Personalizing immunotherapy

Pharmacology and Treatment Selection in Metastatic Cancer

Daan Hurkmans

Personalizing Immunotherapy

Pharmacology and Treatment Selection in Metastatic Cancer

Daan Hurkmans

ISBN: 978-94-6423-147-2
Cover design: Barry Borsboom
Printed by: ProefschriftMaken || www.proefschriftmaken.nl

The printing was supported by: PamGene International B.V., Pfizer Inc., Chipsoft B.V.

Personalizing Immunotherapy

Pharmacology and Treatment Selection in Metastatic Cancer

Personalisatie van Immunotherapie

Farmacologie en Gerichte Behandeling bij Gemetastaseerde Kanker

Proefschrift

Ter verkrijging van de graad van doctor aan de Erasmus Universiteit Rotterdam

op gezag van de rector magnificus

prof. dr. F.A. van der Duijn Schouten

en volgens het besluit van het College van Promoties.

De openbare verdediging zal plaatsvinden op **woensdag 17 maart 2021 om 15.30 uur.**

Daniël Petrus Hurkmans

geboren te Castricum

Erasmus University Rotterdam

Promotiecommissie

Promotoren:	Prof. dr. A.H.J. Mathijssen
	Prof. dr. J.G.J.V. Aerts
Overige leden:	Prof. dr. F.J. van Kemenade
	Prof. dr. H.J.M. Groen
	Prof. dr. S.H. van der Burg

Voor Linde

Contents

CHAPTER 1

1

Introduction

With the introduction of the immune checkpoint inhibitors (ICIs), a novel category of cancer therapy was created that leads to a cytotoxic immune response against cancer cells. While cytotoxic T-lymphocyte-associated protein 4 (CTLA-4) inhibitors have been introduced in 2011 for the treatment of patients with metastatic melanoma[1], inhibitors targeting the programmed cell death protein 1 (PD-1) receptor or its ligand (PD-L1) are now standard of care for many types of cancer. Durable tumor responses after treatment with ICIs have been observed in metastatic melanoma[2], renal cell cancer (RCC)[3] as well as in non-small cell lung cancer (NSCLC)[4,5]. In this *Introduction*, an overview is given of the available evidence in regard to pharmacokinetics (PK) and predictive markers at the start of this thesis, being March 2017, and which is updated in the *Summary and Future Perspectives* (**Chapter 17**).

Essentially, the clinical implementation of ICIs has differed from strategies traditionally used for cytotoxic drugs in oncology. ICIs are well-tolerated with a high maximum tolerated dose (MTD), whereas chemotherapeutic agents generally have a small therapeutic range and a low MTD. Dose-limiting toxicities are rarely reported. Only one of the main phase 1 trials of ICI monotherapy across several tumor types has identified dose-limiting toxicities[6], as reviewed by Postel-Vinay[7]. Moreover, a profound dose-response relationship has been lacking for ICIs in advanced-stage melanoma or NSCLC (**Table 1**). Previously, a dose-response relationship has not been observed in larger patient cohorts[8,9], with the exception of a phase I trial for ipilimumab (0.3 – 10 mg/kg)[10]. Here, only a small subset of all included metastatic melanoma patients (5%) displayed therapy response, and may consequently be explained by a lack of power. Based on the available trial data, there is a consensus that the serum trough levels achieved with the recommended dosage is well-tolerated and much higher than the required serum concentrations.

Although no efficacy of very low dosing schemes can be expected, a dose-response relationship is lacking in present ICI dosing schemes[11], paving the way for dose optimization. In this context, population PK modeling may support rational dosing across tumor types. Population PK modeling is used to describe the time course of drug exposure in patients and investigates the sources of its variability, which is of particular interest in the real-world setting. Real-world patients, being treated as standard of care, are not identical to trial patients who are subjected to strict inclusion and exclusion criteria. Therefore, we believe that investigation of the source of variability of PK is particularly informative in a real-world setting where physicians are often challenged by patients with a higher age, comorbidities, advanced progression, worse clinical performance or brain metastases.

PK modeling aims to integrate data, knowledge and biological mechanisms to guide rational decisions regarding drug dosing.[12]

Table 1. Therapeutic response in different dose levels of PD-1 or CTLA-4 inhibitors

ICI monotherapy	Indication	Dose	ORR (%)	Reference
CTLA-4	MM			
Ipilimumab	Pretreated MM	0.3 mg/kg Q3W	0	Wolchok et al., Lancet Oncol 2010[10]
		3 mg/kg Q3W	4.2	
		10 mg/kg Q3W	11.1	
Ipilimumab	MM	3 mg/kg Q3W	11	Robert et al., N Engl J Med 2015[8]
PD-1	MM			
Pembrolizumab	Ipilimumab-refractory MM	2 mg/kg Q3W	26	Robert et al., Lancet 2014[13]
		10 mg/kg Q3W	26	
Pembrolizumab	Pretreated MM	10 mg/kg Q2W	33.7	Robert et al., N Engl J Med 2015[8]
		10 mg/kg Q3W	32.9	
Nivolumab	Pretreated MM	0.1 mg/kg Q2W	35.3	Topalian et al., J Clin Oncol 2014[14]
		0.3 mg/kg Q2W	27.8	
		1 mg/kg Q2W	31.4	
		3 mg/kg Q2W	41.2	
		10 mg/kg Q2W	20	
Nivolumab	Previously untreated MM	2 mg/kg Q3W	40	Robert et al., N Engl J Med 2015[2]
PD-1	NSCLC			
Pembrolizumab	Pretreated stage IV NSCLC	2 mg/kg Q3W	18	Herbst et al., Lancet 2016[15]
		10 mg/kg Q3W	18.5	
Nivolumab	Pretreated Stage IV NSCLC	1 mg/kg Q2W 3 mg/kg Q2W	6 32	Topalian et al., N Engl J Med 2012[16]
		10 mg/kg Q2W	18	

Summary of the objective response rate (ORR) in different dose levels for CTLA-4 and PD-1 inhibitors derived from phase I/II/III trials in metastatic melanoma (MM) and non-small cell lung cancer (NSCLC). ORR was based on best overall response (CR or PR defining radiological response) using RECIST v1.1[17].

Selection of patients is essential as ICIs come with high costs, relatively low response rates and high rates of immune-related adverse events (irAEs). Up to the beginning of this thesis,

efforts to predict response (**Box 1**) have yielded various markers for NSCLC and melanoma, including peripheral blood cells, soluble blood-based molecules, characteristics of the tumor genome or microenvironment (TME) and commensal microbiome (**Table 2**).

Box 1 Understanding biomarkers Generally, misunderstanding occurs for the terms prognostic, predictive and (early) monitoring biomarkers in this immune-oncology setting. To clarify, an example about the difference between prognostic and predictive biomarkers is shown in the figure. Additional categories of biomarkers (e.g. susceptibility, diagnostic or safety biomarkers) are out of the scope of this thesis.

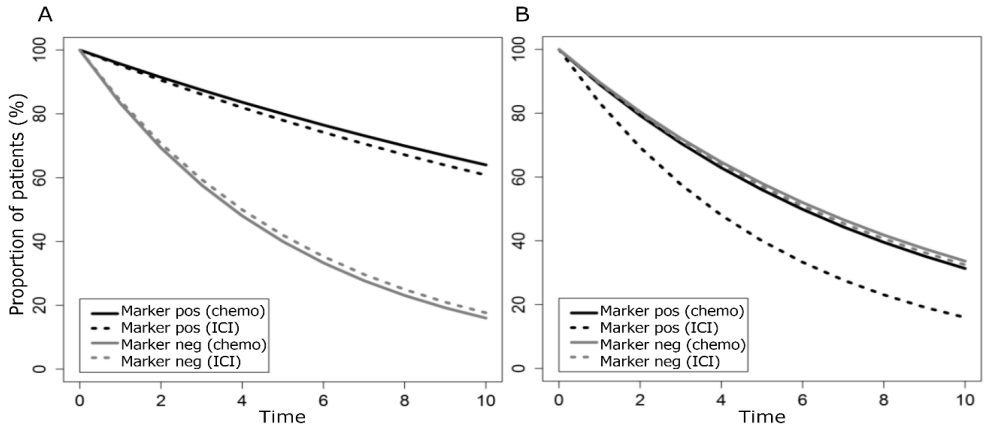

Figure Box 1. A) example of a biomarker that is prognostic. Assume that patients have received either immune checkpoint inhibition (ICI) or chemotherapy (chemo). The survival outcomes of both groups are similar, illustrating prognostic value. In contrast, B) illustrates a negative predictive biomarker reflected in worse survival in patients who received ICI and who are positive for the biomarker. Figure adapted from the BEST (Biomarkers, EndpointS, and other Tools) Resource[18].

Prognostic biomarkers are generally used to identify the likelihood of a clinical event (death, progressive disease) in a patient population, while predictive or early biomarkers are utilized to predict clinical outcome after treatment or are monitored during treatment to evaluate the efficacy.

Biologically, the binding of PD-L1 to the inhibitory immune checkpoint PD-1 aids cancer cells to evade the host immune system. PD-L1 expression in cancer tissue has emerged in 2010 as a predictive biomarker to select patients who are more likely to have an objective response to PD-1 inhibitors[19]. PD-L1 negative tumors have shown a lower probability of therapy response and higher PD-L1 expression has been correlated with improved efficacy[16]. Hence, some clinical trials used PD-L1 positivity as an inclusion criteria. This has led to approval of a PD-1 inhibitor for NSCLC patients whose tumors are positive for PD-L1[20]. Nonetheless, PD-L1 expression in tumor as a predictive biomarker has many

drawbacks. PD-L1 expression in tumor have proven to be variable among different assays[21] or cutoffs, inter-tumoral[22] or intra-tumor heterogeneity[23], and variability after exposure to prior therapies[24]. Therefore, PD-L1 expression in tumor tissue is considered unreliable to properly guide treatment decisions.

Up to March 2017, a number of blood parameters have been associated with clinical outcome after ICI therapy. For instance, myeloid-derived suppressor cells (MDSCs), discriminated from other immune cells of the myeloid lineage by immunosuppressive activity, were consistently negatively correlated with clinical outcome[25-28]. Moreover, the absolute numbers of peripheral monocytes have been related to resistance to CTLA-4 inhibitors[25], and peripheral eosinophils were predominantly associated with response to PD-1 inhibition in metastatic melanoma[29].

Serum lactate dehydrogenase (LDH) has been proposed as a negative predictor for ICIs in metastatic melanoma[29-32]. However, LDH is generally recognized a negative prognostic factor of metastatic melanoma[33], and no differences in ICI efficacy have been observed in a subgroup analysis between patients with normal and elevated LDH[34], supporting prognostic value for LDH. In the same way, preliminary data from a proteomic study have indicated that serum of PD-1 resistant patients is characterized by acute phase, complement and wound healing molecules[35], but failed to distinguish a predictive rather than a prognostic biomarker.

The potential impact of the microbiome was demonstrated by early findings that the antitumor effects of CTLA-4 inhibition relies on distinct gut bacteria, and may be overcome by fecal microbial transplantation in mice[36].

Essentially, higher rates of proliferating cytotoxic T cells recognizing tumor antigens have been detected in blood from patients with clinical benefit after ICIs in patients with NSCLC and melanoma[37], as well as its density in the TME[38-40]. Recognition of tumor antigens by tumor-infiltrating lymphocytes (TILs) is proposed to be a prerequisite for the efficacy of ICI, when presented at the tumor cell surface in the context of classical HLA. Firstly, preliminary data has indicated a relation of T cell receptor (TCR) diversity in blood with response to CTLA-4 inhibitors[41]. A more diverse TCR repertoire was related to clinical benefit, suggesting that in those patients an antitumor T cell population is present that can proliferate and recognize tumor antigens. Secondly, the tumor mutation burden (TMB) was strongly associated with improved clinical outcome after ICIs in advanced-stage NSCLC[37,42,43] and melanoma[44,45]. TMB is a measurement of the frequency of mutations in tumor cells, and relates to the number of tumor antigens that can be recognized by cytotoxic T cells[37,46]. Consistently, thirdly, solid tumors with defects in DNA damage repair (DDR) genes are more likely to benefit from ICIs[47]. This may be illustrated by the observations that defects of the mismatch repair (MMR) machinery lead to hypermutation[48] and associate to higher density of TILs in the TME[49]. Fourthly, mutations related to attenuated presentation of tumor antigens at the cell surface (e.g. *B2M* mutation or *HLA* homozygosity) have been related with resistance mechanisms of ICIs[50,51]. Although other genes have also been

suggested to impact response and resistance to ICIs (e.g. mutations in *STK11*, *BRAF*, *EGFR*, *NF1* or *JAK1/2*)[51-54], their predictive value remains uncertain. Lastly, an interferon-γ gene signature was associated with improved clinical outcome after PD-L1 inhibition (and not for the chemotherapy arm of this trial)[55]. Taken together, the above five lines of evidence emphasize the key role for cytotoxic functions of lymphocytes in ICI therapy.

Table 2. Literature overview (up to March 2017) of proposed biomarkers for immune checkpoint inhibitors

Agent	Tumor	Marker	Association	Reference
Peripheral blood cells				
CTLA-4 inhibitors	MM	MDSCs	Negative	Meyer et al., Cancer Immunol Immunother 2014[26]
CTLA-4 inhibitors	MM	MDSCs	Negative	Kitano et al., Cancer Immunol Res 2014[27]
CTLA-4 inhibitors	MM	MDSCs	Negative	Gebhardt et al., Clin Cancer Res 2015[28]
CTLA-4 inhibitors	MM	TCR richness TCR evenness	Positive Positive	Postow et al., J Immunother Cancer 2015[41]
CTLA-4 inhibitors	MM	AMC MDSCs	Negative Negative	Martens et al., Clin Cancer Res 2016[25]
PD-1 inhibitors	MM	AEC	Positive	Weide et al., Clin Cancer Res 2016[29]
PD-1 inhibitors	MM	Th9 cells	Positive	Nonomura et al., Oncoimmunology 2016[56]
Blood-based molecules				
CTLA-4 inhibitors	MM	LDH	Negative	Kelderman et al., Cancer Immunol Immunother 2014[32]
PD-1 inhibitors	MM	LDH	Negative	Diem et al., Br J Cancer 2016[31]
PD-1 inhibitors	MM	LDH	Negative	Weide et al., Clin Cancer Res 2016[29]
PD-1 inhibitors	MM	LDH	Negative	Ribas et al., JAMA 2016[30]
PD-1 inhibitors	MM	Serum signature[a]	Positive	Weber et al., Cancer Immunol Res 2016[35]
PD-1 inhibitors	MM	TGF-β	Positive	Nonomura et al., Oncoimmunology 2016[56]
Tumor genome				
CTLA-4 inhibitors	MM	TMB[b]	Positive	Van Rooij et al., J Clin Oncol 2013[57]
PD-1 inhibitors	NSCLC	TMB	Positive	Rizvi et al., Science 2015[42]
PD-(L1) inhibitors	MM	*NRAS/BRAF* mutation *NF1* mutation	Uncertain Positive	Johnson et al., Cancer Immunol Res 2015[52]
CTLA-4 inhibitors	MM	*BRAF* mutation	Uncertain	Mangana et al., PLos One 2015[58]
PD-1 inhibitors	Solid tumors	MMR deficiency	Positive	Le et al., N Engl J Med 2015[47]
PD-1 inhibitors	NSCLC	TMB	Positive	Campesato et al. Oncotarget 2016[43]
PD-1 inhibitors	NSCLC	TMB[c]	Positive	McGranahan et al. Science 2016[37]
	NSCLC	*EGFR* mutation	Negative	Peng et al., Cancer Discov 2016[54]

PD-1 inhibitors	MM	TMB	Positive	Hugo et al., Cell 2016[44]
PD-1 inhibitors	MM/ NSCLC	TMB	Positive	Roszik et al., BMC Med 2016[45]
PD-(L)1 inhibitors	MM	*HLA* homozygosity	Negative	Inoue et al., OncoImmunology 2016[50]
PD-1 inhibitors	MM	*JAK1/2* mutation *B2M* mutation	Negative Negative	Zaretsky et al., N Engl J Med 2016[51]
Tumor microenvironment				
PD-1 inhibitors	MM	IHC signature[d]	Positive	Tumeh et al., Nature 2014[59]
PD-L1 inhibitors	NSCLC	PD-L1 expression	Positive	Herbst et al., Nature 2014[60]
CTLA-4 and PD-1 inhibitors	MM	PD-L1 expression	Positive	Larkin et al., N Engl J Med 2015[61]
PD-1 inhibitors	NSCLC	PD-L1 expression	Positive	Borghaei et al., N Engl J Med 2015[46]
CTLA-4 inhibitors PD-1 inhibitors	MM	IHC signature[e] IHC signature[f]	Uncertain Positive	Chen et al., Cancer Discov 2016[62]
PD-L1 inhibitors	NSCLC	PD-L1 expression	Positive	Fehrenbacher et al., Lancet 2016[55]
PD-1 inhibitors	NSCLC	PD-L1 expression	Positive	Herbst et al., Lancet 2016[63]
PD-1 inhibitors	NSCLC	PD-L1 expression	Positive	Reck et al., N Engl J Med 2016[64]
PD-1 inhibitors	NSCLC	PD-L1 expression	Positive	Roach et al., Appl IHC Mol Morphol 2016[65]
CTLA-4 or PD-1 inhibitors	NSCLC/ MM	$CD8^+$ T cells[g]	Positive	McGranahan et al., Science 2016[37]
PD-L1 inhibitors	NSCLC	IFN-γ signature[h]	Positive	Fehrenbacher et al., Lancet 2016[55]
Commensal microbiotica				
CTLA-4 inhibitors	MM	*Bacteroides* species	Uncertain	Vetizou et al., Science 2015[36]

Literature overview of markers that correlate with clinical outcome after immune checkpoint inhibitors for metastatic melanoma (MM) or non-small cell lung cancer (NSCLC). Data cutoff was set at March 2017, at the start of this thesis. An update is provided in the discussion and future perspectives of this thesis, including an extended overview of biomarkers after March 2017. Abbreviations: tumor mutation burden (TMB), absolute monocyte count (AMC), myeloid-derived suppressor cell (MDSC), absolute eosinophil count (AEC), lactate dehydrogenase (LDH), T cell receptor (TCR), not applicable (NA), immunohistochemistry (IHC). [a]Serum protein profile consisting of molecules involved in wound healing, acute phase reactants and complement system. [b]TMB and neo-antigen-specific T cell reactivity. [c]TMB and clonal neo-antigens. [d]Higher numbers of CD8, PD1, and PD-L1 expressing cells and clonal TCR repertoire in tumor. Early on-treatment tumor biopsies revealed a distinct IHC signature consisting of [e]CD8 for CTLA-4 and of [f]CD4, CD8, CD3, PD-1, PD-L1, LAG3, FOXP3 and granzyme B for PD-1 inhibition. [g]Proliferating $CD8^+$ T cells. [h]Interferon-γ gene signature defined by expression of CD8A, GZMA, GZMB, IFNG, EOMES, CXCL9, CXCL10, and TBX21.

This thesis is divided in five parts. **Part I** describes the pharmacology of ICIs, where we studied the relationship between pharmacokinetic parameters (such as drug exposure, drug clearance) and efficacy. We developed a PK model in a real-world cohort to assess the impact of patient factors on the pharmacokinetics of nivolumab and pembrolizumab. **Part II and III** involve treatment selection of immunotherapy of predominantly NSCLC and melanoma, among other tumor types. **Part IV** provides a summary of all findings and the future perspectives of the pharmacology and treatment selection of ICIs, including an updated literature overview. **Part V** contains the appendix.

References

1. Hodi FS, O'Day SJ, McDermott DF, et al. Improved survival with ipilimumab in patients with metastatic melanoma. *N Engl J Med.* 2010;363(8):711-723.
2. Robert C, Long GV, Brady B, et al. Nivolumab in previously untreated melanoma without BRAF mutation. *N Engl J Med.* 2015;372(4):320-330.
3. Motzer RJ, Escudier B, McDermott DF, et al. Nivolumab versus Everolimus in Advanced Renal-Cell Carcinoma. *N Engl J Med.* 2015;373(19):1803-1813.
4. Borghaei H, Paz-Ares L, Horn L, et al. Nivolumab versus Docetaxel in Advanced Nonsquamous Non-Small-Cell Lung Cancer. *N Engl J Med.* 2015;373(17):1627-1639.
5. Brahmer J, Reckamp KL, Baas P, et al. Nivolumab versus Docetaxel in Advanced Squamous-Cell Non-Small-Cell Lung Cancer. *N Engl J Med.* 2015;373(2):123-135.
6. Ribas A, Camacho LH, Lopez-Berestein G, et al. Antitumor activity in melanoma and anti-self responses in a phase I trial with the anti-cytotoxic T lymphocyte-associated antigen 4 monoclonal antibody CP-675,206. *J Clin Oncol.* 2005;23(35):8968-8977.
7. Postel-Vinay S, Aspeslagh S, Lanoy E, Robert C, Soria JC, Marabelle A. Challenges of phase 1 clinical trials evaluating immune checkpoint-targeted antibodies. *Ann Oncol.* 2016;27(2):214-224.
8. Robert C, Schachter J, Long GV, et al. Pembrolizumab versus Ipilimumab in Advanced Melanoma. *N Engl J Med.* 2015;372(26):2521-2532.
9. Robert C, Schadendorf D, Messina M, Hodi FS, O'Day S, investigators MDX. Efficacy and safety of retreatment with ipilimumab in patients with pretreated advanced melanoma who progressed after initially achieving disease control. *Clin Cancer Res.* 2013;19(8):2232-2239.
10. Wolchok JD, Neyns B, Linette G, et al. Ipilimumab monotherapy in patients with pretreated advanced melanoma: a randomised, double-blind, multicentre, phase 2, dose-ranging study. *Lancet Oncol.* 2010;11(2):155-164.
11. Gettinger SN, Horn L, Gandhi L, et al. Overall Survival and Long-Term Safety of Nivolumab (Anti-Programmed Death 1 Antibody, BMS-936558, ONO-4538) in Patients With Previously Treated Advanced Non-Small-Cell Lung Cancer. *J Clin Oncol.* 2015;33(18):2004-2012.
12. Mould DR, Upton RN. Basic concepts in population modeling, simulation, and model-based drug development-part 2: introduction to pharmacokinetic modeling methods. *CPT Pharmacometrics Syst Pharmacol.* 2013;2:e38.
13. Robert C, Ribas A, Wolchok JD, et al. Anti-programmed-death-receptor-1 treatment with pembrolizumab in ipilimumab-refractory advanced melanoma: a randomised dose-comparison cohort of a phase 1 trial. *Lancet.* 2014;384(9948):1109-1117.
14. Topalian SL, Sznol M, McDermott DF, et al. Survival, durable tumor remission, and long-term safety in patients with advanced melanoma receiving nivolumab. *J Clin Oncol.* 2014;32(10):1020-1030.
15. Herbst RS, Baas P, Kim DW, et al. Pembrolizumab versus docetaxel for previously treated, PD-L1-positive, advanced non-small-cell lung cancer (KEYNOTE-010): a randomised controlled trial. *Lancet.* 2016;387(10027):1540-1550.

16. Topalian SL, Hodi FS, Brahmer JR, et al. Safety, activity, and immune correlates of anti-PD-1 antibody in cancer. *N Engl J Med.* 2012;366(26):2443-2454.
17. Eisenhauer EA, Therasse P, Bogaerts J, et al. New response evaluation criteria in solid tumours: revised RECIST guideline (version 1.1). *Eur J Cancer.* 2009;45(2):228-247.
18. Group F-NBW. 2016.
19. Brahmer JR, Drake CG, Wollner I, et al. Phase I study of single-agent anti-programmed death-1 (MDX-1106) in refractory solid tumors: safety, clinical activity, pharmacodynamics, and immunologic correlates. *J Clin Oncol.* 2010;28(19):3167-3175.
20. Garon EB, Rizvi NA, Hui R, et al. Pembrolizumab for the treatment of non-small-cell lung cancer. *N Engl J Med.* 2015;372(21):2018-2028.
21. Fujimoto D, Sato Y, Uehara K, et al. Predictive Performance of Four Programmed Cell Death Ligand 1 Assay Systems on Nivolumab Response in Previously Treated Patients with Non-Small Cell Lung Cancer. *J Thorac Oncol.* 2018;13(3):377-386.
22. Mansfield AS, Aubry MC, Moser JC, et al. Temporal and spatial discordance of programmed cell death-ligand 1 expression and lymphocyte tumor infiltration between paired primary lesions and brain metastases in lung cancer. *Ann Oncol.* 2016;27(10):1953-1958.
23. Ilie M, Long-Mira E, Bence C, et al. Comparative study of the PD-L1 status between surgically resected specimens and matched biopsies of NSCLC patients reveal major discordances: a potential issue for anti-PD-L1 therapeutic strategies. *Ann Oncol.* 2016;27(1):147-153.
24. Zhang J, Dang F, Ren J, Wei W. Biochemical Aspects of PD-L1 Regulation in Cancer Immunotherapy. *Trends Biochem Sci.* 2018;43(12):1014-1032.
25. Martens A, Wistuba-Hamprecht K, Geukes Foppen M, et al. Baseline Peripheral Blood Biomarkers Associated with Clinical Outcome of Advanced Melanoma Patients Treated with Ipilimumab. *Clin Cancer Res.* 2016;22(12):2908-2918.
26. Meyer C, Cagnon L, Costa-Nunes CM, et al. Frequencies of circulating MDSC correlate with clinical outcome of melanoma patients treated with ipilimumab. *Cancer Immunol Immunother.* 2014;63(3):247-257.
27. Kitano S, Postow MA, Ziegler CG, et al. Computational algorithm-driven evaluation of monocytic myeloid-derived suppressor cell frequency for prediction of clinical outcomes. *Cancer Immunol Res.* 2014;2(8):812-821.
28. Gebhardt C, Sevko A, Jiang H, et al. Myeloid Cells and Related Chronic Inflammatory Factors as Novel Predictive Markers in Melanoma Treatment with Ipilimumab. *Clin Cancer Res.* 2015;21(24):5453-5459.
29. Weide B, Martens A, Hassel JC, et al. Baseline Biomarkers for Outcome of Melanoma Patients Treated with Pembrolizumab. *Clin Cancer Res.* 2016;22(22):5487-5496.
30. Ribas A, Hamid O, Daud A, et al. Association of Pembrolizumab With Tumor Response and Survival Among Patients With Advanced Melanoma. *Jama.* 2016;315(15):1600-1609.
31. Diem S, Kasenda B, Spain L, et al. Serum lactate dehydrogenase as an early marker for outcome in patients treated with anti-PD-1 therapy in metastatic melanoma. *Br J Cancer.* 2016;114(3):256-261.

32. Kelderman S, Heemskerk B, van Tinteren H, et al. Lactate dehydrogenase as a selection criterion for ipilimumab treatment in metastatic melanoma. *Cancer Immunol Immunother.* 2014;63(5):449-458.
33. O'Sullivan B, Brierley J, Byrd D, et al. The TNM classification of malignant tumours-towards common understanding and reasonable expectations. *Lancet Oncol.* 2017;18(7):849-851.
34. Ribas A, Puzanov I, Dummer R, et al. Pembrolizumab versus investigator-choice chemotherapy for ipilimumab-refractory melanoma (KEYNOTE-002): a randomised, controlled, phase 2 trial. *Lancet Oncol.* 2015;16(8):908-918.
35. Weber JS, Sznol M, Sullivan RJ, et al. A Serum Protein Signature Associated with Outcome after Anti-PD-1 Therapy in Metastatic Melanoma. *Cancer Immunol Res.* 2018;6(1):79-86.
36. Vétizou M, Pitt JM, Daillère R, et al. Anticancer immunotherapy by CTLA-4 blockade relies on the gut microbiota. *Science.* 2015;350(6264):1079-1084.
37. McGranahan N, Furness AJ, Rosenthal R, et al. Clonal neoantigens elicit T cell immunoreactivity and sensitivity to immune checkpoint blockade. *Science.* 2016;351(6280):1463-1469.
38. Zeng DQ, Yu YF, Ou QY, et al. Prognostic and predictive value of tumor-infiltrating lymphocytes for clinical therapeutic research in patients with non-small cell lung cancer. *Oncotarget.* 2016;7(12):13765-13781.
39. Brambilla E, Le Teuff G, Marguet S, et al. Prognostic Effect of Tumor Lymphocytic Infiltration in Resectable Non-Small-Cell Lung Cancer. *J Clin Oncol.* 2016;34(11):1223-1230.
40. Fridman WH, Pagès F, Sautès-Fridman C, Galon J. The immune contexture in human tumours: impact on clinical outcome. *Nat Rev Cancer.* 2012;12(4):298-306.
41. Postow MA, Manuel M, Wong P, et al. Peripheral T cell receptor diversity is associated with clinical outcomes following ipilimumab treatment in metastatic melanoma. *J Immunother Cancer.* 2015;3:23.
42. Rizvi NA, Hellmann MD, Snyder A, et al. Cancer immunology. Mutational landscape determines sensitivity to PD-1 blockade in non-small cell lung cancer. *Science.* 2015;348(6230):124-128.
43. Campesato LF, Barroso-Sousa R, Jimenez L, et al. Comprehensive cancer-gene panels can be used to estimate mutational load and predict clinical benefit to PD-1 blockade in clinical practice. *Oncotarget.* 2015;6(33):34221-34227.
44. Hugo W, Zaretsky JM, Sun L, et al. Genomic and Transcriptomic Features of Response to Anti-PD-1 Therapy in Metastatic Melanoma. *Cell.* 2016;165(1):35-44.
45. Roszik J, Haydu LE, Hess KR, et al. Novel algorithmic approach predicts tumor mutation load and correlates with immunotherapy clinical outcomes using a defined gene mutation set. *BMC Med.* 2016;14(1):168.
46. Borghaei H, Paz-Ares L, Horn L, et al. Nivolumab versus Docetaxel in Advanced Nonsquamous Non-Small-Cell Lung Cancer. *N Engl J Med.* 2015;373(17):1627-1639.
47. Le DT, Uram JN, Wang H, et al. PD-1 Blockade in Tumors with Mismatch-Repair Deficiency. *N Engl J Med.* 2015;372(26):2509-2520.
48. Timmermann B, Kerick M, Roehr C, et al. Somatic mutation profiles of MSI and MSS colorectal cancer identified by whole exome next generation sequencing and bioinformatics analysis. *PLoS One.* 2010;5(12):e15661.

49. Dolcetti R, Viel A, Doglioni C, et al. High prevalence of activated intraepithelial cytotoxic T lymphocytes and increased neoplastic cell apoptosis in colorectal carcinomas with microsatellite instability. *Am J Pathol.* 1999;154(6):1805-1813.
50. Inoue H, Park JH, Kiyotani K, et al. Intratumoral expression levels of PD-L1, GZMA, and HLA-A along with oligoclonal T cell expansion associate with response to nivolumab in metastatic melanoma. *Oncoimmunology.* 2016;5(9):e1204507.
51. Zaretsky JM, Garcia-Diaz A, Shin DS, et al. Mutations Associated with Acquired Resistance to PD-1 Blockade in Melanoma. *N Engl J Med.* 2016;375(9):819-829.
52. Johnson DB, Frampton GM, Rioth MJ, et al. Targeted Next Generation Sequencing Identifies Markers of Response to PD-1 Blockade. *Cancer Immunol Res.* 2016;4(11):959-967.
53. Skoulidis F, Goldberg ME, Greenawalt DM, et al. STK11/LKB1 Mutations and PD-1 Inhibitor Resistance in KRAS-Mutant Lung Adenocarcinoma. *Cancer Discov.* 2018;8(7):822-835.
54. Peng W, Chen JQ, Liu C, et al. Loss of PTEN Promotes Resistance to T Cell-Mediated Immunotherapy. *Cancer Discov.* 2016;6(2):202-216.
55. Fehrenbacher L, Spira A, Ballinger M, et al. Atezolizumab versus docetaxel for patients with previously treated non-small-cell lung cancer (POPLAR): a multicentre, open-label, phase 2 randomised controlled trial. *Lancet.* 2016;387(10030):1837-1846.
56. Nonomura Y, Otsuka A, Nakashima C, et al. Peripheral blood Th9 cells are a possible pharmacodynamic biomarker of nivolumab treatment efficacy in metastatic melanoma patients. *Oncoimmunology.* 2016;5(12):e1248327.
57. van Rooij N, van Buuren MM, Philips D, et al. Tumor exome analysis reveals neoantigen-specific T-cell reactivity in an ipilimumab-responsive melanoma. *J Clin Oncol.* 2013;31(32):e439-442.
58. Mangana J, Cheng PF, Schindler K, et al. Analysis of BRAF and NRAS Mutation Status in Advanced Melanoma Patients Treated with Anti-CTLA-4 Antibodies: Association with Overall Survival? *PLoS One.* 2015;10(10):e0139438.
59. Tumeh PC, Harview CL, Yearley JH, et al. PD-1 blockade induces responses by inhibiting adaptive immune resistance. *Nature.* 2014;515(7528):568-571.
60. Herbst RS, Soria JC, Kowanetz M, et al. Predictive correlates of response to the anti-PD-L1 antibody MPDL3280A in cancer patients. *Nature.* 2014;515(7528):563-567.
61. Larkin J, Chiarion-Sileni V, Gonzalez R, et al. Combined Nivolumab and Ipilimumab or Monotherapy in Untreated Melanoma. *N Engl J Med.* 2015;373(1):23-34.
62. Chen PL, Roh W, Reuben A, et al. Analysis of Immune Signatures in Longitudinal Tumor Samples Yields Insight into Biomarkers of Response and Mechanisms of Resistance to Immune Checkpoint Blockade. *Cancer Discov.* 2016;6(8):827-837.
63. Herbst RS, Baas P, Kim DW, et al. Pembrolizumab versus docetaxel for previously treated, PD-L1-positive, advanced non-small-cell lung cancer (KEYNOTE-010): a randomised controlled trial. *Lancet.* 2016;387(10027):1540-1550.
64. Reck M, Rodriguez-Abreu D, Robinson AG, et al. Pembrolizumab versus Chemotherapy for PD-L1-Positive Non-Small-Cell Lung Cancer. *N Engl J Med.* 2016;375(19):1823-1833.

65. Roach C, Zhang N, Corigliano E, et al. Development of a Companion Diagnostic PD-L1 Immunohistochemistry Assay for Pembrolizumab Therapy in Non-Small-cell Lung Cancer. *Appl Immunohistochem Mol Morphol*. 2016;24(6):392-397.

PART I

Pharmacology

CHAPTER 2

2

Correlation between nivolumab exposure and treatment outcomes in non-small cell lung cancer

Edwin A. Basak, Stijn L.W. Koolen, Daan P. Hurkmans, Marco W.J. Schreurs, Sander Bins, Esther Oomen-de Hoop, Annemarie J.M. Wijkhuijs, Ilse den Besten, Stefan Sleijfer, Reno Debets, Astrid A.M. van der Veldt, Joachim G.J.V. Aerts, Ron H.J. Mathijssen

European Journal of Cancer, March 2019, 109: page 12-20

Introduction: Nivolumab treatment is subject to large interpatient variability in both efficacy and toxicity, which may partly be explained by differences in nivolumab exposure. Exposure-response relationships in regular healthcare have not been extensively investigated for nivolumab. Therefore, we aimed to identify possible exposure-response relationships in nivolumab treated non-small cell lung cancer (NSCLC) patients.

Materials and Methods: NSCLC patients who started 2nd line nivolumab therapy (3 mg/kg Q2W) between May 5th 2016 and August 1st 2017, and from whom serial blood samples, toxicity data, and outcome data were prospectively collected, were included. Follow-up was carried out until November 1st 2017. Patients were classified according to best objective response (BOR) based on RECIST v1.1, and toxicities according to CTCAE. Nivolumab trough concentrations were measured after 2, 4, and 10 weeks of treatment, excluding dose delays, and calculated geometric means were tested versus BOR or toxicity using ANOVA and an independent samples *t*-test, respectively. Overall survival (OS) and progression free survival were compared between high and low trough concentration groups.

Results: Seventy-six patients were evaluable for analyses. Responders (n=15) had higher mean trough concentrations than patients with progression (n=33): 47% higher after 2 weeks (p=0.001), 53% higher after 4 weeks (p=0.008), and 73% higher after 10 weeks (p=0.002). Higher trough concentrations were associated with longer OS (p=0.001).

Discussion: This study shows that NSCLC patients with a response to nivolumab had a higher nivolumab exposure than patients with progression, indicating a potential exposure-response relationship. Further clinical research should focus on clarifying these exposure-response relationships.

Abstract

INTRODUCTION

Nivolumab is a human immunoglobin G4 monoclonal antibody directed against programmed death 1 (PD-1) protein, reinvigorating intratumoral T-cells, which often have become inactivated in a T-cell co-stimulation-deprived micro-environment.{Nishimura, 1999 #1}[1] Nivolumab is currently approved for the treatment of various solid and hematological malignancies.

PD-1 receptor occupancy on circulating CD3+ T cells in nivolumab treated melanoma patients has been demonstrated to be saturated at doses above 0.3 mg/kg, as patients receiving higher doses did not achieve a higher PD-1 receptor occupancy. However, response rates in these patients were higher in doses > 0.3 mg/kg,[2,3] indicating the presence of unexplored mechanisms which determine response to nivolumab treatment. Comparable results are reported for nivolumab treated NSCLC patients: response rates in patients dosed at 3 mg/kg Q2W were higher than those dosed at 1 mg/kg Q2W (24% versus 3%). However, no increase in response rates was observed in patients receiving 10 mg/kg Q2W compared to 3 mg/kg Q2W.[2,3] Moreover, the occurrence of serious adverse events did not increase in patients who received nivolumab doses of 1.0 mg/kg or higher.[3] Therefore, the dose of 3 mg/kg Q2W was used in consecutive phase 3 trials.[4,5] As a consequence, subtle exposure-response relationships in NSCLC patients receiving the nivolumab dose of 3 mg/kg may have been overlooked.

So far, exposure-response relationships in nivolumab treated patients have not been reported,[6] whereas various other monoclonal antibodies used for the treatment of solid tumors and hematologic malignancies have shown exposure-response relationships.[7-11] For example, breast cancer patients treated with trastuzumab with an exposure in the lowest quartile after cycle 1, had 8 months shorter median overall survival than patients in other quartiles, without a difference in the occurrence of toxicities. Colorectal cancer patients with a below median cetuximab exposure, experienced significantly shorter median progression free survival (PFS) than other patients (3.3 versus 7.8 months). Furthermore, in patients with advanced melanoma, ipilimumab 10 mg/kg resulted in significantly longer median overall survival (OS) than ipilimumab 3 mg/kg (15.7 versus 11.5 months).[12] For the first time, we studied exposure-response relationships in standard of care nivolumab treated NSCLC patients, treated with a dosing regimen of 3 mg/kg Q2W.

MATERIALS AND METHODS

Design

Stage IV NSCLC patients who started nivolumab treatment between May 5th 2016 and August 1st 2017 at the Erasmus MC Cancer Institute, were included prospectively in this study (Dutch Trial Registry number NTR7015), allowing for serial sampling during standard

of care nivolumab treatment. Data cut-off was at November 1st 2017. Blood was drawn prior to every 2-weekly nivolumab infusion to measure nivolumab trough concentrations (i.e. concentration immediately prior to following infusion). Patient characteristics and clinical data were included from the hospital's electronic patient record system. Best overall response (BOR) was assessed according to RECIST v1.1 with a minimal follow-up time of 90 days.[13] If treatment was discontinued before 90 days due to rapid progression or death, BOR was classified as progressive disease (PD). A minimum duration of 90 days for stable disease (SD) was necessary. Confirmation of partial response (PR) or complete response was not required for best response determination. In patients treated beyond radiologic progression, subsequent response assessments accounted for BOR. Adverse events were registered from start of treatment until end of follow-up according to National Cancer Institute Common Terminology Criteria for Adverse Events (NCI-CTCAE) v4.03.

Nivolumab serum measurements

Four mL of serum was obtained before every nivolumab infusion, of which 5 µL was used to measure nivolumab serum concentrations. All nivolumab concentrations were measured with an in-house developed and validated ELISA.[14] Measurements were performed as follows: 96-well EIA/RIA microtiter plates (Corning, NY, USA) were coated overnight at 4° C with 100 µL/well of 0.1 µg/mL capture antigen (recombinant human PD-1 Fc chimera, R&D, Minneapolis, MN, USA), diluted in PBS (BioWhittaker Inc, Walkersville, MD, USA), pH 7.4. The plates were washed three times in washing buffer (0.05% Tween 20 in PBS, pH 7.4) and incubated for 1 hour at room temperature (RT) with 300 µL/well blocking solution (1% BSA/0.05% Tween20 in PBS, pH 7.4). After three washes, nivolumab calibration standards, ranging from 25 to 0.20 ng/mL and serum samples, 1:4000 diluted in blocking solution were added in duplicate to the wells and subsequently, the plates were incubated for 2 hours at RT on a shaker set at 300 rpm. After three additional washes, 100 µl/well of 0.2 µg/mL detection antibody (Human IgG4-HRP, BioRad, Hercules, CA, USA), diluted in blocking solution, was added to the plates, followed by incubation for 2 hours at RT on a shaker. Subsequently, plates were washed three times and 100 µl/well tetramethylbenzidine peroxidase substrate was added. Plates were incubated for 15 minutes in the dark and the reaction was stopped with 2 M H_2SO_4. Results were read using VersaMax Tunable microplate reader (Molecular Devices) at an optical density of 450 nm, corrected at wavelength of 570 nm. Results were calculated by averaging all duplicate readings and using a standard curve, generated by a 5 parameter logistic curve-fit.

Statistics and data analysis

Patients were divided according to BOR in PD, SD and PR, and according to toxicity (occurrence of grade ≥3 or grade ≤2 adverse events). Trough concentrations were compared on the log-scale at week 2, 4, and 10 between BOR groups with ANOVA and between toxicity groups with an independent samples t-test. Patients with dose-delays until time point of

analysis were excluded for that particular --and following-- time points. If significant, a *post hoc* analysis with Tukey HSD test was performed between BOR groups. The assumption of equal variances in log transformed trough concentrations between groups was assessed with Levene's test. A Log Rank test was performed to assess potential differences in OS and PFS between the groups with 50% lowest trough concentrations (low exposure) and 50% highest trough concentrations (high exposure). Patients dying without progression were censored. Data collection and statistical analysis were performed using R v3.3.1 and IBM SPSS Statistics v24 (Chicago, IL). A two-sided p value <0.05 was considered significant.

Table 1. Patient characteristics

	Total Number of patients (n=76)	Non-responders (n=33)	Partial responders (n=15)
Gender			
Male	46 (61%)	21 (64%)	6 (40%)
Female	30 (40%)	12 (36%)	9 (60%)
Age at start (years)			
Mean (±SD)	63 (±8.9)	60 (±9.7)	65 (±6.6)
WHO performance status			
0	17 (22%)	5 (15%)	3 (20%)
1	39 (51%)	20 (61%)	10 (67%)
2	1 (1%)	1 (3%)	0 (0%)
Unknown	19 (25%)	7 (21%)	2 (13%)
Primary lung tumor			
Adenocarcinoma	50 (66%)	22 (67%)	12 (80%)
Squamous cell carcinoma	23 (30%)	10 (30%)	2 (13%)
Large cell carcinoma	3 (4%)	1 (3%)	1 (7%)
Number of pre-treatment lines[a]			
1	60 (79%)	23 (70%)	14 (93%)
2	14 (18%)	10 (30%)	0 (0%)
3	2 (3%)	0 (0%)	1 (7%)

[a]All patients with pre-treatment received a platinum containing regimen.

RESULTS

Out of 84 patients, 76 were evaluable (see **table 1**), since 4 patients were non-evaluable according to RECIST and 4 patients had no follow-up blood samples available as their treatment was discontinued after the first cycle (3 patients because of rapid clinical deterioration and 1 patient because of grade 3 skin toxicity). According to BOR, 33, 28, and 15 patients had PD, SD and PR, respectively. Grade ≥3 toxicities occurred in 15 patients. Median follow-up time was 246 days (IQR 127–379 days).

Figure 1. Median nivolumab trough concentrations

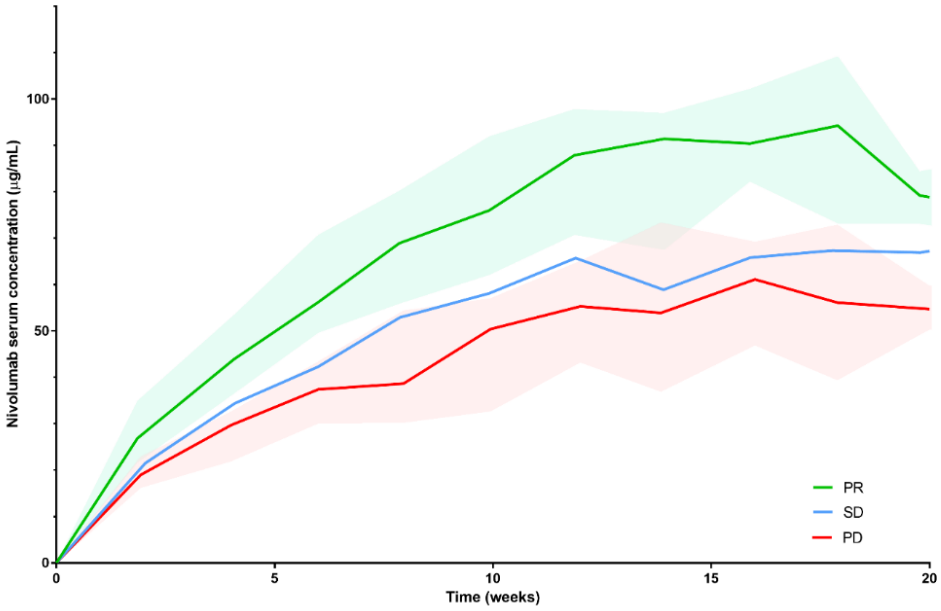

Nivolumab trough concentrations for each response category, measured prior to every nivolumab infusion and 2 weeks after a previous infusion. Lines represent median values for PR (green), SD (blue), and PD (red), respectively. Shaded area represents interquartile ranges for partial responders (green) and patients with progressive disease (red).

The courses of median nivolumab trough concentrations per response group until 20 weeks after treatment start are shown in **figure 1**. Comparisons of median trough levels and the number of evaluable patients per response group at week 2, 4, and 10 are shown in **figure 2**. In **figure 3a** and **3b** Kaplan-Meier curves are shown for OS and PFS per group of trough concentration, whereas median trough concentrations and the number of evaluable patients per toxicity group are shown in **figure 4**. For each time point, geometric mean trough concentrations were significantly different between response groups: at week 2: p=0.001; at week 4: p=0.01; at week 10: p=0.002. *Post hoc* comparisons showed that at week 2, PR patients (27.4 µg/mL, 95%CI: 22.3-33.6 µg/mL) had 47% (95%CI: 34-61%) higher geometric mean trough concentrations than PD patients (18.7 µg/mL, 95%CI: 16.7-20.9 µg/mL; p=0.001), and 30% (95%CI: 20-42%) higher trough concentrations than SD patients (21.0 µg/mL, 95%CI: 18.6-23.7 µg/mL; p=0.034). At week 4, PR patients (46.2 µg/mL, 95%CI: 37.4-57.0 µg/mL) had 53% (95%CI: 50-57%) higher trough concentrations than PD patients (30.2 µg/mL, 95%CI: 25.0-36.4 µg/mL; p=0.008), and 40% (95%CI: 32-48%) higher trough concentrations than SD patients (33.0 µg/mL, 95%CI: 28.3-38.5 µg/mL; p=0.047). At week 10, PR patients (79.4 µg/mL, 95%CI: 60.7-103.8

Figure 2. Nivolumab trough concentrations per time point according to BOR

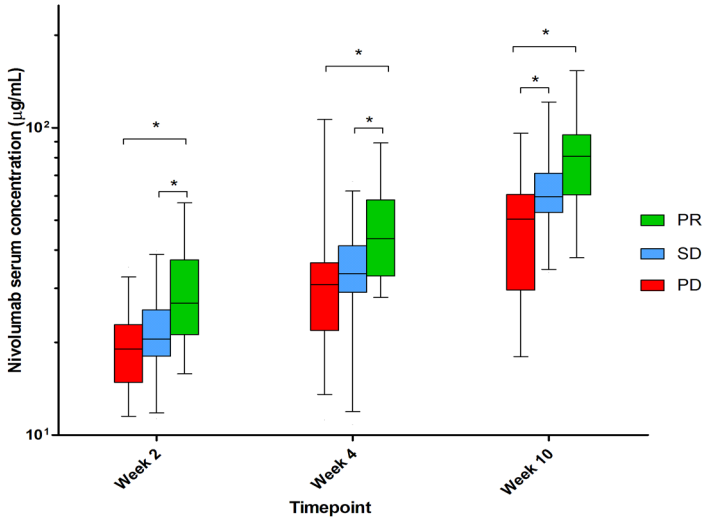

BOR	N	N	N
PD	29	27	15
SD	24[a]	25	20
PR	14	14	11

Nivolumab trough concentrations per response category per time point. Red, blue, and green boxes represent the median and interquartile ranges for the PD, SD, and PR groups, respectively. Whiskers show 5 - 95% percentile. *Indicates significant difference ($p<0.05$); [a]One missing sample.

Figure 3. OS and PFS versus nivolumab trough concentrations

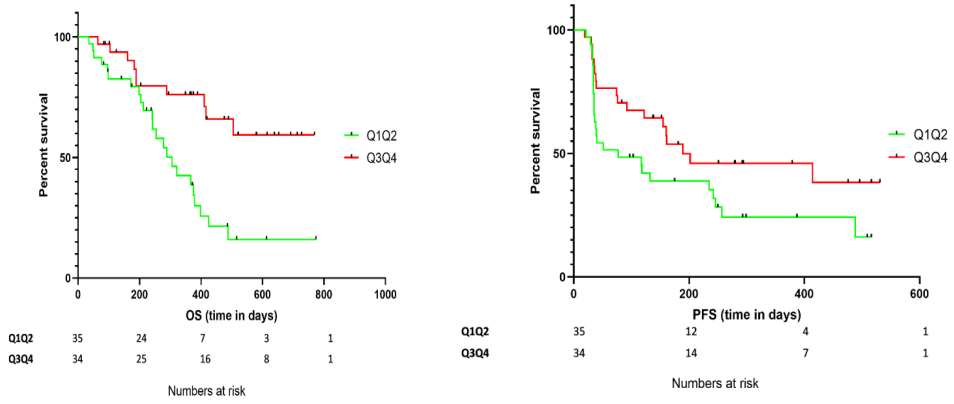

Kaplan-Meier curve for overall survival (a) and progression free survival (b) stratified for the groups with 50% lowest trough concentrations (Q1Q2) and 50% highest trough concentrations (Q3Q4).

Figure 4. Nivolumab trough concentrations per time point according to toxicity

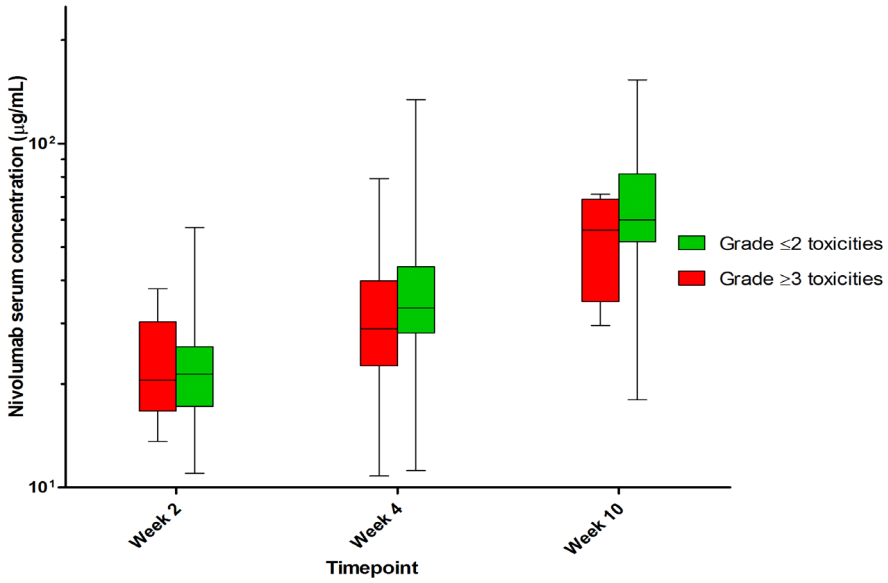

Toxicity	N	N	N
Grade 3 or higher	11	10	4
Grade 2 or lower	56	56	42

Nivolumab trough concentrations per toxicity category per time point. Green and red boxes represent the median and interquartile ranges for the grade ≤2 toxicity and grade ≥3 toxicity groups, respectively. Whiskers show 5 - 95% percentile.

µg/mL) had 73% (95%CI: 71-76%) higher trough concentrations than PD patients (45.8 µg/mL, 95%CI: 35.6-58.9 µg/mL; p=0.002), whereas trough concentrations in SD patients were 36% (95%CI: 21-54%) higher than in PD patients (62.5 µg/mL, 95%CI: 54.9-71.3 µg/mL; p=0.048). The high exposure group experienced significant longer OS (median: not reached versus 306 days; p=0.001), whereas no significant difference was found for PFS (median: 189 versus 77 days; p=0.061).

No difference in exposure was found when comparing patients with and without grade ≥3 toxicity during all time points: 4% (95%CI: 3–5%) difference at week 2 (p=0.732), 21% (95%CI: 20–23%) difference at week 4 (p=0.216, and 20% (95%CI: 12–32%) difference at week 10 (p=0.413). Assumption of equal variances between BOR groups and between toxicity groups was met at each investigated time point.

Only after 4 weeks of treatment, a difference in exposure between males and females was found (30.4 µg/mL versus 41.3 µg/mL; p=0.005).

DISCUSSION

In this study, we aimed to assess the relationship between nivolumab exposure and clinical outcome in NSCLC patients. We demonstrated for the first time that patients, treated with an equivalent dose per kg and with an objective radiographical response to nivolumab therapy, have a significantly higher exposure than non-responders at all the time points measured (i.e. after 2, 4, and 10 weeks of treatment). The high exposure group experienced longer OS, whereas no difference was found for PFS. No association was found between the occurrence of grade ≥3 adverse events and drug exposure, which is in line with earlier phase I studies, where no maximum tolerated dose could be defined for nivolumab in the dose range of 0.3 to 10 mg/kg.[15]

These observations might reflect a true exposure-response relationship for nivolumab. On the other hand, a target concentration of 10 µg/mL was sufficient in an *ex vivo* model for reaching >90% of the maximum achievable receptor occupancy,[16] which is already reached after the first cycle in all treatment groups. Furthermore, it has recently been suggested that the exposure-response relationship for immune checkpoint inhibitors is confounded by the catabolic state due to cancer cachexia, which would lead to lower nivolumab concentrations due to accelerated IgG breakdown and would shorten survival.[17] In that study, however, the exposure-response relationship could not be explained by cachexia alone and other factors than only peripheral PD-1 receptor occupancy are likely involved in a response to treatment too, as has been suggested earlier.[2] Moreover, our primary endpoint (i.e. best objective response) is less likely to be affected by cachexia than overall survival is. Currently available evidence is therefore not sufficient to rule out an exposure-dependent anti-cancer effect of nivolumab and it remains vital to further elucidate the relationship between exposure and response. Additionally, an increasing response rate until a nivolumab dose of 3.0 mg/kg Q2W in NSCLC patients[2,3] supports a possible exposure-response relationship in patient groups receiving 3.0 mg/kg Q2W.

If exposure appears to determine response (at least partially), we hypothesize that PD and SD patients would have had a better response if they had reached higher systemic exposure at an earlier moment, since nivolumab trough concentrations are higher in PR patients in an early phase of treatment. To achieve this a loading dose could be considered, e.g. by doubling the first dose of nivolumab. The long terminal half-life of the nivolumab IgG antibody, leading to a long time until steady-state is reached, supports such a loading dose, which is applied for many other therapeutic IgG antibodies too.[18] Many factors have been demonstrated or are thought to influence the pharmacokinetics of monoclonal antibodies. Along with cachexia, the influence of other parameters on monoclonal antibody exposure needs to be quantified, body weight has been correlated with the clearance of monoclonal antibodies.[19] And clearance itself is associated with overall survival in pembrolizumab treated patients.[17] Also, it is thought that endothelial wall inflammation may influence the distribution of monoclonal antibodies.[20] Furthermore,

(epi)genetic variation in the neonatal Fc-receptor (FcRn) may influence pharmacokinetics of certain antibodies.[21] Target-mediated clearance and thus PD-1 expression may affect exposure too.[22,23] Furthermore, the formation of antidrug antibodies (ADA) influences pharmacokinetics of administered antibodies.[21] Although a negligible effect was seen on efficacy, and no effect was seen on clearance, 12.7% of nivolumab treated patients experience ADA formation.[24]

In our analysis, the high exposure group experienced longer OS, whereas no difference was found for PFS. This may indicate that trough concentrations are affected by mechanisms influencing OS, but less PFS, such as cachexia. However, subsequent treatment lines after nivolumab may also influence OS, whereas PFS is not affected.

Male patients experienced lower exposure only after 4 weeks of treatment, this is in line with earlier findings, reporting higher clearance in males.[17,25]

Serial sampling of blood allowed us to include time points prior to a radiologic assessment, and therefore to study a high number of patients treated with an equivalent dose per kg. The prospective character of this study, the inclusion of a uniform cohort treated with a similar nivolumab dosage, the distribution of the response groups comparable to earlier reported trials and intensive sampling prior nivolumab administration provide a solid background for interpretation of results. Intensive measurements of C_{trough} levels are --to our opinion-- excellent means to study exposure response relationship because it is relatively convenient for patients and it is the most informative pharmacokinetic sample to quantify exposure in a single pharmacokinetic sample strategy. Moreover, minimum and median follow-up time (3 and 8.1 months, respectively) well exceeded median time to response (2.1-2.2 months)[4,5] and toxicity, that generally occurs within 3 months.[26] Therefore, only few data on the clinical endpoints is lacking in this analysis. In a real world setting, physicians occasionally decide for treatment beyond progression, two patients had 'pseudo-progression'. Both patients eventually achieved PR during nivolumab therapy, and were therefore classified accordingly. Regarding the PK data, one should notice that patients with serious adverse events or progressive disease were excluded from analysis at week 4 and 10 relatively more frequent because of interruption or discontinuation of treatment, respectively, which may lead to a higher decrease of included patients at later time points in those subgroups. Some caution when interpreting the data should be taken, since potential factors associated with treatment outcome, such as tumor load, the occurrence of pre-existent cachexia or clearance[17], and their influence on exposure, are not included in this analysis. Also, the included number of patients in this analysis is relatively low. We did not perform a multivariable analysis due to potential sparse-data bias. Although it has been noted that exposure-response relationships in nivolumab treated patients may be biased by decreased clearance in responding patients, this finding is shown to be of less relevance in an early stage of treatment.[27] This emphasizes the need for further research following our results, despite earlier analysis showing a relatively flat exposure-response relationship over various nivolumab doses.[28]

This is the first study showing an exposure-response relation for nivolumab. We argue that further clarification of exposure-response relationships and its covariates in patients treated with nivolumab is highly warranted, and new dosing strategies or combination therapies aiming at increasing the dosage should be explored. In particular, as toxicity does not increase with a higher systemic exposure, future nivolumab dosing adjustments based on exposure may improve treatment outcome.

REFERENCES

1. Nishimura H, Nose M, Hiai H, Minato N, Honjo T. Development of lupus-like autoimmune diseases by disruption of the PD-1 gene encoding an ITIM motif-carrying immunoreceptor. *Immunity.* 1999;11(2):141-151.
2. Agrawal S, Feng Y, Roy A, Kollia G, Lestini B. Nivolumab dose selection: challenges, opportunities, and lessons learned for cancer immunotherapy. *J Immunother Cancer.* 2016;4:72.
3. Topalian SL, Hodi FS, Brahmer JR, et al. Safety, activity, and immune correlates of anti-PD-1 antibody in cancer. *N Engl J Med.* 2012;366(26):2443-2454.
4. Borghaei H, Paz-Ares L, Horn L, et al. Nivolumab versus Docetaxel in Advanced Nonsquamous Non-Small-Cell Lung Cancer. *N Engl J Med.* 2015;373(17):1627-1639.
5. Brahmer J, Reckamp KL, Baas P, et al. Nivolumab versus Docetaxel in Advanced Squamous-Cell Non-Small-Cell Lung Cancer. *N Engl J Med.* 2015;373(2):123-135.
6. Callahan MK, Postow MA, Wolchok JD. Targeting T Cell Co-receptors for Cancer Therapy. *Immunity.* 2016;44(5):1069-1078.
7. Yang J, Zhao H, Garnett C, et al. The combination of exposure-response and case-control analyses in regulatory decision making. *J Clin Pharmacol.* 2013;53(2):160-166.
8. Wang J, Song P, Schrieber S, et al. Exposure-response relationship of T-DM1: insight into dose optimization for patients with HER2-positive metastatic breast cancer. *Clin Pharmacol Ther.* 2014;95(5):558-564.
9. Azzopardi N, Lecomte T, Ternant D, et al. Cetuximab pharmacokinetics influences progression-free survival of metastatic colorectal cancer patients. *Clin Cancer Res.* 2011;17(19):6329-6337.
10. Mould DR, Dubinsky MC. Dashboard systems: Pharmacokinetic/pharmacodynamic mediated dose optimization for monoclonal antibodies. *J Clin Pharmacol.* 2015;55 Suppl 3:S51-59.
11. Gibiansky E, Gibiansky L, Carlile DJ, Jamois C, Buchheit V, Frey N. Population Pharmacokinetics of Obinutuzumab (GA101) in Chronic Lymphocytic Leukemia (CLL) and Non-Hodgkin's Lymphoma and Exposure-Response in CLL. *CPT Pharmacometrics Syst Pharmacol.* 2014;3:e144.
12. Feng Y, Roy A, Masson E, Chen TT, Humphrey R, Weber JS. Exposure-response relationships of the efficacy and safety of ipilimumab in patients with advanced melanoma. *Clin Cancer Res.* 2013;19(14):3977-3986.
13. Eisenhauer EA, Therasse P, Bogaerts J, et al. New response evaluation criteria in solid tumours: revised RECIST guideline (version 1.1). *Eur J Cancer.* 2009;45(2):228-247.
14. Basak EA, Wijkhuijs AJM, Mathijssen RHJ, Koolen SLW, Schreurs MWJ. Development of an Enzyme-Linked Immune Sorbent Assay to Measure Nivolumab and Pembrolizumab Serum Concentrations. *Therapeutic drug monitoring.* 2018;40(5):596-601.
15. Brahmer JR, Drake CG, Wollner I, et al. Phase I study of single-agent anti-programmed death-1 (MDX-1106) in refractory solid tumors: safety, clinical activity, pharmacodynamics, and immunologic correlates. *J Clin Oncol.* 2010;28(19):3167-3175.

16. Ogungbenro K, Patel A, Duncombe R, Nuttall R, Clark J, Lorigan P. Dose Rationalization of Pembrolizumab and Nivolumab Using Pharmacokinetic Modeling and Simulation and Cost Analysis. *Clin Pharmacol Ther.* 2018;103(4):582-590.
17. Turner D, Kondic AG, Anderson KM, et al. Pembrolizumab exposure-response assessments challenged by association of cancer cachexia and catabolic clearance. *Clin Cancer Res.* 2018, https://doi.org/10.1158/1078-0432.CCR-18-0415.
18. Leyland-Jones B, Colomer R, Trudeau ME, et al. Intensive loading dose of trastuzumab achieves higher-than-steady-state serum concentrations and is well tolerated. *J Clin Oncol.* 2010;28(6):960-966.
19. Mould DR, Green B. Pharmacokinetics and pharmacodynamics of monoclonal antibodies: concepts and lessons for drug development. *BioDrugs.* 2010;24(1):23-39.
20. Vugmeyster Y, Harrold J, Xu X. Absorption, distribution, metabolism, and excretion (ADME) studies of biotherapeutics for autoimmune and inflammatory conditions. *AAPS J.* 2012;14(4):714-727.
21. Ghetie V, Ward ES. Multiple roles for the major histocompatibility complex class I- related receptor FcRn. *Annu Rev Immunol.* 2000;18:739-766.
22. Lammerts van Bueren JJ, Bleeker WK, Bogh HO, et al. Effect of target dynamics on pharmacokinetics of a novel therapeutic antibody against the epidermal growth factor receptor: implications for the mechanisms of action. *Cancer Res.* 2006;66(15):7630-7638.
23. Coffey GP, Stefanich E, Palmieri S, et al. In vitro internalization, intracellular transport, and clearance of an anti-CD11a antibody (Raptiva) by human T-cells. *J Pharmacol Exp Ther.* 2004;310(3):896-904.
24. Agrawal S, Statkevich P, Bajaj G, et al. Evaluation of Immunogenicity of Nivolumab Monotherapy and Its Clinical Relevance in Patients With Metastatic Solid Tumors. *J Clin Pharmacol.* 2017;57(3):394-400.
25. Bajaj G, Wang X, Agrawal S, Gupta M, Roy A, Feng Y. Model-Based Population Pharmacokinetic Analysis of Nivolumab in Patients With Solid Tumors. *CPT Pharmacometrics Syst Pharmacol.* 2017;6(1):58-66.
26. Champiat S, Lambotte O, Barreau E, et al. Management of immune checkpoint blockade dysimmune toxicities: a collaborative position paper. *Ann Oncol.* 2016;27(4):559-574.
27. Liu C, Yu J, Li H, et al. Association of time-varying clearance of nivolumab with disease dynamics and its implications on exposure response analysis. *Clin Pharmacol Ther.* 2017;101(5):657-666.
28. Feng Y, Wang X, Bajaj G, et al. Nivolumab Exposure-Response Analyses of Efficacy and Safety in Previously Treated Squamous or Nonsquamous Non-Small Cell Lung Cancer. *Clin Cancer Res.* 2017;23(18):5394-5405.

CHAPTER 3

3

A prospective cohort study on the pharmacokinetics of nivolumab in metastatic non-small cell lung cancer, melanoma, and renal cell cancer patients

Daan P. Hurkmans, Edwin A. Basak, Tanja van Dijk, Darlene Mercieca, Marco W.J. Schreurs, Annemarie J.M. Wijkhuijs, Sander Bins, Esther Oomen-de Hoop, Reno Debets, Markus Joerger, Arlette Odink, Astrid A.M. van der Veldt, Cor H. van der Leest, Joachim G.J.V. Aerts, Ron H.J. Mathijssen, Stijn L.W. Koolen

Journal for ImmunoTherapy of Cancer, July 2019, 7: 192

Abstract

Background*:* Nivolumab is administered in a weight-based or fixed-flat dosing regimen. For patients with non-small cell lung cancer (NSCLC), a potential exposure-response relationship has recently been reported and may argue against the current dosing strategies. The primary objectives were to determine nivolumab pharmacokinetics (PK) and to assess the relationship between drug clearance and clinical outcome in NSCLC, melanoma, and renal cell cancer (RCC).

Materials and Methods*:* In this prospective observational cohort study, individual estimates of nivolumab clearance and the impact of baseline covariates were determined using a population-PK model. Clearance was related to best overall response (RECISTv1.1), and stratified by tumor type.

Results*:* Two-hundred-twenty-one patients with metastatic cancer receiving nivolumab-monotherapy were included of whom 1,715 plasma samples were analyzed. Three baseline parameters had a significant effect on drug clearance and were internally validated in the population-PK model: gender, BSA, and serum albumin. Women had 22% lower clearance compared to men, while the threshold of BSA and albumin that led to >20% increase of clearance was > 2.2m^2 and <37.5g/L, respectively. For NSCLC, drug clearance was 42% higher in patients with progressive disease(mean: 0.24; 95%CI: 0.22-0.27 L/day) compared to patients with partial/ complete response(0.17; 0.15-0.19). A similar trend was observed in RCC, however, no clearance-response relationship was observed in melanoma.

Discussion*:* Based on the first real-world population-PK model of nivolumab, covariate analysis revealed a significant effect of gender, BSA, and albumin on nivolumab clearance. A clearance-response relationship was observed in NSCLC, with a non-significant trend in RCC, but not in melanoma. Individual pharmacology of nivolumab in NSCLC appears important and should be prospectively studied.

BACKGROUND

Nivolumab is a human immunoglobulin G4 (IgG4) monoclonal antibody (MoAb) that inhibits the interaction between the co-inhibitory immune receptor programmed death-1 (PD-1) and its ligands, PD-L1 and PD-L2. Nivolumab monotherapy has been approved for several indications, including advanced and metastatic melanoma[1], advanced clear-cell renal cell cancer (RCC), and metastatic non-small-cell lung cancer (NSCLC)[2,3]. IgG4 MoAbs, such as nivolumab, are characterized by a relatively high molecular mass, leading to a slow distribution in tissues[4]. The elimination of nivolumab is very much alike endogenous immunoglobulins with a half-life of approximately 27 days[5] and a steady-state at 12 weeks. In current clinical practice, nivolumab is administered in different schedules including 3 mg/kg Q2W, 240 mg flat dosing Q2W, and 480 mg flat dosing Q4W. The dosing of 3 mg/kg Q2W --approved by the Food and Drug Administration (FDA) in 2014 -- was based on dose-finding phase I/II studies, showing tolerability for the wide range of 0.1 to 10 mg/kg, and showing activity at 0.1 mg/kg Q2W and higher[6]. However, approval of nivolumab flat dosing (in March 2018), however, was solely based on *in silico* studies: selected flat doses were based on equivalence with initial dosing at median body weight of 80 kg. Population pharmacokinetic (PPK) modeling of data from approximately 100 clinical trials was used to simulate nivolumab concentrations and to compare flat dosing regimens (240 mg Q2W, 480 mg Q4W) with 3 mg/kg Q2W dosing.[7,8] It is noteworthy that a previous model-based PPK analysis resulted in significant but not clinically relevant covariate effects, of which gender and body weight were the most important[9].

Few studies have assessed dose-response (D-R) and exposure-response (E-R) relationships of nivolumab. In a quantitative analysis[10] of a phase 1b dose-escalation study in 129 patients with NSCLC[6], a positive D-R relationship was found at 3 or 10 mg/kg versus 1 mg/kg. In addition, trough concentrations at steady state were correlated with objective response (OR) at 0.1 to 3 mg/kg in another cohort of patients with NSCLC[10]. A D-R relationship could not be demonstrated in patients with melanoma (n=107) nor RCC (n=34) at this dose range, but was only observed at 0.1 up to 1 mg/kg. In 221 melanoma patients treated in phase 1b[6] and 3 studies[11], absence of an E-R relationship was confirmed utilizing PPK modeling by relating the time-averaged nivolumab concentration to OR[12].

In a recent real-world study performed by our group, a steep positive E-R relationship of nivolumab was found for NSCLC (n=76). Here, patients with a partial response (PR) had significant higher mean trough levels during therapy than patients with progressive disease (PD), and high exposure correlated significantly with better overall survival (OS).[13]

The present study addresses the PK of nivolumab in a real-world setting. The main objectives were 1) to define patient parameters influencing nivolumab pharmacokinetics and 2) to describe the relationship of systemic nivolumab clearance with objective response in patients with NSCLC, melanoma, and RCC. Secondary objectives include an

exploratory analysis in regard to immune-related adverse events (irAEs), progression-free survival (PFS), and OS.

METHODS

Patients and study design

Patients with advanced cancer who were treated with nivolumab between 20th April 2016 and 30th October 2018 at the Erasmus MC Cancer Institute (Rotterdam, The Netherlands) and the Amphia Hospital (Breda, The Netherlands) were included prospectively in this study (Dutch Trial Register number NTR7015/ NL6828), allowing for serial blood sampling during standard of care nivolumab treatment. The study was approved by the independent ethics committee (MEC 16-011) and all patients provided written informed consent. Blood samples were drawn prior to every 2-weekly nivolumab to measure trough concentrations. For those patients who gave extensive informed consent, intensive sampling was performed between the first and second administration of nivolumab. Patient characteristics and clinical data were prospectively collected.

Pharmacokinetic measurements

For all patients (n=221), nivolumab trough concentrations were determined for a selection of serum samples until end of treatment. Nivolumab serum concentrations were determined by an in-house developed and validated enzyme-linked immune sorbent assay (ELISA, as described previously[14]. Serum samples were selected to determine trough concentrations prior to each administration for the first 12 weeks, thereafter at evenly 12-weekly intervals until the end of treatment. For some patients (n=3), intensive sampling allowed to determine nivolumab concentrations at 2 hours, 2 days, and 1 week after the first administration in order to estimate a best-fit compartmental model.

Data collection

The following baseline patient parameters were collected: gender, race, tumor type, performance status, age, body weight, body surface area (BSA), total volumetric tumor burden, serum creatinine, renal function, total serum protein, serum albumin, lactate dehydrogenase (LD) and leucocyte count. Performance status was determined according to Eastern Cooperative Oncology Group[15]. For NSCLC patients, weight loss was recorded and defined as a percentage of 2.5 or higher[16] during a period of three months prior to the first administration of nivolumab. BSA was calculated by the Mosteller equation[17]. Renal function was estimated using the Chronic Kidney Disease Epidemiology Collaboration (CKD-EPI) formula[18].

For a subgroup of NSCLC patients (n=30), total volumetric tumor burden at baseline was assessed by a thoracic radiologist (A.O.) in a blinded manner using IntelliSpace Portal

version 8 (Philips Medical Systems Nederland B.V., The Netherlands). Only primary tumor lesions with a long axis ≥10 mm, lymph nodes with a short axis ≥15 mm and metastatic lesions with a long axis ≥10 mm were included. Total volumetric tumor burden was not assessed if the primary tumor was not identifiable or its boundaries could not be defined, e.g. due to surrounding atelectasis or radiation effects.

Best overall response (BOR) was assessed according to Response Evaluation Criteria in Solid Tumors version 1.1 (RECIST v1.1)[19]. A minimum duration of 90 days for stable disease (SD) was required. Confirmation of PR or complete response (CR) was not required. PFS was defined as the time from the first administration of nivolumab until PD or death due to any cause, whichever occurred first. OS was defined as the time from the first administration of nivolumab until death due to any cause. IrAEs were registered from start of treatment until end of follow-up according to National Cancer Institute Common Terminology Criteria for Adverse Events version 4.03 (NCI-CTCAE v4.03). Data cut-off for these analyses was set at 1st of January 2019.

Pharmacokinetic modeling

To determine patient parameters influencing nivolumab PK (primary objective 1), nonlinear mixed effect modeling software, NONMEM (version 7.4; ICON, Development Solutions, MD) was used to analyze the PK data. The first-order conditional estimation method with interaction was used for parameter estimation. Pirana software version 2.9.7 (Pirana, www.pirana-software.com) was used as a modeling environment, and data were further handled in the latest R desktop version 1.1.453 (R-project, www.rproject.org).

A two-compartment PPK model was developed to best fit the nivolumab pharmacokinetics with individual estimates of systemic drug clearance (schematically shown in **Suppl. Figure 1**). Two-compartment PPK models have previously been described to best fit pharmacokinetics of monoclonal antibodies in blood[20]. Since we had only trough PK levels available, modelling of nivolumab distribution was challenging. Hence, we assumed that the central volume (V1) equals the peripheral volume of distribution (V2) as previously described for nivolumab[21].

Between-subject variability (BSV) was tested for clearance and distribution volume. The inclusion of BSV was evaluated according to the change of objective function value (OFV, $P<0.05$) and shrinkage. A shrinkage value below 25% was considered acceptable[22].

BSV was modelled according to equation 1:

$$P_i = P \cdot exp(\eta_i) \quad (1)$$

where P_i represents the parameter estimate for each individual patient (*i*), P represents the typical population parameter estimate and η_i represents BSV distributed according to $N(0, \omega^2)$.

Residual errors were described by a proportional error model (equation 2):

$$C_{obs,ij} = C_{pred,ij} \times (1 + \varepsilon_{p,ij}) \quad (2)$$

where $C_{obs,ij}$ and $C_{pred,ij}$ represent the observed and predicted concentration for the (*i*)th subject and the (*j*)th measurement, respectively. $\varepsilon_{p,ij}$ represents the proportional error distributed according to $N(0,\sigma^2)$.

Covariates were added to the PPK model (initial model M_i) to obtain a final model (final model M_f). Potential covariates were selected based on clinical plausibility and tested by a stepwise approach with forward inclusion (threshold $p<0.01$) and backward elimination (threshold $p<0.005$)[23-25]. The covariates were tested on clearance (CL) by multiplying a typical clearance value (CL_{TV}) with a factor for categorical ($Factor_{cat}$) and continuous ($Factor_{con}$) covariates (equation 3).

$$CL = CL_{TV} \times Factor_{cat} \times Factor_{con} \quad (3)$$

Categorical covariates were scored as '0' or '1'. Equation 4 was applied for patients who scored '1' in which θ_x represents the covariate effect size estimate. Continuous variables were tested with the PK model using equation 5 where *cov* represents the covariate measure, cov_{median} the population median of the covariate, and θ_y the covariate effect measure.

$$Factor_{cat} = 1 + \theta_x \quad (4)$$

$$Factor_{con} = \left(\frac{cov}{cov_{median}}\right)^{\theta_y} \quad (5)$$

Data analysis

Descriptive statistics included frequency and the median with range and inter-quartile range (IQR) of covariates. To analyze the relationship of systemic nivolumab clearance, which is inversely proportional to drug exposure, with treatment outcome (primary objective 2), patients were stratified by tumor type (NSCLC, melanoma, and RCC) and ranked according to BOR. To avoid potential confounding from covariates that may correlate with response, the initial model M_i was used to compare individual drug clearance estimates between different BOR groups (PD, SD, PR/CR). Equal variances among groups were assessed with Levene's test, normal distribution was assessed using the skewness and kurtosis. Comparison of individual drug clearance was assessed for the three BOR groups by ANOVA and post-hoc independent samples t-tests.

To investigate the relationship of systemic nivolumab clearance with toxicity, patients were stratified by tumor type, grouped based on the occurrence of grade 0-2 or grade $\geq$3 irAEs, and analyzed by independent samples t-test. To relate systemic nivolumab clearance to PFS and OS, NSCLC patients were grouped into quartiles: patients with low clearance (Q1) were compared with patients with high clearance (Q4) by the Kaplan-Meier approach. The relative risk of death or death/progression was assessed by the Cox proportional hazards model. Additional patient characteristics were included grouped by clearance quartile (Q1-Q4). A two-sided p-value <0.05 was considered significant.

Post-processing of NONMEM generated data and statistical analysis was conducted with R and IBM SPSS Statistics version 24.0.0.1 (Chicago, IL).

RESULTS

A total of 221 nivolumab-treated cancer patients were included in the PPK model (M_i and M_f): NSCLC (71.4%), melanoma (21.7%), RCC (6.3%), and one mesothelioma patient. The patient characteristics are shown in **Table 1**. One patient received ipilimumab after initial treatment with nivolumab monotherapy, and was excluded from clearance-response, clearance-survival and clearance-toxicity analysis. Dosing was based on body weight (3mg/kg Q2W), with an average dose of 240 mg per administration (IQR: 200 – 280 mg). The average number of nivolumab cycles administered per patient was 12. The overall median follow up time (from first administration of nivolumab to censoring) was 338 days (IQR: 145 – 487 days). A total of 1,715 measurements were available for PK analysis (average of 8 measurements per patient). Examples of nivolumab measurements and administrations over time from two patients, one with and one without dose delays, are shown in **Figure 1**.

Figure 1. Patient examples

A

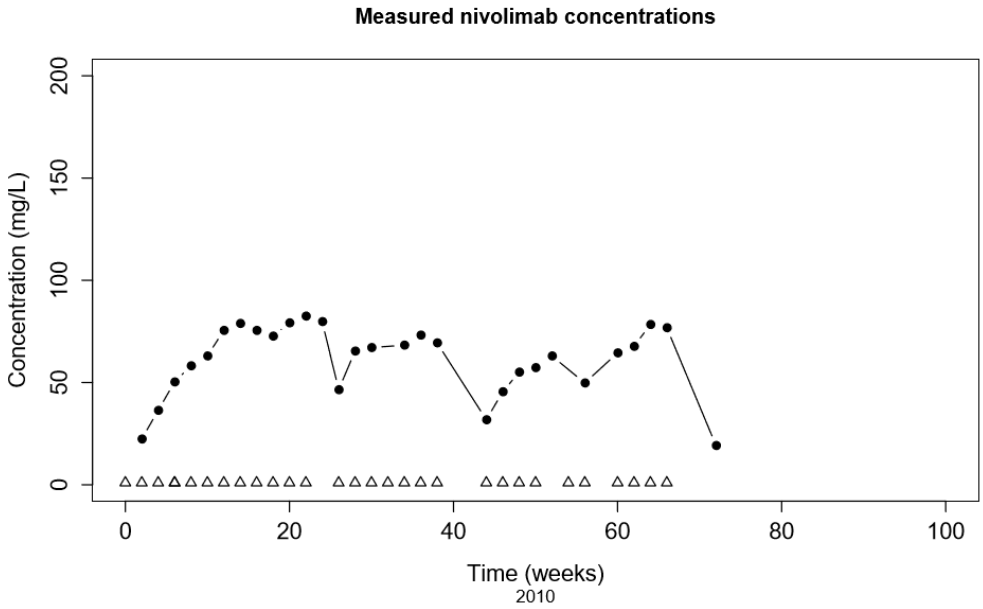

B

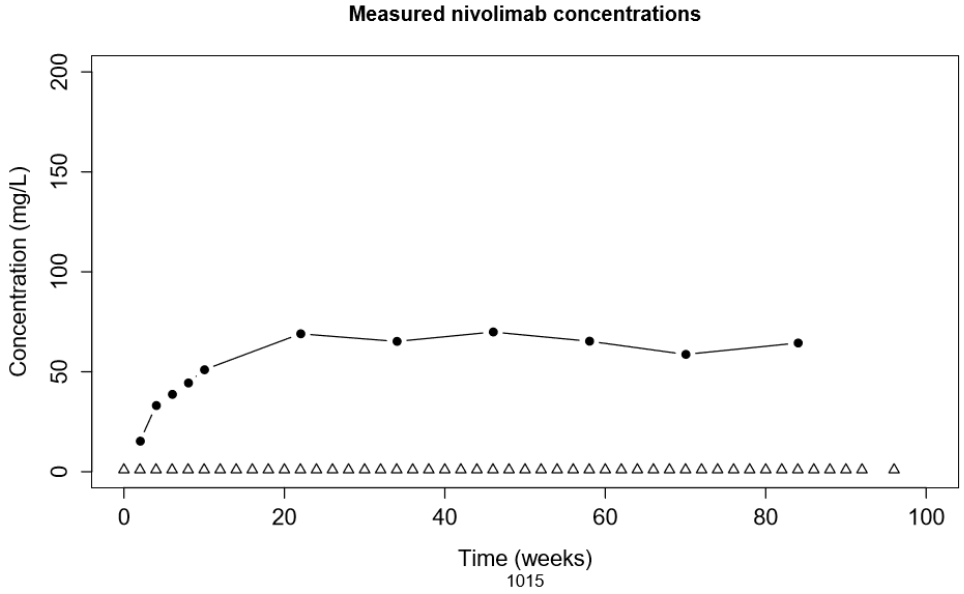

Example of two subjects (2010: NSCLC, 1015: melanoma patient) showing concentrations of nivolumab (mg/L) versus time (weeks), with received administrations of nivolumab being marked as open triangles. Single measurements are represented by closed circles. A) Note that patient 2010 experienced several dose delays followed by a decrease of nivolumab concentrations that was in line with the approximate half-life time of 25 days, whereas B) patient 2015 has had no dose delays and demonstrated a time to steady state concentrations of approximately 20 weeks.

Table 1. Patient characteristics

Demographic Covariates Categorical		**n (%)**
Tumor Type		
NSCLC all types		158 (71.5)
Non-Squamous		96
Squamous		42
Unknown NSCLC type		20
Melanoma		48 (21.7)
RCC		14 (6.3)
Mesothelioma		1 (0.5)
Treatment		
Nivolumab monotherapy (3 mg/kg Q2W)		221 (100)
Gender		
Male		138 (62.4)
Female		83 (37.6)
Race		
Caucasian		195 (88.2)
Other		5 (2.3)
Unknown		21 (9.5)
WHO Performance Status		
0		63 (28.5)
1		103 (46.6)
2		4 (1.8)
Unknown		51 (23.1)
Weight loss prior to start therapy (only in NSCLC)		
Yes		36 (16.3)
No		81 (36.7)
Unknown		104 (47.1)
Demographic and Laboratory Covariates Continuous	**Median (IQR)**	**n (%)**
Age (yr)	65 (59-71)	221 (100)
Body Weight (kg)	78.5 (70-88)	220 (99.5)
Body Surface Area (m^2)	1.95 (1.81-2.09)	205 (93)
Tumor Burden 3D (cm^3; only in NSCLC)	18.6 (66-98)	25 (11)
Creatinine (µmol/L)	81 (66-98)	203 (92)
CKD (mL/min)	81 (62-90)	203 (92)
Total Protein (g/L)	73 (69-90)	163 (74)
Albumine (g/L)	42 (42-45)	174 (79)
LD (U/L)	215 (183-275)	196 (89)
Leucocytes (10^9 cells/L)	7.7 (6.3-10.2)	203 (92)

Baseline covariates of patients. Abbreviations: number of patients (n), inter-quartile range (IQR), CKD-EPI renal clearance (CKD), lactate dehydrogenase (LD).

Gender, BSA and albumin influence nivolumab pharmacokinetics

Continuous and categorical clinical covariates were incorporated in the final two-compartment model by forward inclusion and backward elimination (**Suppl. Table 1**), resulting in four covariates reaching the significance threshold, namely: gender, BSA, albumin, and body weight. BSA had a higher impact on nivolumab pharmacokinetics than weight; the latter being rejected by the backward elimination step. The parameter estimates according to the M_f are shown in **Table 2** including the results of internal validation. The NONMEM model can be found **Suppl. Appendix 1**. Inter-individual variance was reduced from 37% (as indicated by M_i) to 30.7% by incorporating these three covariates. Women had 22% lower clearance than men, as evidenced by a mean clearance of 0.185 and 0.237 L/day, respectively. The thresholds of BSA and baseline serum albumin that led to an estimated >20% increase of systemic nivolumab clearance were > 2.2 m^2 (BSA) and <37.5 g/L (albumin), respectively (**Figure 2**).

Table 2. Parameter estimates

Parameters	Units	Estimate	RSE (%)	Bootstrap estimate	Bootstrap 95% CI
Population parameters					
Clearance (CL)	L/day	0.211	3.5	0.211	0.196 to 0.226
Central volume of distribution (V1)	L	3.46	5.8	3.46	3.09 to 3.83
Peripheral volume of distribution (V2)	L	3.46	5.8	3.46	3.09 to 3.84
Inter-compartmental clearance (Q)	L/day	0.48	<0.1	0.48	0.48 to 0.48
Covariate effects					
Female gender on CL	-	-0.17	29.1	-0.17	-0.27 to -0.06
BSA effect on CL	-	0.97	24.1	0.96	0.48 to 1.45
Albumin effect on CL	-	-1.34	19.8	-1.33	-1.83 to -0.86
Between-subject variability					
Clearance (CL)	CV%	30.7	9	30.3	24.8 to 35.6
Residual unexplained variability					
Proportional error	CV%	31.8	8	31.8	29.1 to 34.2

Table 2. Population parameters, covariate effects and between-subject variability according to the final population pharmacokinetic model (Mf). Abbreviations: clearance (CL), relative standard error (RSE), percentage coefficient of variation (CV%), confidence interval (CI). The shrinkage of the between-subject variability of clearance and the proportional error was 9.2% and 4%, respectively.

Correlation between drug clearance and clinical outcome

Clinical outcome and occurrence of toxicity are shown in **Suppl. Table 2**. The initial model (M_i) was used to investigate the relationship between individual clearance of nivolumab and clinical response or toxicity in NSCLC, melanoma, and RCC (**Figure 3B-D**). A negative clearance-response relationship

Figure 2. Parameter effect on clearance

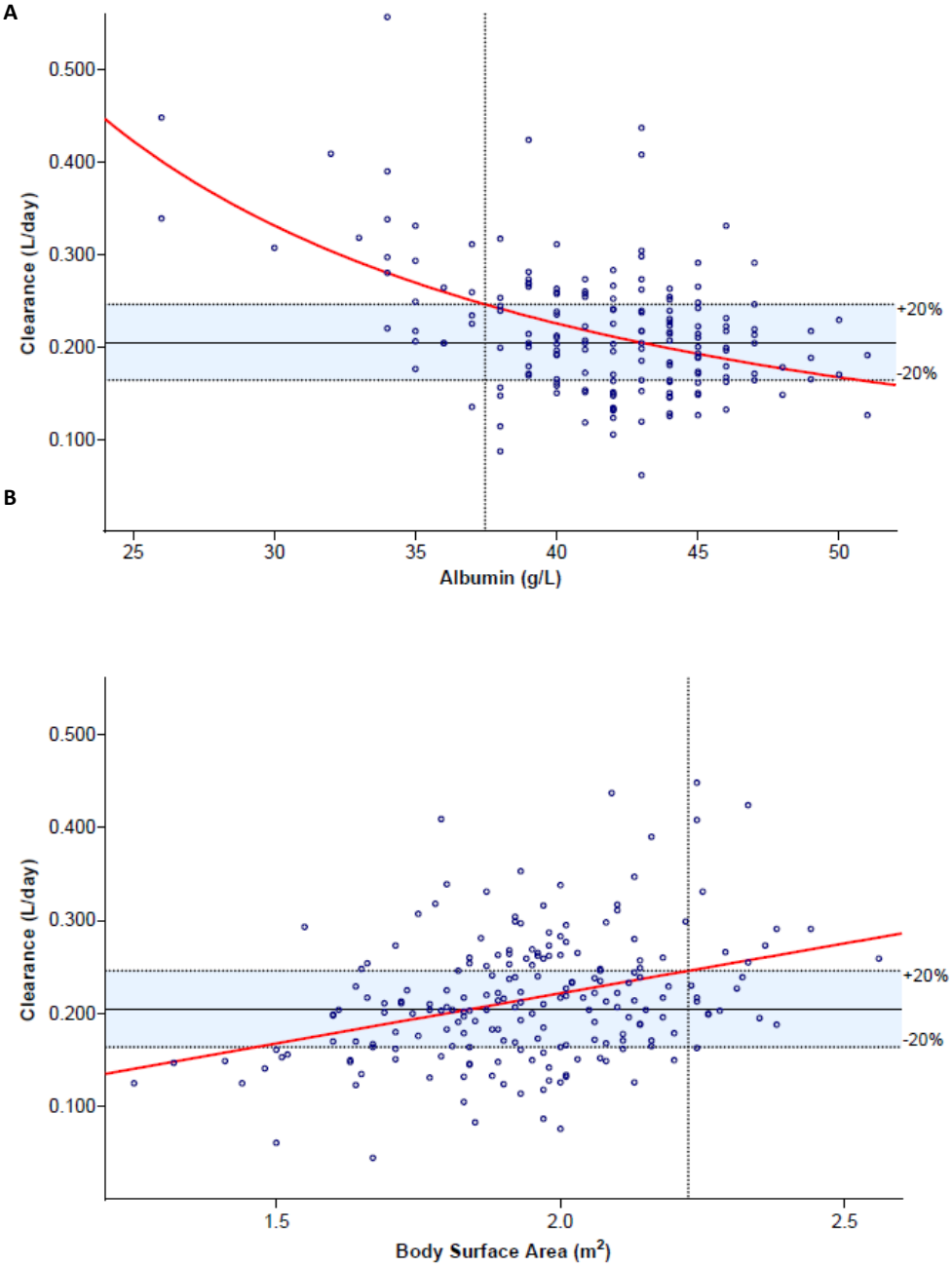

A) Estimated nivolumab clearance (L/day) as a function of A) baseline serum albumin (g/L) and B) body surface area (BSA; m^2). Single measurements are represented by open circles. The red line predicts clearance according to the final PPK model (M_f). The horizontal dotted lines mark the 20% increase of clearance, taking the mean clearance as reference (solid line). The vertical dotted line mark the threshold where nivolumab clearance is expected to be increased by >20%.

Figure 3. Clearance-response analysis

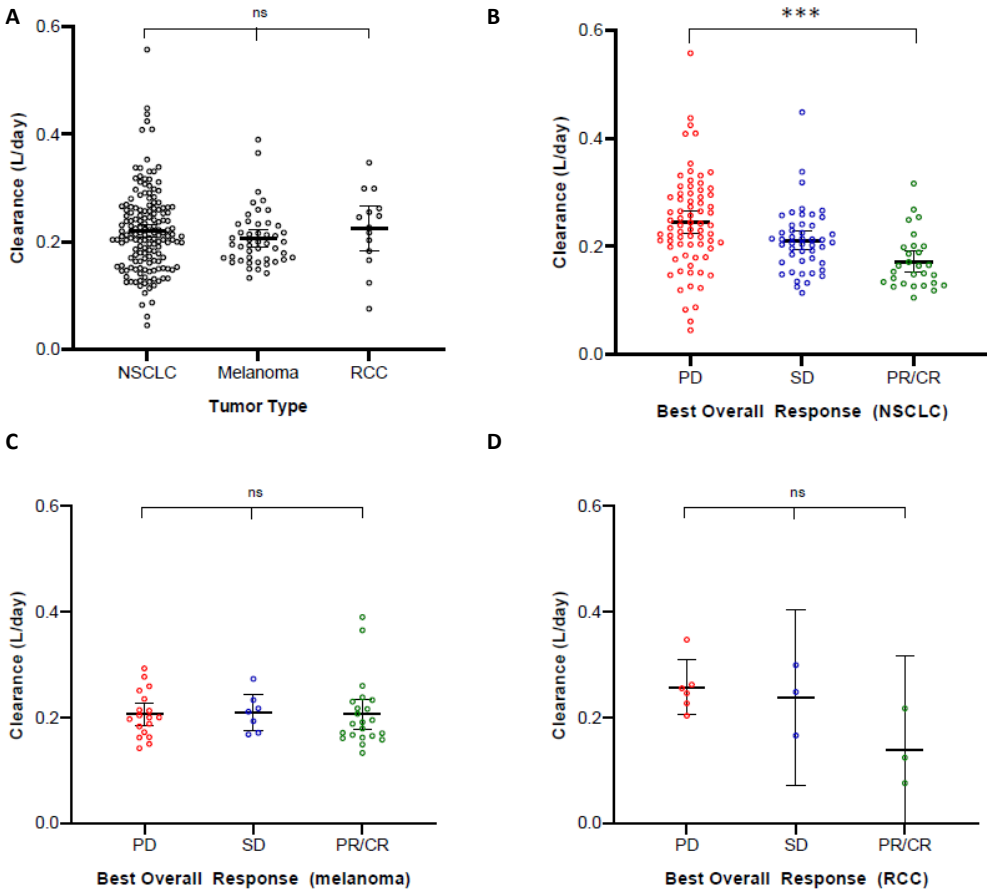

A) Nivolumab clearance (L/day) of A) all patients receiving nivolumab monotherapy grouped by best overall response (BOR), and stratified by B) NSCLC, C) melanoma, and D) RCC. Single measurements are represented by open circles. Bars indicate the 95% confidence interval of the mean. Abbreviations: progressive disease (PD), stable disease (SD) and partial response/ complete response (PR/CR). P-values indicated by ***<0.001 (post-hoc independent samples t-test).

was found in patients with NSCLC (p<0.001), as a significantly higher clearance of 41.8% was observed in patients with PD (mean: 0.244; 95%CI: 0.223 – 0.265 L/day) compared to patients with PR/CR (0.172; 0.152 – 0.192). Patients with SD were identified as an intermediate group (0.211; 0.193 – 0.228). A non-significant trend similarly to NSCLC was observed in RCC (p=0.054). Of note, no clearance-response relationship was observed in melanoma (p=0.987). A clearance-irAE relationship was not found for NSCLC, melanoma, or RCC (respectively p=0.28, p=0.84 and p=0.92; **Suppl. Figure 2B-D**), nor for all three tumor types pooled together (p=0.31; **Suppl. Figure 2A**).

There was no significant difference in drug clearance between tumor types (p=0.47; **Figure 3A**), corresponding with above-mentioned PPK modeling where tumor type as a categorical covariate did not reach the significance threshold. Notably, when patients with NSCLC were grouped by clearance, the lowest quartile of clearance was significantly associated with better PFS (HR 0.32; 95%CI: 0.18 – 0.57, p<0.001) and OS (HR: 0.25; 95%CI: 0.12 – 0.51, p<0.001) compared to patients with the highest quartile of clearance (**Figure 4A-B**). Additionally, the patient characteristics grouped by quartile of clearance are shown in **Supplementary Table 3**.

Figure 4. Kaplan-Meier curves

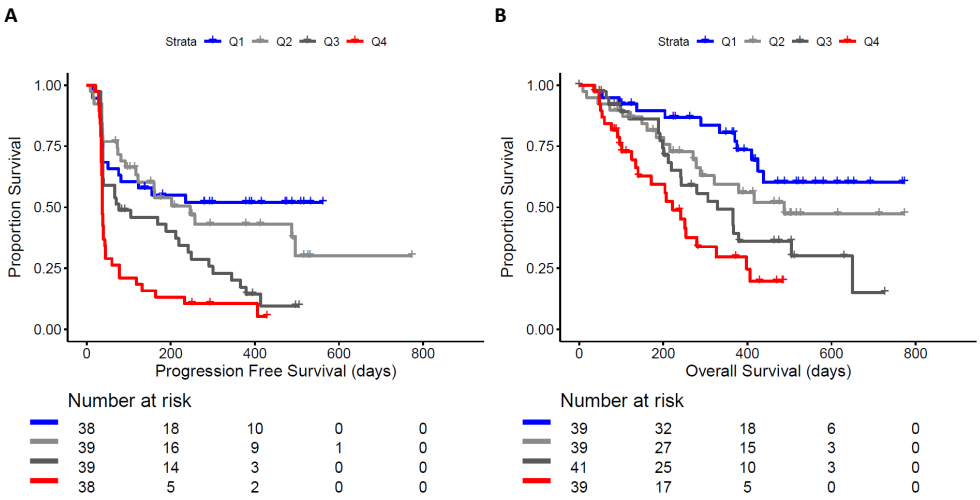

A) progression-free survival (PFS) and B) overall survival (OS) of NSCLC patients receiving nivolumab monotherapy stratified by clearance into 4 quartiles of clearance displayed by Kaplan-Meier methodology: Q1 [first quartile (blue); lowest clearance] - Q4 [fourth quartile (red); highest clearance].

DISCUSSION

In the current study, we showed that gender, baseline BSA, and serum albumin had a significant effect on the systemic clearance of nivolumab in the two compartment PPK model. These three covariates partially explained the high inter-individual variance (~37%) of drug clearance. Secondly, we have demonstrated the relationship between nivolumab pharmacokinetics and radiological response to therapy. By stratifying tumor types, the negative clearance-response relationship was highly significant in NSCLC, and

a non-significant trend was seen in RCC. The clearance-response relationship could not be confirmed in melanoma.

Our developed PPK model was comparable to previously described models for different MoAbs and nivolumab. In a model-based meta-analysis for four different MoAbs a robust fit was obtained using a two-compartment model with estimates for systemic clearance and volume of distribution of 0.200 L/day and 3.6 L, respectively, and with a 31% inter-subject variability of clearance[20]. This was similar to recently published parameter estimates of a nivolumab-based two-compartment model described by Bajaj and colleagues (clearance 0.226 L/day; compartmental volume 3.6; 35% inter-subject variability of clearance)[9]. Although the time-varying pharmacokinetics as described by Liu *et al.*[21] could not be confirmed in our analysis, our time-stationary PPK model worked with sufficient accuracy. Important to note is that we observed that trough levels reached steady state concentrations and remained stable over time in individual patients (as illustrated by **Figure 1B**).

Estimated systemic drug clearance according to the PPK model, which is inversely proportional to exposure, was utilized in this study to correlate clearance with response, survival, and occurrence of irAEs. It is important to realize that correlating systemic clearance to treatment outcome using a PPK model may potentially be influenced by those incorporated baseline covariates that are related to the efficacy of immunotherapy. To avoid such confounding, we utilized the initial model to demonstrate the relationship of systemic clearance with clinical outcome, which was further grouped by tumor type. Two patients were excluded from these analyses: a patient with mesothelioma and a patient who was treated with concomitant ipilimumab from the second cycle of nivolumab, at which point he was censored from the analyses.

The differential clearance-response relationship of nivolumab in NSCLC compared to melanoma remains to be elucidated. This may be explained by different tumor intrinsic as well as extrinsic factors, such as tumor immunogenicity and patient immunity (e.g. microbiota, environmental factors) respectively. In addition, positive D-R relationships were found for NSCLC at doses from 0.1 to 3 mg/kg Q2W[10], whereas for melanoma this was only observed at doses from 0.1 to 1 mg/kg Q2W[10]. In this respect it is noteworthy that the ORR of nivolumab in metastatic melanoma is superior compared to metastatic NSCLC[1-3]. In our study, patients with melanoma demonstrated better performance than patients with NSCLC before initiation of nivolumab monotherapy (WHO performance score of 0: 76% and 23%, respectively). Taken together, we cannot exclude that nivolumab may be effective at lower doses for patients with melanoma than for NSCLC, and that patients with NSCLC may be more sensitive for changes in exposure than patients with melanoma. Consequently, nivolumab dosing based on weighted parameters may be relevant to optimize efficacy, particularly for NSCLC patients.

Whether the inverse clearance-response relation for nivolumab in NSCLC indicate a true causal effect on clinical outcome remains to be clarified. The issue was discussed

by Badawi in a comment on our previous work showing a positive E-R relationship of nivolumab for NSCLC[13,26]. Of note, an absent E-R relationship but a strong negative clearance-OS association has been described for pembrolizumab, another PD-1 blocking monoclonal antibody, in solid tumors[27]. The efficacy of pembrolizumab seemed to be independent of absolute doses from 2 to 10 mg/kg Q2W or flat dose 200 mg Q3W. Turner and colleagues argued that this clearance-OS relationship was confounded by the cachectic state of patients, which caused more rapid protein (and thus antibody) turnover and worse survival.[27] Given the circular reasoning in their study design, however, this hypothesis may not have been supported by appropriate evidence[28]. Although we did not find a covariate effect of prior weight loss or the performance score on the PPK model, serum albumin was inversely correlated with nivolumab clearance. Albumin may be considered as a surrogate marker for protein clearance, coinciding with clearance of endogenous immunoglobulins and nivolumab. This may provide supporting evidence to the hypothesis that the exposure-response (or inverse clearance-response) relationship is affected by the metabolic state of patients, although we cannot rule out the possibility of a true causal relationship.

The elimination and recycling mechanisms of nivolumab is expected to exhibit similarities to those of endogenous immunoglobulins with a central role for the neonatal Fc receptor (FcRn)[29]. The FcRn is being widely expressed in human tissue (www.proteinatlas.org), particularly in myeloid cells, and reported to play a key role in the metabolism of albumin in blood[30]. Interestingly, myeloid cells have emerged as major regulators of cancer immune response by presenting tumor antigens to T cells and controlling the activity of cytotoxic cells, where myeloid-derived suppressor cells (MDSCs) suppress T cell responses and are implicated in tumor metastasis[31,32]. In fact, MDSCs were negatively associated with response to treatment and survival in NSCLC[33,34]. Monocytic myeloid cells in peripheral blood prior to anti-PD-1 nivolumab and pembrolizumab are associated with inferior PFS and OS[35]. We expect that by further exploring the interaction between the peripheral immune system, e.g. FcRn in the myeloid lineage, and nivolumab pharmacokinetics, understanding of immune checkpoint inhibitor treatment could be significantly enhanced.

CONCLUSIONS

In oncology, pharmacokinetic modeling is widely used to optimize drug dosing. For immune checkpoint inhibitors, approved flat dosing regimens for nivolumab have been solely based on simulations from dose-finding clinical trials. In this prospective real-life patient cohort study, we observed an effect of gender, body surface area, and baseline serum albumin on systemic drug clearance, thereby providing understanding of the high inter-individual variance of clearance. We demonstrate a strong inverse correlation of drug clearance and response in NSCLC, and a similar trend in RCC, but a clearance-

response relationship was not observed in melanoma. Considering the recent approval of nivolumab fixed dosing regimens --which was solely based on simulating PK data from clinical studies-- this real-world study suggests that dosing regimens based on patient parameters may be considered to improve efficacy, particularly in NSCLC, and should be prospectively studied.

REFERENCES

1. Robert C, Long GV, Brady B, et al. Nivolumab in previously untreated melanoma without BRAF mutation. *N Engl J Med.* 2015;372(4):320-330.
2. Borghaei H, Paz-Ares L, Horn L, et al. Nivolumab versus Docetaxel in Advanced Nonsquamous Non-Small-Cell Lung Cancer. *N Engl J Med.* 2015;373(17):1627-1639.
3. Brahmer J, Reckamp KL, Baas P, et al. Nivolumab versus Docetaxel in Advanced Squamous-Cell Non-Small-Cell Lung Cancer. *N Engl J Med.* 2015;373(2):123-135.
4. Jadhav SB, Khaowroongrueng V, Fueth M, Otteneder MB, Richter W, Derendorf H. Tissue Distribution of a Therapeutic Monoclonal Antibody Determined by Large Pore Microdialysis. *J Pharm Sci.* 2017;106(9):2853-2859.
5. EMA. *Assessment report Opdivo, Yervoy.* 15 November 2018.
6. Topalian SL, Hodi FS, Brahmer JR, et al. Safety, activity, and immune correlates of anti-PD-1 antibody in cancer. *N Engl J Med.* 2012;366(26):2443-2454.
7. Long GV, Tykodi SS, Schneider JG, et al. Assessment of nivolumab exposure and clinical safety of 480 mg every 4 weeks flat-dosing schedule in patients with cancer. *Ann Oncol.* 2018;29(11):2208-2213.
8. Zhao X, Suryawanshi S, Hruska M, et al. Assessment of nivolumab benefit-risk profile of a 240-mg flat dose relative to a 3-mg/kg dosing regimen in patients with advanced tumors. *Ann Oncol.* 2017;28(8):2002-2008.
9. Bajaj G, Wang X, Agrawal S, Gupta M, Roy A, Feng Y. Model-Based Population Pharmacokinetic Analysis of Nivolumab in Patients With Solid Tumors. *CPT Pharmacometrics Syst Pharmacol.* 2017;6(1):58-66.
10. Agrawal S, Feng Y, Roy A, Kollia G, Lestini B. Nivolumab dose selection: challenges, opportunities, and lessons learned for cancer immunotherapy. *J Immunother Cancer.* 2016;4:72.
11. Weber JS, D'Angelo SP, Minor D, et al. Nivolumab versus chemotherapy in patients with advanced melanoma who progressed after anti-CTLA-4 treatment (CheckMate 037): a randomised, controlled, open-label, phase 3 trial. *Lancet Oncol.* 2015;16(4):375-384.
12. Wang X, Feng Y, Bajaj G, et al. Quantitative Characterization of the Exposure-Response Relationship for Cancer Immunotherapy: A Case Study of Nivolumab in Patients With Advanced Melanoma. *CPT Pharmacometrics Syst Pharmacol.* 2017;6(1):40-48.
13. Basak EA, Koolen SLW, Hurkmans DP, et al. Correlation between nivolumab exposure and treatment outcomes in non-small-cell lung cancer. *Eur J Cancer.* 2019;109:12-20.
14. Basak EA, Wijkhuijs AJM, Mathijssen RHJ, Koolen SLW, Schreurs MWJ. Development of an Enzyme-Linked Immune Sorbent Assay to Measure Nivolumab and Pembrolizumab Serum Concentrations. *Ther Drug Monit.* 2018;40(5):596-601.
15. Oken MM, Creech RH, Tormey DC, et al. Toxicity and response criteria of the Eastern Cooperative Oncology Group. *Am J Clin Oncol.* 1982;5(6):649-655.
16. Martin L, Senesse P, Gioulbasanis I, et al. Diagnostic criteria for the classification of cancer-associated weight loss. *J Clin Oncol.* 2015;33(1):90-99.
17. Mosteller RD. Simplified calculation of body-surface area. *N Engl J Med.* 1987;317(17):1098.

18. Stevens LA, Claybon MA, Schmid CH, et al. Evaluation of the Chronic Kidney Disease Epidemiology Collaboration equation for estimating the glomerular filtration rate in multiple ethnicities. *Kidney Int.* 2011;79(5):555-562.
19. Eisenhauer EA, Therasse P, Bogaerts J, et al. New response evaluation criteria in solid tumours: revised RECIST guideline (version 1.1). *Eur J Cancer.* 2009;45(2):228-247.
20. Davda JP, Dodds MG, Gibbs MA, Wisdom W, Gibbs J. A model-based meta-analysis of monoclonal antibody pharmacokinetics to guide optimal first-in-human study design. *MAbs.* 2014;6(4):1094-1102.
21. Liu C, Yu J, Li H, et al. Association of time-varying clearance of nivolumab with disease dynamics and its implications on exposure response analysis. *Clin Pharmacol Ther.* 2017;101(5):657-666.
22. Savic RM, Karlsson MO. Importance of shrinkage in empirical bayes estimates for diagnostics: problems and solutions. *AAPS J.* 2009;11(3):558-569.
23. Mould DR, Upton RN. Basic concepts in population modeling, simulation, and model-based drug development. *CPT Pharmacometrics Syst Pharmacol.* 2012;1:e6.
24. Mould DR, Upton RN. Basic concepts in population modeling, simulation, and model-based drug development-part 2: introduction to pharmacokinetic modeling methods. *CPT Pharmacometrics Syst Pharmacol.* 2013;2:e38.
25. Upton RN, Mould DR. Basic concepts in population modeling, simulation, and model-based drug development: part 3-introduction to pharmacodynamic modeling methods. *CPT Pharmacometrics Syst Pharmacol.* 2014;3:e88.
26. Badawi M, Coss CC, Phelps MA. Letter to the Editor: Exposure-response or clearance-response relationship in immune checkpoint therapy?-A comment on 'correlation between nivolumab exposure and treatment outcomes in non-small-cell lung cancer' by Basak et al. *Eur J Cancer.* 2019;114:25-26.
27. Turner DC, Kondic AG, Anderson KM, et al. Pembrolizumab Exposure-Response Assessments Challenged by Association of Cancer Cachexia and Catabolic Clearance. *Clin Cancer Res.* 2018;24(23):5841-5849.
28. Bins S, Koolen SLW, Mathijssen RHJ. Pembrolizumab Exposure-Response Assessments Challenged by Association of Cancer Cachexia and Catabolic Clearance-Letter. *Clin Cancer Res.* 2019;25(10):3192.
29. Pyzik M, Rath T, Lencer WI, Baker K, Blumberg RS. FcRn: The Architect Behind the Immune and Nonimmune Functions of IgG and Albumin. *J Immunol.* 2015;194(10):4595-4603.
30. Zhu X, Meng G, Dickinson BL, et al. MHC class I-related neonatal Fc receptor for IgG is functionally expressed in monocytes, intestinal macrophages, and dendritic cells. *J Immunol.* 2001;166(5):3266-3276.
31. Gabrilovich DI, Ostrand-Rosenberg S, Bronte V. Coordinated regulation of myeloid cells by tumours. *Nat Rev Immunol.* 2012;12(4):253-268.
32. Parker KH, Beury DW, Ostrand-Rosenberg S. Myeloid-Derived Suppressor Cells: Critical Cells Driving Immune Suppression in the Tumor Microenvironment. *Adv Cancer Res.* 2015;128:95-139.

33. Huang A, Zhang B, Wang B, Zhang F, Fan KX, Guo YJ. Increased CD14(+)HLA-DR (-/low) myeloid-derived suppressor cells correlate with extrathoracic metastasis and poor response to chemotherapy in non-small cell lung cancer patients. *Cancer Immunol Immunother.* 2013;62(9):1439-1451.
34. de Goeje PL, Bezemer K, Heuvers ME, et al. Immunoglobulin-like transcript 3 is expressed by myeloid-derived suppressor cells and correlates with survival in patients with non-small cell lung cancer. *Oncoimmunology.* 2015;4(7):e1014242.
35. Soyano AE, Dholaria B, Marin-Acevedo JA, et al. Peripheral blood biomarkers correlate with outcomes in advanced non-small cell lung Cancer patients treated with anti-PD-1 antibodies. *J Immunother Cancer.* 2018;6(1):129.

SUPPLEMENTARY MATERIALS

Supplementary Figure 1. PPK model

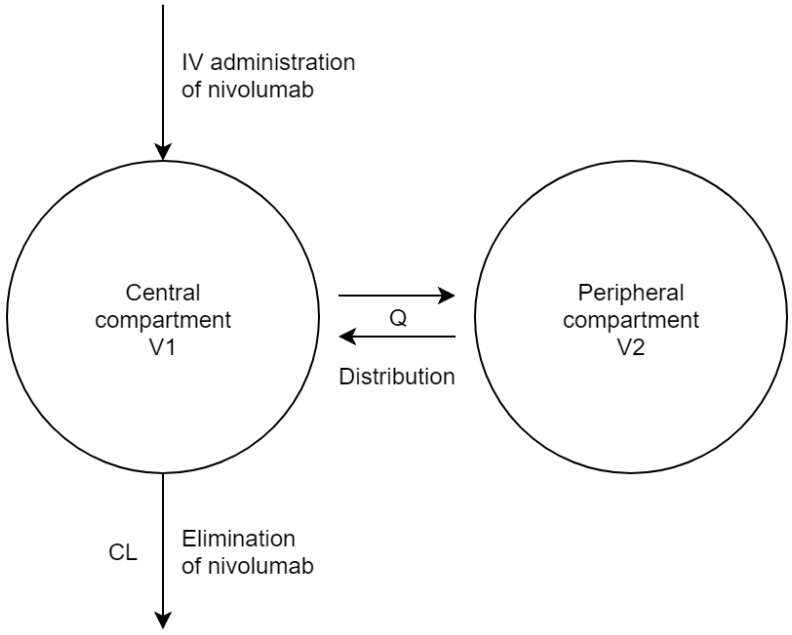

Schematic overview of the two-compartmental PPK model of nivolumab.

Supplementary Figure 2. Clearance-toxicity analysis

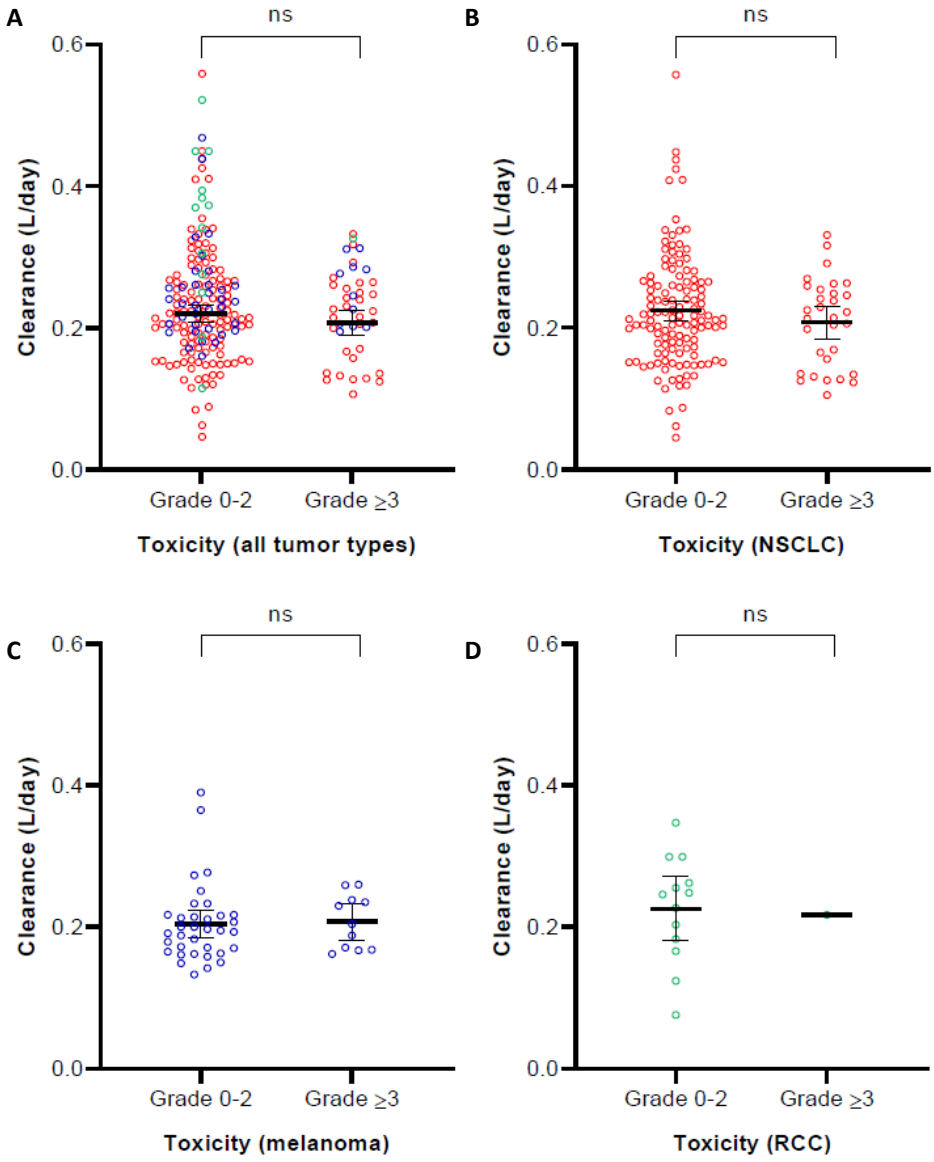

A) Drug clearance (L/day), according to initial model Mi, grouped by toxicity (irAEs; grade 0-2 vs. grade >3) of A) all patients, B) NSCLC (in red), C) melanoma (in blue) and D) renal cell cancer (RCC; in green) receiving nivolumab monotherapy. Single measurements are represented by open circles. Bars indicate the 95% confidence interval of the mean.

Supplementary Figure 3. Goodness of fit

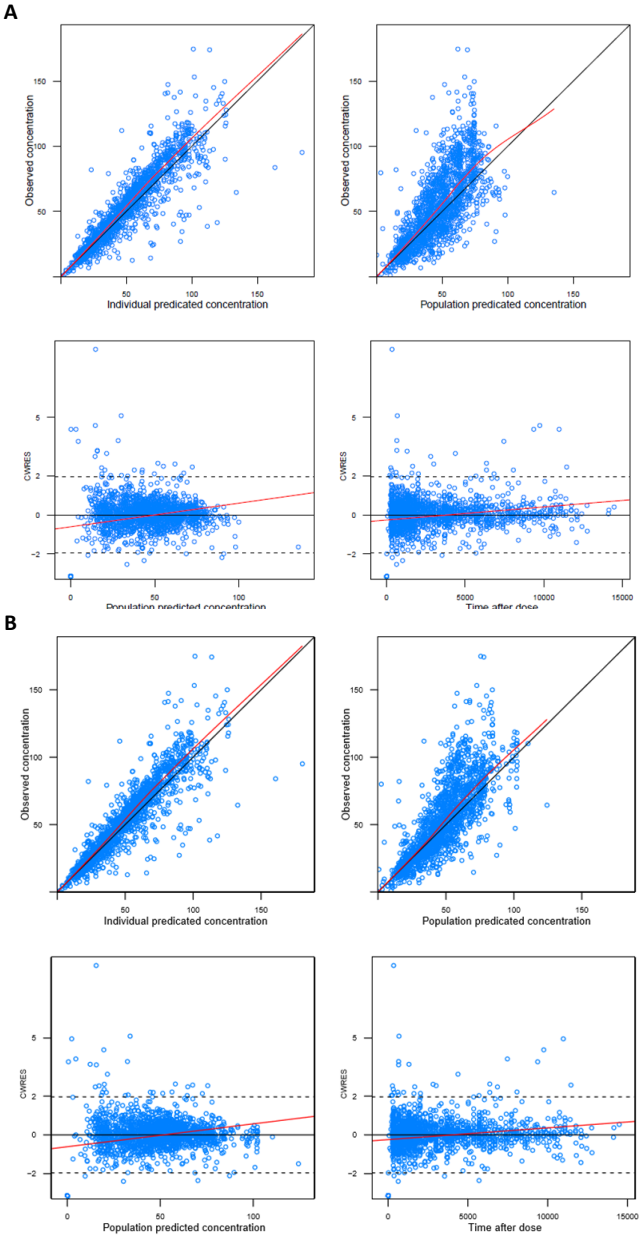

Standard goodness of fit of the A) initial (Mi) and B) final model (Mf). Single observations are represented by open circles. Red and black lines mark locally estimated scatterplot smoothing lines, lines of identity (diagonal) or ordinate value of 0 (horizontal), respectively. The figures include observations versus individual predictions (a), observations vs population predictions (b), conditional weighted residuals (CWRES) versus population predictions (c) and CWRES versus time after dose (d).

Supplementary Table 1. Parameter estimates

Categorical Covariates	Estimates	dOFD
NSCLC vs. other tumor types	-0.03	-0.251
Melanoma vs. other tumor types	0.05	-0.449
Female vs. Male	-0.26	-29.685
WHO=0 vs. Rest (including unknowns)	0.08	-1.682
Weight Loss Present vs. Rest (including unknowns)	0.09	-1.406
Continuous Covariates	**Estimates**	**dOFD**
Age (yr)	0.12	-0.604
Body Weight (kg)	0.60	-18.716
Body Surface Area (m^2)	1.22	-25.519
Tumor Burden 3D (cm^3)	0.09	-2.252
Creatinine (µmol/L)	-0.01	-0.003
CKD (mL/min)	0.01	-0.307
Total Protein (g/L)	0.25	-0.300
Albumine (g/L)	-1.31	-18.989
LD (U/L)	0.0004	-
Leucocytes (10^9 cells/L)	0.07	-0.648

Categorical and continuous covariates shown as estimates and difference in objective function value according to initial model Mi (dOFD). Abbreviations: CKD-EPI renal clearance (CKD), lactate dehydrogenase (LD).

Supplementary Table 2. Clinical outcome and toxicity

	Total n(%)	NSCLC n(%)	Mel n(%)	RCC n(%)
BOR (RECIST v1.1)				
PR/CR	53 (24.2)	28 (17.7)	22 (46.8)	3 (21.4)
SD	57 (26.0)	47 (29.7)	7 (14.9)	3 (21.4)
PD	97 (44.3)	73 (46.2)	18 (38.3)	6 (42.9)
Non-evaluable	12 (5.5)	10 (6.3)	-	2 (14.3)
IrAEs (CTCAE 4.03)				
Grade 0-2	175 (79.9)	127 (80.4)	35 (74.5)	13 (92.9)
Grade ≥3	43 (19.6)	31 (19.6)	11 (23.4)	1 (7.1)
Unknown	1 (0.5)	-	1 (2.1)	-

Distributions of best overall response (BOR) by RECIST v1.1 and irAEs by CTCAE v4.03 for all patients receiving nivolumab monotherapy and grouped by tumor type. Abbreviations: melanoma (Mel), renal cell carcinoma (RCC).

Supplementary Table 3. Patient characteristics by quartiles of drug clearance

	Q1	Q2	Q3	Q4
Tumor type *n (% within quartile)*				
NSCLC	*n=39*	*n=40*	*n=40*	*n=39*
Adenocarcinoma	23 (59)	30 (75)	23 (57.5)	20 (51)
Squamous cell carcinoma	11 (28)	7 (17.5)	10 (25)	14 (36)
Unknown	5 (13)	3 (7.5)	7 (17.5)	5 (13)
WHO performance score *n (% within quartile)*				
0	5 (13)	8 (20)	7 (17.5)	5 (13)
1	25 (64)	16 (40)	19 (47.5)	23 (59)
2	-	1 (2.5)	-	1 (2.5)
Unknown	9 (23)	15 (37.5)	14 (35)	10 (25.5)
Weight loss prior to start therapy *n (% within quartile)*				
Yes	12 (31)	12 (30)	5 (12.5)	7 (18)
No	17 (43.5)	19 (47.5)	21 (52.5)	23 (59)
Unknown	10 (25.5)	9 (22.5)	14 (35)	9 (23)
Gender *n (% within quartile)*				
Male	11 (28)	23 (57.5)	29 (72.5)	35 (90)
Female	28 (72)	17 (42.5)	11 (27.5)	4 (10)
Body Surface Area (m^2) *median (IQR)*	1.81 (1.55-1.97)	1.85 (1.76-2.06)	1.95 (1.84-2.10)	2.00 (1.91-2.13)
Albumin (g/L) *median (IQR)*	42 (41-44)	43 (40-45)	42 (40-45)	39 (34-43)

Patient characteristics including important patient parameters (gender, BSA and serum albumin) grouped by quartile of drug clearance (Q1-Q4), which was utilized for the clearance-survival analysis. The percentage within the quartiles is shown, leaving out the unknown parameters. Abbreviations: Q1-4 (quartile 1-4), IQR (inter-quartile range).

Supplementary Appendix 1.

The final and initial models were internally validated using VPC **(Suppl. Figure 3)** and a bootstrap procedure. Bootstrap analysis was performed with replacement by randomly selecting patients from the dataset.

Syntax of initial PPK model M_i:

```
$PROBLEM PK
$INPUT DROP ID CYCLE TIME DV AMT RATE MDV EVID CMT DAY WEEK TAD RESPONS GRTT
$DATA FINAL_PK_MULTOMAB_NSCLC_RCC_MEL.csv IGNORE=#;concentration mg/L
$SUBROUTINES ADVAN3 TRANS4
$PK
```

```
CL = THETA(1)*EXP(ETA(1))
V1  = THETA(2)
V2 = THETA(2)
Q= THETA(3)
S1 = V1

$ERROR
TY=F
IF(F.LT.0.001) TY=0.001
IPRED = TY
Y=IPRED*(1+ERR(1))
IRES = DV-IPRED
IWRES = IRES/IPRED

$THETA
(0, 0.01) ; CL
(0, 5) ; V1
0.02 FIX; Q

$OMEGA
(0.1) ; IIV CL

$SIGMA
0.05  ;   prop paz

$EST METHOD=1 INTER MAXEVAL=2000 NOABORT SIG=3 PRINT=1 POSTHOC
$COV
```

Syntax of final PPK model M_f:

```
$PROBLEM PK
$INPUT DROP ID CYCLE TIME DV AMT RATE MDV EVID CMT DAY WEEK TAD RESPONS
     GRTT SEX RACE DISEASE AGE WHO LGT WGT BSA TWOD THREED CREAT CKD TPRO ALB
     LD LEU GRAN EOS NEUIMM NEUMAT BC MON DC TC CDF CDE CDFP CDEP WLB WLP

$DATA FINAL_PK_MULTOMAB_NSCLC_RCC_MEL.csv IGNORE=#;concentration mg/L

$SUBROUTINES ADVAN3 TRANS4
```

```
$PK
;CLSEX-DEFINITION START
IF(SEX.EQ.0) CLSEX = 1 ; Most common
IF(SEX.EQ.1) CLSEX = 1 + THETA(4)
;CLSEX-DEFINITION END

;CLBSA-DEFINITION START
IF(BSA.EQ.999) THEN
CLBSA=1
ELSE
CLBSA=(BSA/1.9)**THETA(5)
ENDIF
;CLBSA-DEFINITION END

;CLALB-DEFINITION START
IF(ALB.EQ.999) THEN
CLALB=1
ELSE
CLALB=(ALB/42)**THETA(6)
ENDIF
;CLALB-DEFINITION END

;CL-RELATION START
CLCOV=CLSEX*CLBSA*CLALB
;CL-RELATION END

TVCL=THETA(1)

CL = TVCL*CLCOV*EXP(ETA(1))
V1  = THETA(2)
V2 = THETA(2)
Q= THETA(3)
S1 = V1

$ERROR
TY=F
IF(F.LT.0.001) TY=0.001
IPRED = TY
Y=IPRED*(1+ERR(1))
IRES = DV-IPRED
```

```
IWRES = IRES/IPRED

$THETA
0.0085 ; CL
3.45 ; V1
0.02 FIX; Q
(-3,-.261) ; CLSEX
(-3,1.22) ; CLBSA
(-3,-1.31) ; CLALB

$OMEGA
(0.1) ; IIV CL

$SIGMA
0.05  ;   prop paz

$EST METHOD=1 INTER MAXEVAL=2000 NOABORT SIG=3 PRINT=1 POSTHOC
$COV
```

CHAPTER 6

6

A serum protein classifier identifying patients with advanced non-small cell lung cancer who derive clinical benefit from treatment with immune checkpoint inhibitors

Mirte Muller*, Karlijn Hummelink*, Daan P. Hurkmans, Anna-Larissa Niemeijer, Kim Monkhorst, Joanna Roder, Carlos Oliveira, Heinrich Roder, Joachim G. Aerts*, Egbert F. Smit*

*Shared first/senior authorship

Clinical Cancer Research, October 2020, 26: page 5188-5197

Introduction: Pretreatment selection of patients with non–small cell lung cancer (NSCLC) who would derive clinical benefit from treatment with immune checkpoint inhibitors (CPIs) would fulfill an unmet clinical need by reducing unnecessary toxicities from treatment and result in substantial health care savings.

Material and Methods: In a retrospective study, mass spectrometry (MS)-based proteomic analysis was performed on pretreatment sera derived from patients with advanced NSCLC treated with nivolumab as part of routine clinical care (n = 289). Machine learning combined spectral and clinical data to stratify patients into three groups with good ("sensitive"), intermediate, and poor ("resistant") outcomes following treatment in the second-line setting. The test was applied to three independent patient cohorts and its biology was investigated using protein set enrichment analyses (PSEA).

Results: A signature consisting of 274 MS features derived from a development set of 116 patients was associated with progression-free survival (PFS) and overall survival (OS) across two validation cohorts (N = 98 and N = 75). In pooled analysis, significantly better OS was demonstrated for "sensitive" relative to "not sensitive" patients treated with nivolumab; HR, 0.58 (95% confidence interval, 0.38–0–87; P = 0.009). There was no significant association with clinical factors including PD-L1 expression, available from 133 of 289 patients. The test demonstrated no significant association with PFS or OS in a historical cohort (n = 68) of second-line NSCLC patients treated with docetaxel. PSEA revealed proteomic classification to be significantly associated with complement and wound-healing cascades.

Discussion: This serum-derived protein signature successfully stratified outcomes in cohorts of patients with advanced NSCLC treated with second-line PD-1 CPIs and deserves further prospective study.

Abstract

STATEMENT OF TRANSLATIONAL RELEVANCE

Predictive biomarkers for the efficacy of PD-(L)1 inhibition in non-small cell lung cancer 54 (NSCLC) beyond PD-L1 are lacking. We retrospectively developed a pretreatment proteomic 55 signature derived from peripheral blood that was able to stratify patients for benefit of 56 Nivolumab in treatment of relapsed NSCLC. A signature consisting of 274 mass spectral 57 features derived from a development set of 116 patients was associated with progression 58 free survival (PFS) and overall survival (OS) across 2 validation cohorts (N=98 and N=75). 59 In pooled analysis, a significantly better OS was demonstrated for "sensitive" relative to "not 60 sensitive" patients, hazard ratio (HR) 0.58 (95% CI 0.38-0-87, P=0.009). There was no 61 significant association with clinical factors including PD-L1 immunohistochemistry. Further 62 prospective exploration of the predictive capabilities of this assay is underway.

INTRODUCTION

The addition of immune checkpoint inhibitors (CPIs) to the armamentarium of medical treatment of advanced non–small cell lung cancer (NSCLC) has increased survival for a minority of patients. Historically, in patients with metastatic disease, 2-year survival rates following platinum-based chemotherapy were 10%–20% (1). In recent phase III studies, either comparing CPIs alone or CPI chemotherapy to chemotherapy (2), 2-year survival rates in the CPI arms range from 32% to 67%. In addition, long-term follow-up of patients treated in early single-agent CPI studies indicates that 5-year survival of 15%–20% may be expected, even in heavily pretreated patients (3, 4).

At the same time, it is clear that not all patients benefit from treatment with CPIs. Indeed, response rates and survival times can be augmented by pretreatment selection based on tumor characteristics

such as PD-L1 expression (5), staining of CD8-positive cells (6), tumor mutational burden (TMB; ref. 7), and other genomic markers (8, 9). The predictive power of the best studied of these PD-L1 IHC is far from perfect. For example, in patients with previously treated NSCLC with PD-L1 staining of at least 50%, the objective response rate to pembrolizumab was 44% (5). Thus, alternative predictive biomarkers for response and clinical benefit are needed. We sought to develop a serum-based, pretreatment protein test to avoid the need for tissue biopsies, which are typically required to analyze tumor-related biomarkers. Here, we report on the development of such a test in advanced NSCLC treated with single-agent CPI in the second-line setting.

MATERIALS AND METHODS

Patient cohorts and sample sets

Pretreatment serum samples, collected within 1 month of immunotherapy initiation, were available from four cohorts of patients. The development set consisted of 116 samples from patients treated at the Netherlands Cancer Institute (Amsterdam, the Netherlands) between May 2015 and March 2017. Validation set 1 consisted of 98 samples from patients treated at the Vrije Universiteit Medical Center (Amsterdam, the Netherlands) or the Netherlands Cancer Institute (Amsterdam, the Netherlands) between June 2015 and July 2018. Validation set 2 comprised samples from 75 patients treated at the Erasmus University Medical Centre (Rotterdam, the Netherlands) between April 2016 and July 2017. Patients, identified according to criteria established in the phase III trials demonstrating benefit for nivolumab over docetaxel (10, 11), received nivolumab 3 mg/kg, administered as an intravenous infusion, every 2 weeks, for advanced NSCLC after platinum-containing chemotherapy as part of routine clinical care. Patients in the development cohort and validation set 2 were treated in second-line. Validation set 1 contained 58 patients treated in second-line and 40 patients treated in higher lines. The cohorts comprised all patients in the respective institutions who provided pretreatment serum samples available for analysis, were eligible for immunotherapy as routine care, and who received at least one dose of nivolumab. Response to treatment was evaluated according to RECIST v1.1 every 6 weeks for the first 12 weeks and every 3 months thereafter. In addition, a fourth cohort of pretreatment serum samples (chemotherapy cohort) was collected from patients with advanced NSCLC treated in second-line with chemotherapy while enrolled in a clinical trial (NCT00989690; ref. 12). Samples were available for 68 of the 74 patients who received docetaxel (75 mg/ m^2 every 21 days) in this study. Trial inclusion and exclusion criteria have been published elsewhere (12). All samples were obtained in the context of biobanking protocols or a clinical trial for which institutional review board approval was sought and obtained. All patients provided written informed consent according to local ethical standards and adhered to standards set out in the Declaration of Helsinki. Progression-free survival (PFS) was measured from start of treatment until progression of disease, death, or loss to follow-up. Overall survival (OS) was defined as time from start of therapy until death or loss to follow-up.

PD-L1 IHC

Tumor PD-L1 expression scoring was performed according to the instruction manual of the qualitative IHC assay developed as a complementary diagnostic tool for nivolumab (PD-L1 IHC 22C3 pharmDx, Dako). PD-L1 expression levels were determined by observing complete circumferential or partial linear expression (at any intensity) of PD-L1 on the plasma cell membrane of viable tumor cells. In parallel, the pattern of staining in CD4-stained slides, which also stain CD4þ lymphocytes and macrophages, was evaluated and

compared with PD-L1-stained slides to avoid false positive assessment due to PD-L1–expressing macrophages in between tumor cells. Assessment of expression levels was performed in sections that included at least 100 tumor cells that could be evaluated.

Spectral acquisition and processing

Samples were processed using standardized operating procedures. We used the Deep matrix-assisted laser desorption/ionization (MALDI) method of mass spectrometry on a MALDI Time-ofFlight Mass Spectrometer (SimulTof Systems) to generate reproducible mass spectra from small amounts of serum (3 mL; ref. 13). This approach reveals mass spectral (MS) peaks with a greater dynamic range than previously possible by exposing the samples to 400,000 MALDI laser "shots," rather than the several thousand used in standard applications. The spectra were processed to render them comparable between patients, and 274 MS features (peaks) were selected for further analysis for their known reproducibility and stability (listed in **Supplementary Data**). Sample processing and MS analysis followed methods presented previously (14, 15) and are outlined in the Supplementary Materials and Methods. Parameters for these procedures were established using only the 116-sample development set, and this fixed procedure was applied to all other sample sets without modification.

Test development

Test development was carried out using the Diagnostic Cortex platform (16), which has been used previously to design tests that were able to stratify patients by outcome in various settings, for example, to identify patients with advanced melanoma likely to be sensitive to CPIs (14, 15). The approach incorporates machine learning concepts and elements of deep learning (17) to facilitate test development in cases where there are more measured attributes than samples. The potential for overfitting was minimized, thus allowing the creation of tests that can generalize to unseen datasets. Tests were created averaging over many splits of the development set into training and test sets, and reliable test performance estimates can be obtained from the development set by restricting averages to the test set evaluations ("out-of-bag estimates"; ref. 18).

For successful supervised learning, suitable training class labels are required. We used a semisupervised approach (19) that does not require accurate prespecification of patients into better or worse outcome training classes and allows us to be guided by the gold standard time-to-event outcomes of OS and PFS. An approximation was made for training classes, with patients with the lowest time-to-event outcome times assigned to the "negative" class and those with the highest time-to-event outcome times assigned to the "positive" class. A classifier was constructed using these training classes and used to generate classifications for all samples in the development set using out-of-bag evaluations. These resulting classifications were then used as improved training class labels for a second iteration of classifier construction. This simultaneous iterative refinement of

the classifier and the classes used in training generally converges quickly and reveals the underlying structure of the MS data and its association with clinical outcomes (19). Full details of the application of the method in this setting are provided in the Supplementary Materials and Methods

One classifier previously developed with the Diagnostic Cortex platform was used as part of the developed test. BDX008 was created to stratify patients with advanced melanoma into groups with better and worse outcomes when treated with nivolumab (15). It has been validated in multiple independent cohorts of patients with melanoma treated with CPIs (15, 20). Also, it has demonstrated some ability to stratify OS of patients with advanced NSCLC treated with nivolumab (21). A version of BDX008, adapted for the spectral preprocessing parameters and feature definitions in this project, was created (see Supplementary Data: Supplementary Materials and Methods for details).

Preliminary statistical considerations showed a binary split of the development set into equal-sized groups would allow detection of a HR between the groups of 0.55 with 90% power, assuming fully mature clinical data and a significance level of 95%. Similar considerations for a ternary split into equal size subgroups would allow detection of an HR of 0.48 under the same specifications.

All reference data and test parameters were generated solely using the development set. Validation sets and the chemotherapy cohort were never used in the creation of any components of the test. All elements of the classification algorithms were locked prior to running the test on the validation sets and chemotherapy cohort

Protein set enrichment analysis

This analysis applies the gene set enrichment analysis (GSEA) method (22) to protein expression data. The method identifies expression differences that are consistent across prespecified groups or sets of attributes, in this case, sets of proteins that are associated with particular biological processes. Two additional independent reference sets of serum samples with matched MS data and protein expression data were used for this set enrichment analysis. One sample set was composed of 49 samples with protein expression data from a panel of 1,129 proteins; the second set had 100 samples with protein expression data from a panel of 1,305 proteins (protein expression measurements were generated by SomaLogic). Specific protein sets were created as the intersection of the list of the panel targets and results of queries for biological functions from gene ontology, using AmiGO2 tools (http:// amigo.geneontology.org/amigo) and UniProt databases (https:// www. uniprot.org/). The protein set enrichment analyses (PSEA) method associated test classification with these biological functions via a rankbased correlation of the measured protein expressions with the test classifications of the reference samples (23). The mass spectral features associated with biological processes (in particular immune response type 2) were determined using Spearman correlation of the measured protein expressions with the mass spectral features (23) using the 49- sample reference set only. While the

implementation closely follows the GSEA approach, we employed an extension of the standard method that increases the statistical power to detect associations between phenotype (test classification subgroup) and biological process (24). The PSEA was carried out using a C# implementation and MATLAB (MathWorks). PSEA P values were defined as described by Subramanian and colleagues (20). FDRs for the PSEA calculations were assessed using the method of Benjamini and Hochberg (25).

Other statistical analysis

All analyses, except the PSEA, were carried out using SAS9.3 (SAS Institute) or PRISM (GraphPad). Survival/PFS plots and medians were generated using the Kaplan–Meier method. Association between test classification and categorical or continuous variables was assessed using Fisher exact test and Mann–Whitney test, respectively. All P values are two-sided.

RESULTS

Patient characteristics and overall outcomes for all four cohorts are summarized in **Table 1** and were typical of patients with advanced NSCLC treated predominantly in the second-line setting. Clinicopathologic characteristics were generally similar between the four cohorts, although the proportion of patients with performance status 2 or higher was larger in the development cohort and validation set 1, and the proportion of patients with performance status 0 was higher in the chemotherapy cohort. PD-L1 status was not available for the chemotherapy cohort and was missing for at least one-third of patients in the other three cohorts.

Table 1. Patient characteristics and outcomes for all cohorts: development, validation set 1, validation set 2, and chemotherapy cohort

		Development ($n = 116$)	Validation 1 ($n = 98$)	Validation 2 ($n = 75$)	Chemotherapy ($n = 68$)
Age, median (range)		65 (43–83)	64 (29–77)	65 (35–78)	64 (39–77)
Gender, *n* (%)	Male	66 (57)	51 (52)	48 (64)	52 (76)
	Female	50 (43)	47 (48)	27 (36)	16 (24)
PS, *n* (%)	0	36 (32)	20 (20)	18 (32)	35 (51)
	1	60 (54)	65 (66)	37 (66)	29 (43)
	2+	15 (14)	13 (13)	1 (2)	4 (6)
Smoking	Ever	104 (91)	88 (92)	61 (92)	64 (94)
status, *n* (%)	Never	10 (9)	8 (8)	5 (8)	4 (6)
Histology,	Adeno	77 (66)	42 (74)	49 (65)	47 (75)
n (%)	Squamous	26 (22)	10 (18)	17 (23)	12 (19)
	Other	13 (11)	5 (9)	9 (12)	4 (6)
PD-L1, *n* (%)	≥1%	33 (28)	12 (14)	16(21)	0 (0)
	<1%	43 (37)	30 (29)	9 (12)	0 (0)
	NA	40 (34)	56 (57)	50 (67)	68 (100)
Response, *n* (%)	CR	1 (1)	1 (0)	0 (0)	0 (0)
	PR	16 (14)	28 (28)	15 (20)	7 (10)
	SD	19 (16)	26 (33)	25 (33)	23 (34)
	PD	65 (56)	37 (33)	31 (41)	22 (32)
	NA/NE	15 (13)	6 (7)	4 (5)	16 (24)
PFS (months)	Median	2.6	4.1	4.3	3.5
OS (months)	Median	8.5	8.4	12.0	8.0

Abbreviations: %, % of patients with available data; adeno, adenocarcinoma; NA, not available; NE, not evaluable; PD, progressive disease; PD-L1, PD-L1 expression; PS, performance status; SD, stable disease.

Development of the test

A ternary test was developed that was able to stratify the development set of 116 samples into three groups with different outcomes after anti-PD-1 treatment, that is, the resistant group (with poor outcomes), the intermediate group (with intermediate outcomes), and the sensitive group (with good outcomes). The ternary test result was generated by combining the results of three binary classification algorithms (classifiers). Each of the three classifiers stratified patients into two groups: "positive" with better outcomes and "negative" with worse outcomes. The binary results were integrated as shown in **Fig. 1** to yield the final test result. First, classifications were generated for all samples by classifier A, the version of the preexisting BDX008 test adapted to the spectral processing used in this project. To identify a group of patients least likely to have good outcomes, the patients classified as negative by classifier A were subsequently classified by classifier C. This classifier was developed using the subset of MS features found to be associated with immune response type 2 by PSEA and a subset of the development cohort enriched for inferior outcomes, by excluding patients designated as BDX008þ and having performance status 0 (the MS features in this subset are listed in the Supplementary Materials and Methods). Samples designated as negative by both classifier A and classifier C were classified as "resistant." To identify a group of patients likely to have the best outcomes, the patients classified as positive by classifier A were further classified by classifier B. This classifier was developed using all 274 mass spectral features on a subset of the development set enriched for better outcomes, by excluding patients who were classified both as BDX008 and negative by classifier C. Samples designated positive by both classifier A and classifier B were classified as "sensitive." All samples not classified as "sensitive" or "resistant" were classified as "intermediate." More details of the test development process and parameters are provided in the Supplementary Data. Reproducibility was assessed by running the test on the 98 serum samples of validation set 1 twice, 13 months apart. Concordance between classifications was 85%. For identification of patients with resistant outcomes (resistant vs. not resistant, i.e., sensitive and intermediate), concordance was 91% and for identification of patients with sensitive outcomes (sensitive vs. not sensitive, i.e., resistant and intermediate), concordance was 93%.

The test was able to stratify patients into three groups (sensitive, intermediate, and resistant) with different OS and PFS. Of the 116 samples in the development set, 41 (35%) were classified as resistant, 43 (37%) as intermediate, and 32 (28%) as sensitive. Kaplan–Meier plots of OS and PFS by classification groups are shown in **Fig. 2A and B**. PFS for the resistant subgroup was significantly shorter than for the other groups [resistant vs. sensitive: HR, 0.33 (95% confidence interval (CI), 0.19–0.58); $P < 0.001$ and resistant vs. intermediate: HR, 0.59 (95% CI, 0.37–0.96); $P = 0.035$]. Median PFS was 1.4 (95% CI, 1.3–2.3) months for the resistant group, 4.3 (95% CI, 1.4–5.7) months for the intermediate group, and 9.1 (95% CI, 2.5–undefined) months for the sensitive group. OS for the resistant subgroup was significantly shorter than for the sensitive subgroup and numerically shorter than for the intermediate group (resistant

vs. sensitive: HR, 0.34 (95% CI, 0.19–0.64); P < 0.001 and resistant vs. intermediate: HR, 0.63 (95% CI, 0.38–1.06); P = 0.083]. Median OS was 4.3 (95% CI, 2.0–7.9) months for the resistant subgroup, 10.4 (95% CI, 5.9–11.4) months for the intermediate group, and 17.3 (95% CI, 8.5–undefined) months for the sensitive group. Test classification was also associated with response (P < 0.001, see Supplementary Data: Supplementary Results; Supplementary Table S12). Eighty-five percent of patients classified as resistant experienced progressive disease as best response and only 10% had a response (all partial). In the sensitive group, only 28% of patients had progressive disease as best response and 28% achieved a response [one complete response (CR) and eight partial responses (PR) as best response of 32 patients].

Figure 1.

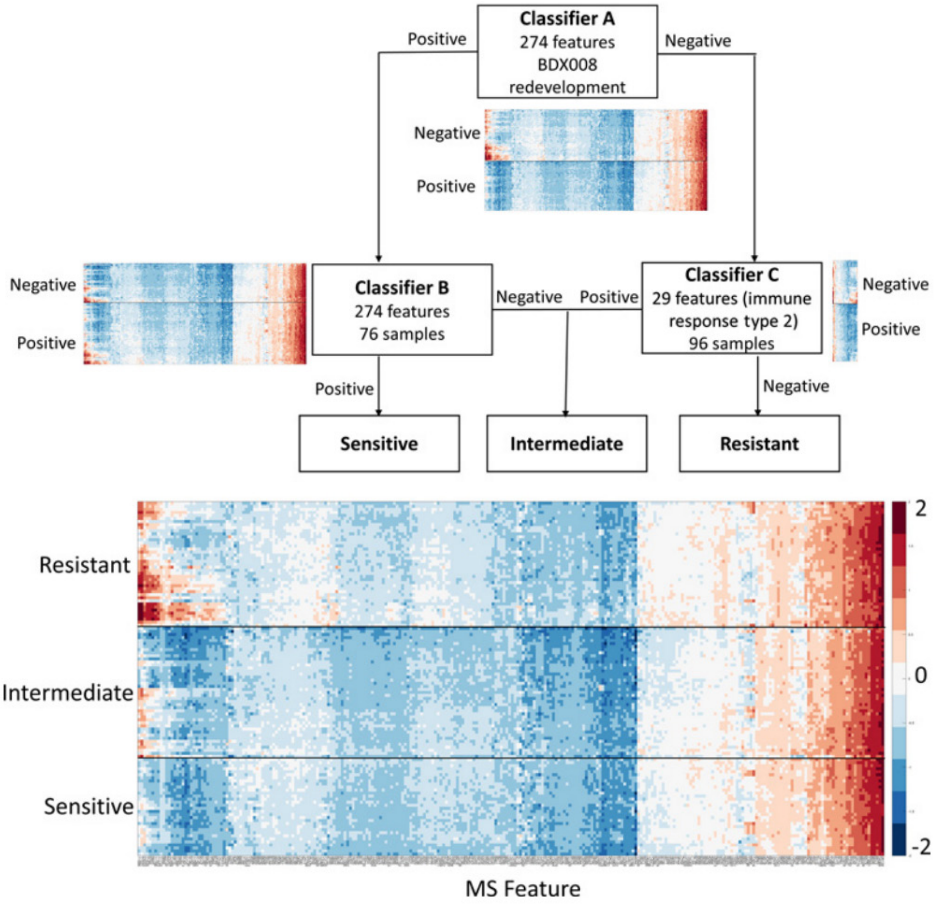

Heatmaps within the schema show log10 values of features used in each classifier (x-axis) for the development cohort of 116 samples, grouped by individual classifier results, negative or positive. The heatmap below the schema shows the log10 values of all 274 features used within the test for all samples in the development cohort, grouped by test classification (resistant, intermediate, or sensitive). Larger versions of the heatmaps are in the Supplementary Data.

Figure 2.

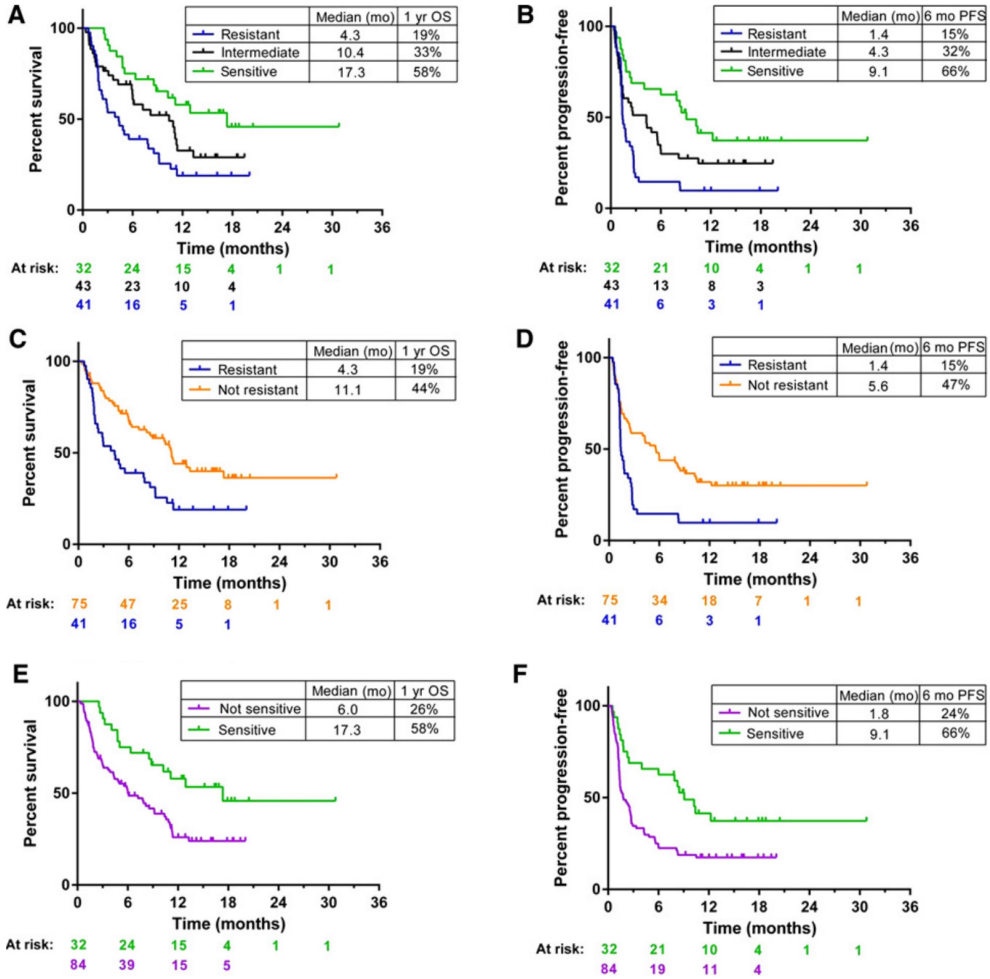

Outcomes by test classification for the development cohort.

For differentiating patients with the worst outcome from the remainder of the cohort, we compared the resistant subgroup with the "not resistant" group, that is, the combination of intermediate and sensitive subgroups, see **Fig. 2C and D**. The resistant subgroup had significantly inferior OS and PFS than the other subgroups [HR, 0.48 (95% CI, 0.30–0.77); P = 0.002 for OS and HR, 0.46 (95% CI, 0.30– 0.71); P < 0.001 for PFS]. These differences remained significant for PFS (P = 0.015) and trended to significance for OS (P = 0.062) in multivariate analysis when adjusted for other baseline characteristics, including performance status and PD-L1 expression.

The patients with the best outcomes (sensitive subgroup) were compared with the "not sensitive" group, that is, the remainder of the cohort (resistant þ intermediate subgroups; **Fig. 2E and F**). Patients classified as sensitive had significantly better OS and PFS than patients classified as not sensitive [HR, 0.45 (95% CI, 0.25– 0.79); P = 0.006 for OS and HR, 0.45 (95% CI, 0.27–0.76); P = 0.003 for PFS]. Median OS was 17.3 (95% CI, 8.5–undefined) months for the sensitive group, compared with 6.0 (95% CI, 4.3–9.2) months for the not sensitive group; median PFS was 9.1 (95% CI, 2.5–undefined) months for the sensitive group, compared with only 1.8 (95% CI, 1.4–2.7) months for the not sensitive group. In multivariate analyses, while the effect sizes for OS and PFS remained substantial (HR, 0.60 and 0.63, respectively), classification of sensitive versus not sensitive did not retain its independent significance as a predictive factor (Supplementary Data: Supplementary Results; Supplementary Tables S13 and S14).

Baseline patient characteristics showed no association with test classification for $P < 0.05$ (Supplementary Data: Supplementary Results; Supplementary Table S15). In particular, PD-L1 expression was not significantly correlated with test classification ($P < 0.387$ for ternary classification vs. PD-L1$^+$/PD-L1$^-$/NA).

Validation

The locked test was applied to samples from validation sets 1 and 2 and the chemotherapy cohort. Validation set 1 had been used in a previous investigation (26) and, therefore, while it was not used in test development, validation set 1 could not be run blinded to clinical data. The chemotherapy cohort was a subset of a previously analyzed clinical trial comparing chemotherapy and targeted therapy, and hence, could also not be tested blinded to clinical data. Testing of validation set 2 was completely blinded to all clinical data. Statistical consideration of power to detect the effect sizes observed in the development cohort for each validation set and the chemotherapy cohort is outlined in the Supplementary Data.

Within the validation sets, the number and proportions of patients assigned to each classification group were 37 (38%)/32 (43%) resistant, 30 (31%)/19 (25%) intermediate, and 31 (32%)/24 (32%) sensitive for set 1/set 2, respectively. Kaplan–Meier plots of OS by test classification, resistant versus not resistant and sensitive versus not sensitive, are shown for the validation sets in **Fig. 3A–D**. In validation set 1, **Fig. 3A and B**, patients classified as resistant had significantly worse OS than not resistant patients [HR, 0.60 (95% CI, 0.37–0.97); P = 0.037] and patients classified as sensitive had significantly better OS than not sensitive patients [HR, 0.56 (95% CI, 0.33–0.97); P = 0.038]. One-year survival for the sensitive group was 65% and the corresponding median was 15.3 (95% CI, 8.8–undefined) months. In contrast, median OS was only 4.8 (95% CI, 2.9–9.3) months in the resistant group, with 29% OS at 1 year. PFS was numerically superior in the sensitive group and inferior in the resistant group, but the differences in outcome were smaller and did not reach statistical significance (see Supplementary Data: Supplementary

Results; Supplementary Figs. S1 and S2). Analysis of the subgroup of patients treated with nivolumab in third- or higher line (N = 40), showed similar behavior in OS and PFS, with resistant patients showing a trend to shorter outcomes [HR, 0.49 (95% CI, 0.23–1.04); P = 0.062 for OS and HR, 0.50 (95% CI, 0.25–1.02); P = 0.057 for PFS] and sensitive patients showing numerically longer survival [HR, 0.48 (95% CI, 0.21–1.10); P = 0.082 for OS and HR, 0.62 (95% CI, 0.31–1.23); P = 0.172 for PFS]. Kaplan–Meier plots for this subgroup are shown in the Supplementary Data.

Figure 3.

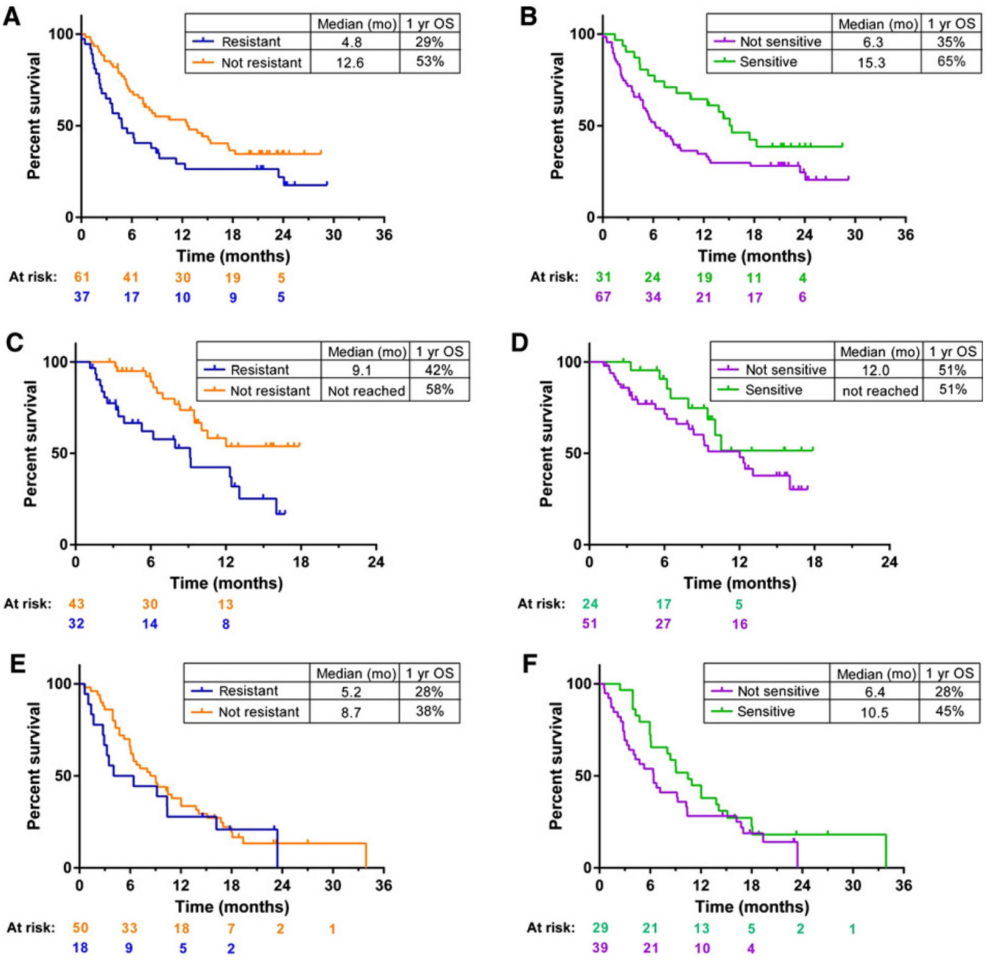

Kaplan–Meier plots of OS for the validation sets and the chemotherapy cohort. A, Validation set 1 resistant versus not resistant. B, Validation set 1 sensitive versus not sensitive. C, Validation set 2 resistant versus not resistant. D, Validation set 2 sensitive versus not sensitive. E, Chemotherapy cohort sensitive versus not sensitive. F, Chemotherapy cohort resistant versus not resistant.

Results for validation set 2 are shown in **Fig. 3C and D**. Patients classified as resistant had worse OS than not resistant patients [HR, 0.39 (95% CI, 0.19–0.77); P = 0.007]. The comparison of OS between the sensitive group and the not sensitive patients yielded an HR of 0.58, but did not show a significant difference (P = 0.179). However, for ternary test classifications, the sensitive group had longer OS than the resistant group [HR, 0.41 (95% CI, 0.18–0.94); P = 0.036]. Full analysis for the sensitive/intermediate/resistant classifications can be found in Supplementary Data: Supplementary Results. Analysis of PFS showed only numerical differences between classification groups.

As results were consistent across cohorts, within the limits of relatively small subgroup sizes, a pooled analysis of all patients treated in second-line setting with nivolumab was carried out stratified by cohort (N = 249). There was no indication of any correlation of PD-L1 expression with test classification (P = 0.292, 0.810, and 0.337 for ternary, resistant vs. not resistant, and sensitive vs. not sensitive test classifications), although positive PD-L1 expression was a predictor of improved OS and PFS in the pooled analysis [HR, 1.60 (95% CI, 1.01–2.54); P = 0.046 for OS and HR, 1.61 (95% CI, 1.07–2.44); P = 0.023 for PFS]. Indeed, analysis including test classification and PD-L1 expression demonstrated both to be independent predictors of PFS (see Supplementary Data). Within the pooled second-line population, multivariate analysis showed that the resistant versus not resistant stratification was a significant independent predictor of OS (P < 0.001) and PFS (P = 0.006) when adjusted for multiple baseline factors (**Table 2**). The sensitive versus not sensitive stratification was a significant independent predictor of OS (P = 0.009) and showed a trend for prediction of PFS (P = 0.079).

Figure 3E and **F** show OS for classification groups obtained by applying the test to pretreatment samples of the chemotherapy cohort, in which patients received docetaxel as second-line therapy. There was no indication that the test was able to stratify patients by outcome following this single-agent chemotherapy (P = 0.471 and P = 0.165 for OS comparison of resistant vs. not resistant and sensitive vs. not sensitive, respectively).

Table 2. Multivariate analysis of OS and PFS stratified by cohort for the pooled second-line population for test classification resistant versus not resistant (analysis 1) and test classification sensitive versus not sensitive (analysis 2)

		OS		PFS
Analysis 1		**HR (95% CI)**	***P***	**HR (95% CI)**
Test classification (vs. resistant)	Not resistant	0.52 (0.37–0.74)	<0.001	0.64 (0.47–0.88)
Histology (vs. adeno)	Squamous	0.83 (0.54–1.28)	0.403	1.10 (0.75–1.60)
	NA/other	1.10 (0.66–1.85)	0.711	1.09 (0.69–1.70)
Age (vs. ≥65)	<65	1.14 (0.80–1.63)	0.455	1.27 (0.93–1.73)
Gender (vs. male)	Female	0.52 (0.35–0.76)	0.001	0.69 (0.50–0.96)
PS (vs. 0)	1	1.56 (1.02–2.39)	0.040	1.37 (0.96–1.97)
	2+	3.66 (2.00–6.67)	<0.001	2.30 (1.31–4.06)
	NA	2.29 (1.15–4.54)	0.018	1.90 (1.05–3.46)
Smoking (vs. ever)	Never	1.87 (0.96–3.64)	0.064	1.47 (0.81–2.67)
	NA	0.76 (0.30–1.92)	0.559	0.76 (0.33–1.76)
PD-L1 (vs. positive)	Negative	1.20 (0.74–1.94)	0.461	1.31 (0.85–2.03)
	NA	0.84 (0.52–1.36)	0.474	0.86 (0.57–1.30)
Analysis 2		**HR (95% CI)**	***P***	**HR (95% CI)**
Test classification (vs. not sensitive)	Sensitive	0.58 (0.38–0.87)	0.009	0.73 (0.51–1.04)
Histology (vs. adeno)	Squamous	0.84 (0.54–1.30)	0.428	1.12 (0.76–1.63)
	NA/other	1.13 (0.68–1.87)	0.648	1.10 (0.70–1.71)
Age (vs. ≥65)	<65	1.06 (0.75–1.51)	0.750	1.21 (0.89–1.65)
Gender (vs. male)	Female	0.49 (0.33–0.72)	<0.001	0.66 (0.47–0.91)
PS (vs. 0)	1	1.41 (0.92–2.17)	0.116	1.32 (0.92–1.90)
	2+	3.31 (1.78–6.13)	<0.001	2.19 (1.22–3.91)
	NA	2.25 (1.14–4.45)	0.020	1.95 (1.07–3.55)
Smoking (vs. ever)	Never	1.82 (0.93–3.57)	0.082	1.48 (0.81–2.71)
	NA	0.83 (0.33–2.11)	0.693	0.84 (0.36–1.95)
PD-L1 (vs. positive)	Negative	1.22 (0.75–1.98)	0.417	1.34 (0.87–2.07)

Abbreviations: Adeno, adenocarcinoma; NA, not available; PS, performance status.

Protein set enrichment

To examine the potential biological mechanisms underlying the test, the association of test classification with various biological processes was assessed using PSEA methods (22–24). The results are summarized in **Table 3**. Acute phase response, acute inflammatory response, wound healing, and complement activation were identified as associated with test classification with $P < 0.001$. In addition, innate immune response and chronic inflammatory response were identified as associated with $P < 0.01$. Similar analysis was performed comparing the sensitive subgroup with the remaining patients. Only immune tolerance and suppression were identified as associated with test classification with $P < 0.01$ (FDR < 0.1). Full results for sensitive versus not sensitive phenotype are contained in the Supplementary Data: Supplementary Results; Supplementary Table S21.

Table 3. Results of PSEA of test classifications resistant versus not resistant

Biological process	*P* value of association	FDR
Acute phase response	<0.0001	<0.002
Acute inflammatory response	0.0001	<0.002
Wound healing	0.0002	<0.002
Complement activation	0.0005	<0.003
Innate immune response	0.0014	<0.01
Chronic inflammatory response	0.0044	<0.02
Extra cellular matrix	0.0231	<0.08
IFN type 1	0.0315	<0.1
Cellular component morphogenesis	0.0317	<0.1
Immune tolerance and suppression	0.0526	<0.2
B-cell–mediated immunity	0.0526	<0.2
Angiogenesis	0.0753	<0.2
NK-cell–mediated immunity	0.1222	<0.3
Behavior	0.1270	<0.3
Cytokine production involved in immune response	0.3198	<0.5
Glycolysis and positive regulators	0.3560	<0.6
Epithelial–mesenchymal transition	0.4548	<0.6
Type 17 immune response	0.4668	<0.6
Type 1 immune response	0.5102	<0.7
Type 2 immune response	0.7791	<0.9
Response to hypoxia	0.9287	<1
T-cell–mediated immunity	0.9861	<1
IFNγ	0.9884	<1

Abbreviation: NK, natural killer.

DISCUSSION

Here, we report the establishment of a pretreatment serum proteomic classifier that separates those patients who obtain little from those that obtain durable clinical benefit from treatment with the PD-1 inhibitor, nivolumab, as second-line treatment for advanced NSCLC. On the basis of 274 MS features, patients could be classified as being resistant, intermediate, or sensitive. The difference in OS between resistant and not resistant patients was highly significant: the HR was 0.48, and median survival times were 4.3 months versus 11.1 months, respectively. The test was validated while blinded to clinical outcome data with an independent set of patients with advanced NSCLC, treated at a different institution. The classifier failed to stratify outcomes within a historical cohort of patients with advanced NSCLC treated with docetaxel as second-line therapy. Moreover, test classification, as expected, was independent of well-established clinical factors and notably showed no evidence of association with PD-L1 expression.

A serum test would have obvious advantages, such as ease of detection using one blood draw. Also, the test may avoid the issue of intrapatient tumor heterogeneity and could assess host factors that are not captured by examination of the tumor microenvironment in histologic samples. Further characterization of the classifier revealed that the classification phenotypes identified are associated with biological processes known to confer a poor prognosis in lung cancer. Several lines of research indicate that complement, as a member of a diverse family of innate immune proteins, is involved in dysregulation of mitogenic signaling and escape from immune surveillance (27, 28). Complement activation, as measured by Cd4, a stable complement degradation product, in serum of patients with early-stage NSCLC was significantly associated with poor prognosis (29). A number of authors have identified the ratio of the acute phase protein, serum C-Reactive protein, to albumin as a negative prognostic factor in both early and advanced NSCLC (30). Intratumoral wound-healing signatures, as measured by mRNA expression arrays, are considered to be T-cell suppressive and have been observed in several tumor types, among them NSCLC (31). Interestingly, sera derived from patients with tumors exhibiting woundhealing signatures elicited identical signatures from nontumorassociated fibroblasts, which were found to be a powerful predictor of an unfavorable clinical course (32). These observations may provide the biological basis of our findings, although a direct link between the abundance of these circulating proteins and absence of a response to PD-1 inhibitors remains to be established.

The results obtained in this study do not stand alone. Weber and colleagues identified a protein classifier from sera of patients with melanoma treated with PD-1 inhibitors, employing the same technology that was used in our study. This was validated in multiple patient cohorts treated with PD-1 inhibitors and CTLA4 antagonists. (14) As here, they were able to identify, prior to initiation of treatment, patients who had a favorable outcome following treatment. Biological processes associated with that classifier included

complement, wound healing, and acute phase pathways, all upregulated in the poor prognosis group, corroborating our results. Further evidence that the pretreatment circulating proteome provides important information on checkpoint efficacy was provided in the context of a phase II study where atezolizumab was compared with docetaxel as second-line treatment in 272 patients with advanced NSCLC (33). Similar to our results, a serum protein classifier was established that identified patients with poor [median OS, 7.3 months; n ¼ 60 (45%)] and good [median OS, not reached; n = 73 (55%)] outcomes. This classifier was shown in blinded validation to be predictive for atezolizumab versus docetaxel for OS and PFS (Pinteraction < 0.01). In that study, as in our own, there was no association between test classification and tumor PD-L1 expression; there was also no association with TMB. Also, among the biological processes that were most significantly associated with classification by PSEA, acute inflammation and complement activation ranked in the top three.

There are some limitations to our results. Obviously, the number of patients was low and all three immunotherapy-treated cohorts came from one geographic area and were investigated retrospectively. Also, for historical reasons, validation blinded to all clinical data was only possible for validation set 2. Although we made strong efforts to obtain sufficient tumor tissue samples, we were not able to obtain PD-L1 expression data on all patients. Several factors contributed to this: many patients are diagnosed on the basis of cytology alone and so have no tissue available for PD-L1 analysis; at the time of treatment initiation for these patients, use of PD-L1 expression was still somewhat investigational; and positive PD-L1 expression status was not mandatory for administration of nivolumab in the second- and higher-line setting. Unfortunately, TMB data were not collected. Investigation of larger cohorts with more complete information on TMB and PD-L1 expression would be useful to examine with more precision the level of association of these markers and how much complementary information each can provide to predict outcome. The nonimmunotherapy-treated control set was small and restricted to one therapy. It would be of interest to study the performance of the test in larger control cohorts in other standard-of-care nonimmunotherapy regimens to be able to explore the test's predictive potential.

Additional validation of the test in other larger cohorts of patients treated with CPIs is necessary. So far, we have investigated the ability of the test to stratify outcome for patients receiving checkpoint blockade monotherapy in the second- and higher-line setting, after platinum-based chemotherapy. However, now immunotherapy is moving into the first-line setting, either as monotherapy for patients with PD-L1 expression greater than 50%, or in combination with chemotherapy. It is of interest to evaluate the performance of the test in these first-line settings. A prospective trial, comparing outcomes between mono-immunotherapy and the chemo-immunotherapy combination in first-line patients with high PD-L1 expression is in the final stages of design. Studies in earlier stage patients receiving durvalumab with chemoradiation would also be informative. Evaluation of

the test with appropriate comparator nonimmunotherapy regimens in a prospective, randomized setting would be required to unequivocally determine its predictive power and clinical utility.

REFERENCES

1. Goldstraw P, Chansky K, Crowley J, Rami-Porta R, Asamura H, Eberhardt WEE, et al. The IASLC Lung Cancer Staging Project: proposals for revision of the TNM stage groupings in the forthcoming (eighth) edition of the TNM classification for lung cancer. J Thor Oncol 2016;11:39–51.
2. Peters S, Reck M, Smit EF, Mok TS, Hellman MD. How to make best use of immunotherapy as first-line treatment for advanced/metastatic non-small cell lung cancer? Ann Oncol 2019;30:884–96.
3. Gettinger S, Horn L, Jackman D, Spigel D, Antonia S, Hellmann M, et al. Five year follow up of nivolumab in previously treated advanced non-smallcell lung cancer: results from the CA209-003 study. J Clin Oncol 2018;36: 1675–84.
4. Garon EB, Hellman MD, Rizvi NA, Carcereny E, Leighl NB, Ahn MJ, et al. Fiveyear overall survival for patients with advanced non-small-cell lung cancer treated with pembrolizumab: results from the Keynote-001 study. J Clin Oncol 2019;37:2518–27.
5. Garon EB, Rizvi NH, Hui R, Leighl N, Balmanoukian AS, Eder JP, et al. Pembrolizumab for the treatment of non-small-cell lung cancer. New Eng J Med 2015;372:2018–28.
6. Sun R, Linkin EJ, Vakalopoulou M, Derde L, Champiat S, Han SR, et al. A radiomics approach to assess tumor-infiltrating CD8 cells and response to anti-PD-1 or anti-PD-L1 immunotherapy: an imaging biomarker, retrospective multicohort study. Lancet Oncol 2018;19;1180–91.
7. Hellmann M, Nathanson T, Rizvi H, Creelan BC, Sanchez-Vega F, Ahuja A, et al. Genomic features of response to combination immunotherapy in patients with advanced non-small-cell lung cancer. Cancer Cell 2018;33:843–52.
8. Duruisseaux M, Martiniz-Cardus A, Calleja-Cervantes ME, Moran S, Castro de Moura M, Davalos V, et al. Epigenetic prediction of response to anti-PD-1 treatment in non-small-cell lung cancer: a multicenter, retrospective analysis. Lancet Respir Med 2018;6:771–81.
9. Cristescu R, Mogg R, Ayers M, Albright A, Murphy E, Yearly J, et al. Pan-tumor genomic biomarkers for PD-1 checkpoint blockade-based immunotherapy. Science 2018;362:197.
10. Brahmer J, Reckamp KL, Baas O, Crino L, Eberhardt WE, Poddubstaya E, et al. Nivolumab versus docetaxel in advanced squamous-cell non-small-cell lung cancer. N Engl J Med 2015;373:123–35.
11. Borghaei H, Paz-Ares L, Horn L, Spigel DR, Steins M, Ready NE, et al. Nivolumab versus docetaxel in advanced nonsquamous non-small-cell lung cancer. N Engl J Med 2015;373:1627–39.
12. Gregorc V, Novello S, Lazzari C, Barni S, Aieta M, Mencoboni M, et al. Predictive value of a proteomic signature in patients with non-small-cell lung cancer treated with second-line erlotinib or chemotherapy (PROSE): a biomarker-stratified, randomized phase 3 trial. Lancet Oncology 2014;15:713–21.
13. Tsypin M, Asmellash S, Meyer K, Touchet B, Roder H. Extending the information content of the MALDI analysis of biological fluids via multi-million shot analysis. PLoS One 2019;14:e0226012.
14. Weber JS, Sznol M, Sullivan R, Blackmon S, Boland C, Kluger H, et al. A serum protein signature associated with outcome after anti-PD-1 therapy in metastatic melanoma. Cancer Immunol Res 2018;6:79–86.

15. Ascierto PA, Capone M, Grimaldi AM, Mallardo D, Simeone E, Madonna G, et al. Proteomic test for anti-PD-1 checkpoint blockade treatment of metastatic melanoma with and without BRAF mutations. J Immunother Cancer 2019;7:91.
16. Roder J, Oliveira C, Net L, Tsypin M, Linstid B, Roder H. A dropout-regularized classifier development approach optimized for precision medicine test discovery from omics data. BMC Bioinformatics 2019;20:325.
17. Goodfellow I, Bengio Y, Courville A. Deep learning. Cambridge, MA: MIT Press; 2016. p. 5–11.
18. Breiman L. Out-of-bag estimation. Technical Report. Berkeley, CA: Department of Statistics, University of California; 1996.
19. Roder H, Oliveira C, Net L, Linstid B, Tsypin M, Roder J. Robust identification of molecular phenotypes using semi-supervised learning. BMC Bioinformatics 2019;20:273.
20. Weber J, Martinez AJ, Roder H, Roder J, Meyer K, Asmellash S, et al. Pretreatment patient selection for nivolumab benefit based on serum mass spectra. J Immunother Cancer 2015:3:P103.
21. Grossi F, Rijavec E, Biello F, Barletta G, Maggioni C, Genova C, et al. Evaluation of pretreatment serum tests for nivolumab benefit in patients with non-small cell lung cancer. J Thorac Oncol 2017;12:S1322.
22. Subramanian A, Tamayo P, Mootha VK, Mukherjee S, Ebert BL, Gilette MA, et al. Gene set enrichment analysis: a knowledge-based approach for interpreting genome-wide expression profiles. Proc Natl Acad Sci U S A 2005;102: 15545–50.
23. Grigorieva J, Asmellash S, Oliveira C, Roder H, Net L, Roder J. Application of protein set enrichment analysis to correlation of protein functional sets with mass spectral features and multivariate proteomic tests. Clin Mass Spectrometry 2020;15:44–53.
24. Roder J, Linstid B, Oliveira C. Improving the power of gene set enrichment analyses. BMC Bioinformatics 2019;20:257.
25. Benjamini Y, Hochberg Y. Controlling the false discovery rate: a practical and powerful approach to multiple testing. J Royal Stat Soc. Series B (Methods) 1995; 57:289–300.
26. Goldberg SB, Jilaveany L, Kluger HM, Chiang V, Mahajan A, Xia B, et al. Mass spectrometry-based test predicts outcome on anti-PD-1 therapy for patients with advanced non-small cell lung cancer with brain metastases. J Immunother Cancer 2017;5:86.
27. Rutkowski MJ, Sughrue ME, Kane AJ, Mills SA, Parsa AT. Cancer and the complement cascade. Mol Cancer Res 2010;8:1453–65.
28. Wang Y, Sun SN, Liu Q, Yu YY, Guo J, Wang K, et al. Autocrine complement inhibits IL-10 dependent T-cell-mediated antitumor immunity to promote tumor progression. Cancer Discov 2016:6;1022–35.
29. Ajona D, Pajares MJ, Corrales L, Perez-Gracia JL, Agorreta J, Lozano MD, et al. Investigation of complement activation product c4d as a diagnostic and prognostic biomarker for lung cancer. J Natl Cancer Inst 2013;105: 1385–93.
30. McMillan DC. The systemic inflammation-based Glasgow score: a decade of experience in patients with cancer. Cancer Treat Rev 2013;39:534–40.

31. Hugo W, Zaretsky JM, Sun L, Song C, Moreno BH, Hu-Lieskovan S, et al. Genomic and transcriptomic features of response to anti-PD-1 therapy in metastatic melanoma. Cell 2016;165:35–44.
32. Chang HY, Sneddon JB, Alizadeh AA, Sood R, West RB, Montgomery K, et al. Gene expression signature of fibroblast serum response predicts human cancer progression: similarities between tumors and wounds. PLoS Biol 2004; 2:0206.
33. Kowanetz M, Leng N, Roder J, Oliveira C, Asmellash S, Meyer K, et al. Evaluation of immune-related markers in the circulating proteome and their association with atezolizumab efficacy in patients with 2Lþ NSCLC. J Immunother Cancer 2018;6:114.

CHAPTER 7

7

Tumour growth rate as a tool for response evaluation during PD-1 treatment for non-small cell lung cancer: a retrospective analysis

Deirdre M.H.J. ten Berge, Daan P. Hurkmans, Ilse den Besten, Jeroen S. Kloover, Ron H.J. Mathijssen, Reno J.E.M.A. Debets, Egbert F. Smit, Joachim G.J.V. Aerts

European Respiratory Journal Open Research, December 2019, 5:179

Abstract

Introduction: Immune checkpoint inhibitors have emerged as a standard of care treatment for non-small cell lung cancer (NSCLC). To get insight into variations in tumor growth kinetics and their potential predictive values for outcome we evaluated tumor growth rate (TGR) in patients receiving PD-1 checkpoint inhibitors.

Materials and Methods: Differences in TGR before and after the start of treatment were calculated by entering the sum of the longest diameters from CT-scans before and after the initiation of therapy into a formula that assumes a volumetric exponential tumor growth. TGR variations, possible predictors for TGR changes and its relationship to overall survival (OS) were studied. For comparison tumor response was assessed using Response Evaluation Criteria in Solid Tumors version 1.1 (RECIST v1.1).

Results: Among the 58 evaluable patients, 37 patients (64%) showed deceleration of TGR and 16 patients (27%) showed an acceleration of TGR after initiation of therapy, with a significant difference in median OS of 18.0 versus 6.0 months (HR=0.35; 95%CI:0.18-0.71) between these groups. Four patients (7%) were defined as having HPD. In 5 patients (9%), the tumor growth remained stable. These TGR categories were not significantly different according to age, gender, histology, smoking or previous radiotherapy. Of the patients defined as having progressive disease by RECIST1.1 at first follow up 40% showed response to CPI by a decrease in tumor growth rate.

Discussion: Tumor growth kinetics can be used as a clinically relevant predictor for OS in anti-PD1 treated NSCLC patients, and may provide additional information to RECIST measurements.

INTRODUCTION

In recent years, programmed cell death (PD)-(L)1 immune checkpoint inhibitors have emerged as a standard of care treatment option with an increase in survival and this has changed the way patients with cancer are managed[1]. Checkpoint inhibitor (CPI) treatment is associated with novel patterns of tumor response, and evidence suggests that treatment with these immunotherapeutic agents may even backfire in certain patients[2]. In current practice, the anti-tumor activity of therapeutic agents is assessed using the Response Evaluation Criteria in Solid Tumors (RECIST) guidelines, originally published in 2000 and revised in 2009 as RECIST1.1[3]. This utilizes unidimensional diameter measurements for response evaluation. Progression is defined at an increase in tumor size (which is the summation of the longest diameter of 5 target lesions) of more than 20% compared to the lowest determined tumor size at any point in time. The possibility of pseudoprogression[4–6] necessitated a second update of RECIST and in 2017 iRECIST was adopted as novel tumor response evaluation tool in patients with immunotherapy treatment[7]. Several authors have suggested that RECIST criteria may be inadequate to capture the response to immunotherapies[8–13].

At first, anecdotal evidence of rapid disease progression in patients treated with immunotherapy was reported[14, 15]. This was followed by a review of the tumor growth rate in 131 patients with different tumor histology upon treatment with anti-PD-1 therapies, which revealed that 9% of patients developed accelerated tumor growth which was subsequently characterized as hyperprogressive disease (HPD)[16]. To identify tumors showing HPD, tumor growth kinetics were integrated into the response evaluation method and implemented in multiple recent studies[16–20]. (**Table 1**) In all five the definitions of HPD, tumor kinetics and time are taken into account, which are both not part of the RECIST measurements. For example, tumor growth rate (TGR) uses the same computed tomography (CT) measurements as RECIST but assumes that volumetric tumor growth follows an exponential law. Also, it integrates the time intervals between CT scans allowing a quantitative assessment of the dynamics and kinetics of the tumor. In both RECIST and TGR, each patient is used as his or her own control. TGR has already been successfully used to evaluate the activity of multiple agents other than CPIs and in other tumor types[16, 21–24] and for this study the authors believe that it can be instrumental to identify therapeutic effects in the treatment with immunotherapeutic agents other than for HPD.

In this study, it is hypothesized that tumor growth kinetics based on CT measurements provides clinically relevant information in CPI treatment for NSCLC and is associated with clinical outcome. RECIST measurements and TGR differences before and after initiation of CPI treatment were analyzed in NSCLC to assess the variations in tumor growth kinetics and their potential predictive values for outcome.

Table 1. Definitions of Hyperprogressive disease in immunotherapy using tumor growth kinetics

Definition of Hyperprogressive disease	Tumor type	No. of patients	Reference
A Response Evaluation Criteria in Solid Tumors progression at the first evaluation with a 2-fold or greater increase in Tumor growth rate (TGR) between the period prior to treatment and upon therapy	All histologies treated with anti-PD1/PDL1	131	Champiat et al. (2017)
A tumor growth kinetics ratio ≥2, being the ratio between the slope of tumor growth prior to treatment and after start of therapy	Head and neck squamous cell carcinoma	34	Saâda-Bouzid et al. (2017)
Time-to-treatment failure of less than 2 months, >50% increase in tumor burden compared with pre-immunotherapy imaging, and >2-fold increase in progression pace	Stage IV cancer, different tumor types	155	Kato et al. (2017)
A disease progression at the first evaluation with ΔTGR exceeding 50%. With ΔTGR being the variation per month between tumor growth rate before and during treatment.	Non-small cell lung cancer	406	Ferrara et al. (2018)
An absolute increase of delta TGR by 50%, with delta TGR being the variation per month of TGR before and after initiation of therapy	Non-small cell lung cancer	242	Ferrara et al. (2017)

MATERIALS AND METHODS

Patient selection

Between June 2015 and September 2017, 196 NSCLC patients were treated with the anti-PD1 immune checkpoint inhibitor nivolumab as a second line therapy in an early access program (EAP) and as standard of care at the Erasmus MC, Erasmus University Medical Center (Rotterdam, The Netherlands). The Erasmus MC is a tertiary hospital to which patients were referred from other hospitals for CPI treatment. Nivolumab was administered intravenously at a dose of 3 mg/kg every two weeks.

Out of these, 58 were eligible for inclusion (**Figure 1A**). These patients had: (1) a baseline CT-scan prior to the initiation of therapy (< 2weeks); (2) at least one pre-baseline CT-scan taken before the baseline CT-scan, during which interval no treatment was provided; and (3) at least one follow-up CT-scan following immunotherapy available for adequate review. For the pre-baseline CT-scan, the last CT-scan from the referring hospitals was frequently used. As patients were referred for CPI treatment from other hospitals and given the EAP application procedure, there is a time lag between the determination of progression on last systemic treatment and the start of the new therapy. The median time between the pre-baseline and baseline CT-scan is 1.8 months, ranging from 1.3 to 6.8 months. A small window between the baseline CT and the start of therapy of no more than two weeks was

required. Follow-up scans were performed according to the treating physicians' discretion as a part of clinical care without predefined intervals. There was an expected average time of 6 to 8 weeks between the baseline CT scan and response assessment.

Figure 1.

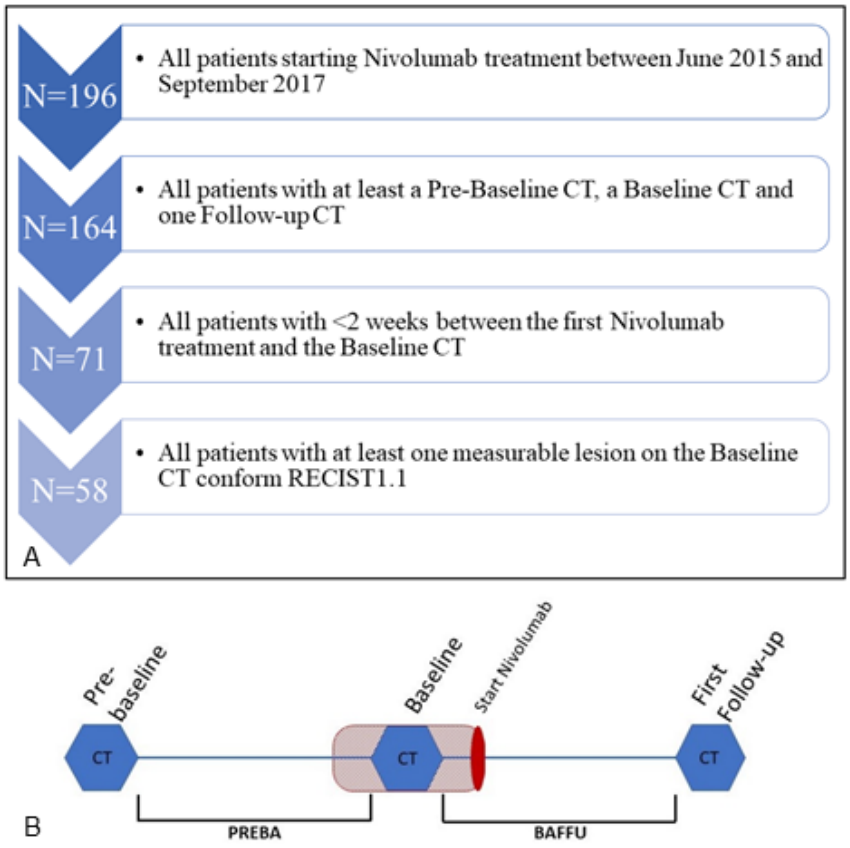

A: Patient selection flow chart. B: Reviewed CT scan moments. PREBA (pre-baseline to baseline) = time between pre-baseline and baseline CT scan. BAFFU (baseline to first follow up = time between baseline and first follow up CT. Red marked area = time between baseline CT and start Nivolumab which was < 2 weeks.

Assessment of tumor growth kinetics

The pre-baseline, baseline and first follow-up (FU) CT scans were retrospectively reviewed for the assessment of tumor burden and identification of target lesions (**Figure 1B**). Identification of target lesions and tumor size measurements were quantitatively assessed by the radiologists using RECIST v1.1[10]. In brief, target lesions (≥10 mm in the longest

diameter for non-nodal lesions and ≥15 mm in short axis for nodal lesions) were selected on baseline scans with a slice thickness no greater than 5 mm, allowing up to 2 lesions per organ and up to 5 lesions in total[10]. Only patients with at least one target lesion on baseline scan were included. Follow-up scans were performed according to the treating providers' discretion as a part of clinical care without predefined intervals.

Definitions

Tumor size was defined as the sum of the longest diameters (SLD) of the target lesions for pre-baseline, baseline and the first FU scan as per RECIST v1.1. According to RECIST v1.1, the tumor response was classified as: complete response (CR), partial response (PR), stable disease (SD), and progressive disease (PD)[5]. To report the tumor size difference between PREBA (pre-baseline to baseline) and BAFFU (baseline to first follow up) in a clinically meaningful way, time was taken into account as a factor. This was expressed as the percentage difference in SLD of the target lesions for the reference period of 6 weeks, which is the planned time between follow up CT scans (SLDdiff):

$SLDdiff_{PREBA} = ((((SLD_{Baseline} - SLD_{Pre\text{-}baseline})/SLD_{Pre\text{-}baseline}))*100)/Time_{PREBA}(weeks))*6$

$SLDdiff_{BAFFU} = ((((SLD_{Follow\text{-}up} - SLD_{Baseline})/SLD_{Baseline}))*100)/Time_{BAFFU}(weeks))*6$

$SLDdifference = SLD_{BAFFU} - SLD_{PREBA}$

TGR was calculated across the same clinically relevant treatment periods (and if relevant between follow up scans thereafter). Tumor size was expressed in the same way, using SLD. Let *t* be the time expressed in months for the period between CT-scans. The tumor volume at time t is equal to $V_t = V_0 \exp(TG*t)$, assuming the tumor growth follows an exponential law. V_0 is the volume at baseline and TG is a measure of tumor growth. We approximated the tumor volume (V) by $V = 4 \pi R^3 /3$, where R, the radius of the sphere is equal to SLD/2[25]. TG is than equal to $TG = 3 \text{ Log}(SLD_t/SLD_0)/t$. To report the TGR results in a clinically meaningful way, we expressed TGR as a percentage increase in tumor volume during 1 month using the following transformation: TGR ¼ 100 [exp(TG) 1], where exp(TG) represents the exponential of TG. TG and TGR were calculated using the following transformation:

$TG_{PREBA} = (3* LN(SLD_{Baseline}/SLD_{Pre\text{-}baseline}))/Time_{PREBA}(months)$

$TG_{BAFFU} = (3* LN(SLD_{Follow\text{-}up}/SLD_{baseline}))/Time_{BAFFU}(months)$

$TGR_{PREBA} = 100*(\exp(TG_{PREBA})-1)$

$TGR_{BAFFU} = 100*(\exp(TG_{BAFFU})-1)$

For patients who had disease progression with new lesions, the SLDdifference and TGR were computed on the target lesions only (new lesions were not included in the SLD). Hyperprogressive disease was defined as a 2-fold or greater increase in TGR from baseline. True hyperprogressive disease (True-HPD) was defined as a 2-fold or greater increase in TGR from baseline and PD as defined by RECIST v1.1 at the first follow up evaluation, according to the definition of Champiat *et al.*[16].

Statistical analysis

Overall survival (OS) was determined as the time between the first administration of nivolumab and the time of death by any cause, patients with loss to follow up were censored. OS was estimated and presented graphically using the Kaplan-Meier method. Survival curves were compared using the Log-rank test. Hazard ratios (HR) were estimated from Cox proportional hazard models. Statistical comparisons were performed using the X^2 or Fisher's exact test for categorical data, t-test were used for continuous variables. All the tests were 2-sided and significance was assumed if $P < 0.05$. All the analyses were done using IBM SPSS statistics version 23.

RESULTS

The majority of the 58 patients included for analysis were male (59%) and the mean age was 63 (range 35-79). Ten percent of patients were non-smokers, 83% were either current or an ex-smokers and for 7%, this was unknown. Histological types were: adenocarcinoma (71%), squamous cell carcinoma (22%), Large cell in (2%), NSCLC NOS (2%), and unknown (3%) (**Suppl. table 1**).

All patients received prior chemotherapy with a median of 4.1 months between the last administration of chemotherapy and the administration of CPI, ranging from 0.7 to 24.6 months in the 53 patients with the exact stop date known. Thirty-nine percent of 56 patients received prior radiotherapy to the chest with a median time of 9.6 months between the last radiation dose and the first administration of CPI, ranging from -2.1 to 24.6 months. In two patients this was not recorded.

Figure 2.

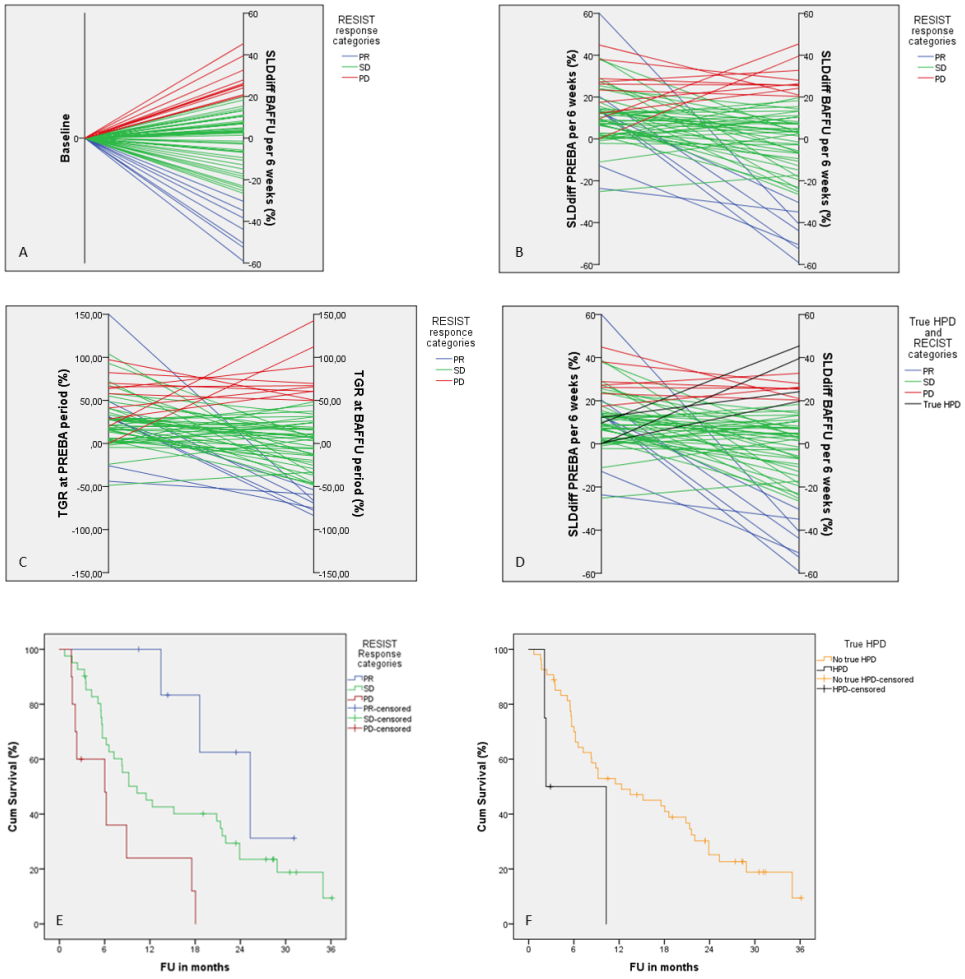

RECIST categories at first follow up A. Tumor growth in SLD difference between baseline and first follow-up. B. SLD difference before and after baseline. C. Tumor growth in TGR before and after baseline. D. Tumor growth in SLD difference with patients showing hyperprogressive disease. E. Overall survival (OS) when differentiated according to RECIST response categories (Log Rank P= 0.004). F. OS according to HPD (Log Rank P= 0.041).True-HPD (black) = hyperprogressive disease defined as PD at the first evaluation with a 2-fold or greater increase in tumor growth rate (TGR) from baseline; No hyperprogressive disease (yellow) = patients not showing HPD at fist follow up. PREBA = Pre-baseline period; BAFFU = period from baseline to first follow-up.

The median OS was 11.5 ± 2.8 months. The median number of months on treatment was 4 (Range 0 – 25). The mean time from the pre-baseline to baseline ($Time_{PREBA}$) CT-scan was

10.5 ± 5.1 weeks. And the mean time from baseline to first follow up ($Time_{BAFFU}$) was 5.8 ± 1.7 weeks. At first follow-up CT scan, patients were categorized by RECIST v1.1 into: CR 0 (0%), PR 7 (12%), SD 41 (71%), and PD 10 (17%) patients. **Figure 2A** shows how follow-up CT's are classically evaluated, taking the baseline CT as the zero point, and categorizing tumor growth at follow-up according to RECIST. Lines ending above zero represent tumor growth, with a 20% increase in total tumor size being the cut-off for PD. Lines ending below zero represent tumor shrinkage, with -30% being the cut-off for partial response.

Next, we compared the above change in sum of the diameters according to RECIST after start of treatment to the change in sum of the diameters before the start of treatment (**Figure 2B).** Of the 10 patients showing PD at first follow up, CPI caused a decrease in growth rate in 4 patients (40%), an increase in tumor growth rate in 5 patients (50%) and in 1 patient (10%) the tumor growth did not significantly change (defined as a change of ≤5%). Of the 41 patients showing SD at first follow up, CPI caused a decrease in growth rate in 26 patients (63%), an increase in tumor growth rate in 11 patients (27%) and in 4 patients (10%) the tumor growth did not significantly change. In all 7 patients showing PR at first follow up, CPI caused a decrease in tumor growth.

Tumor growth rate (TGR) is derived from the SLD but accounts for an assumption for tumor volume. In **Figure 2C** the TGR before and after initiation of CPI therapy is shown. and although this gives a similar representation of the changes in growth pattern it is harder to correlate with the RECIST criteria than **Figure 2B**.

In total 11 patients (19%) fulfill the definition of HPD based on TGR alone defined as a >50% increase in TGR between PREBA and BAFFU. Four patients (7%), were defined as having True-HPD, because they showed PD according to RECIST at the first follow up on top of the >50% increase in TGR. In **figure 2D**, these patients with True-HPD are visualized within the RECIST categories.

OS was differentiated according to RECIST v1.1 response categories: PR 25.3 ± 5.3 months, SD 10.3 ± 2.5 months and PD 6.0 ± 2.6 months. (Log Rank *P= 0.004*) (**Figure 2E**). When differentiating according to HPD status an OS of: no True-HPD 12.3 ± 4.3 months versus True-HPD 2.3 ± 2.7 months was observed. (Log Rank *P= 0.041*) (**Figure 2F**)

The distribution of TGR across the 2 periods is as follows; PREBA period: median 28.0 (range: -48.6 to 293.7) and BAFFU period: median 6.9 (range: -83.8 to 142.6). The group was divided into patients showing tumor growth acceleration (TGR/SLDdiff at BAFFU > PREBA) 16 (27%) and patients showing tumor growth deceleration and/or shrinkage (TGR/SLDdiff at BAFFU < PREBA) 37 (64%) after the initiation of therapy, excluding patients with stable TGR 5(9%) (<5% difference in TGR per month) (**Figure 3A**). Comparison of acceleration in TGR with deceleration in TGR provided a significant difference in median OS of 6.0 ± 0.6 vs 18.0 ± 4.4 months, Log Rank *P= 0.002*. (**Figure 3C**). Deceleration of TGR reduced the risk of early death with a HR of 0.35; 95% CI of 0.18 to 0.71. By only taking into account the 48 patients showing tumor growth before the start of CPI, the TGR could be further

divided into a group that showed tumor shrinkage after initiation of therapy (*N=21*, 44%), tumors that kept growing but with a decreased growth rate (*N=14*, 29%) and tumors that kept growing but increased their growth rate (*N=13*, 27%). (**Figure 3B**) This provided a significant difference in median OS of 25.3 ± 3.6 vs 8.9 ± 2.5 vs 5.5 ± 0.7 months, Log Rank *P<0.001*. (**Figure 3D**). When plotting OS against growth rate in SLDdifference at 6 weeks after baseline, the effect of these growth patterns can be appreciated. **Figure 4**.

Figure 3.

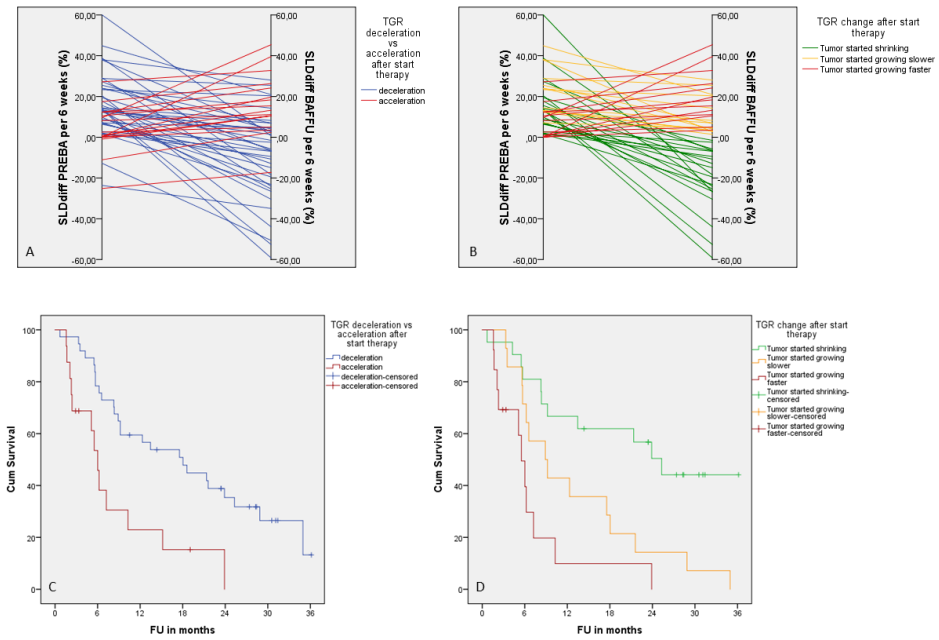

A. TGR acceleration versus deceleration after start of therapy. B. Patients showing growth before the start of therapy grouped according to change in growth pattern after start of therapy. C OS according to increase versus decreased TGR after start of therapy (Log Rank: P= 0.002). D. OS according to change in TGR after initiation of therapy (Log Rank: P< 0.001). TGR = Tumor growth rate; OS = overall survival; FU = Follow up.

Figure 4.

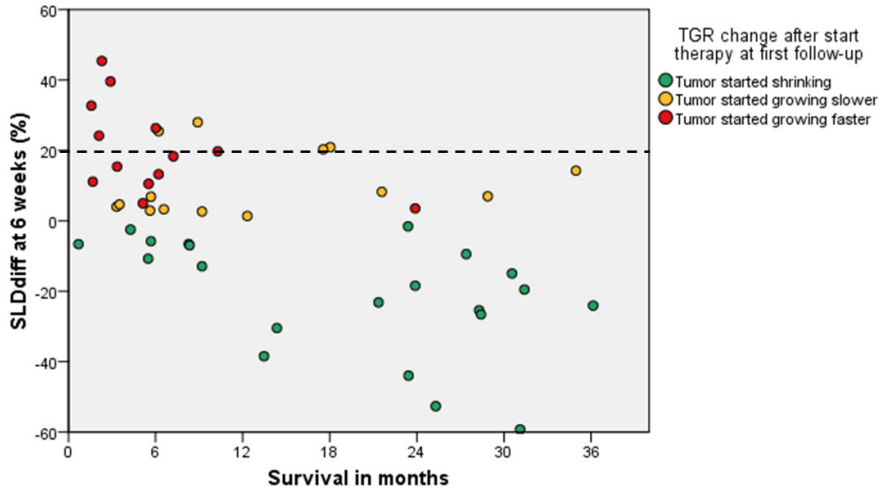

Overall survival plotted against the SLDdifference at six weeks after the start of CPI in the patients that showed tumor growth before the start of therapy. The patients were divided into groups according to tumor growth rate change. Patients showing tumor growth with an increased growth rate (red) as well as with a decreased growth rate (yellow) go over the 20% growth line, defining progressive disease at first follow up.

No correlation between TGR or SLDdifference during PREBA and during BAFFU was found. No significant correlations were observed in gender, age, histology, smoking and previous radiotherapy for patients showing tumor growth acceleration when compared to patients showing growth deceleration. For the patients showing True-HPD no significant correlations were observed in gender, age, histology, smoking and previous radiotherapy when compared to the rest of the studied population. 3 out of 4 patients with True-HPD were ≥65 years, the fourth patient was 46 years old.

DISCUSSION

This study explores the dynamics of tumor growth in patients treated with CPI for NSCLC. We confirm the presence and incidence of HPD but we also describe a novel phenomenon that in those tumors that keep growing, a decrease in tumor growth rate induced by CPI is associated with improved survival. The division of the group into patients showing deceleration in TGR versus acceleration in TGR at first follow up after the start of CPI therapy, provided a significant and clinically relevant difference in OS of 12 months.

This is relevant as the patients in each group fall into different RECIST categories. For example, patients with a decrease in TGR on CPI might still be growing fast enough to be categorized as having PD at the first response assessment. However, these patients have a significant better OS than a patient with a tumor that responded with an increase in TGR. Of the patients showing PD according to RECIST criteria by an increase of SLD of ≥ 20%, 40% actually had a decrease in tumor growth. In these patients, after determination of PD, in general the immune therapy will be withheld, potentially deteriorating the outcome of the patient. In this particular group, treatment beyond progression was given when a patient was in good clinical condition, given the option of pseudo-progression. This may also (partly) explain why we did find this increase in OS, but a further treatment may be beneficial for these patients. As far as the authors are aware, only Lahmar *et al*.[15] recently presented an abstract describing a similar analysis in 58 NSCLC patients treated with CPIs and categorized their response patterns according to increasing or decreasing TGR after the initiation of therapy[15]. In line with our findings, they also found a significant relationship between treatment TGR and OS after immunotherapy.

When the growth patterns were further divided into three groups, (i.e. a group that showed tumor shrinkage after initiation of therapy; tumors that kept growing but with a decreased TGR; and tumors that kept growing but with an increased TGR), significant differences in median OS of respectively 25.3, 8.9 and 5.5 months were found. When comparing just the two groups that kept growing, only a tendency towards significance was found, P=0.065, possibly due to the small number of patients. No significant differences for the patients showing TGR acceleration were observed in gender, histology, smoking and previous radiotherapy when compared to the patients showing deceleration.

Of the 58 patients found eligible for inclusion in this study, four (7%) were having True-HPD defined as showing PD according to RECIST at the first evaluation with a 2-fold or larger increase in TGR between the period prior to treatment (PREBA) and upon therapy (BAFFU). This is a comparable range as found by Champiat *et al*.[16] who used the same definition for HPD[16]. In a recent review incidences of HPD up to 21% were described in NSCLC patients specifically[8]. In other histologies incidences up to 29%[17–19] were found but these used different, and often less strict, definitions. Comparable to the study by Champiat *et al*.[16] we only included patients that had a follow up CT scan, and excluded the patients who became too ill to be scanned or who died before the first follow-up CT scan. True-HPD was, in this study, a significant negative predictive value for OS. Patients showing True-HPD had a median OS of only 2.3 while the other patients had an OS of more than one year. This result is, again, in line with the observations by Champiat *et al*. and Ferrera *et al*.[16, 19].

Many patients in the available patient cohort were not eligible for inclusion due to the relatively long time of more than two weeks between the baseline scan and the start of CPI treatment. To be able to use TGR in a more standardized way we recommend stricter follow up protocols with the baseline CT scan and start of therapy ideally being on the

same day. In the case of this study, up to 47% extra patients could have been included if this stricter follow up protocol would have been implemented. Another limitation of the current study is that it is a retrospective analysis. The selection of target lesions may not perfectly reflect the evolution of the whole tumor burden and new lesions were not accounted for. Moreover, we assumed that tumors do grow as spheres, while we know this is not always the case[26]. It remains to be determined whether response assessment using RECIST is the optimal basis to determine the TGR in immunotherapy. To differentiate early HPD from pseudo-progression is another pitfall in this treatment type, further underlining the importance of imaging at defined intervals, close monitoring and clear definitions.

To date, there is no definition of TGR for growth assessment in treatment with immunotherapeutic agents and it is still unclear which factors influence TGR. Tumor growth rate integrates the time interval between CT-scans allowing a quantitative assessment of the dynamics and kinetics of the tumor. But, as can be seen in figures 2B and C, TGR is more difficult to correlate with the RECIST criteria because the percentage in which TGR is expressed does not match the RECIST thresholds. To make TGR more related to the way tumor evaluation takes place using RECIST, the factor time was integrated into the SLD measurements, resulting in a SLDdifference in percentage over 6 weeks. This could possibly be a more accessible expression in everyday practice for tumor growth kinetics when used only to evaluate if tumor growth is increasing, decreasing or if it is shrinking. To find the predictors and to understand the biological mechanisms underlying the variable therapeutic effects, prospective studies with close monitoring and biopsies are necessary. But, by starting to visualize and monitor tumor growth kinetics before and after onset of therapy, insight into the response patterns in immunotherapy treatment can already be improved. In current clinical practice, we are already calculating the SLDdifference of the target lesion to evaluate RECIST response between two CT-scans at a certain treatment point. If these results are put in a graph from the first available scan, a visual representation of the growth rate changes over time and how treatments are influencing these, will be obtained. Because TGR is calculated from the same measurements that determine RECIST, extra work for the radiologist would be avoided. Ideally, an integrated software application or a web page would be developed in which the SLD is entered, after which it visualizes the tumor growth kinetics in a graph that represents the evolution over the different follow up moments. When more widely used, and more data becomes available, graphs could be validated and cut off values for treatment planning could be determined. In summary, in this study, tumor growth dynamics provide clinically relevant information and additional information about response to using RECIST alone. In the current computer driven medical world, calculating and visualizing tumor growth kinetics before and during treatment can potentially improve treatment planning, and might help to decide early which patients might, and might not benefit from their treatment with CPI.

REFERENCES

1. Berger KN, Pu JJ. PD-1 pathway and its clinical application: A 20year journey after discovery of the complete human PD-1 gene. Gene 2018; 638: 20–25.
2. Ledford H. Promising cancer drugs may speed tumours in some patients. Nature 2017; 544: 13–14.
3. Eisenhauer EA, Therasse P, Bogaerts J, Schwartz LH, Sargent D, Ford R, Dancey J, Arbuck S, Gwyther S, Mooney M, Rubinstein L, Shankar L, Dodd L, Kaplan R, Lacombe D, Verweij J. New response evaluation criteria in solid tumours: revised RECIST guideline (version 1.1). Eur. J. Cancer Oxf. Engl. 1990 2009; 45: 228–247.
4. Chiou VL, Burotto M. Pseudoprogression and Immune-Related Response in Solid Tumors. J. Clin. Oncol. 2015; 33: 3541–3543.
5. Kurra V, Sullivan RJ, Gainor JF, Hodi FS, Gandhi L, Sadow CA, Harris GJ, Flaherty K, Lee S. Pseudoprogression in cancer immunotherapy: Rates, time course and patient outcomes. J. Clin. Oncol. 2016; 34: 6580–6580.
6. Kurman JS, Murgu SD. Hyperprogressive disease in patients with non-small cell lung cancer on immunotherapy. J. Thorac. Dis. 2018; 10: 1124–1128.
7. Seymour L, Bogaerts J, Perrone A, Ford R, Schwartz LH, Mandrekar S, Lin NU, Litière S, Dancey J, Chen A, Hodi FS, Therasse P, Hoekstra OS, Shankar LK, Wolchok JD, Ballinger M, Caramella C, de Vries EGE. iRECIST: guidelines for response criteria for use in trials testing immunotherapeutics. Lancet Oncol. 2017; 18: e143–e152.
8. Champiat S, Ferrara R, Massard C, Besse B, Marabelle A, Soria J-C, Ferté C. Hyperprogressive disease: recognizing a novel pattern to improve patient management. Nat. Rev. Clin. Oncol. 2018; 15: 748–762.
9. Benjamin RS, Choi H, Macapinlac HA, Burgess MA, Patel SR, Chen LL, Podoloff DA, Charnsangavej C. We should desist using RECIST, at least in GIST. J. Clin. Oncol. Off. J. Am. Soc. Clin. Oncol. 2007; 25: 1760–1764.
10. Ratain MJ, Eckhardt SG. Phase II studies of modern drugs directed against new targets: if you are fazed, too, then resist RECIST. J. Clin. Oncol. Off. J. Am. Soc. Clin. Oncol. 2004; 22: 4442–4445.
11. Maitland ML, Schwartz LH, Ratain MJ. Time to tumor growth: a model end point and new metric system for oncology clinical trials. J. Clin. Oncol. Off. J. Am. Soc. Clin. Oncol. 2013; 31: 2070–2072.
12. Nathan PD, Vinayan A, Stott D, Juttla J, Goh V. CT response assessment combining reduction in both size and arterial phase density correlates with time to progression in metastatic renal cancer patients treated with targeted therapies. Cancer Biol. Ther. 2010; 9: 15–19.
13. Grande E, Martínez-Sáez O, Gajate-Borau P, Alonso-Gordoa T. Translating new data to the daily practice in second line treatment of renal cell carcinoma: The role of tumor growth rate. World J. Clin. Oncol. 2017; 8: 100–105.
14. Saada-Bouzid E, Defaucheux C, Karabajakian A, Palomar Coloma V, Servois V, Paoletti X, Even C, Fayette J, Guigay J, Loirat D, Romano E, Le Tourneau C. Tumor's flare-up and patterns of recurrence in patients (pts) with recurrent and/or metastatic (R/M) head and neck squamous cell carcinoma (HNSCC) treated with anti-PD1/PD-L1 inhibitors. J. Clin. Oncol. 2016; 34: 6072–6072.

15. Lahmar J, Facchinetti F, Koscielny S, Ferte C, Mezquita L, Bluthgen MV, Lindsay CR, Adam J, Planchard D, Soria J-C, Besse B, Caramella C. Effect of tumor growth rate (TGR) on response patterns of checkpoint inhibitors in non-small cell lung cancer (NSCLC). J. Clin. Oncol. 2016; 34: 9034–9034.
16. Champiat S, Dercle L, Ammari S, Massard C, Hollebecque A, Postel-Vinay S, Chaput N, Eggermont A, Marabelle A, Soria J-C, Ferté C. Hyperprogressive Disease Is a New Pattern of Progression in Cancer Patients Treated by Anti-PD-1/PD-L1. Clin. Cancer Res. Off. J. Am. Assoc. Cancer Res. 2017; 23: 1920–1928.
17. Saâda-Bouzid E, Defaucheux C, Karabajakian A, Coloma VP, Servois V, Paoletti X, Even C, Fayette J, Guigay J, Loirat D, Peyrade F, Alt M, Gal J, Le Tourneau C. Hyperprogression during anti-PD-1/PD-L1 therapy in patients with recurrent and/or metastatic head and neck squamous cell carcinoma. Ann. Oncol. Off. J. Eur. Soc. Med. Oncol. 2017; 28: 1605–1611.
18. Kato S, Goodman A, Walavalkar V, Barkauskas DA, Sharabi A, Kurzrock R. Hyperprogressors after Immunotherapy: Analysis of Genomic Alterations Associated with Accelerated Growth Rate. Clin. Cancer Res. Off. J. Am. Assoc. Cancer Res. 2017; 23: 4242–4250.
19. Ferrara R, Caramella C, Texier M, Audigier Valette C, Tessonnier L, Mezquita L, Lahmar J, Mazieres J, Zalcman G, Brosseau S, Westeel V, Le Moulec S, Leroy L, Duchemann B, Veillon R, Planchard D, Boucher M, Koscielny S, Soria J-C, Besse B. Hyperprogressive disease (HPD) is frequent in non-small cell lung cancer (NSCLC) patients (pts) treated with anti PD1/PD-L1 monoclonal antibodies. Annals of Oncology 2017; : suppl_5.
20. Ferrara R, Mezquita L, Texier M, Lahmar J, Audigier-Valette C, Tessonnier L, Mazieres J, Zalcman G, Brosseau S, Moulec SL, Leroy L, Duchemann B, Lefebvre C, Veillon R, Westeel V, Koscielny S, Champiat S, Ferté C, Planchard D, Remon J, Boucher M-E, Gazzah A, Adam J, Bria E, Tortora G, Soria J-C, Besse B, Caramella C. Hyperprogressive Disease in Patients With Advanced Non-Small Cell Lung Cancer Treated With PD-1/PD-L1 Inhibitors or With Single-Agent Chemotherapy. JAMA Oncol. 2018; 4: 1543–1552.
21. Stein WD, Wilkerson J, Kim ST, Huang X, Motzer RJ, Fojo AT, Bates SE. Analyzing the pivotal trial that compared sunitinib and IFN-α in renal cell carcinoma, using a method that assesses tumor regression and growth. Clin. Cancer Res. Off. J. Am. Assoc. Cancer Res. 2012; 18: 2374–2381.
22. Ferté C, Fernandez M, Hollebecque A, Koscielny S, Levy A, Massard C, Balheda R, Bot B, Gomez-Roca C, Dromain C, Ammari S, Soria J-C. Tumor growth rate is an early indicator of antitumor drug activity in phase I clinical trials. Clin. Cancer Res. Off. J. Am. Assoc. Cancer Res. 2014; 20: 246–252.
23. Ferté C, Koscielny S, Albiges L, Rocher L, Soria J-C, Iacovelli R, Loriot Y, Fizazi K, Escudier B. Tumor growth rate provides useful information to evaluate sorafenib and everolimus treatment in metastatic renal cell carcinoma patients: an integrated analysis of the TARGET and RECORD phase 3 trial data. Eur. Urol. 2014; 65: 713–720.
24. Gomez-Roca C, Koscielny S, Ribrag V, Dromain C, Marzouk I, Bidault F, Bahleda R, Ferté C, Massard C, Soria J-C. Tumour growth rates and RECIST criteria in early drug development. Eur. J. Cancer Oxf. Engl. 1990 2011; 47: 2512-2516.

25. Schiavon G, Ruggiero A, Schöffski P, van der Holt B, Bekers DJ, Eechoute K, Vandecaveye V, Krestin GP, Verweij J, Sleijfer S, Mathijssen RHJ. Tumor volume as an alternative response measurement for imatinib treated GIST patients. PloS One 2012; 7: e48372.
26. Schiavon G, Ruggiero A, Bekers DJ, Barry PA, Sleijfer S, Kloth J, Krestin GP, Schöffski P, Verweij J, Mathijssen RHJ. The effect of baseline morphology and its change during treatment on the accuracy of Response Evaluation Criteria in Solid Tumours in assessment of liver metastases. Eur. J. Cancer Oxf. Engl. 1990 2014; 50: 972–980.

SUPPLEMENTARY INFORMATION

Supplementary Table 1. Patient and tumor characteristics at the start of checkpoint inhibitor therapy

Characteristic	N	%
Gender		
Male	34	59%
Female	24	41%
Age		
Median	64	
Mean	63	
Range	35 - 79	
Diagnosis		
Invasive adenocarcinoma	41	71%
Squamous cell carcinoma	13	22%
NSCLC NOS	1	2%
Great cell	1	2%
unknown	2	3%
Smoking		
Never	6	10%
Ex	34	59%
Current	11	19%
Ex/current	3	5%
unknown	4	7%
Therapies before start		
Chemotherapy	58	100%
Thoracic radiotherapy (*N=56*)	22	39%
No. months Nivolumab (*N=55*)		
Median	4	
Mean	6	
Range	0 – 25	
Best overall response Nivolumab		
Complete response	1	2%
Partial response	16	28%
Stable disease	16	28%
Progressive disease	13	21%
Not evaluable/Unknown	13	21%

CHAPTER 8

Tumor mutational load, CD8+ T cells, expression of PD-L1 and HLA class I to guide immunotherapy decisions in NSCLC patients

Daan P. Hurkmans, Merian E. Kuipers, Jasper Smit, Ronald van Marion, Ron H.J. Mathijssen, Piet E. Postmus, Pieter S. Hiemstra, Joachim G.J.V. Aerts, Jan H. von der Thüsen*, Sjoerd H. van der Burg*

*shared senior authorship

Cancer Immunology Immunotherapy, May 2020, 69: page 771-777

Introduction: A minority of NSCLC patients benefit from anti-PD1 immune checkpoint inhibitors. A rational combination of biomarkers is needed. The objective was to determine the predictive value of tumor mutational load (TML), $CD8^+$ T cell infiltration, HLA class-I and PD-L1 expression in the tumor.

Materials and Methods: Metastatic NSCLC patients were prospectively included in an immune-monitoring trial (NTR7015) between April 2016-August 2017, retrospectively analyzed in FFPE tissue for TML (NGS: 409 cancer-related-genes) and by IHC staining to score PD-L1, $CD8^+$ T cell infiltration, HLA class-I. PFS (RECISTv1.1) and OS were analyzed by Kaplan-Meier methodology.

Results: 30 patients with adenocarcinoma (67%) or squamous cell carcinoma (33%) were included. High TML was associated with better PFS (p=0.004) and OS (p=0.025). Interaction analyses revealed that patients with both high TML and high total $CD8^+$ T cell infiltrate (p=0.023) or no loss of HLA class-I (p=0.026), patients with high total $CD8^+$ T cell infiltrate and no loss of HLA class-I (p=0.041) or patients with both high PD-L1 and high TML (p=0.003) or no loss of HLA class-I (p=0.032) were significantly associated with better PFS. Unsupervised cluster analysis based on these markers revealed three sub-clusters, of which cluster-1A was overrepresented by patients with progressive disease (15 out of 16), with significant effect on PFS (p=0.007).

Discussion: This proof-of-concept study suggests that a combination of PD-L1 expression, TML, $CD8^+$ T cell infiltration and HLA class-I functions as a better predictive biomarker for response to anti-PD-1 immunotherapy. Consequently, refinement of this set of biomarkers and validation in a larger set of patients is warranted.

Précis

The findings suggest that a rational combination of biomarkers – PD-L1, TML, CD8+ T cell infiltration and classical HLA – improves response prediction of immunotherapy in lung cancer.

Abstract

INTRODUCTION

Tumors evade T-cell mediated destruction by exploiting inhibitory immune checkpoints such as the PD-1/ PD-L1 pathway. The efficacy of treatment with immune checkpoint inhibitors (ICIs) targeting this pathway in non–small-cell lung cancer (NSCLC) is limited, and better use of biomarkers is needed to predict response to treatment [1].

The currently most widely used biomarker is PD-L1 expression in the tumor, as assessed by the PD-L1 tumor proportion score (TPS), which is positively associated with a response to ICI treatment in metastatic NSCLC patients [2]. However, the performance of the PD-L1 assay to predict clinical response remains poor [3].

The presence of tumor infiltrating $CD8^+$ T cells which recognize tumor antigens, when presented at the tumor cell surface in the context of HLA class I, is a prerequisite for successful ICI treatment. A surrogate marker for recognition of tumor antigens is tumor mutational load (TML), a measurement of the frequency of mutations in tumor cells, that correlates with the number of neoantigens that can be recognized by $CD8^+$ T cells [4]. Next-generation genome sequencing (NGS) panels composed of about 300-600 cancer-related genes are designed to predict the TML with similar accuracy as whole exome sequencing [5]. A strong $CD8^+$ type 1 T cell infiltration of tumors critically contributes to a better clinical outcome in cancer, including NSCLC [4]. Conversely, (partial) loss of HLA occurs in a sizeable fraction of NSCLC tumors, as well as HLA diversity modulate the prognostic impact of tumor-infiltrating $CD8^+$ T cells, and thus survival after checkpoint blockade [6-9]. While TML is an emerging biomarker, $CD8^+$ T cell infiltration and HLA expression have not been considered as predictive biomarkers in NSCLC.

Therefore, this study is the first to determine the predictive value of the TML, $CD8^+$ T cells and HLA class I expression in combination with the PD-L1 expression in anti-PD-1 treated NSCLC.

MATERIALS AND METHODS

Study population

Patients with stage IV NSCLC who started nivolumab monotherapy between April 2016 and August 2017 at the Erasmus University Medical Center, Rotterdam, The Netherlands, were included prospectively in the MULTOMAB study (Dutch Trial Registry NTR7015/ NL6828). The study was approved by the independent ethics committee (Medical Research Ethics Committee Erasmus MC; MEC 16-011) and all patients provided written informed consent. Patients were randomly selected and assessed for eligibility. Patients with NSCLC stage IV were included who had been treated with nivolumab monotherapy (weight-based dosing: 3mg/kg i.v., Q2W) and who were evaluable by RECIST v1.1. Patients who were treated with a prior line of immunotherapy were excluded. The median follow-

up time was 27 weeks (interquartile range: 14-46 weeks) and the median time between diagnostic biopsy and first administration of nivolumab was 5 weeks (interquartile range: 1-41 weeks). The use of archival formalin-fixed, paraffin-embedded (FFPE) samples was in accordance with guidelines from the Dutch Federation of Medical Research and was approved by the independent ethics committee (Medical Research Ethics Committee Erasmus MC; MEC 17-1186). Specimen handling and all biomarker assay analyses were undertaken blinded; a unique code was assigned for each patient, with a separate list linking these codes with the patient characteristics and outcomes.

TML assay

Mutational load was determined by the Oncomine TML assay (ThermoFisher Scientific, Waltham, MA) according to manufacturer's protocol on an Ion Torrent S5 XL next-generation sequencing platform (Gilford, NH). Mutational load is defined as the number of somatic nonsynonymous variants (missense and nonsense single nucleotide variants plus insertions and deletions) detected per megabase of exonic sequence with sufficient coverage. Germline variants were filtered out using the Mutation Load Calculation Filter Chain in Ion Reporter software 5.10 (ThermoFisher Scientific, Waltham, MA). A TML cut-off of 11 mut/Mb was used to differentiate between tumors with low or high TML.

Immunohistochemistry on FFPE samples

Expression patterns of classical HLA (HLA-A and HLA-B/C) were assessed according to the Ruiter scoring system [10] as described before [8]. The intensity and percentage of cells in the tumor were determined based on the sum of the intensity of staining (ranging from 0-3) and percentage positive cells (ranging from 0-5). Loss of HLA class I was defined by a low Ruiter score (0-3) of both HLA-A and HLA-B/C. Patients were dichotomized for low or high total $CD8^+$ T cell infiltration based on the mean $CD8^+$ T cell infiltration for all patients, and for low (<50%) or high (≥50%) PD-L1 TPS (using the ready-to-use SP263 Ab clone on a Ventana Benchmark Ultra (both form Roche Diagnostics, Tucson, AZ) system according to the manufacturer's instructions. Mouse monoclonal Abs HCA-2 and HC-10 (tissue culture supernatant respectively anti HLA-A, 1:500, and anti HLA-B/-C, 1:750; a generous gift from Prof. dr. J. Neefjes, Department of Cell and Chemical Biology, LUMC) were used to detect the free heavy chain of the classical HLA-A and HLA- B/-C molecule). The detection of $CD8^+$ T-cells was done by using mouse monoclonal CD8 Ab (clone IA5, Leica Biosystems, Germany, 1:500). PD-L1 TPS was determined by using clone SP263 (Ventana PD-L1 assay, Roche, Switzerland).

Statistical analysis

Best overall response (BOR) was assessed according to RECIST v1.1 for complete response (CR), partial response (PR), stable disease (SD) and progressive disease (PD): minimum duration of 90 days for SD was required, confirmation of CR or PR was not necessary. PFS

was defined as the time between the first administration of nivolumab until PD or death due to any cause, and OS until death due to any case. Survival was compared by log-rank test using Kaplan-Meier methodology. Group comparisons of categorical data were performed by 2-tailed χ^2 or Fisher's Exact test. Differences with two-sided P values <0.05 were considered significant. No power analysis was performed in this proof-of-concept study. R version 1.1.453 (R-project, www.rproject.org) was used for hierarchical cluster analysis with complete linkage by Manhattan distance measure, using the mean for missing values, statistical software package SPSS v24.0.0.1 (SPSS, Chicago, USA) was used for further statistical analysis.

RESULTS

A total of 99 patients were assessed for eligibility, of whom 69 patients were excluded because of either insufficient or poor quality of samples (n=33), or failure to obtain FFPE material from referring hospitals (n=36). 30 patients were analyzed (**Table 1**). The mean duration of nivolumab treatment was 5.4 months (SD: 4.6). Two patients (6%) developed severe immune-related toxicity (grade 3/4, according to CTCAE 4.03). All patients had at least one prior line of chemotherapy, consisting of platinum-based doublet chemotherapy, and three patients were also treated with an EGFR tyrosine kinase inhibitor. The mean duration of response to first line chemotherapy was 7.2 months (SD: 4.7). Examples of two representative patients are shown in **Fig. 1a**, displaying TML and IHC staining of classical HLA, $CD8^+$ T cells and PD-L1.

First, the prognostic effect of each parameter on PFS (**Fig. 2a-d**) and OS (**Fig. S1a-d**) was determined. High TML was significantly associated with better PFS (p=0.004) and OS (p=0.025). PD-L1 was associated with improved PFS (p=0.027), but not with OS (p=0.121). $CD8^+$ T cells and HLA as individual biomarkers were not significantly associated with better OS or PFS, which was expected [8], although normal expression of HLA class I resulted in the better OS and PFS when compared to complete or partial loss of HLA expression. Complete loss was defined by a low score (0-2), partial loss by an intermediate score (3-6), and normal expression by a high score (7-8). Patients with complete loss had impaired PFS compared to patients with partial loss or normal expression of HLA class I (**Fig. S2**).

Table 1: Patient characteristics, TML and IHC patterns at baseline.

Patient characteristics		**number**	**mean (SD)**
Age (years), *number, mean (SD)*		30	64 (8.6)
		number	**(%)**
Gender			
	Male	18	(60.0)
	Female	12	(40.0)
NSCLC type			
	SCC	10	(33.3)
	Adenocarcinoma	20	(66.6)
Regimen			
	Nivolumab	30	(100)
Prior chemotherapy			
	Yes	30	(100)
History of smoking			
	Yes	23	(88.5)
	No	2	(11.5)
TML			
	Low	17	(68.0)
	High	8	(32.0
HLA-A			
	Low	14	(48.3)
	High	15	(51.7)
HLA-B/C			
	Low	12	(41.4)
	High	17	(58.6)
Total $CD8^+$			
	Low	16	(57.1)
	High	12	(42.9)
PD-L1 (TPS)			
	Neg (0%)	11	(40.7)
	Pos ($\geq$1%)	16	(59.3)

From a total of 99 eligible patients, 69 were non-evaluable for this analysis, because either there was no sufficient archived FFPE tissue (n=31), FFPE tissue could not be obtained from the referring hospital (n=36) or the tissue was of poor quality (n=2). The expression patterns of HLA-A and HLA-B/C as well as the total $CD8^+$ T cell infiltration in these patients were similar to what we reported before in a comparable group of NSCLC patients (10).

Figure 1. Patient examples and cluster analysis

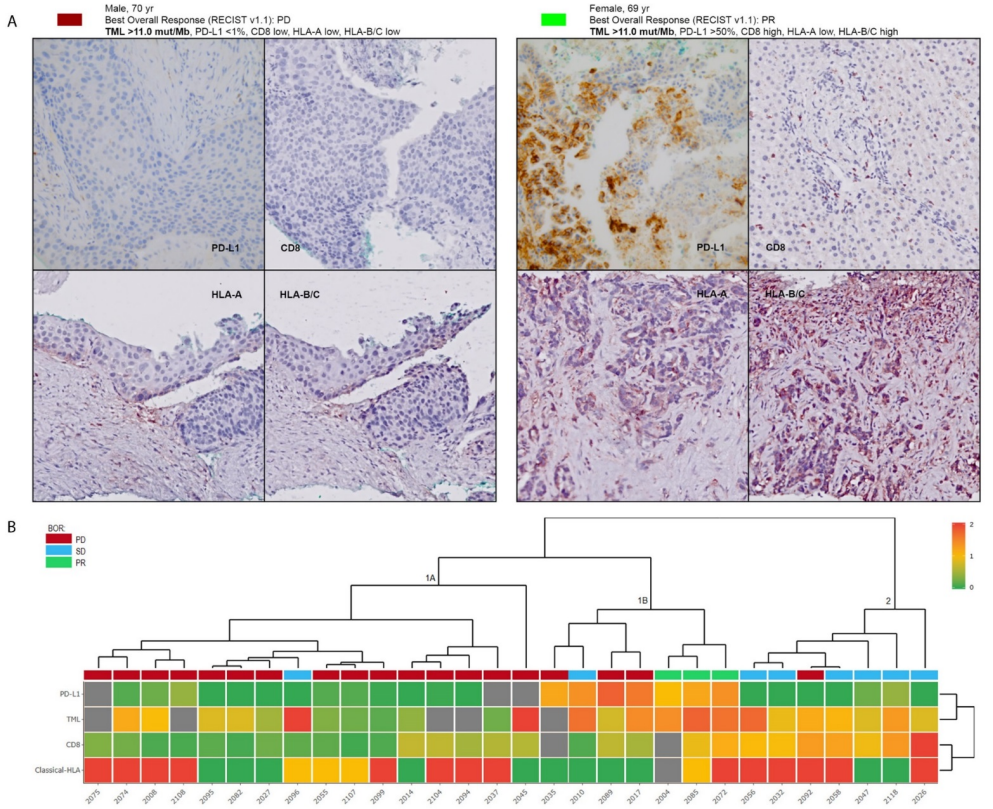

Example of two patients showing the BOR (RECIST v1.1): TML NGS output, and the IHC of HLA-A, HLA-B/C, total CD8+ and PD-L1. For HLA, the percentage of positive tumor cells was classified (0-5) and the intensity of the staining (0-3), resulting in a final score based on both (0-8) and was categorized as 0-3 (low) or 4-8 (high); according to the Ruiter scoring system. Loss of classical HLA was defined as absent expression (0-3) of both HLA-A and HLA-B/C IHC. Magnification x20. b Heat map of unsupervised cluster analysis based on classical HLA, total CD8 tumor infiltration, TML and PD-L1 revealing three distinct clusters (1-3). BOR by RECIST v1.1 was incorporated in the heat map.

Figure 2. PFS analysis

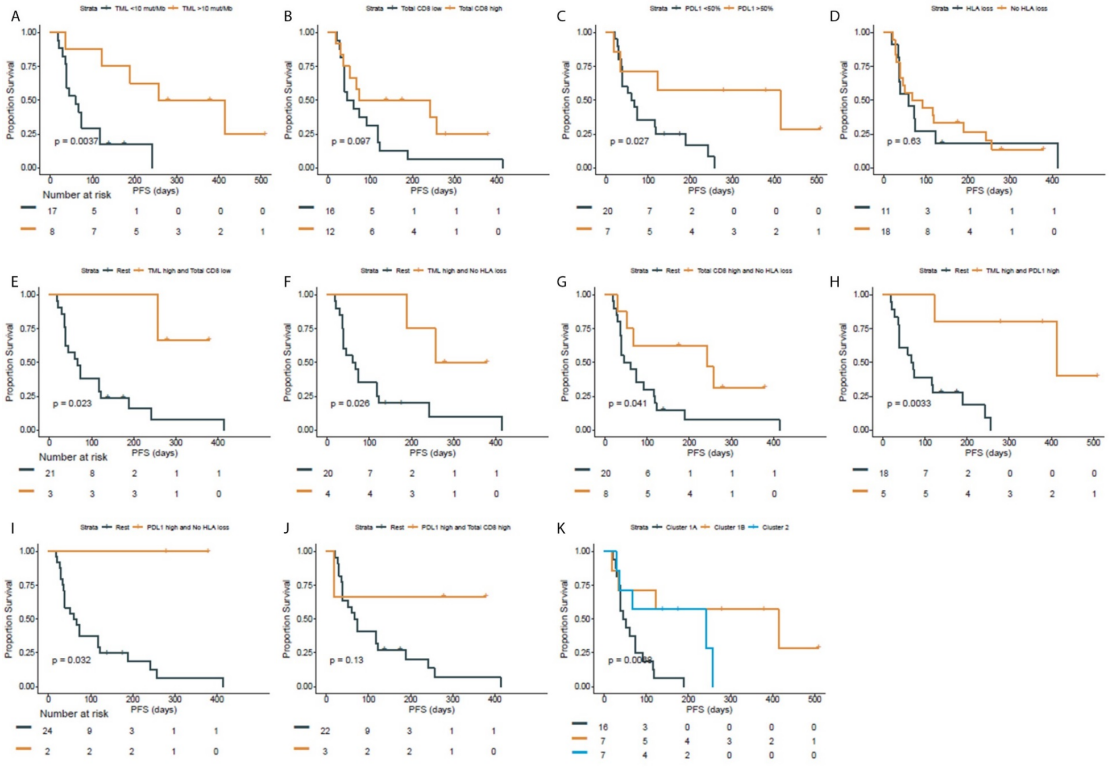

Kaplan-Meier plots showing the PFS by a TML high (>11 mut/Mb) vs. low (<11 mut/Mb), b CD8+ T cell infiltration high vs. low, c PD-L1 high (>50%) vs low, d classical HLA (-A and –B/C) loss vs. rest, e TML high and total CD8+ high vs. rest, f TML high and no loss of classical HLA vs. rest, g total CD8+ high and no loss of classical HLA vs. rest, h TML high and PD-L1 high vs. rest, i PD-L1 high and no loss of classical HLA vs. rest, j PD-L1 high and CD8+ high vs. rest and k cluster (cluster 1A, 1B and 2).

However, interaction analyses between these two markers and the other markers revealed that each combination of two markers was significantly associated with better PFS (**Fig. 2e-j**), except for PD-L1 with $CD8^+$ T cells due to low power. Specifically, 1) high TML and either high total $CD8^+$ T cell infiltration (p=0.023) or no loss of HLA class I (p=0.026), 2) high total $CD8^+$ T cell infiltration and no loss of HLA class I (p=0.041), and 3) high PD-L1 and either high TML (p=0.003) or no loss of HLA class I (p=0.032) was associated with better PFS.

Next, the patients were divided into two groups on the basis of a clinical response (CR/PR/SD) or failure to respond (PD) to nivolumab treatment (**Table S1**). This revealed a significant overrepresentation of patients with a high TML (p=0.043) and/or more profound total $CD8^+$ T cell infiltration (p=0.005) among clinical responders. This association was not found for HLA class I expression or PD-L1 (TPS $\geq$1% or $\geq$50%).

A comparison of the absolute values for all these parameters confirmed that the mean TML (p=0.001) and mean total $CD8^+$ T cell infiltrate (p=0.004) were higher in the group of patients with a treatment response (**Table S2**). Notably, the TML was not directly correlated with $CD8^+$ T-cell infiltration or HLA expression, but was positively associated with PD-L1 (p=0.035; **Table S3**).

Lastly, an unsupervised cluster analysis based on the four parameters was performed. This revealed two major clusters and a total of three sub-clusters **(Fig. 1b**). Cluster 1A was overrepresented by patients with PD (15 out of 16) of which the tumors were negative for 2-3 of the 4 biomarkers. Cluster 2 almost exclusively comprised patients with SD of which the tumor was positive for 2-3 biomarkers but did not express PD-L1. Survival analyses of the 3 different clusters (**Fig. 2k** and **Fig. S1k**) indicate a significant effect on PFS (p=0.007), while the OS (p=0.74) was significant in a post-hoc comparison of cluster 1A with 1B (p=0.048).

DISCUSSION

The present proof-of-concept study suggests that in addition to PD-L1 expression also TML, $CD8^+$ T cell infiltration and HLA class I expression are associated with PFS and predict the response to anti-PD-1 immunotherapy. Interestingly, unsupervised cluster analysis of the patients based on all four markers revealed one cluster pattern that almost exclusively identified non-responders (cluster 1A). In the current real-life setting, only a small amount of archival material could be used for TML determination and IHC staining, derived from routine biopsy specimens from the primary tumor and following initial diagnostic procedures (including routine NGS testing for driver mutations in some cases). We were able to demonstrate the clinical value of TML analysis in this immuno-oncology setting, and we believe this is the first study to do so in combination with a range of IHC biomarkers in small, realistic biopsy specimens.

Our findings are consistent with previous studies in different settings, although those studies cannot be generalized. Associations between TMB and immune signatures are generally cancer type dependent [11], and it can be assumed that they are also tumor stage dependent. In addition, a prospective study in early-stage untreated NSCLC patients demonstrated a significant and independent association of low immune-evasion capacity (defined as tumors with no immune editing potential, no HLA loss and no antigen processing machinery [APM] defects) and high number of neoantigens with increased disease-free survival [12].

Moreover, release of checkpoint blockade by nivolumab may result in a series of dynamic changes in the composition of the tumor microenvironment [13] which override the current prediction (false negatives), but this was not taken into account as we were limited to the use of archival material prior to ICI therapy. Notably, a significant correlation between PD-L1 expression and TML was determined, which may contradict accumulating evidence from clinical trials [14]. This may be related to the limited number of patients, but may also result from the use of continuous covariates rather than stratified data in clinical trials where true correlations may easily be overlooked. Based on our findings, it could not be established that TML and PD-L1 serve as an independent biomarker for clinical outcome.

An interesting finding of this study is the added value of expression of HLA class I molecules on cancer cells, which is known to be crucial for the recognition of tumor cells by CD8+ TCs. In our opinion, the actual detection of HLA class I expression is more valuable as a future biomarker for ICIs than genetic, epigenetic, transcriptional, post-transcriptional or post-translational aberrations, such as loss of heterozygosity in *HLA* or *B2M* mutations, since protein expression is the ultimate outcome of all those changes. For instance, genetic studies have revealed that *NLRC5*, an HLA class I transactivator, is an important target for cancer immune evasion. The expression of *NLRC5* correlated with that of HLA class I and negatively correlated with OS in stage III NSCLC [15]. We focused primarily on the expression of HLA class I and did not determine selective APM defects, while this could also affect the recognition of tumor antigens by the immune system. For HLA peptides to be presented to CD8+ T cells, peptides must be processed by proteolysis, trimmed by enzymes to fit into the groove of HLA molecules, and transported intracellularly by peptide transporters, endoplasmic reticulum chaperones and the Golgi apparatus. The antigen presenting pathway often is altered in cancer, including lung cancer [16,17]. Further studies should be directed at investigating the impact of the APM defects on response to ICIs. Last but not least, due to the relatively low patient numbers, we decided to take complete loss defined as a low score (0-3) of both HLA-A and HLA-B/C, but not partial HLA class I loss into consideration. However, a subgroup analysis showed that patients with complete loss have impaired OS and PFS compared to patients with no loss of HLA class I. The PFS of patients with partial loss was comparable to that of patients with no loss of HLA class I.

Taken together, the findings support the hypothesis that a rational combination of biomarkers – based on the biological requirements for the ICIs to work – may contribute to a more adequate response prediction of ICI treatment in NSCLC. Consequently, refinement of this proposed set of biomarkers and validation in a greater set of patients is warranted.

REFERENCES

1. Sacher AG, Gandhi L. Biomarkers for the Clinical Use of PD-1/PD-L1 Inhibitors in Non-Small-Cell Lung Cancer: A Review. *JAMA Oncol.* 2016;2(9):1217-1222.
2. Topalian SL, Taube JM, Anders RA, Pardoll DM. Mechanism-driven biomarkers to guide immune checkpoint blockade in cancer therapy. *Nat Rev Cancer.* 2016;16(5):275-287.
3. Fujimoto D, Sato Y, Uehara K, et al. Predictive Performance of Four Programmed Cell Death Ligand 1 Assay Systems on Nivolumab Response in Previously Treated Patients with Non-Small Cell Lung Cancer. *J Thorac Oncol.* 2018;13(3):377-386.
4. Rizvi NA, Hellmann MD, Snyder A, et al. Cancer immunology. Mutational landscape determines sensitivity to PD-1 blockade in non-small cell lung cancer. *Science.* 2015;348(6230):124-128.
5. Chaudhary R, Quagliata L, Martin JP, et al. A scalable solution for tumor mutational burden from formalin-fixed, paraffin-embedded samples using the Oncomine Tumor Mutation Load Assay. *Transl Lung Cancer Res.* 2018;7(6):616-630.
6. Mehta AM, Jordanova ES, Kenter GG, Ferrone S, Fleuren GJ. Association of antigen processing machinery and HLA class I defects with clinicopathological outcome in cervical carcinoma. *Cancer Immunol Immunother.* 2008;57(2):197-206.
7. McGranahan N, Rosenthal R, Hiley CT, et al. Allele-Specific HLA Loss and Immune Escape in Lung Cancer Evolution. *Cell.* 2017;171(6):1259-1271 e1211.
8. Talebian Yazdi M, van Riet S, van Schadewijk A, et al. The positive prognostic effect of stromal CD8+ tumor-infiltrating T cells is restrained by the expression of HLA-E in non-small cell lung carcinoma. *Oncotarget.* 2016;7(3):3477-3488.
9. Chowell D, Morris LGT, Grigg CM, et al. Patient HLA class I genotype influences cancer response to checkpoint blockade immunotherapy. *Science.* 2018;359(6375):582-587.
10. Ruiter DJ, Ferrier CM, van Muijen GN, et al. Quality control of immunohistochemical evaluation of tumour-associated plasminogen activators and related components. European BIOMED-1 Concerted Action on Clinical Relevance of Proteases in Tumour Invasion and Metastasis. *Eur J Cancer.* 1998;34(9):1334-1340.
11. Wang X, Li M. Correlate tumor mutation burden with immune signatures in human cancers. *BMC Immunol.* 2019;20(1):4.
12. Rosenthal R, Cadieux EL, Salgado R, et al. Neoantigen-directed immune escape in lung cancer evolution. *Nature.* 2019;567(7749):479-485.
13. Buck MD, Sowell RT, Kaech SM, Pearce EL. Metabolic Instruction of Immunity. *Cell.* 2017;169(4):570-586.
14. Gandara DR, Paul SM, Kowanetz M, et al. Blood-based tumor mutational burden as a predictor of clinical benefit in non-small-cell lung cancer patients treated with atezolizumab. *Nat Med.* 2018;24(9):1441-1448.
15. Weber JS, D'Angelo SP, Minor D, et al. Nivolumab versus chemotherapy in patients with advanced melanoma who progressed after anti-CTLA-4 treatment (CheckMate 037): a randomised, controlled, open-label, phase 3 trial. *Lancet Oncol.* 2015;16(4):375-384.

16. Durgeau A, Virk Y, Gros G, et al. Human preprocalcitonin self-antigen generates TAP-dependent and -independent epitopes triggering optimised T-cell responses toward immune-escaped tumours. *Nat Commun.* 2018;9(1):5097.
17. Marijt KA, Van Der Burg SH, van Hall T. TEIPP peptides: exploration of unTAPped cancer antigens. *Oncoimmunology.* 2019;8(8):1599639.

SUPPLEMENTARY INFORMATION

Supplementary Table 1. Best overall response analysis.

	Response Number (%)		No response Number (%)		p-value
TML					0.043
Low (<11 mut/Mb)	5	(45.5%)	12	(85.7%)	
High (>11 mut/Mb)	6	(54.5%)	2	(14.3%)	
HLA-A					0.4
Low	4	(40.0%)	10	(52.6%)	
High	6	(60.0%)	9	(47.4%)	
HLA-B/C					0.615
Low	4	(40.0%)	8	(42.1%)	
High	6	(60.0%)	11	(57.9%)	
Total CD8$^+$					0.005
Low	2	(20.0%)	14	(77.8%)	
High	8	(80.0%)	4	(22.2%)	
PD-L1 (TPS)					0.492
Neg (0%)	5	(45.5%)	6	(37.5%)	
Pos (>1%)	6	(54.5%)	10	(62.5%)	
PD-L1 (TPS)					0.279
Low (<50%)	7	(63.6%)	13	(81.3%)	
High (>50%)	4	(36.4%)	3	(18.8%)	

Patient grouping by response to anti-PD1 ICI therapy, comparing TML low vs. high, HLA-A low vs. high, HLA-B/C low vs. high, total CD8+ low vs. high, PD-L1 negative (neg) vs. positive (pos), PD-L1 low (<50%) vs. high (>50%). P-values (1-tailed) by Fisher's Exact test.

Supplementary Table 2. Test of between-subjects effects

	Response Mean (SE)		Non-response Mean (SE)		p-value
TML	10.2	(1.0)	5.2	(0.9)	0.001
HLA-A	5.2	(0.9)	3.2	(0.8)	0.098
HLA-B/C	4.8	(0.8)	3.9	(0.7)	0.407
Total CD8$^+$	58.5	(9.2)	18.5	(8.4)	0.004
PD-L1 (TPS)	23.0	(10.0)	16.3	(9.1)	0.629

Tests of Between-Subjects Effects (n=22) of response comparing individual predictive absolute values of: TML (mut/Mb), HLA-A and HLA-B/C (Ruiter scoring), total CD8$^+$ (cells/mm2), PD-L1 (TPS; %). P-values (1-tailed) by Multivariate testing, excluding patients with missing values.

Supplementary Table 3. Correlation matrix

		PD-L1	Total CD8+	TML	HLA-A	HLA-B/C
PD-L1 (TPS; %)	Correlation Coefficient		0.022	,440*	-0.184	-0.227
	Sig. (2-tailed)		0.916	0.035	0.240	0.147
	Number		25	23	26	26
Total CD8+ (cells/mm2)	Correlation Coefficient	0.022		0.067	0.163	0.086
	Sig. (2-tailed)	0.916		0.754	0.249	0.546
	Number	25		24	28	28
TML (mut/Mb)	Correlation Coefficient	,440*	0.067		0.064	-0.035
	Sig. (2-tailed)	0.035	0.754		0.682	0.820
	Number	23	24		24	24
HLA-A (Ruiter scoring)	Correlation Coefficient	-0.184	0.163	0.064		,623**
	Sig. (2-tailed)	0.240	0.249	0.682		0.000
	Number	26	28	24		29
HLA-B/C (Ruiter scoring)	Correlation Coefficient	-0.227	0.086	-0.035	,623**	
	Sig. (2-tailed)	0.147	0.546	0.820	0.000	
	Number	26	28	24	29	

Correlation matrix of PD-L1 tumor proportional score (TPS; %), total CD8+ T cell infiltration (cells/mm2), TML (mutations/Mb), HLA-A and HLA-B/C (Ruiter Score). Parametric correlations were performed by Pearson correlation coefficient, non-parametric correlations by Kendall's Tau. TML was significantly correlated with PD-L1 (r2=0.440, p=0.035), HLA-A was significantly correlated with HLA-B/C (r2=0.623, p=0.000001).

Supplementary Figure 1. OS analysis

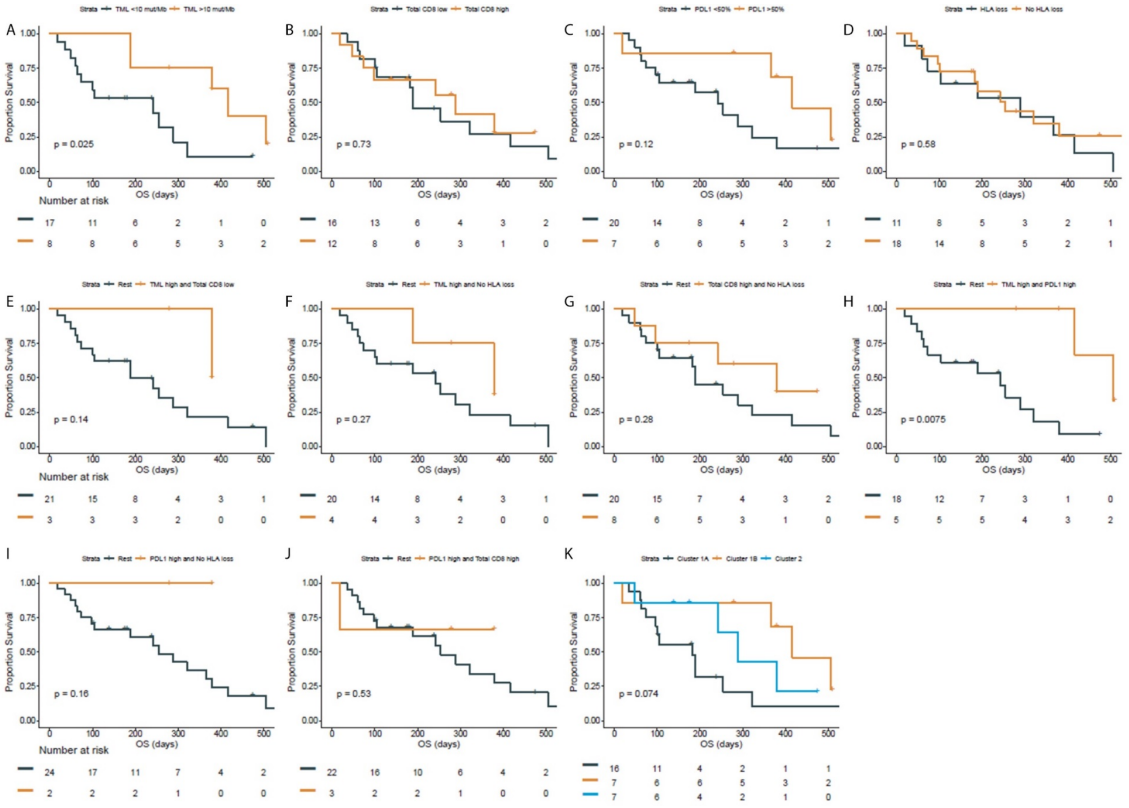

Kaplan-Meier plots showing the overall survival by a TML high (>11 mut/Mb) vs. low (<11 mut/Mb), b CD8+ T cell infiltration high vs. low, c PD-L1 high (>50%) vs low, d classical HLA (-A and –B/C) loss vs. rest, e TML high and total CD8+ high vs. rest, f TML high and no loss of classical HLA vs. rest, g total CD8+ high and no loss of classical HLA vs. rest, h TML high and PD-L1 high vs. rest, i PD-L1 high and no loss of classical HLA vs. rest, j PD-L1 high and CD8+ high vs. rest, k cluster (cluster 1A, 1B and 2).

Supplementary Figure 2. Kaplan-Meier curves based on HLA class I expression

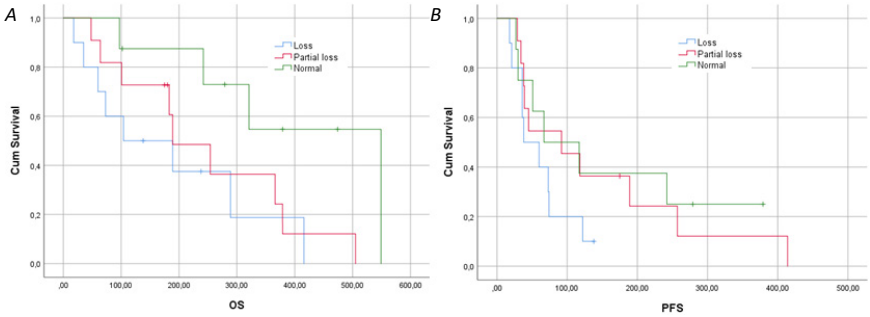

Kaplan-Meier curves showing the a OS en b PFS of patients based on the HLA class I expression: complete loss vs. partial loss vs. no loss of HLA class I. Here, complete loss was defined as 0-2, partial loss as 3-6, and no loss as 7-8. This resulted in a separate score for HLA-A and HLA-B/C. These scores were combined into a single score for HLA class I expression. Statistical tests were non-significant for OS (log rank p=0.055) and PFS (log-rank p=0.298).

CHAPTER 9

9

Granzyme B is correlated with clinical outcome after PD-1-blockade in patients with stage IV non-small-cell lung cancer

Daan P. Hurkmans, Edwin A. Basak, Nina Schepers, E. Oomen – de Hoop, Cor H. van der Leest, Samira El Bouazzaoui, Sander Bins, Stijn L.W. Koolen, Stefan Sleijfer, Astrid A.M. van der Veldt, Reno Debets, Ron H.N. van Schaik, Joachim G.J.V. Aerts, Ron H.J. Mathijssen

Journal for ImmunoTherapy of Cancer, May 2020, 8: 586

Abstract

Introduction: A minority of advanced non-small-cell lung cancer (NSCLC) patients benefit from treatment with immune checkpoint inhibitors (ICIs). Ineffective effector function of activated T and NK cells may lead to reduced tumor cell death, even when these activated effector cells are released from their immune checkpoint brake. Hence, in this study we aimed to assess the association of baseline serum granzyme B, as well as germline variation of the *GZMB* gene, with clinical outcome to PD-1 blockade.

Materials and Methods: A total of 347 stage IV NSCLC patients who started nivolumab treatment between June 2013 and June 2017 were prospectively included. Baseline serum and whole blood was available, allowing for protein quantification and targeted DNA sequencing. Clinical outcome was based on best overall response (BOR) according to RECIST v1.1, PFS, and OS.

Results: Patients with low serum levels of granzyme B had worse PFS (HR 1.96; 95%CI 1.12-3.43; p=0.018) and worse OS (HR 2.08; 95%CI 1.12-3.87; p=0.021) than patients with high baseline serum levels. To validate the findings, germline variation of *GZMB* rs8192917 was assessed. Patients with homozygous and heterozygous variants of *GZMB* rs8192917 had worse BOR (OR:1.60; 95%CI:1.01-2.52; p=0.044) and worse PFS (HR:1.38; 95%CI:1.02-1.87; p=0.036) than wild types.

Discussion: A low baseline serum level of granzyme B and germline variation of *GZMB* was associated with worse clinical outcome in NSCLC, emphasizing the relevance and additional value of monitoring germline genetic variations which mirror cytotoxic functions of T cells in ICI therapy.

INTRODUCTION

Immune checkpoint inhibitors (ICIs) target immune effector cells, predominantly T cells, which may lead to an effective immune response towards tumor cells [1,2]. Although ICIs have shown to significantly improve overall survival (OS) in advanced non-small-cell lung cancer (NSCLC), only a minority of patients benefits from treatment, with an objective response in about one out of five patients [3,4].

The molecular mechanisms underlying resistance to ICI therapy are only partly explained. It is postulated that a combination of factors contribute to response, involving tumor biology, tumor microenvironment, the peripheral immune system, as well as germline genetics [5,6]. PD-1-mediated inhibition targets signalling downstream of the T cell receptor via its downstream phosphatase SHP-2, as well as co-stimulatory molecules [7,8]. Importantly, distorted effector function of activated T and NK cells may lead to reduced tumor cell death, even when these activated effector cells are released from their PD-1 brake.

Previously, it has been demonstrated that immunohistochemical staining and *in vivo* imaging, using positron emission tomography (PET), of intratumoral granzyme B may serve as a predictive biomarker for PD-1 blockade in melanoma [9]. Granzyme B is a key serine protease that is secreted to induce apoptosis, primarily by activated T cells and NK cells [10]. Distortion of granzyme B activity could be linked to reduced entry, trafficking, and accumulation within the cytoplasm of target cells (e.g. tumor cells), and/or linked to reduced enzymatic activity, and hence decreased cleavage of intracellular substrates, such as caspase-3 [11-13].

Taken together, we hypothesise that low baseline serum levels of granzyme B, and consequently alterations of the *GZMB* locus, may contribute to resistance mechanisms of PD-1 blockade. The primary objectives of the current analysis were to assess the association of baseline serum granzyme B levels with progression-free survival (PFS) and overall survival (OS) after PD-1 blockade in NSCLC patients. As a validation, genetic variants of the *GZMB* gene were related with PFS, OS and best overall response (BOR). Secondary objectives were to assess the relationship between serum granzyme B as well as genetic variations of *GZMB* and cytotoxic immune cell populations in blood.

MATERIALS AND METHODS

Study design and data collection

Patients with advanced NSCLC who were treated with PD-1 ICIs between June 2013 and June 2017 at the Erasmus University MC (Rotterdam, The Netherlands) and the Amphia Hospital (Breda, The Netherlands) were prospectively included. Patients with NSCLC stage IV were included who had been treated with nivolumab monotherapy (3mg/kg i.v., Q2W), patients were excluded who were treated with a prior line of immunotherapy.

The study was approved by the independent ethics committee board (MEC 02-1002 and MEC 16-011) and all patients provided written informed consent. Whole blood and baseline serum were available for DNA analysis and protein quantification, respectively. All assays were performed blinded to study endpoints; patients were assigned to a subject number. Patient characteristics included demographic and clinical data. BOR was assessed according to the Response Evaluation Criteria in Solid Tumors version 1.1 (RECIST v1.1) [14]. A minimum duration of 90 days for stable disease (SD) was required. Confirmation of partial response (PR) or complete response (CR) was not required. After treatment initiation, radiological evaluation by computed tomography (CT) was usually performed every 6 weeks. Progression-free survival (PFS) was defined as the time from the first administration of nivolumab until progressive disease (PD), or death due to any cause, whichever occurred first. OS was defined as the time from the first administration of nivolumab until death due to any cause.

Quantitative protein measurement and DNA analysis

Quantitative analysis of granzyme B in serum was performed by a magnetic bead-based assay, using a 1x96-well microplate and magnetic anti-granzyme-B-coated beads (Human Magnetic Luminex Assay, R&D Systems Inc., MN). *GZMB* c.128T>C (rs8192917) was selected primarily based on its presumed contribution to resistance mechanisms of ICIs [9]. A total of twelve single-nucleotide polymorphisms (SNPs) were selected in eight genes based on their contribution to T cell immunity and their correlation with overt T cell responses, such as the autoimmune diseases (AIDs) systemic lupus erythematosus and rheumatoid arthritis. A summary of the correlation of selected SNPs with overt T cell responses is displayed in **suppl. table 1**. SNPs with a minor allele frequency (MAF) of <5% were excluded from the analysis. Linkage disequilibrium was tested using the application LDmatrix of LDlink version 5 (https://ldlink.nci.nih.gov/). Distribution of genotypes was tested for Hardy-Weinberg equilibrium (HWE) using the χ^2 test. Deviations from HWE may reflect genotyping errors, though, may also be a signal of disease association[15], e.g. mutation of tumor suppressor genes. DNA isolation and genotyping for *GZMB* rs8192917, *HLA-A* rs60131261, *IL10* rs3024493, *IL2RA* rs3024493, *IFNG* rs2430561/rs2069705/rs2069718, *PDCD1* rs2227981/rs10204525/rs2227982, *PTPN11* rs2301756 and *ZAP70* rs13420683 has been performed using TaqMan analysis as previously described [16]. Whole-blood specimens was used for extraction of DNA. Genotyping was performed using predesigned Taqman allelic discrimination assays, consisting of two allele-specific minor groove binding probes. Polymerase chain reactions (PCR) were performed in a reaction volume containing DNA, primers, and the specific probes were labelled with fluorescent dye.

Flow cytometry

Peripheral blood samples were analysed multiplex flow cytometry as previously described by Kunert et al.[6]. In short, absolute cell counts of immune cell populations were determined

on whole blood after lysis of red blood cells, and frequencies of particular subsets were determined in more detail on cryopreserved peripheral blood mononuclear cell samples that were stained with a mix of antibodies.

Mutational burden and expression of PD-L1 in tumor tissue

Expression of PD-L1 and tumor mutational burden (TMB) have previously been determined in a subset of patients of cohort 1 (n=26; stage IV NSCLC patients) using archival formalin-fixed, paraffin-embedded tissue samples[17]. Baseline expression of PD-L1 has been determined using antibody clone SP263 (Roche Diagnostics, Tucson, AZ), whereas TMB has been measured using the Oncomine TML assay (Thermofisher Scientific, Waltham, MA).

Statistical analysis

To study the relationship between baseline protein levels or SNPs and survival (PFS and OS), Cox regression analysis was used. Patient survival was visualised by the Kaplan-Meier approach. Patients were dichotomized for low or high granzyme B serum levels based on the median value of all patients. Dominant, recessive, and additive models [18] were used to test associations between SNPs and clinical outcomes including BOR, PFS and OS. Hazard ratios (HR) and 95% CIs were calculated. For the association of SNPs with radiological response, BOR was utilized as an ordered categorical variable with three levels, namely: CR/PR (pooled), SD and PD, by means of ordinal logistic regression analysis. This method assumes that the relationship between each pair of outcome groups is the same. The proportional odds assumption was checked for all analyses. Univariate ordinal logistic regression was applied for both SNPs and patient factors, and odds ratio (OR) and 95% confidence intervals (CI) were calculated. Multivariable ordinal logistic analysis was performed including both single SNPs and patient factors, with $p < 0.1$ according to the univariate analyses. All analyses with a significant relation ($p < 0.05$) between SNP and clinical outcome, were internally validated by bootstrapping[19], where 1,000 bootstrap samples were generated (with replacement) and 95% CIs were calculated for either ORs or HRs. Furthermore, bias and bias-corrected 95% CIs were calculated. In general, a p-value < 0.05 was considered to be statistically significant. Analyses were performed using IBM SPSS Statistics version 24.0.0.1 (Chicago, IL) and STATA version 15.1 (StataCorp LP, TX).

RESULTS

Patient characteristics

Baseline serum from a total of 78 (cohort 1) and DNA from a total of 322 stage IV NSCLC patients (cohort 2) was available for analysis (**table 1**). There was a 16.5% subject overlap between the patient cohorts. All patients were treated with at least one dose of nivolumab

at 3 mg/kg Q2W. Overall, median absolute starting dose was 222 mg (interquartile range [IQR] 192 - 263 mg). The objective response rate (ORR) was similar in cohort 1 and cohort 2, respectively 19.2% and 16.6%. A minority of all patients (7%) could not be evaluated for response by RECIST v1.1 due to early death, loss to follow-up or incomplete or absent follow-up tumor assessments. In the univariate analysis of cohort 2, WHO performance status (0 vs. $\geq$1) and sex (male vs. female) were significantly associated with PFS (HR 0.66; 95%CI 0.46-0.95; p=0.027 and HR 1.38; 95%CI 1.06-1.80; p=0.18, respectively) and OS (HR 0.52; 95%CI 0.34-0.77; p=0.001 and HR 1.40; 95%CI 1.05-1.86; p=0.023, respectively). In the multivariable analysis, only WHO performance status and primary tumor type remained significant for their association with respectively PFS or OS and BOR.

Serum levels of granzyme B are associated with clinical outcome

Serum levels of granzyme B were determined in cohort 1 (**Suppl. Fig. 1**), having a median concentration of 1.27 pg/mL, which was used as the cut-off to dichotomize patients with low and high levels of serum granzyme B (as described in the method section). Patients with low baseline serum levels of granzyme B had a significant worse PFS (HR 1.96; 95%CI 1.12-3.43; p=0.018, **figure 1a**) than patients with high levels of baseline serum granzyme B. Likewise, low levels of granzyme B were significantly associated with worse OS (HR 2.08; 95%CI 1.12-3.87; p=0.021, **figure 1b**) compared to high levels of granzyme B.

Table 1. Patient characteristics

		Cohort 1 (n=78)		Cohort 2 (n=322)	
Age at start	*Mean (range in years)*	63.6(35-78)		64.7(29-85)	
		n	%	n	%
Sex					
	Male	48	61.5	202	62.7
	Female	30	38.5	120	37.3
Primary tumor					
	Adenocarcinoma	52	66.7	200	62.1
	Squamous cell carcinoma	17	21.8	96	29.8
	Large cell carcinoma	-	-	22	6.8
	Lung cancer with unknown pathology	9	11.5	4	1.2
WHO PS					
	0	18	23.1	54	16.8
	1	39	50.0	188	58.4
	2	1	1.3	7	2.2
	3	-	-	1	0.3
	Unknown	20	25.6	72	22.4
Prior lines					
	0	2	2.6	1	0.3
	1	60	76.9	217	67.4
	2	13	16.7	82	25.5
	3	2	2.6	15	4.7
	4	1	1.3	6	1.9
	5	-	-	1	0.3
Smoking status					
	History or current smoker	56	71.8	238	73.9
	Never smoker	8	10.3	20	6.2
	Unknown	14	17.9	64	19.9
Ethnicity					
	Caucasian	74	94.9	308	95
	Other	4	5.1	5	2
	Unknown	0	-	9	3

Baseline characteristics of NSCLC cohort 1 and cohort 2. 16.5% of the patients (n=53) from cohort 2 were overlapping with cohort 2. Abbreviations: number (n) WHO performance status (WHO PS).

Figure 1. Association of serum granzyme b and *GZMB* genotype with survival

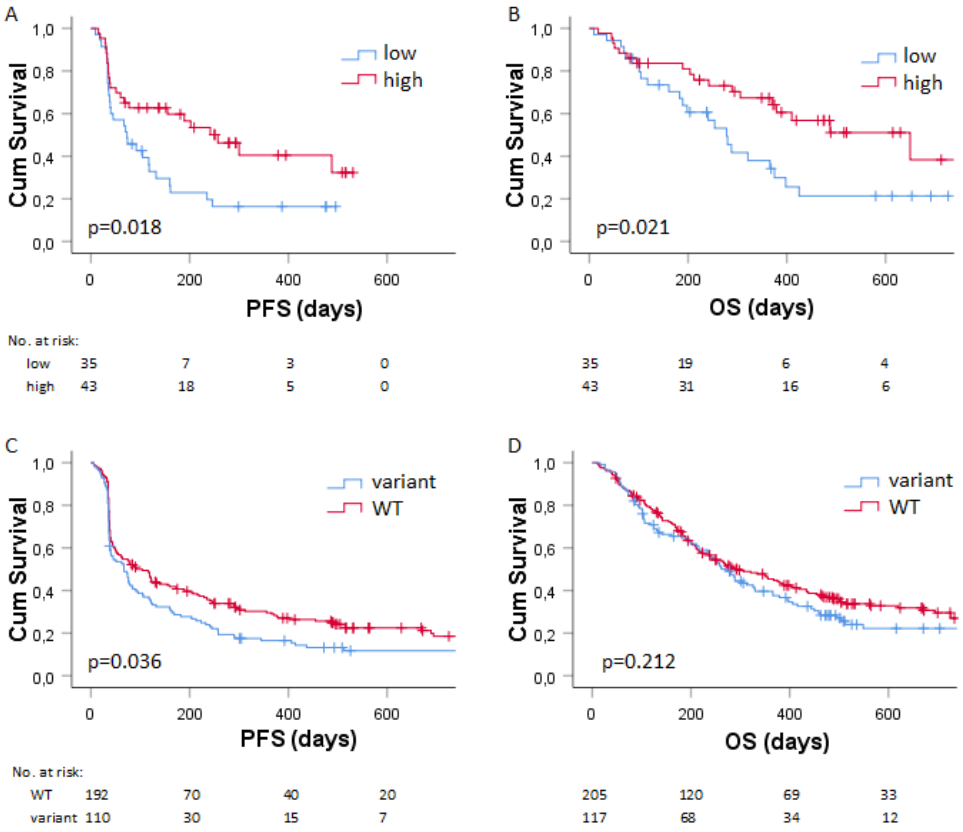

A) Kaplan-Meier plots showing the A) progression-free survival (PFS; in days) and B) overall survival (OS; in days) of patients in cohort 2 (n=78) with low (in blue) vs. high (in red) baseline serum levels of granzyme B. The C) PFS and D) OS of patients in cohort 2 (n=322) with wild type (in red) vs. variant germline GZMB (in blue). Numbers at risk shown below the graph.

Germline variation of GZMB is associated with clinical outcome

To validate the findings in a second cohort by a different approach [20], genetic alterations of *GZMB* c.128T>C (rs8192917), together with a mechanism-of-action based panel of other SNPs, were related to PFS, OS and BOR in cohort 2. Investigated SNPs with the corresponding haplotype frequencies, MAF and HWE statistics are shown in **suppl. table 2**. After correction for WHO performance status and sex in multivariable analysis, patients with homozygous and heterozygous variants of *GZMB* rs8192917 had worse PFS (HR 1.38; 95%CI 1.02-1.87; p=0.036; **table 2**; **figure 1c**). This finding could be internally validated (HR 95%CI 1.02-1.87; bias 0.003; bias-corrected 95%CI 1.03-1.88; p=0.036; **suppl. table 3**). Remaining SNPs were not associated with PFS after correction for patient factors (**table 3**).

No significant association of SNPs with OS was observed after correction of patient factors (**table 3**). Of note, homozygous and heterozygous variants of *GZMB* rs8192917 were not significantly associated with OS (HR 1.19; 95%CI 0.91-1.57; p=0.212; **table 2**; **figure 1d**). Homozygous and heterozygous variants of *GZMB* rs8192917 were significantly associated with worse BOR (OR 1.60; 95%CI 1.01-2.52; p=0.044; **table 2**) and could be internally validated for the association with BOR (OR 95%CI 1.05-2.55, bias 0.007; bias-corrected 95%CI 1.09-2.57; p=0.030, **suppl. table 3**). All the results from both univariate ($p < 0.1$) and multivariate analyses of the association with PFS, OS or BOR are shown in **table 3**. Results from the internal validation of factors that were significantly associated after correction for patient factors (p-value < 0.05) are shown in **suppl. table 3**. For a subset of patients, both serum levels of granzyme B and germline variation of *GZMB* c.128T>C (rs8192917) were available for analysis. Patients with homozygous and heterozygous variants of *GZMB* rs8192917 (n=19) had significant lower serum levels of granzyme B compared to patients with wild type *GZMB* (n=34; mean difference 8.6 pg/mL, 95% CI 1.77-15.38, p=0.015).

Table 2. Association between GZMB genotype and clinical outcome

PFS		**Univariate analysis**		**Multivariate analysis**	
Parameter	**Test variables**	**HR (95%CI)**	**P-value**	**HR (95%CI)**	**P-value**
GZMB c.128T>C	CC+CT vs. TT	1.39(1.07-1.80)	0.013*	1.38(1.02-1.87)	0.036*
WHO	0 vs. ≥1	0.66(0.46-0.95)	0.027*	0.61(0.42-0.89)	0.01*
Sex	Male vs. female	1.38(1.06-1.80)	0.018*	1.29(0.95-1.76)	0.103

OS		**Univariate analysis**	
Parameter	**Test variables**	**HR (95%CI)**	**P-value**
GZMB c.128T>C	CC+CT vs. TT	1.19(0.91-1.57)	0.212
WHO	0 vs. ≥1	0.52(0.35-0.77)	0.001*
Sex	Male vs. female	1.40(1.05-1.86)	0.023*

BOR		**Univariate analysis**		**Multivariate analysis**	
Parameter	**Test variables**	**OR (95%CI)**	**P-value**	**OR (95% CI)**	**P-value**
GZMB c.128T>C	CC + CT vs. TT	1.63 (1.04-2.57)	0.033*	1.60 (1.01-2.52)	0.044*
Primary tumor	Other vs. adeno	0.63 (0.40-0.98)	0.041*	0.63 (0.41-0.99)	0.045*

Univariate and multivariate analysis of the association of germline variation of GZMB and progression-free survival (PFS), overall survival (OS) or best overall response (BOR). Patient factors associated with OS/PFS (p-value < 0.1) were included in the multivariate analysis. Significance is marked by *. Abbreviations: hazard ratio (HR), 95% confidence interval (95%CI), WHO performance status (WHO).

Table 3. Association between investigated SNPs and clinical outcome

Univariate analysis (PFS)			
Parameter	**Test variables**	**HR (95%CI)**	**P-value**
IFNG c.874T>A	AA+AT vs. TT	0.76(0.58-0.99)	0.045
IL2RA c.64+5006T>C	CC+CT vs. TT	0.80(0.62-1.04)	0.098
WHO performance status	0 vs. ≥1	0.66(0.46-0.95)	0.027
Sex	Male vs. female	1.38(1.06-1.80)	0.018
Multivariate analysis (PFS)			
Parameter	**Test variables**	**HR (95% CI)**	**P-value**
IFNG c.874T>A	AA+AT vs. TT	0.79(0.58-1.07)	0.131
WHO performance status	0 vs. ≥1	0.66(0.45-0.95)	0.024
Sex	Male vs. female	1.26(0.92-1.71)	0.148
IL2RA c.64+5006T>C	CC+CT vs. TT	0.81(0.60-1.10)	0.177
WHO performance status	0 vs. ≥1	0.65(0.45-0.93)	0.019
Sex	Male vs. female	1.29(0.95-1.76)	0.101
IFNG c.874T>A	AA+AT vs. TT	0.76(0.55-1.05)	0.093
WHO performance status	0 vs. ≥1	0.52(0.34-0.77)	0.001
Sex	Male vs. female	1.45(1.03-2.02)	0.32
Univariate analysis (OS)			
Parameter	**Test variables**	**HR (95% CI)**	**P-value**
IFNG c.874T>A	AA+AT vs. TT	0.72(0.55-0.95)	0.021
WHO performance status	0 vs. ≥1	0.52(0.35-0.77)	0.001
Sex	Male vs. female	1.40(1.05-1.86)	0.023
Multivariate analysis (OS)			
Parameter	**Test variables**	**HR (95% CI)**	**P-value**
IFNG c.874T>A	AA+AT vs. TT	0.76(0.55-1.05)	0.093
WHO performance status	0 vs. ≥1	0.52(0.34-0.77)	0.001
Sex	Male vs. female	1.45(1.03-2.02)	0.32
Univariate analysis (BOR)			
Parameter	**Test variables**	**OR (95%CI)**	**P-value**
IL10 c.387+284C>A	AA vs. AA +AC	0.25 (0.07-0.89)	0.033
ZAP70 -21-4127C>A	AA vs. CC+AC	0.50 (0.25-0.98)	0.045
Primary tumor	Other vs. adeno	0.63 (0.40-0.98)	0.041
Multivariate analysis (BOR)			
Parameter	**Test variables**	**OR (95% CI)**	**P-value**
IL10 c.387+284C>A	AA vs. AA +AC	0.24 (0.07-0.84)	0.026
Primary tumor	Other vs. adeno	0.61 (0.39-0.96)	0.031
ZAP70 -21-4127C>A	AA vs. CC+AC	0.49 (0.24-0.97)	0.042
Primary tumor	Other vs. adeno	0.61 (0.39-0.96)	0.033

Univariate and multivariate analysis of the association between germline SNPs (except those related to GZMB variation; those are shown in table 2) and progression-free survival (PFS), overall survival (OS) or best overall response (BOR). Only SNPs that were associated with OS/PFS/BOR (p-value < 0.1) are shown and included in the multivariate analysis. Significance is marked by *. Abbreviations: hazard ratio (HR), 95% confidence interval (95%CI), WHO performance status (WHO).

Serum levels of granzyme B are accompanied by presence of T cells with terminal differentiation and exhausted phenotype

Next, we assessed the relationship between serum granzyme B as well as genetic variations of *GZMB* and cytotoxic immune cell populations in blood. Overall, there was a tendency that patients with lower serum granzyme B levels had lower absolute numbers of peripheral CD56+NK cells (mean 141 vs. 205 cells/µL, p=0.16; **suppl. fig. 2**) and $CD8^+$ T cells (346 vs. 463 cells/µL, p=0.41; **figure 2a**) when compared to patients with higher serum granzyme B levels. In fact, patients with homozygous or heterozygous variants of *GZMB* rs8192917 had a higher number of $CD8^+$ T cells but not CD56+ NK cells than patients with wild type *GZMB* (**figure 2b** and **suppl. fig. 2b**). Further, we studied whether granzyme B levels or *GZMB* genotypes correlate with frequencies of those immune cell phenotypes that correspond to either terminal differentiation ($CCR7^-CD45RA^+$) or exhaustion ($PD1^+$ and $TIM3^+$) of $CD8^+$ T cells, as signs

Figure 2. Association between serum granzyme B and T cell populations with phenotypes that correspond to functional responses

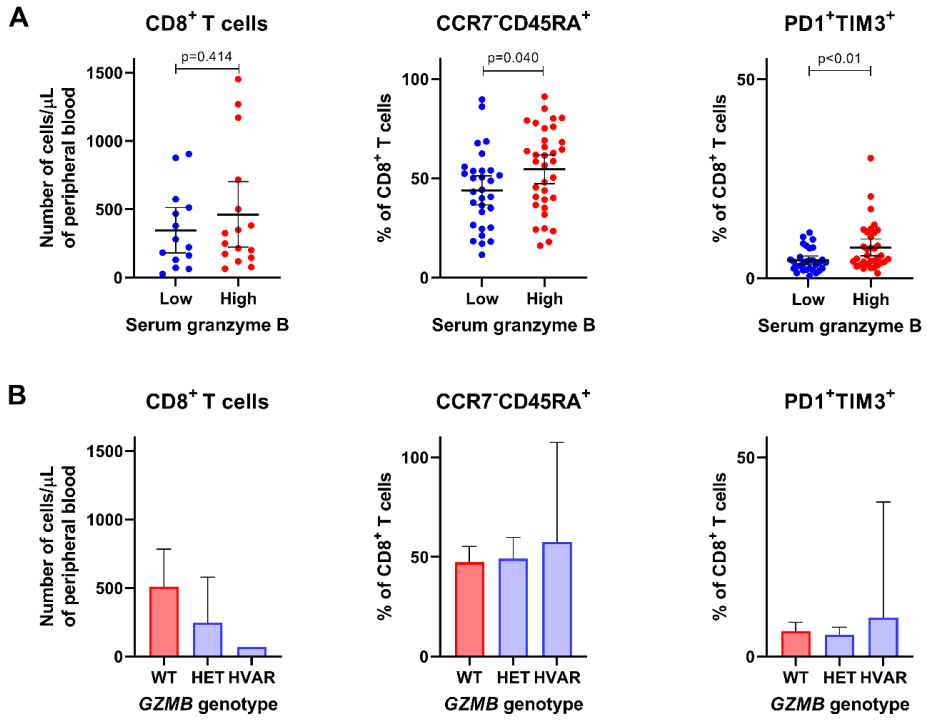

Associations are shown between A) serum granzyme B levels or B) GZMB genotype and T cell populations in blood. CD8+ T cells is considered as a subset of T lymphocytes with cytotoxic functions. CCR7-CD45RA+ cytotoxic T cells correspond with terminal differentiation, and PD1+TIM3+ cytotoxic T cells correspond with exhaustion, both signs of T cell activation or cytotoxicity. Abbreviations: wild type (WT), heterozygous variant (HET) and homozygous variant (HVAR).

of T cell cytotoxicity. Interestingly, patients with lower serum granzyme B levels had a lower proportion of $CCR7^{-}CD45RA^{+}CD8^{+}$ T cells (mean 44 vs. 54 %, p=0.040) as well as $PD1^{+}TIM3^{+}CD8^{+}$ T cells (mean 4.5 vs. 7.8 %, p=0.001; **figure 2a**). No significant association nor trend could be observed between *GZMB* genotype and frequencies of T cells with these phenotypes (**figure 2b**).

Relationship between serum granzyme B, expression of PD-L1 and TMB

Interaction analysis for PFS and OS was performed between serum granzyme B, and PD-L1 and TMB in a subset of evaluable patients. In the univariate analysis, TMB (HR 7.31; 95%CI: 1.5-34.7; p=0.01) was significantly correlated with PFS, while expression of PD-L1 (HR 4.30; 95%CI: 0.9-19.8; p=0.06) or serum granzyme B (HR 2.34; 95%CI: 0.9-5.9; p=0.07) did not meet the threshold for significance (**suppl. table 4**). Moreover, only serum granzyme B was significantly correlated with OS (HR: 2.95; 95%CI: 1.09-7.93; p=0.03; **suppl. table 5**). Multivariate analysis of these biomarkers (namely: serum granzyme B, PD-L1 and TMB) for PFS and OS did not meet significance. Of note, the hazard ratios were in favor of higher levels of PD-L1 ($\geq$50%), TMB ($\geq$10 mut/Mb) and serum granzyme B ($\geq$1.27 pg/mL), yet expression of PD-L1 (%), TMB (mut/Mb) and serum granzyme B levels (pg/mL) were not significantly correlated with each other (**suppl. table 6**).

DISCUSSION

The present study demonstrates that serum levels of granzyme B and alterations of the *GZMB* locus may contribute to resistance mechanisms of PD-1 blockade. This concept (**figure 3**) is based on our findings that 1) low serum levels of granzyme B and 2) a common germline polymorphism of the *GZMB* gene were associated with worse clinical outcome after PD-1 blockade in metastatic NSCLC patients. Moreover, serum levels of granzyme B were positively correlated with peripheral abundance of T cell populations that were highly differentiated or were expressing the immune checkpoints PD1 and TIM3. The results are in line with our hypothesis that cytotoxic effector functions of lymphocytes (i.e., through granzymes) are critical for the anti-PD-1 antibody-mediated immune effects. Granzyme B levels were determined at baseline in stage IV NSCLC patients prior to start with PD-1 ICIs. The median granzyme B level in this cohort was 1.27 pg/mL (range 0 – 88 pg/mL), which was lower than reported levels in healthy controls, e.g. a median plasma granzyme B of 5.7 pg/mL (IQR 3.7 – 7.1 pg/mL; n=38) [21] or 11.5 pg/mL (range 1 – 130 pg/mL; n=54) [22]. Measurements of granzyme B in serum were consistent with measurements in plasma [22]. Our findings confirm the hypothesis that lower granzyme B levels in metastatic cancer patients mirrors the immune micro-environment of tumors favoring tumor growth by halting the anti-tumor response of cytotoxic immune cells. This may be a result of those germline variations that impact cytotoxic functions of lymphocytes.

Figure 3. Mechanism of action

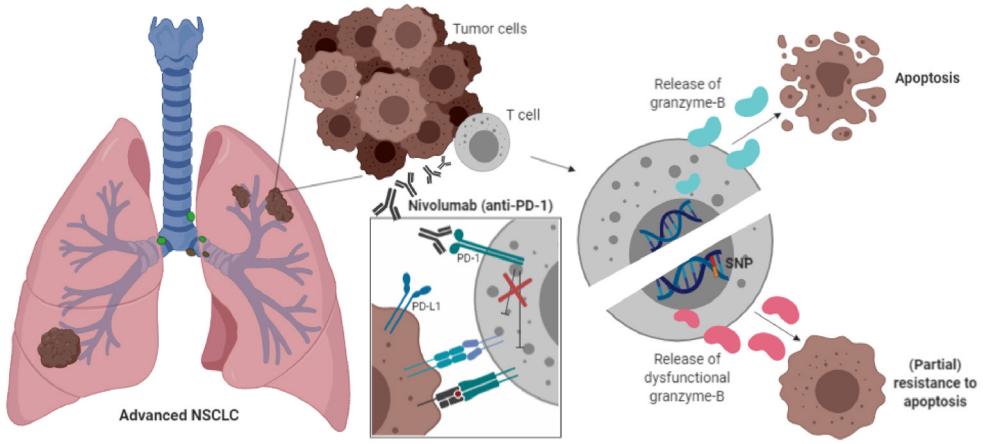

Schematic overview of the proposed mechanism of action of the GZMB SNP. Presence of the GZMB c.128T>C SNP indicates the expression of variant granzyme B isotypes (indicated as pink granzyme B molecules) that might lead to impaired cytotoxic effector functions of T cells, resulting in impaired apoptosis of tumor cells and partial resistance to anti-PD-1 blockade. The molecular mechanism of the PD-1 antibody nivolumab is shown in the white box. This figure was created by DH in BioRender.com.

Besides germline polymorphisms in the *GZMB* gene, polymorphisms in other genes have been investigated as well for their association with clinical outcome. Interestingly, these germline variations were not consistently found to correlate with PFS, OS or BOR. Interpretation of these findings are challenging, and do not necessarily implicate an absence of effects of non-*GZMB* SNPs. Although SNPs were rationally selected by their correlations with autoimmunity (**suppl. table 2**), we cannot exclude that SNPs in the investigated genes contribute to therapy resistance, as well as epigenetic or post-transcriptional regulation of gene expression or function. For example, PD-1 ICIs are suggested to only minimally target responses mediated by T cell receptors (involving *ZAP70*) and their primary method of action is most likely explained by relieving SHP-2 inhibition of the CD28 co-stimulatory pathway [8]. Genomic alterations in tumors may involve loss of tumor antigens that are recognized by T cells, loss of antigen-presenting machinery components, tumor-induced inactivation of T cell signalling and insensitivity to effector functions of lymphocytes, death receptors or interferons [23].

The nonsynonymous substitution of *GZMB* c.128T>C (rs8192917) was found to be in strong linkage disequilibrium with other common (MAF>15%) exonic variants, representing a haplotype block (data publicly available from The Single Nucleotide Polymorphism Database (https://www.ncbi.nlm.nih.gov/snp/; **suppl. figure 3**). This indicates that

two predominant isoforms of granzyme B are expressed in the European population, defining two predominant isoforms, and is consistent with previous reports that genetic variation of *GZMB* leads to change of three amino acids of the mature protein ($Q^{48}P^{88}Y^{245}$ to $R^{48}A^{88}H^{245}$) [24,25]. Interestingly, the two isoforms have a similar expression, stability and proteolytic activity, however, the variant granzyme B isotype was observed to be incapable of inducing apoptosis in tumor cell lines in contrast to the functional effects of the more common isotype [26].

Interaction analysis between granzyme B, expression of PD-L1 in tumor and TMB showed that these markers were not inter-correlated, which suggests their value as independent biomarkers for clinical outcome after PD-1 ICIs. Although our findings in regard to serum granzyme B and *GZMB* germline variation are confirmed in a large patient cohort and by internal validation, further investigations need to be performed to determine the clinical value as a predictive or prognostic biomarker of response to PD-1 blockade. These investigations include comparative analysis with these currently used biomarkers in an extended patient cohort, and evaluation of the diagnostic accuracy and mapping of the sensitivity of serum granzyme B in a prospective clinical trial. The results may not be directly applicable to other ethnic groups, as the study was performed in a European population.

An important aspect of our results is that germline genetics related to cytotoxic effector functions of lymphocytes contribute to mechanisms of resistance to ICI therapy. Previously, it has been shown that germline variations in regard to the antigen presentation machinery are related to response to ICIs, i.e. HLA-1 heterozygosity [27]. Considering the urgent need to understand how genetic variation affects response to ICIs, as reviewed by Havel *et al.* [5], further work is warranted to identify novel genetic loci. We believe that apart from genes that are involved in antigen presentation, other immune-modulating genes may also contribute to response and resistance mechanisms of ICIs, of which granzyme B is an example. Determination of germline variations of cancer patients contributing to response to ICIs may well be performed by future genome wide association studies (GWAS).

CONCLUSIONS

While the immune-oncology field rapidly advances, our understanding of ICI resistance mechanisms is limited and effective patient selection is lacking. Our data demonstrate that granzyme B is an important player in the antitumor immunity, as a consequence of the finding that low serum levels of granzyme B and germline variation of the *GZMB* gene contributes to resistance to PD-1 blockade in advanced NSCLC. As recent clinical trial results underline effective biomarker-based patient selection, future trials that incorporate granzyme B into diagnostics is considered as a promising step in this direction.

REFERENCES

1. Sharpe AH, Pauken KE. The diverse functions of the PD1 inhibitory pathway. *Nat Rev Immunol.* 2018;18(3):153-167.
2. Hanahan D, Weinberg RA. Hallmarks of cancer: the next generation. *Cell.* 2011;144(5):646-674.
3. Borghaei H, Paz-Ares L, Horn L, et al. Nivolumab versus Docetaxel in Advanced Nonsquamous Non-Small-Cell Lung Cancer. *N Engl J Med.* 2015;373(17):1627-1639.
4. Brahmer J, Reckamp KL, Baas P, et al. Nivolumab versus Docetaxel in Advanced Squamous-Cell Non-Small-Cell Lung Cancer. *N Engl J Med.* 2015;373(2):123-135.
5. Havel JJ, Chowell D, Chan TA. The evolving landscape of biomarkers for checkpoint inhibitor immunotherapy. *Nat Rev Cancer.* 2019;19(3):133-150.
6. Kunert A, Basak EA, Hurkmans DP, et al. CD45RA(+)CCR7(-) CD8 T cells lacking co-stimulatory receptors demonstrate enhanced frequency in peripheral blood of NSCLC patients responding to nivolumab. *J Immunother Cancer.* 2019;7(1):149.
7. Hui E, Cheung J, Zhu J, et al. T cell costimulatory receptor CD28 is a primary target for PD-1-mediated inhibition. *Science.* 2017;355(6332):1428-1433.
8. Kamphorst AO, Wieland A, Nasti T, et al. Rescue of exhausted CD8 T cells by PD-1-targeted therapies is CD28-dependent. *Science.* 2017;355(6332):1423-1427.
9. Larimer BM, Wehrenberg-Klee E, Dubois F, et al. Granzyme B PET Imaging as a Predictive Biomarker of Immunotherapy Response. *Cancer Res.* 2017;77(9):2318-2327.
10. Voskoboinik I, Whisstock JC, Trapani JA. Perforin and granzymes: function, dysfunction and human pathology. *Nat Rev Immunol.* 2015;15(6):388-400.
11. Cao X, Cai SF, Fehniger TA, et al. Granzyme B and perforin are important for regulatory T cell-mediated suppression of tumor clearance. *Immunity.* 2007;27(4):635-646.
12. Nagata S. Apoptosis by death factor. *Cell.* 1997;88(3):355-365.
13. Pinkoski MJ, Hobman M, Heibein JA, et al. Entry and trafficking of granzyme B in target cells during granzyme B-perforin-mediated apoptosis. *Blood.* 1998;92(3):1044-1054.
14. Eisenhauer EA, Therasse P, Bogaerts J, et al. New response evaluation criteria in solid tumours: revised RECIST guideline (version 1.1). *Eur J Cancer.* 2009;45(2):228-247.
15. Namipashaki A, Razaghi-Moghadam Z, Ansari-Pour N. The Essentiality of Reporting Hardy-Weinberg Equilibrium Calculations in Population-Based Genetic Association Studies. *Cell J.* 2015;17(2):187-192.
16. Bins S, Basak EA, El Bouazzaoui S, et al. Association between single-nucleotide polymorphisms and adverse events in nivolumab-treated non-small cell lung cancer patients. *Br J Cancer.* 2018;118(10):1296-1301.
17. Hurkmans DP, Kuipers ME, Smit J, et al. Tumor mutational load, CD8(+) T cells, expression of PD-L1 and HLA class I to guide immunotherapy decisions in NSCLC patients. *Cancer Immunol Immunother.* 2020.
18. Lewis CM. Genetic association studies: design, analysis and interpretation. *Brief Bioinform.* 2002;3(2):146-153.

19. Efron B. Bootstrap methods: Another look at the jackknife. *The annals of Statistics*. 1979;7:1-26.
20. Editorial. It's time to talk about ditching statistical significance. *Nature*. 2019;567(7748):283.
21. de Jong HK, Garcia-Laorden MI, Hoogendijk AJ, et al. Expression of intra- and extracellular granzymes in patients with typhoid fever. *PLoS Negl Trop Dis*. 2017;11(7):e0005823.
22. Spaeny-Dekking EH, Hanna WL, Wolbink AM, et al. Extracellular granzymes A and B in humans: detection of native species during CTL responses in vitro and in vivo. *J Immunol*. 1998;160(7):3610-3616.
23. Zaretsky JM, Garcia-Diaz A, Shin DS, et al. Mutations Associated with Acquired Resistance to PD-1 Blockade in Melanoma. *N Engl J Med*. 2016;375(9):819-829.
24. Jin Y, Andersen G, Yorgov D, et al. Genome-wide association studies of autoimmune vitiligo identify 23 new risk loci and highlight key pathways and regulatory variants. *Nat Genet*. 2016;48(11):1418-1424.
25. Ferrara TM, Jin Y, Gowan K, Fain PR, Spritz RA. Risk of generalized vitiligo is associated with the common 55R-94A-247H variant haplotype of GZMB (encoding granzyme B). *J Invest Dermatol*. 2013;133(6):1677-1679.
26. McIlroy D, Cartron PF, Tuffery P, et al. A triple-mutated allele of granzyme B incapable of inducing apoptosis. *Proc Natl Acad Sci U S A*. 2003;100(5):2562-2567.
27. Chowell D, Morris LGT, Grigg CM, et al. Patient HLA class I genotype influences cancer response to checkpoint blockade immunotherapy. *Science*. 2018;359(6375):582-587.

SUPPLEMENTARY INFORMATION

Supplementary Figure 1. Frequency histogram

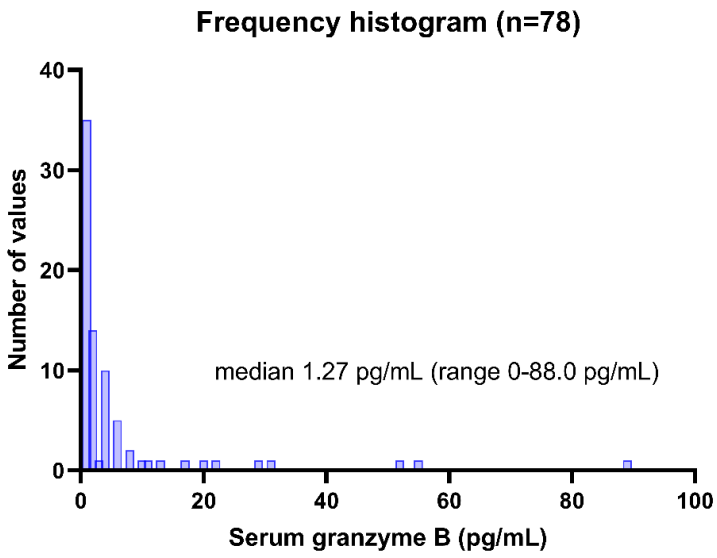

Frequency histogram of granzyme B measurements in serum. In total, baseline measurements were performed in 78 stage IV NSCLC patients. Almost half of the patients had undetectable levels of granzyme B in serum.

Supplementary Figure 2. Lack of association between serum granzyme B or GZMB genotypes and NK cell numbers

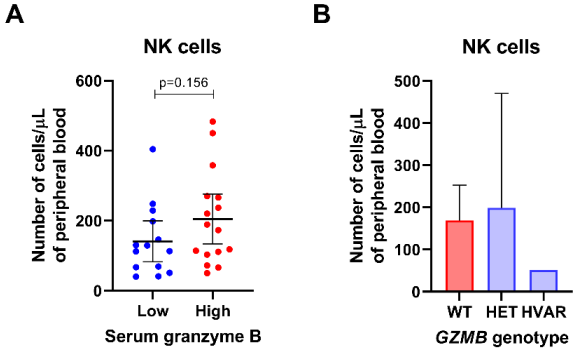

Association is shown between A) serum granzyme B levels or B) GZMB genotype and the number of CD56+ NK cells in blood. Abbreviations: wild type (WT), heterozygous variant (HET) and homozygous variant (HVAR).

Supplementary Figure 3. LD statistics for all common *GZMB* SNPs

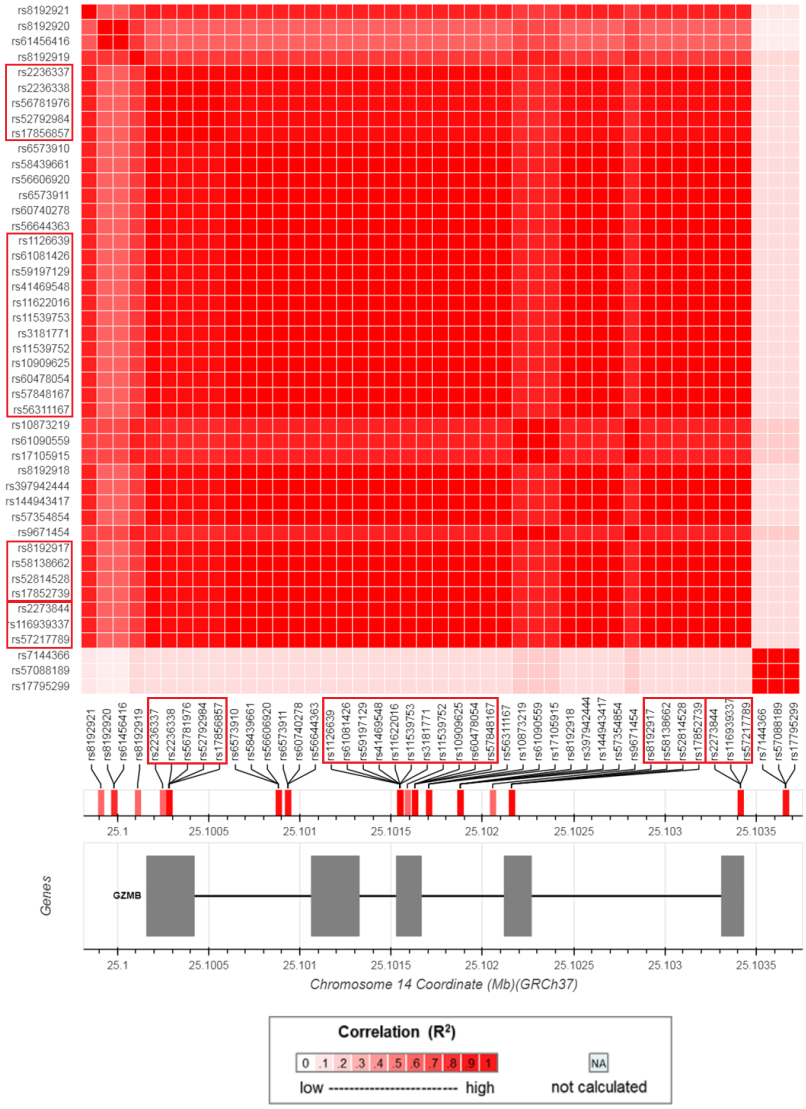

Heatmap matrix of pairwise linkage disequilibrium statistics of common SNPs of GZMB (MAF > 15%; dbSNP database). Exon germline variants (rs-numbers) are marked with the red boxes. Note that all common germline variants present in GZMB exones are in strong linkage disequilibrium, defining two predominant GZMB isoforms in the European population (~70% common GZMB allele). Data derived from publicly available reference haplotypes are used from the 1000 Genomes Project. The R squared as a measure of linkage disequilibrium are shown, red indicates high correlation. Abbreviations: R squared (R2).

Supplementary Table 1. Association of SNPs with AIDs

Gene	Rs-number	Disease	Effect	Key references
HLA-A	rs60131261	Vitiligo	Higher susceptibility (OR 1.53) for AID and associated with elevated expression of HLA-A	Jin, 2016[15]
GZMB	rs8192917	Vitiligo	Higher susceptibility (OR 1.23/1.39) for AID	Jin, 2016[15] Xu, 2018[16]
IL10	rs3024493	SLE, T1D, CD, UC, BeD	Higher susceptibility (OR 1.26) for AIDs	Ramos, 2011[17]
IL2RA	rs2104286	RA, MS	Lower susceptibility (OR 0.81) for RA, higher susceptibility (OR 1.19) for MS	Kurreeman, 2009[18] Wang, 2018[19]
IFNG	rs2430561, rs2069705, and rs2069718	SLE	Higher susceptibility (OR 1.75/2.42) for AID	Lee, 2016[20] Kim, 2010[21]
PDCD1	rs2227981, rs10204525, and rs2227982	AS	Higher susceptibility for AID	Chen, 2016[22] Liu, 2011[23]
PTPN11	rs2301756	UC	Higher susceptibility (OR 1.81) for AID	Narumi, 2009[24]
ZAP70	rs13420683	CD	Higher susceptibility (OR 2.25) for AID	Bouzid, 2013[25]

Germline variations of genes that are implicated in the etiopathogenesis of autoimmune diseases (AIDs). These variants are indicated by gene and rs-number. Abbreviations: Type 1 diabetes (T1D), Crohn's disease (CD), ulcerative colitis (UC), alkylosing spondyloditis (AS), Behcet's disease (BeD), rheumatoid arthritis (RA), multiple sclerosis (MS), systemic lupus erythematosus (SLE).

Supplementary Table 2. Investigated single-nucleotide polymorphisms

Protein	Gene	rs-number	Variant	WT	HET	HVAR	Undet.	MAF	HWE (χ^2)
Granzyme B	*GZMB*	rs8192917	c.128T>C	205	104	13	0	20%	<0.01
HLA-A	*HLA-A*	rs60131261	delTTTA	178	116	28	0	27%	2.05
IL-10	*IL10*	rs3024493	c.387+284C>A	231	81	10	0	16%	0.77
CD25	*IL2RA*	rs2104286	c.64+5006T>C	180	118	22	2	25%	0.2
IFN-γ	*IFNG*	rs2430561	c.874T>A	105	153	63	1	43%	0.29
		rs2069705	−1616T>C	145	135	42	0	34%	1.4
		rs2069718	367–895C>T	112	148	60	2	42%	0.8
PD-1	*PDCD1*	rs2227981	804C>T	94	154	73	1	47%	0.42
		rs10204525	889G>A	271	47	4	0	9%	1.39
		rs2227982	644C>T	320	2	0	0	0.3%	-
SHP-2	*PTPN11*	rs2301756	333–223A>G	259	60	3	0	10%	0.05
ZAP-70	*ZAP70*	rs13420683	−21–4127C>A	177	106	33	6	27%	7.42*

Overview of investigated SNPs. *If $\chi 2 > 3.84$ (p-value <0.05) then SNP is not consistent with HWE. ZAP70 -32-4127C>A (rs13420683) was not consistent with HWE ($\chi 2$ 7.42; $p < 0.01$) but remained in the analysis after excluding the likelihood of a type I error. As PDCD1 644C>T (rs2227982) had a MAF of 0.3% (<5%) in the study cohort, it was excluded from further analyses. All other SNPs were considered suitable for analysis. Abbreviations: wild-type (WT), heterozygote variant (HET), homozygote variant (HVAR), minor allele frequency (MAF), Hardy-Weinberg equilibrium (HWE).

Supplementary Table 3. Internal validation

Multivariate analysis (BOR)					
Factor	**Comparison**	**OR (95%CI)**	**P-value**	**Bias**	**Bias-corrected 95%CI**
GZMB c.128T>C	CC + CT vs. TT	1.019-2.509	0.041	0.006	1.052-2.548
Primary tumor	Other vs. adeno	0.410-0.981	0.041	-0.005	0.425-1.009
IL-10 c.387+284C>A	AA vs. AA +AC	0.010-5.420	0.367	-0.128	0.033-0.908
Primary tumor	Other vs. adeno	0.398-0.946	0.027	-0.006	0.405-0.979
ZAP70 -21-4127C>A	AA vs. CC+AC	0.236-1.019	0.056	0.005	0.246-1.014
Primary tumor	Other vs. adeno	0.395-0.953	0.030	-0.006	0.398-0.987

Multivariate analysis (PFS)					
Factor	**Comparison**	**HR (95%CI)**	**P-value**	**Bias**	**Bias-corrected 95%CI**
GZMB c.128T>C	CC+CT vs. TT	1.022-1.867	0.036	0.003	1.027-1.879
WHO performance	0 vs. ≥1	0.418-0.898	0.012	<-0.001	0.408-0.876
Sex	Male vs. female	0.943-1.771	0.111	<0.001	0.943-1.780

Bootstrap results of the association between SNPs and clinical outcome. Bias measure, bias-corrected 95%CI and p-value of the multivariate analysis are shown in the table for each factor. SNPs associated with BOR, PFS or OS (p<0.1; multivariate analysis) were included. Remaining SNPs and patient factors are not shown.* Abbreviations: hazard ratio (HR), odds ratio (OR), 95% confidence interval (95%CI).

Supplementary Table 4. Association of PD-L1, TMB and serum granzyme B with PFS

PFS			Univariate			Multivariate		
		n	HR	95%CI	p-value	HR	95%CI	p-value
Expression of PD-L1 in tumor	<50 vs. ≥50%	26	4.30	0.93-19.77	0.06	4.04	0.36-45.31	0.26
Tumor mutational burden	<10 vs. ≥10 mut/Mb	22	7.31	1.54-34.67	0.01*	3.42	0.60-19.53	0.17
Serum granzyme B	<1.27 vs. ≥1.27 pg/mL	26	2.34	0.93-5.93	0.07	1.53	0.52-4.51	0.44

Univariate and multivariate analysis of the association between expression of PD-L1 in tumor, tumor mutational burden and serum granzyme B levels with progression-free survival (PFS). Biomarkers associated with PFS (p-value<0.1) were included in the multivariate analysis. COX regression analysis was performed on a subset of patients from cohort 1, of whom baseline parameters and clinical outcome was available. Significance is marked by *. Abbreviations: hazard ratio (HR), 95% confidence interval (95%CI).

Supplementary Table 5. Association of PD-L1, TMB and serum granzyme B with OS

OS			Univariate			Multivariate		
		n	HR	95%CI	p-value	HR	95%CI	p-value
Expression of PD-L1 in tumor	<50 vs. ≥50%	26	4.04	0.90-18.15	0.07	3.22	0.28-36.50	0.35
Tumor mutational burden	<10 vs. ≥10 mut/Mb	22	3.42	0.93-12.66	0.07	1.65	0.36-7.54	0.52
Serum granzyme B	<1.27 vs. ≥1.27 pg/mL	26	2.95	1.09-7.93	0.03*	2.25	0.73-6.91	0.16

Univariate and multivariate analysis of the association between expression of PD-L1 in tumor, tumor mutational burden and serum granzyme B levels with overall survival (OS). Biomarkers associated with OS (p-value<0.1) were included in the multivariate analysis. COX regression analysis was performed on a subset of patients from cohort 1, of whom baseline parameters and clinical outcome was available. Significance is marked by *. Abbreviations: hazard ratio (HR), 95% confidence interval (95%CI).

Supplementary Table 6. Correlation matrix of PD-L1, TMB and granzyme B

		PD-L1 expression	Tumor mutational burden
Tumor mutational burden	Pearson Correlation	0,13	
	p-value (2-tailed)	0,56	
	n	22	
Granzyme B	Pearson Correlation	-0,20	-0,18
	p-value (2-tailed)	0,33	0,42
	n	26	22

Correlation matrix showing the Pearson correlation test outcomes of tumor mutational burden, granzyme B levels and PD-L1 expression in tumor tissue obtained prior to start of PD-1 ICIs in a subset of patients from cohort 1. Abbreviations: number of patients (n).

CHAPTER 10

Molecular data show conserved DNA locations distinguishing lung cancer subtypes and regulation of immune genes

Daan P. Hurkmans*, Menno Tamminga*, Bram van Es, Tom Peters, Wouter Karman, Rogier T.A. van Wijck, Peter J. van der Spek, Tjebbe Tauber, Maureen Los, Anouk van Schetsen, Thu Vu, T. Jeroen. N. Hiltermann, Ed Schuuring, Joachim G.J.V. Aerts, Sissy Chen, Harry J.M. Groen

*shared first authorship

Lung Cancer, August 2020, 146: page 341-349

Abstract

Introduction: Non-small-cell lung cancer exhibits a range of transcriptional and epigenetic patterns that not only define distinct phenotypes, but may also govern immune related genes, which have a major impact on survival.

Materials and Methods: We used open-source RNA expression and DNA methylation data of the Cancer Genome Atlas with matched non-cancerous tissue to evaluate whether these pretreatment molecular patterns also influenced genes related to the immune system and overall survival.

Results: The distinction between lung adenocarcinoma and squamous cell carcinoma are determined by 1,083 conserved methylation loci and RNA expression of 203 genes which differ for >80% of patients between the two subtypes. Using the RNA expression profiles of 6 genes, more than 95% of patients could be correctly classified as having either adeno or squamous cell lung cancer. Comparing tumor tissue with matched normal tissue, no differences in RNA expression were found for costimulatory and co-inhibitory genes, nor genes involved in cytokine release. However, genes involved in antigen presentation had a lower expression and a wider distribution in tumor tissue.

Discussion: Only a small number of genes, influenced by DNA methylation, determine the lung cancer subtype. The antigen presentation of cancer cells is dysfunctional, while other T cell immune functions appear to remain intact.

INTRODUCTION

Smoking induced lung cancer has a large number of DNA mutations while other environmental factors such as air pollution may cause a different distribution in DNA mutations, often observed in non-smokers in genes like *EGFR*, *BRAF*, *HER2* and *ALK* [1]. Lung cancer is traditionally subdivided into small-cell lung cancer and non-small-cell lung cancer (NSCLC) with the latter being divided into two main subtypes, adenocarcinoma and squamous cell carcinoma (SCC).

It is known that DNA methylation is affected by age, smoking, emphysema and histological subtype [2]. Changes in the methylation pattern affects RNA expression, leading not only to different phenotypes, but also to a different effect on the immune activation. This may not only be reflected in the expression of human leukocyte antigen (HLA) or PD-L1 on tumor cells, but also in the tumor microenvironment. The Cancer Genome Atlas group (TCGA) performed molecular studies on lung adenocarcinoma and SCC identifying driver oncogenes and loss-of-function mutations in the HLA-A class I major histocompatibility gene [3,4]. Molecular classification approaches were made by clustering phenotypes on different platforms [5]. In a more recent study, a "cluster-of-clusters" analytic approach on differential DNA expression showed three distinct subtypes within SCC and six within adenocarcinomas [6]. Three of the adenocarcinoma subtypes had high expression of several immune related genes including PD-L1, PD-L2, CD3 and CD8.

To date, the role of epigenetic modifications in relation to tumor responses in NSCLC remains to be clarified. Global DNA hypomethylation at repeated sequences has been identified in tumor cells in combination with DNA hypermethylation at specific loci [7]. CpG dinucleotides are highly represented in repeated sequences of the genome (LINE, SINE) and in the promotor regions of about 65% of the human genome and it is suggested that these play a role in regulation of gene expression. Biopsies of both adenocarcinoma and SCC show differences in methylation and in immune infiltrate [8]. Although their tumor response to checkpoint inhibitors is similar (1 year progression-free survival of 21% and 19% for respectively SCC and non-SCC in the Checkmate studies), different determinants driving tumor response and resistance may be involved [9].

We hypothesized firstly, that a clear separation based on DNA methylation and RNA expression can be made between the NSCLC subtypes, and secondly, that methylation controls immune modulating genes in the tumor DNA and tumor-intrinsic defects must be present.

MATERIALS AND METHODS

Study cohort and data acquisition

Patients with treatment naive NSCLC, adenocarcinoma and SCC, whose DNA methylation and RNA expression data from the resected tumor was available in the public domain, were selected from two different profiling platforms (RNA sequencing resulting in 60,483 mRNA expression values and methylation profiling by Infinium HM450 platform resulting in 485,577 DNA methylation β-values) at the TCGA Research Network (http://cancergenome.nih.gov/). Details on methods and data generation of the RNA sequencing and DNA methylation can be found in the original TCGA landmark papers [3,4] Duplicate samples, those with missing histological diagnosis, and those with disease recurrences were removed. In total, 1,024 unique NSCLC patients with tumor tissue were selected of whom 154 patients provided additional normal tissue. Patients with normal tissue provided 108 samples for the normal RNA expression dataset and 74 samples for the normal DNA methylation dataset; 28 patients provided samples for both methods. The tumor RNA expression dataset consisted of 1,014 tumor samples (513 adenocarcinoma and 501 SCC) and the tumor methylation dataset consisted of 828 tumor samples (458 adenocarcinoma and 370 SCC). We extracted clinical and pathological data on age, gender, histology, stage of disease, tumor cell percentage and survival calculated from time of diagnosis to time of death or last follow-up (**Extended Data Table 4**). The dataset was analyzed during a hackathon session, in which data scientists in collaboration with physicians competed to create a "functioning" product by the end of the 3-day event.

Data curation and statistical methods

All datasets were filtered and curated for non-significantly associated features after preprocessing of the files. ComBat, an empirical Bayes location/scaling method was applied to rule out potential cohort bias in the RNA expression data as a consequence of different study sites and laboratories, whereas BEclear was used in the DNA methylation data (**Supplementary Information**). As co-variant we used gender, because this factor has a high variance over the batches and its value is known for all samples. We started with principal component analysis (PCA) to discern underlying structure of the database, e.g. the total gene expression versus the immune modulating gene groups expressions.

For RNA expression and DNA methylation data we used non-parametric tests. The separation of the cancer types was compared before and after bias correction with both the Kolmogorov-Smirnov test and Mann-Whitney U test. The Kolmogorov-Smirnov tests provides a ks-score, which determines whether the given distributions of two groups are the same or different with a probability of 1-ks-score (**Supplementary Information**).

After we determined differences in distributions of methylation probes, an algorithm was developed using separate cut-off values for DNA methylation and RNA expression to

identify the most predictive genes to classify the NSCLC subtypes. This best split analysis determined whether a cut-off value could provide a split of at least 85% of patients into the correct subtype with a certainty of more than 80%, starting with probes or genes that had the highest differences (fold change). Differences between tumor subtypes based on DNA methylation β value had to be at least 0.1 to increase the probability of biological relevance. Loci with the largest differences for both DNA methylation and RNA expression respectively were determined after the annotating the probes into corresponding genes, an overlap in genes of both lists was established for biological interpretation.

Different immune modulatory genes were selected and grouped according to their function (**Extended Data Table 5**). These include co-stimulatory genes (COSTIM), co-inhibitory genes (COINHIB), antigen presenting genes (AGPRES) and immune modulatory/inflammatory cytokines and chemokines (CYTCHEM). The co-stimulatory immune modulatory gene group included genes that are known to be expressed in tumor cells (e.g. *ICOSL, OX40L, SLAM*), as reviewed by Chen and Flies [30]. Similarly, co-inhibitory genes were included in the analysis (e.g. *VTCN1*, *CD113, CD48*). *HLAE* was included for its protein function as inhibitor ligand for immunocompetent (NK) cells [31,32]. For antigen presentation, genes were selected involved in antigen presentation (e.g. classical HLA) and genes involved in antigen processing (e.g. *TAP1, CIITA, HLAA*) were selected for inclusion in the antigen presentation genes group [33]. Genes coding for cytokines and chemokines (e.g. *IL10, IDO, IFNG*) were selected based on their implication in immune tolerance of cancer through pleiotropic effects in immune regulation and inflammation [34–36].

Gene densities of all AGPRES genes were calculated within R using a kernel density estimate from the distribution of RNA expression of NSCLC and non-cancerous tissue.

To study the relationship between expression of immune related gene groups (AGPRES, COSTIM, COINHIB, CYTCHEM) and overall survival, a multivariate Cox regression analysis was used with age, gender, smoking (pack years), tumor type and stage of disease as covariates (patient factors with $p<0.1$ from univariate analysis included). The expression of pretreatment immune related gene groups was used as a categorical variable with two levels divided by the median (high and low overall expression of all involved genes). Hazard ratios (HR) and 95% confidence intervals (CI) are reported.

To investigate the biological pathways, Ingenuity Pathway Analysis (Qiagen, Hilden, Germany) was used to perform gene enrichment analyses on these gene lists.

RESULTS

Methylation in NSCLC

We used 1,024 unique patients from NSCLC TCGA datasets. Based on DNA methylation a PCA analysis appeared to be capable of separating adenocarcinoma and SCC (**Fig. 1a**). The prediction model based on the PCA outcomes correctly identified all but one of the

included patients as either adenocarcinoma or SCC. Importantly, stratification for high and low purity (indicated as the proportion of tumor cell content) of the processed samples did not influence the findings. Remarkably, of all methylation probes with a ks-score ≥0.95, the mean corrected differences ranged from +0.02 to +0.15 (scale -1 - +1), implicating a very small variation in methylation for these highly conserved loci in both phenotypes and a consistent stronger methylation of adenocarcinoma compared to SCC (**Fig. 2**).

Figure 1. Clustering of main lung cancer phenotypes based on DNA methylation and RNA expression

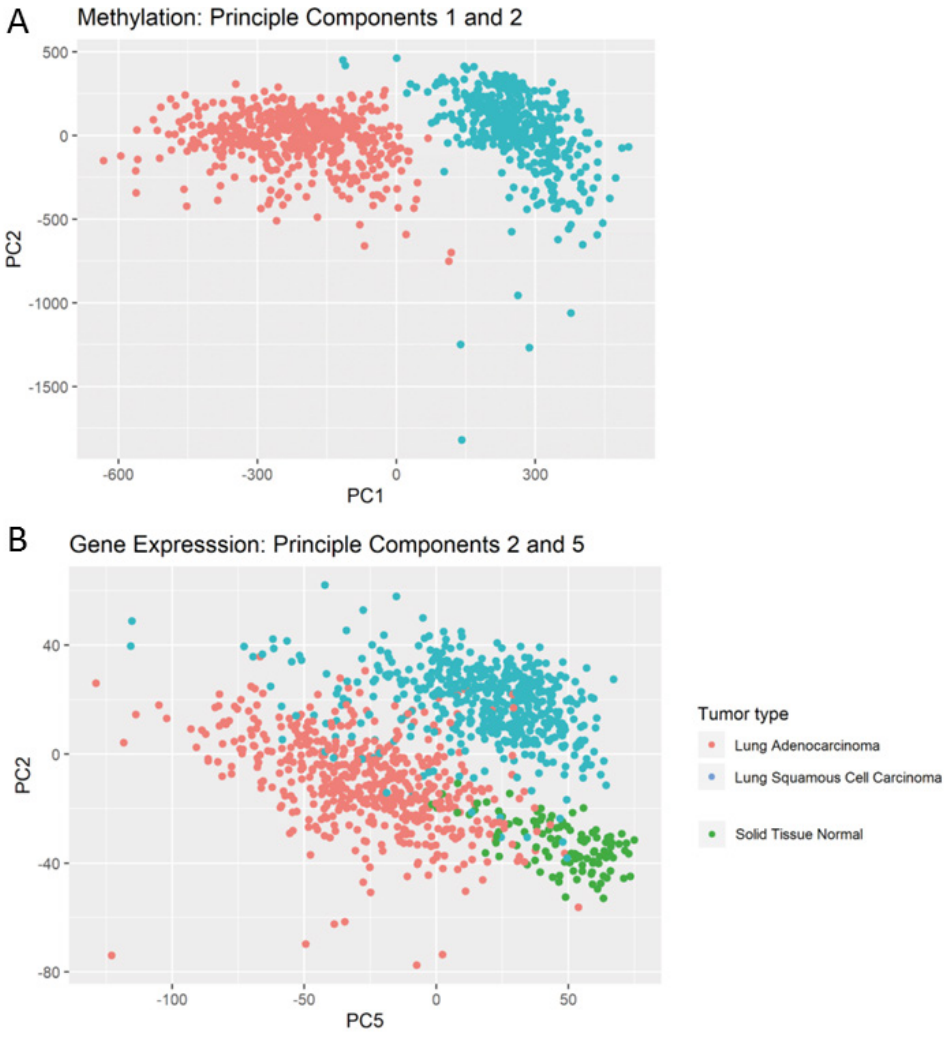

A) Pulmonary adenocarcinoma is distinguished from squamous cell carcinoma by DNA methylation and B) to a slightly lesser extent by RNA expression.

Figure 2. Higher DNA methylation in adenocarcinoma compared to squamous cell carcinoma

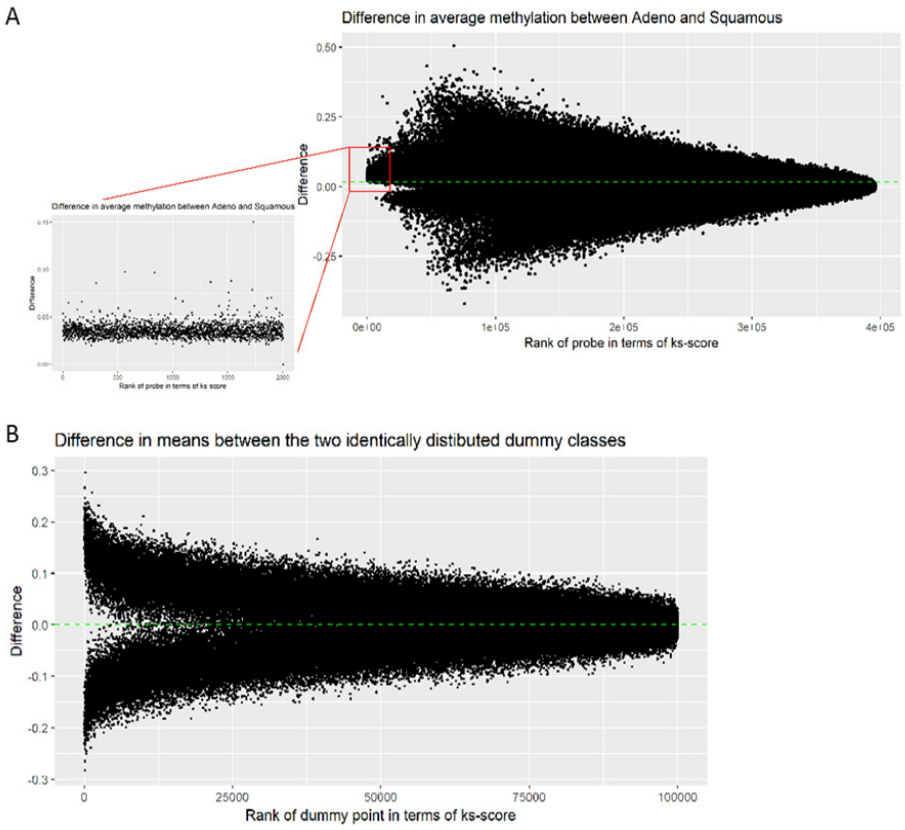

A) Adenocarcinoma contains consistently higher methylated DNA than squamous cell lung carcinoma mainly due to a relative small number of probes at conserved loci compared to B) a theoretical at random model. Overall difference in methylation is 0.017 (positive values on the y-axis indicate higher DNA methylation of adenocarcinoma, negative values indicate higher DNA methylation of squamous cell carcinoma). X-axis ranks the probes according to the ks-score for differentiation between both histological subtypes. Y-axis is the difference between the mean methylation (0 is low methylation and 1 is high methylation) between both subtypes.

After we observed significant differences in methylation probe distribution between the subtypes, we continued with a best split analysis. The algorithm identified 1083 methylation probes (out of a total of 485,577 probes) which individually could be used to correctly classify at least 85% of patients. Next, we looked into the chromosomal position of the different methylated probes. An even distribution along the genome was determined at increasingly stringent ks-scores (**Fig. 3a,b** and **Extended Data Table 1**).

Figure 3. Location of methylation probes along 23 chromosomes that separates adenocarcinoma from squamous cell lung carcinoma at ks ≥ 0.95 and ks ≥ 0.97 level

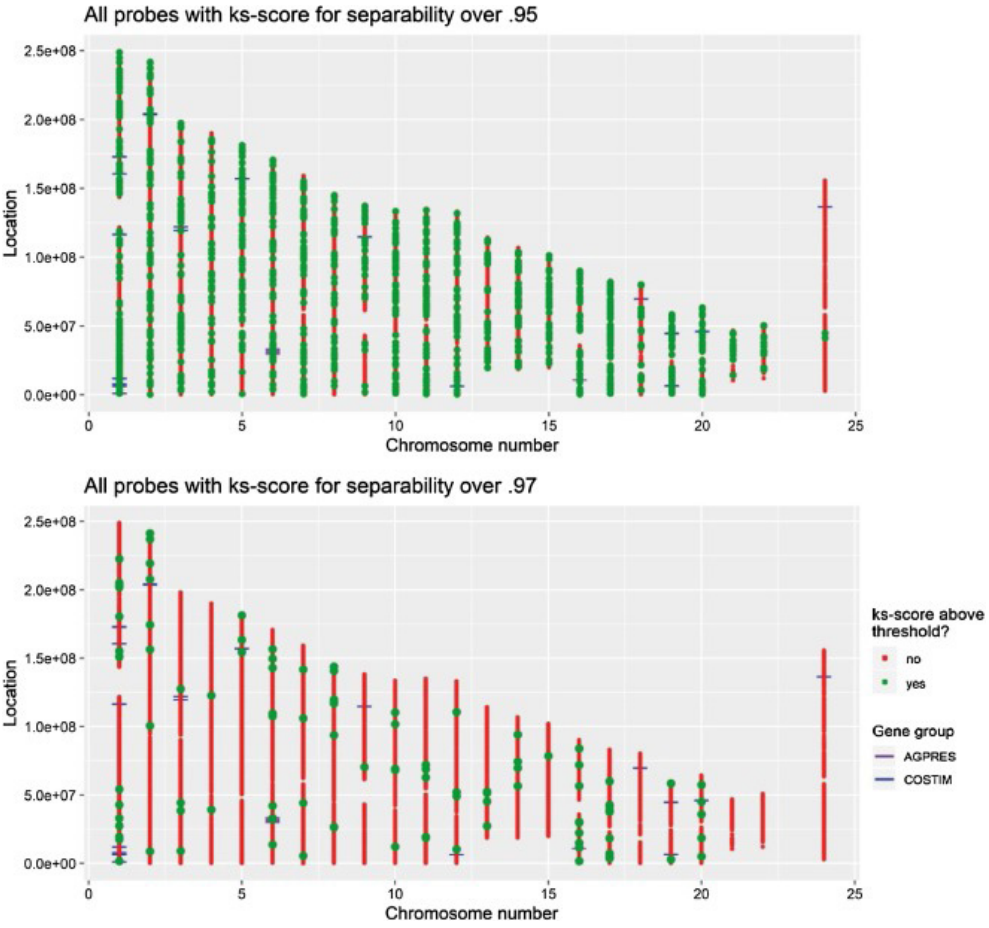

Methylation pattern for each chromosome characterized by their individual probes A) with ks-score for separability between histologic subtypes over 95 % are evenly distributed over chromosomes with an exception for the x-chromosome. B) Probes with ks-score over 97 % show the conserved methylated areas that preserve the difference between subtypes. Mostly they are related to CpG islands located along chromosomes. X-axis and y-axis refer to respectively the chromosome number and individual probe localization on the chromosome according to ks-score for separability. Green dots represent differential probes. Antigen presentation and costimulation genes are flagged for chromosome location. (For interpretation of the references to colour in this figure legend, the reader is referred to the web version of this article).

The higher ks-score indicates a better separability between histologic subtypes (Supplementary Information). The methylation pattern for each chromosome characterized

by individual probes with ks-score ≥ 95% was distributed over all chromosomes except the X-chromosome. Probes with a high ks-score over 97% for separability represented conserved methylated loci that preserve the difference between phenotypes.

To address morphological differences between adenocarcinoma and SCC based on DNA methylation, an enrichment analysis was performed on the gene level based on the methylation probes that are most distinct for phenotype (ks-score >0.95; n=2,101 mapped genes). Remarkably, these and other genes showed a low methylation rate compared to normal tissue. The main canonical pathways that are most distinct for NSCLC subtypes are DNA repair pathways (**Extended Data Fig. 1**). However, based on the relative methylation of these genes, mechanisms involved in response to the category "viral infections" (z-score 10.7, p<0.001;) were more activated in SCC compared to adenocarcinoma, whereas mechanisms involved in cell death (z-score -17.8, p<0.001) were inhibited. Central genes involved in "viral infection" that are found to be differential in SCC compared to adenocarcinoma include *IRF3*, *NFKB1*, *RELA* (also known as *NFKB3*), *STAT3*, *SRPK1* and *TRIM*.

Expression in NSCLC

We next aimed to investigate to what extent methylation influences RNA expression levels. We observed that DNA methylation explains approximately 40 - 55% of the inversely correlated variation in the RNA expression. This percentage, however, is not only dependent on the β-value level that would biologically lead to effective epigenetic gene suppression, but also on the correlation between gene expression and methylation (Fig. 4e). Approximately 60% of methylation probes (different to the random 50%) are inversely correlated with RNA expression by selecting only those methylation probes that are assumed to have an epigenetic suppressive effect (average β-value > 0.25) on DNA transcription and with a significant correlation (correlation coefficient >0.5 or <-0.5). Of note, methylation probes with a negative, positive, or no relationship with gene expression could be determined as illustrated in **Fig. 4b-d** (**Supplementary information, sub 5**). In general, genes that were heavily methylated showed a lower RNA expression than genes that had a moderate or low methylation rate.

Unsupervised principal component analysis of the transcriptome led to a slightly less accurate separation of NSCLC phenotypes (**Fig. 1b**) than that based on DNA methylation data (**Fig. 1a**). Comparing tumor with non-cancerous tissue confirms that the RNA expression pattern is specific for NSCLC (**Fig. 1b**). The best split analysis on RNA data identified 203 genes, of which the expression was different in 85% of cases between SCC and adenocarcinoma. Of these, differences in RNA expression of five genes (*KRT5, DSC3, DSG3, TP63, CALML3*), and one miRNA (*MIR205HG*) combined could separate both subtypes with an accuracy of 95%.

Figure 4. Relation between DNA methylation for immune modulating genes determined by one probe and gene expression at four quartile levels

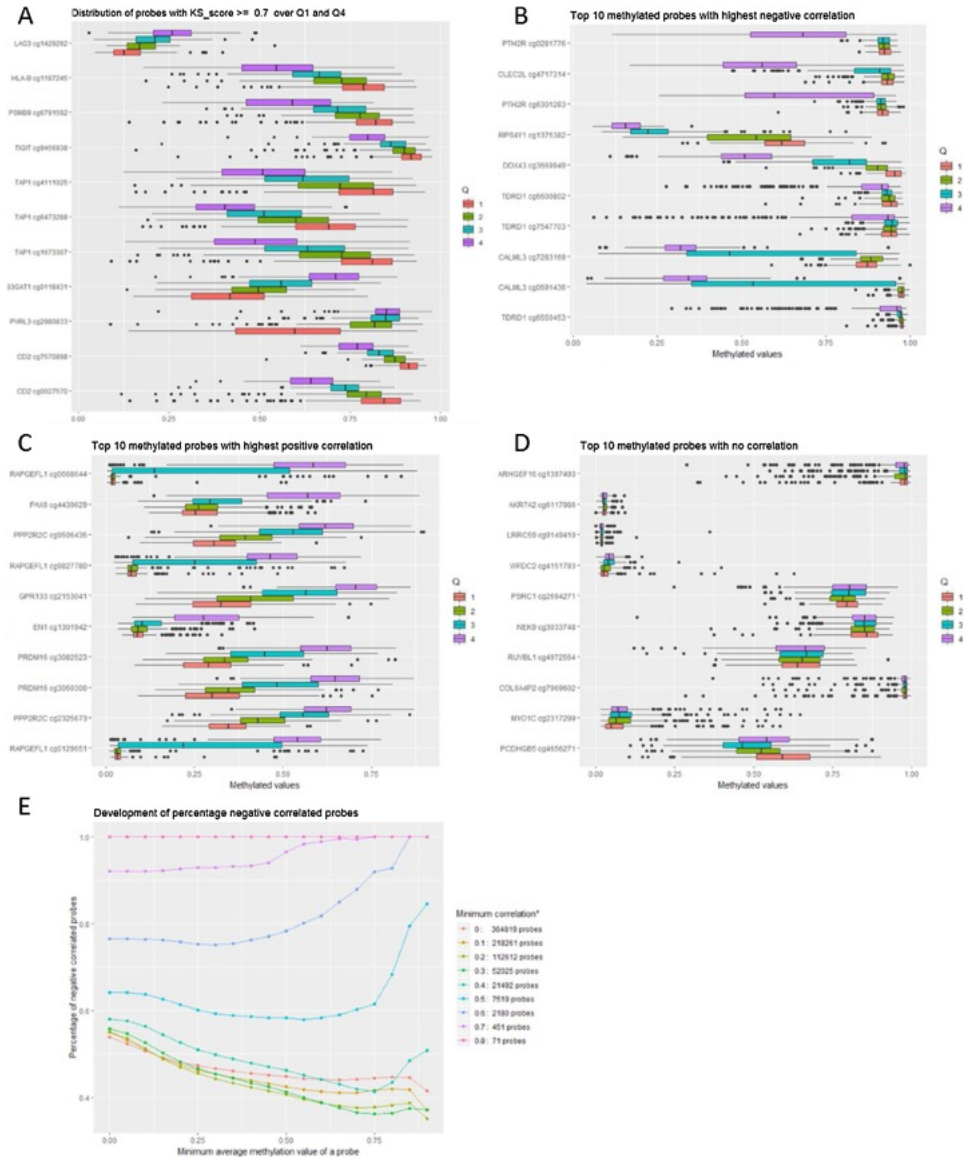

A) Immune modulating genes identified by probes with ks-score ≥ 70 % (adenocarcinoma vs. SCC) show an inverse relationship between expression and methylation for most genes. In this example, LAG3 and B3GAT1 show the opposite expression effect at low and moderate methylation, respectively. Examples are shown of probes with B) the highest negative correlation, C) highest positive correlation and D) no correlation between DNA methylation and RNA expression. E) The percentage of methylation probes that are inversely correlated with RNA expression depends on the cut-off of the correlation between methylation and gene expression of a probe and minimal average methylation.

Bilevel molecular analysis in NSCLC

We selected the top 500 methylation probes with their corresponding genes and the top 500 genes based on RNA expression and found an overlap of 41 genes related to the separation of the NSCLC phenotypes based on both DNA methylation and RNA expression (**Extended Data Table 2**). Gene enrichment analysis by Ingenuity Pathway Analysis revealed that *TP63* was an important upstream regulator, with elevated expression in SCC compared to adenocarcinoma. Target molecules of *TP63* in the list of 41 genes included *CSTA, SNAI2, DST, ACTL6A, KRT7* and the miRNA *MIR205HG*, and their expression was in the same predicted direction as the *TP63* activation in SCC.

Figure 5. Four immune modulatory gene groups as compared with all gene expressions in non-small cell lung cancers shows two clusters of increase (PC3 and PC6-9)

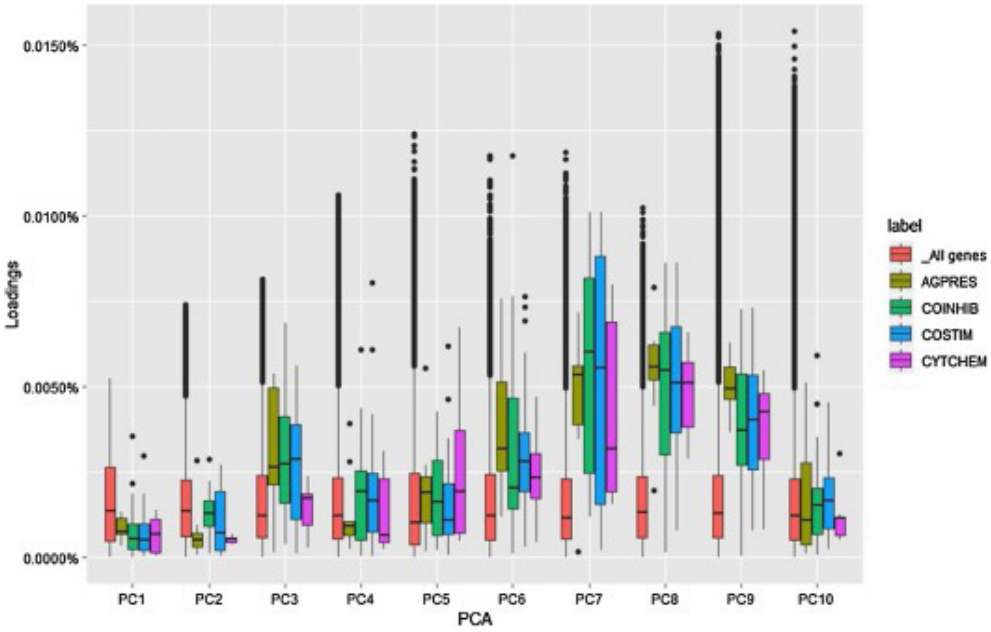

Four main immune modulatory gene groups were distinguished, involved in T cell antigen presentation (AGPRES), T cell co-inhibitory (COINHIB), T cell co-stimulator (COSTIM) and T cell cytokines/chemokines (CYTOCHEM). The influence of these gene groups were investigated on the individual principle components. The y-axis represents the loading of a gene in the DNA expression dataset to a principle component. The red boxes indicate all genes in the DNA expression dataset, whereas the other boxes represent the genes of selected immune modulating gene groups. All immune modulating gene groups are most pronounced in PC7, PC8 and PC9. The midline in the boxplot is the median of data in that component, with the lower and upper limits of the box being the first and third quartile, respectively. By default, the whiskers will extend up to 1.5 times the interquartile range from the top (bottom) of the box. If there are any data beyond that distance, they are represented individually as black dots ('outliers'). (For interpretation of the references to colour in this figure legend, the reader is referred to the web version of this article).

Immune modulating genes and methylation

As expected, methylation was inversely correlated for most methylation probes, e.g. higher level of *HLA-B*, *TAP1*, *CD2* methylation leads to lower RNA expression (**Fig. 4a**). Of note, none of the 1083 methylation probes identified by the best split analysis for histological subtype included any of the selected immune related genes.

We performed a principal component analysis including all RNA expressing genes and determined the weight of each component of immune modulatory gene groups: T cell co-inhibitory (COINHIB), T cell co-stimulator (COSTIM), T cell antigen presentation (AGPRES) and T cell cytokines/chemokines (CYTOCHEM) (**Fig. 5** and **Extended Data Fig. 2**). Genes in the immune related groups were gathered in two clusters, in PC3 and PC6-9. Antigen presenting gene expression was positively associated with co-stimulatory gene expression, not only in tumor but also in non-cancerous tissue (**Extended Data Fig. 2b, c**). Genes involved in the immune response towards endogenous retroviral sequences were also more methylated in adenocarcinoma compared to SCC, but we did not study the repetitive DNA areas with high versus low methylation.

Antigen presenting gene expression in tumor

Average RNA expression of genes in the antigen presenting gene group was lower in tumor than in non-cancerous tissue and showed a larger variation (SD) in expression (**Fig. 6**). *HLAA*, *HLAB* and *TAP2* RNA expression showed a decreased density, suggesting suppression of antigen presentation and processing. The other immune related gene groups in tumors also showed variation, but median values were not significantly different from non-cancerous tissue. At last, we asked ourselves what impact the different immune components have on survival. Interestingly, we were unable to identify survival benefit in an adjusted Cox regression for high expression of genes involved in antigen presentation or costimulatory function (**Extended Data Table 3**). Genes involved in the inhibition of the immune system also were not associated with survival.

Figure 6. RNA expression of immune modulating genes in tumor and their matched non-cancerous tissue

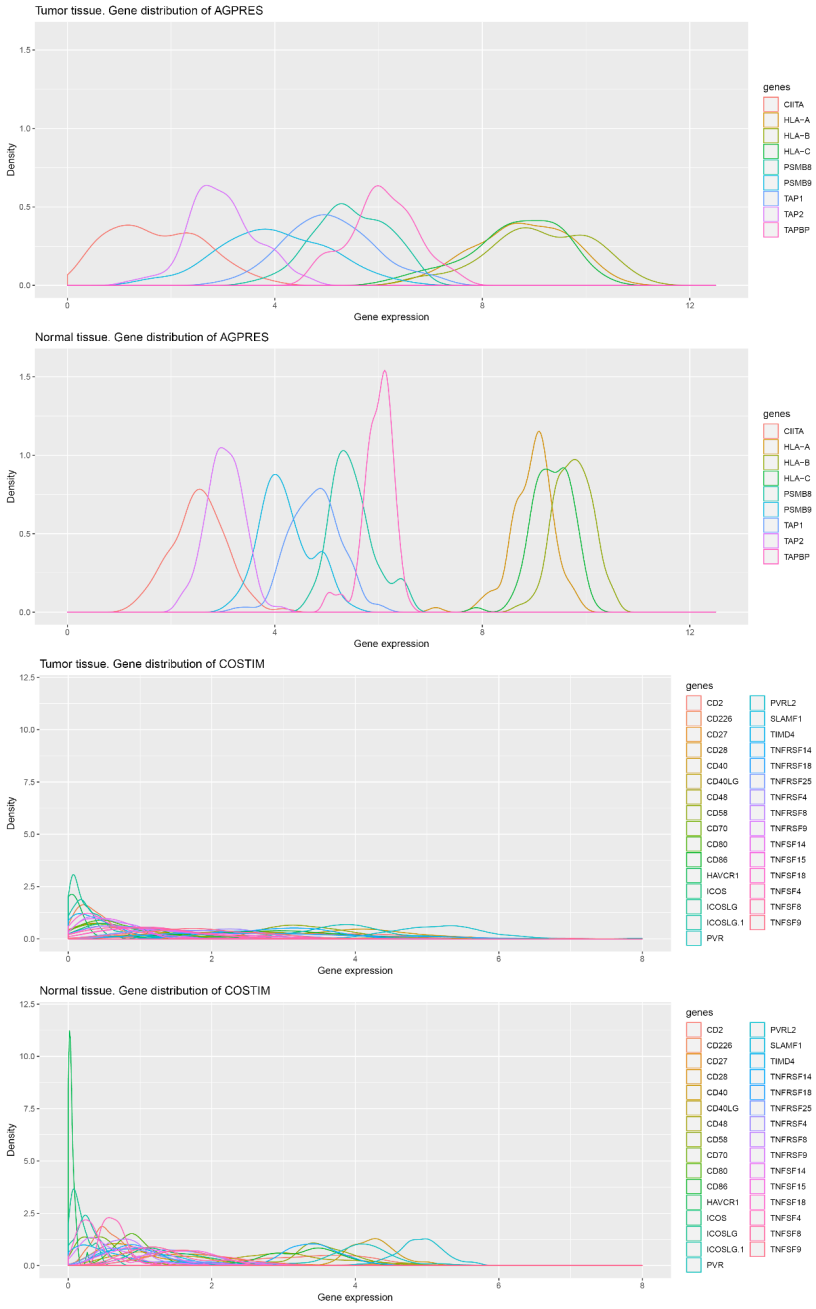

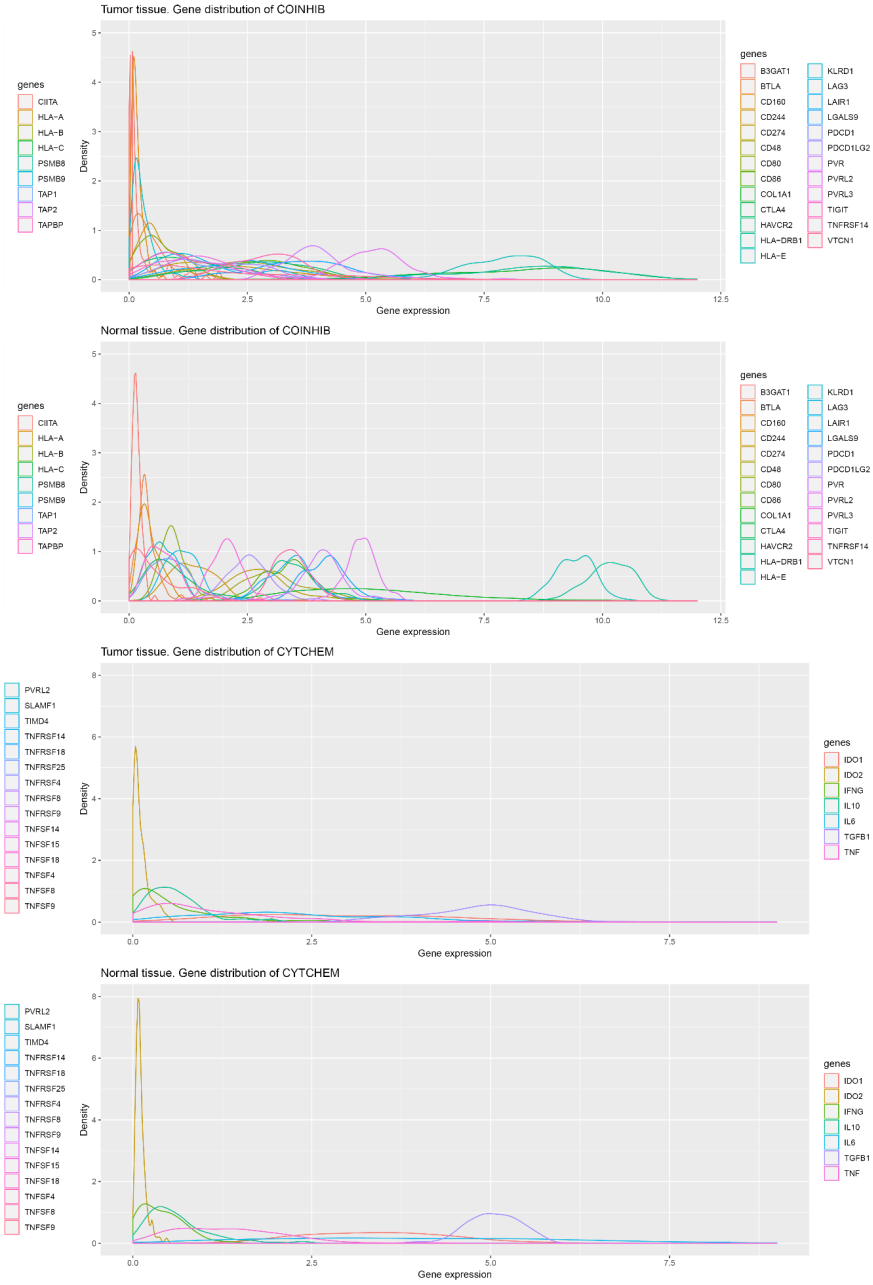

Density distribution of immune modulating gene expressions in 106 NSCLC tumors and their matched non-cancerous tissue. The antigen presenting gene expressions show a different density distribution compared to non-cancerous expressions, while the density of coinhibitory, costimulatory, and cyto- and chemokine gene expressions were largely similar.

DISCUSSION

We identified epigenetic and RNA expression patterns in tumor tissue from NSCLC patients, that distinguished squamous cell lung cancer from adenocarcinoma. Especially the conserved loci with hardly variation in DNA methylation between hundreds of patients were responsible for the distinction between the subtypes. Adenocarcinoma was globally more methylated than squamous cell carcinoma. Immune adaptive mechanisms have also been described such as gene hypermethylation targeting the interleukin-6/Stat3 pathway [10].

Not only methylation but also the differences in the expression values of only six genes could explain the difference between the subtypes in 97% of patients. Involved genes were keratine 5 (*KRT5)*, tumor protein p63 (*TP63)*, *DSC3*, desmoglein 3 (*DSG3)*, calmodulin like 3 (*CALML3)*, and the miRNA *MIR205HG.* All are directly or indirectly involved in tissue morphogenesis, differentiation cell adhesion, and proliferation. The predominant isoform ΔNp63α is overexpressed in SCC and may influence tissue microenvironment by recruiting proinflammatory cells. *TP63* is commonly used in immunohistochemistry to differentiate SCC from adenocarcinoma, which supports the robustness of our analysis [11–13].

Next, we have shown that immune regulatory genes were included in regions marked by methylation probes with a ks-score >95%; these methylation profiles were associated with differential expression in immune modulatory genes before therapy. These genes were located in methylation regions distinguishing pretreatment NSCLC phenotypes by distribution, but were not identified by the best split analysis, indicating that genes involved in subtype morphology and immune regulation are both regulated by methylation but belong to completely distinct gene groups.

Now we have established the relation between methylation and immune expression status, we asked ourselves whether the pretreatment expression of the immune modulating gene groups of early NSCLC patients had survival consequences. We were unable to identify any survival benefit. Compared to non-cancerous tissue we observed a much broader distribution of the expression of immune modulating genes in NSCLC, while the median expression of T cell co-inhibitory, co-stimulatory, and cyto- and chemokine genes remained similar. Only the antigen presenting gene expression in NSCLC was decreased. This group consisted not only of the classical *HLAA*, *HLAB* and *HLAC* whose expression depend on methylation but also *B2M* and *TAP* genes. By multiplexed quantitative immunofluorescence loss of expression of B2M, HLA-I heavy chains and HLA-II was observed in less than 23% of NSCLC patients [14]. Loss of *B2M* expression resulted in decreased or no cell surface expression of MHC class I, which impairs antigen presentation to cytotoxic T cells [15,16]. In melanoma loss of *B2M* and *TAP1* expression reduced overall survival when treated with ipilimumab [17]. Limiting the expression of genes involved in antigen presentation is an important mechanism of tumor cells to evade the immune system [18]. In early NSCLC tumors that have an activated immune system,

extensive immune editing is present in order to fit with the tumor microenvironment, as indicated by the relative depletion of neoantigens in tumors and loss of heterozygosity in *HLA* genes [19]. This allele-specific *HLA* loss may occur in about 40% of NSCLC patients [18]. We observed that in tumor and non-cancerous tissue antigen presenting and co-stimulatory gene expression was positively associated, suggesting that a higher expression of antigen presenting genes is associated with more inflammation. Although our analysis does not provide information on cell types, it suggests that the higher dosage of antigen presenting gene expression in (any) tissue associates with more co-stimulatory gene expressions from T cells. Overall, it may be concluded that the antigen presenting gene group harbors the main immune related defect in NSCLC patients.

Finally, our analysis revealed that higher methylation was observed in genes involved in the immune response towards endogenous retroviral sequences in adenocarcinoma compared to SCC. Disruption of methylation in both subtypes leads to different retroviral expressions. Moreover, analyzing a wide spectrum of over 2,000 involved genes with the highest subtype separability revealed viral involvement, likely retroviral or transposon loci. As we know, human endogenous retroviruses are under epigenetic control and rarely expressed in normal tissue [20,21]. Hypomethylation of the LINE family member L1 occurs in multiple solid cancers and cell lines [22,23]. Lung squamous cell carcinoma has elevated ERVH-5 and other RNA derived endogenous retrovirus expression that were associated with low cytolytic activity [24]. We observed that IRF3, NF-κB and STAT pathways are critical in the production of type I interferons downstream of pathogen recognition receptors. They detect viral RNA and DNA [25]. The genes *SRPK1* and *TRIM4* are found to regulate these virus-induced IFN induction pathways [26,27]. This provides further molecular evidence of the presumed importance of (retro)viral infection in predominantly squamous cell carcinoma as previously observed in squamous cell carcinomas that contained viral DNA [28]. Importantly, a significant proportion of the differentiating methylation probes suppresses viral and retroviral associated genes. Further investigation is needed into the exact nature of those repetitive areas that are hyper- or hypomethylated.

All studies have limitations. Importantly, the tumor samples have varying tumor content (at least 40%) tough, as shown by stratification, this had no consequences for our findings. In order to perform our enrichment analysis of the epigenetic background across NSCLC phenotypes on a gene level methylation signals were averaged. Although this approach resulted in relevant and consistent findings, it may lead to inevitable loss of information as its effect varies across different gene regions. For instance, hypermethylation of high density CpG regions has been recognized to strongly associate with gene expression regulation [29]. Lastly, splicing variants and small cumulative effects within several genes in the same pathway have not taken into consideration in the RNA expression analysis. Alternative splicing may have a functional impact and is increased in cancer compared to normal tissue [29].

Together these results show that NSCLC phenotypes are largely determined by epigenetic regulation of a small conserved group of genes, involved in extracellular matrix and cell structure. Methylation controls immune related genes – also those involved in endogenous retroviral sequences - that show a larger expression diversity in tumor than in non-cancerous tissue. Decreased expression of genes involved in antigen presentation are the main immune related defect in NSCLC, highlighting their importance for immune invasion by the tumor.

REFERENCES

1. H.J.M. Groen, T.J.N. Hiltermann, Air Pollution and Adenocarcinoma in Never-Smokers, J. Thorac. Oncol. 14 (2019) 761–763. https://doi.org/10.1016/j.jtho.2019.02.007.
2. T. Sato, E. Arai, T. Kohno, Y.et al., Epigenetic clustering of lung adenocarcinomas based on DNA methylation profiles in adjacent lung tissue: Its correlation with smoking history and chronic obstructive pulmonary disease, Int. J. Cancer. 135 (2014) 319–334. https://doi.org/10.1002/ijc.28684.
3. P.S. Hammerman, M.S. Lawrence, D. Voet, et al., Comprehensive genomic characterization of squamous cell lung cancers, Nature. 489 (2012) 519–525. https://doi.org/10.1038/nature11404.
4. E.A. Collisson, J.D. Campbell, A.N. Brooks, et al., Comprehensive molecular profiling of lung adenocarcinoma, Nature. 511 (2014) 543–550. https://doi.org/10.1038/nature13385.
5. K.A. Hoadley, C. Yau, D.M. Wolf, et al., Multiplatform analysis of 12 cancer types reveals molecular classification within and across tissues of origin, Cell. 158 (2014) 929–944. https://doi.org/10.1016/j.cell.2014.06.049.
6. F. Chen, Y. Zhang, E. Parra, et al., Multiplatform-based molecular subtypes of non-small-cell lung cancer, Oncogene. 36 (2017) 1384–1393. https://doi.org/10.1038/onc.2016.303.
7. C. Moison, C. Senamaud-Beaufort, L. Fourrière, et al, DNA methylation associated with polycomb repression in retinoic acid receptor β silencing, FASEB J. 27 (2013) 1468–1478. https://doi.org/10.1096/fj.12-210971.
8. A.J. Gentles, S. V. Bratman, L.J. Lee, et al, Integrating Tumor and Stromal Gene Expression Signatures with Clinical Indices for Survival Stratification of Early-Stage Non-Small Cell Lung Cancer, J. Natl. Cancer Inst. 107 (2015) 1–11. https://doi.org/10.1093/jnci/djv211.
9. L. Horn, D.R. Spigel, E.E. Vokes, et al, Nivolumab Versus Docetaxel in Previously Treated Patients With Advanced Non–Small-Cell Lung Cancer: Two-Year Outcomes From Two Randomized, Open-Label, Phase III Trials (CheckMate 017 and CheckMate 057), J. Clin. Oncol. 35 (2017) 3924–3933. https://doi.org/10.1200/jco.2017.74.3062.
10. X. Wang, Y. Wang, G. Xiao, et al, Hypermethylated in cancer 1(HIC1) suppresses non-small cell lung cancer progression by targeting interleukin-6/Stat3 pathway, Oncotarget. 7 (2016) 30350–30364. https://doi.org/10.18632/oncotarget.8734.
11. C.A. Wright, F.R.C. Path, M. Van Der Burg, et al, Diagnosing Mycobacterial Lymphadenitis in Children Using Fine Needle Aspiration Biopsy : Cytomorphology , ZN Staining and Autofluorescence — Making More of Less, Diagn. Cytopathol. 36 (2008) 245–251. https://doi.org/10.1002/dc.
12. W.D. Travis, E. Brambilla, M. Noguchi, et al., International Association for the Study of Lung Cancer/American Thoracic Society/European Respiratory Society International Multidisciplinary Classification of Lung Adenocarcinoma, Physiol. Behav. 176 (2019) 139–148. https://doi.org/10.1016/j.physbeh.2017.03.040.
13. A.G. Nicholson, D. Gonzalez, P. Shah, et al., Refining the diagnosis and EGFR status of non-small cell lung carcinoma in biopsy and cytologic material, using a panel of Mucin staining, TTF-1, cytokeratin 5/6, and P63, and EGFR mutation analysis, J. Thorac. Oncol. 5 (2010) 436–441. https://doi.org/10.1097/JTO.0b013e3181c6ed9b.

14. I. Datar, K. A. Villarroel-Espindola, FranzHenick, Brian S.Syrigos, Konstantinos N.Toki, MariaRimm, David L.Ferrone, SoldanoHerbst, Roy S.Schalper, J. Clin. Oncol. 36 (2018), doi:10.1200/JCO.2018.36.15_suppl.12015.
15. P. Leone, E.C. Shin, F. Perosa, et al., MHC class i antigen processing and presenting machinery: Organization, function, and defects in tumor cells, J. Natl. Cancer Inst. 105 (2013) 1172–1187. https://doi.org/10.1093/jnci/djt184.
16. J.M. Zaretsky, A. Garcia-Diaz, D.S. Shin, et al., Mutations associated with acquired resistance to PD-1 blockade in melanoma, N. Engl. J. Med. 375 (2016) 819–829. https://doi.org/10.1056/NEJMoa1604958.
17. S.J. Patel, N.E. Sanjana, R.J. Kishton, et al., Identification of essential genes for cancer immunotherapy Shashank, Nature. 548 (2015) 537–542. https://doi.org/10.1038/ncomms5930.Genetic.
18. N. McGranahan, R. Rosenthal, C.T. Hiley, et al., Allele-Specific HLA Loss and Immune Escape in Lung Cancer Evolution, Cell. 171 (2017) 1259-1271.e11. https://doi.org/10.1016/j.cell.2017.10.001.
19. R. Rosenthal, E.L. Cadieux, R. Salgado, et al., Neoantigen-directed immune escape in lung cancer evolution, Nature. 567 (2019) 479–485. https://doi.org/10.1038/s41586-019-1032-7.
20. A.S. Attermann, A.M. Bjerregaard, S.K. Saini, et al., Human endogenous retroviruses and their implication for immunotherapeutics of cancer, Ann. Oncol. 29 (2018) 2183–2191. https://doi.org/10.1093/annonc/mdy413.
21. S.R. Richardson, A.J. Doucet, H.C. Kopera, et al., The Influence of LINE-1 and SINE Retrotransposons on Mammalian Genomes, Mob. DNA III. 3 (2015) 1165–1208. https://doi.org/10.1128/microbiolspec.mdna3-0061-2014.
22. E.M. Wolff, H.M. Byun, H.F. Han, et al., Hypomethylation of a LINE-1 promoter activates an alternate transcript of the MET oncogene in bladders with cancer, PLoS Genet. 6 (2010). https://doi.org/10.1371/journal.pgen.1000917.
23. C. Phokaew, S. Kowudtitham, K. Subbalekha,et al., LINE-1 methylation patterns of different loci in normal and cancerous cells., Nucleic Acids Res. 36 (2008) 5704–5712. https://doi.org/10.1093/nar/gkn571.
24. M.S. Rooney, S.A. Shukla, C.J. Wu, et al., Molecular and genetic properties of tumors associated with local immune cytolytic activity, Cell. 160 (2015). https://doi.org/10.1016/j.physbeh.2017.03.040.
25. C.A. Jefferies, Regulating IRFs in IFN driven disease, Front. Immunol. 10 (2019) 1–15. https://doi.org/10.3389/fimmu.2019.00325.
26. L. Nousiainen, M. Sillanpää, M. Jiang, et al., Human kinome analysis reveals novel kinases contributing to virus infection and retinoic-acid inducible gene I-induced type i and type III IFN gene expression, Innate Immun. 19 (2013) 516–530. https://doi.org/10.1177/1753425912473345.
27. J. Yan, Q. Li, A.P. Mao, et al., TRIM4 modulates type i interferon induction and cellular antiviral response by targeting RIG-I for K63-linked ubiquitination, J. Mol. Cell Biol. 6 (2014) 154–163. https://doi.org/10.1093/jmcb/mju005.

28. L.A. Robinson, C.J. Jaing, C. Pierce Campbell, et al., Molecular evidence of viral DNA in non-small cell lung cancer and non-neoplastic lung, Br. J. Cancer. 115 (2016) 497–504. https://doi.org/10.1038/bjc.2016.213.
29. M. Moarii, V. Boeva, J.P. Vert, F. Reyal, Changes in correlation between promoter methylation and gene expression in cancer, BMC Genomics. 16 (2015) 1–14. https://doi.org/10.1186/s12864-015-1994-2.
30. L. Chen, D.B. Flies, Molecular mechanisms of T cell co-stimulation and co-inhibition, Nat. Rev. Immunol. 13 (2013) 227–242. https://doi.org/10.1038/nri3405.
31. N. Lee, M. Llano, M. Carretero, et al., HLA-E is a major ligand for the natural killer inhibitory receptor CD94/NKG2A, Proc. Natl. Acad. Sci. U. S. A. 95 (1998) 5199–5204. https://doi.org/10.1073/pnas.95.9.5199.
32. J. Eugène, N. Jouand, K. Ducoin, et al., The inhibitory receptor CD94/NKG2A on CD8+ tumor-infiltrating lymphocytes in colorectal cancer: a promising new druggable immune checkpoint in the context of HLAE/β2m overexpression, Mod. Pathol. (2019). https://doi.org/10.1038/s41379-019-0322-9.
33. K.S. Kobayashi, P.J. Van Den Elsen, NLRC5: A key regulator of MHC class I-dependent immune responses, Nat. Rev. Immunol. 12 (2012) 813–820. https://doi.org/10.1038/nri3339.
34. J.M. Vahl, J. Friedrich, S. Mittler, et al., Interleukin-10-regulated tumour tolerance in non-small cell lung cancer, Br. J. Cancer. 117 (2017) 1644–1655. https://doi.org/10.1038/bjc.2017.336.
35. D.H. Munn, M.D. Sharma, A.L. Mellor, Ligation of B7-1/B7-2 by Human CD4 + T Cells Triggers Indoleamine 2,3-Dioxygenase Activity in Dendritic Cells , J. Immunol. 172 (2004) 4100–4110. https://doi.org/10.4049/jimmunol.172.7.4100.
36. W.Z. Nisha Nagarsheth, M.S. Wicha, Chemokines in the cancer microenvironment and their relevance in cancer immunotherapy, Nat. Rev. Immunol. 17 (2017) 559–572. https://doi.org/10.1016/j.physbeh.2017.03.040.

SUPPLEMENTARY INFORMATION

1. Data preparation

During the three days of the hackathon sessions, data preparation was performed. Before analysis, a few steps were taken to make data clean and ready for analyses. For the methylation dataset, 89.000 probe IDs with missing methylation value for every patient were removed. For the probe IDs that have missing values for some patients, an imputation method was used. To be specific, the missing values were replaced by the median value of methylation for the corresponding probe IDs on all patients.

For gene expression dataset, gene name and chromosome number and start position are concatenated together to create unique "probe IDs". Duplicated probe IDs are removed from the dataset (25 probe IDs). Similar method as for the methylation dataset was used to handle missing values. Further in the cleaning process, probe IDs with all gene expression values of 0 or with no variance are removed (2.123 probe IDs in total).

2. Cohort bias correction

ComBat, an empirical Bayes location/scaling method, was applied for cohort bias correction. No significant decrease in phenotype separation was observed. However, for the DNA methylation data ComBat correction qualitatively altered the probe wise distributions; basically by removing the bimodality and reducing the differential expression (1). This is further motivated by the fact that the means of the first principal components over the cohorts are approximately centered around the origin for adenocarcinoma and SCC, also the median and mean shift with respect to the median/mean of the entire set is centered around the origin (2). Applying the same statistical tests to separate groups of batches with either only adenocarcinoma or only SCC, a non-significant decrease in batch separation was observed. When looking to the main oncogene drivers in NSCLC and the top six genes that differentiate adenocarcinoma from squamous cell lung cancer, both were unaffected by ComBat correction (Fig. 1,2)

BEclear uses inter-batch ks-scores to decide which probes should be corrected and subsequently uses a matrix factorization method to produce the new probe values. Although one loses signal in cohorts with between-array and within-array corrections, the results for DNA expression data are very limited. If we look into the corrected data dimensions, the number of methylation probes reduced by 8% and gene expression data by 23%.

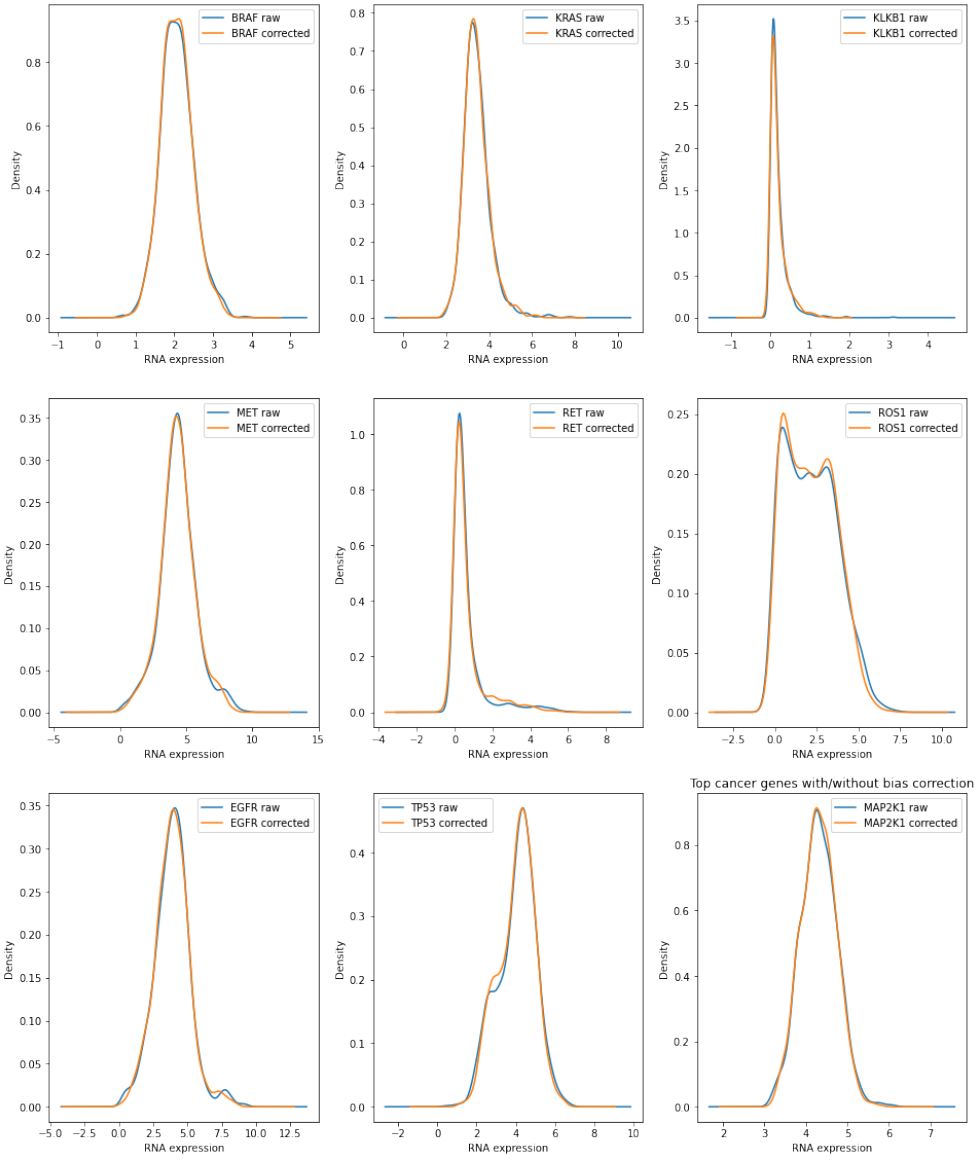

Figure 1. Top cancer genes of NSCLC are unaffected by ComBat correction.

Similarly, for the top 1% percentile of genes with a p-value <0.001, the six genes were found, which are slightly shifted for the non-parametric corrected data.

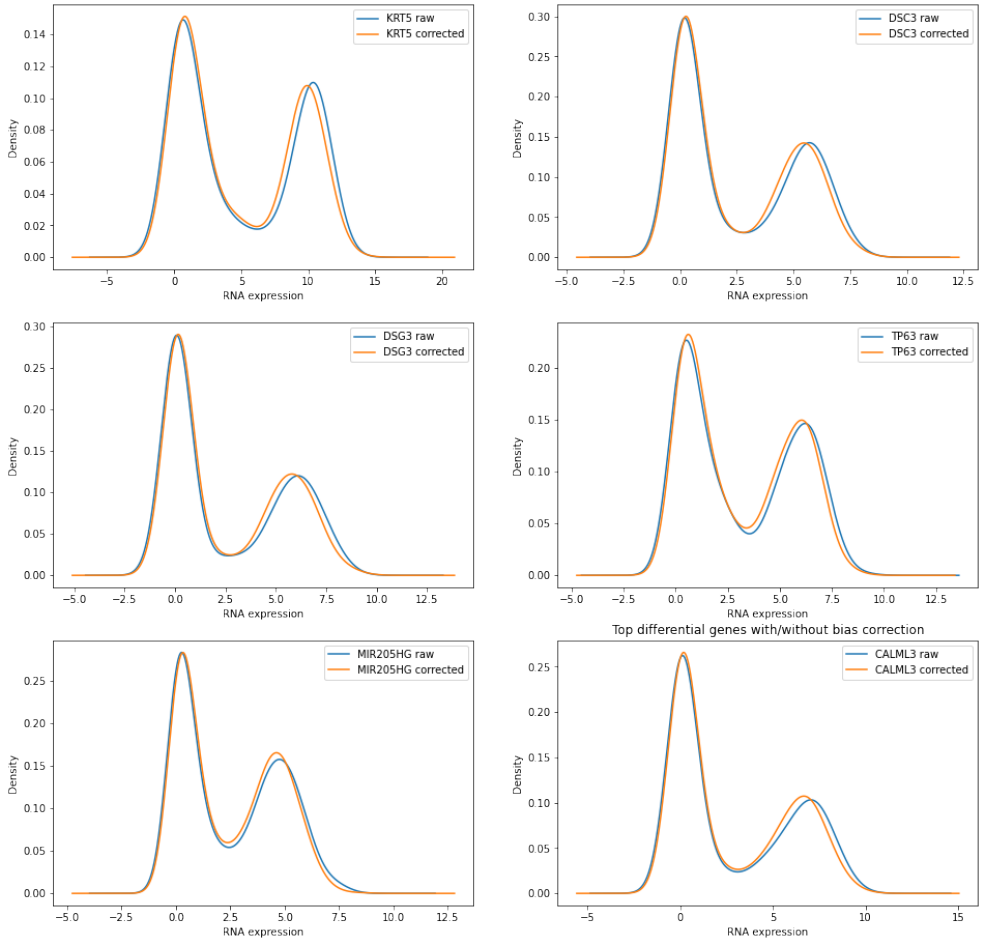

Figure 2. Six top-genes KRT5, DSC3, DSG3, TP63, MIR205HG, CALML3 from DNA expression are non-significantly shifted after ComBat correction tested by Kolmogorov-Smirnov test.

In conclusion, our corrections were performed in such a way that important biological signals are not eliminated by batch and cohort corrections.

3. Principal component analysis (PCA)

PCA is a statistical method, that will reduce the number of dimensions within a dataset. The extracted features, or principle components, have the following properties:

1. For p-dimensional data (x1,…,xp), a principle component PC is a linear combination of the original variables, hence PC=a1.x1+a2.x2+…+ap.xp, where |a|=1.

2. For principle component PCk, the loadings vector ak=a1,…,apk is obtained by finding the linear projection that maximizes the total amount of variance within the dataset.
3. Each new generated principle component is orthogonal to all of the previous principle components. Hence, for the k^{th} principle component, we have ak.aj=0 for each j<k.

By definition of these properties, from a p-dimensional dataset that consist of n observations, at most (n, p) principle components can be extracted.
The optimal number of principle components to select for the analysis is subjective to the application. We have used 10 dimensions. As, by definition of point 2 and 3 above, all principle components are both independent of each other and decreasingly ordered in amount of variance they explain.

4. Separability of adenocarcinoma and squamous cell lung carcinoma

a. by ks-score

The Kolmogorov-Smirnov test (ks test) is a nonparametric test that compares two data samples. The goal of the ks test is to determine whether two data samples come from the same distribution, noting that it is not specified what that common distribution is. The ks-score quantifies a distance between the empirical distribution functions of two samples. The ks-score is mathematically defined by:

$$Dn,m=|F1,nx-F1,mx|\ ,$$

where F1,n and F2,m are the empirical distribution functions of the first and the second sample respectively, and the supremum function. If both samples comes from the same distribution, then Dn,m converges to 0 almost surely in the limit. To conclude, the ks score lays in the interval [0,1], where a score closer to zero indicates that both samples are more likely to be drawn from the same distribution.

We determined the ks-score for each gene x. by methylation probes.

$$\text{ks-score}\ (x) = \frac{Sum\ of\ all\ ks\ scores\ of\ the\ probes\ in\ gene\ x}{Number\ of\ probes\ in\ gene\ x}$$

The ks-score indicates the ability to separate between the subtypes of NSCLC (adenocarcinoma or squamous cell lung carcinoma), where 1 indicates high separability and 0 no separability.

b. Best Split method

To approximate the best split for histological subtypes we used the median for the global distributions for each methylation probe. A more sophisticated method for determining an approximation for the best split is Hartigan's dip test but we found no qualitative difference when applied to a subset of probes. We also applied differential evolution to optimize the

accuracy of the best RNA expression split, but this approach did not noticeably increase the accuracy. Because of the balanced presence of the subtypes adenocarcinoma and squamous cell carcinoma we used the medians of the methylation and RNA expressions distributions. Given the approximate split, we established for each split the accuracy and recall in separating the two subtypes. We required a minimum precision of 85% for both subtypes. This operation was performed over the probes, ordered by descending fold change, until the number of successive failures to meet the minimum precision exceeded a threshold (in this case 50).

5. Bridge between DNA methylation and RNA expression

Methylation values of the genes (β-value for a probe per sample ranged from 0 to 1(0: unmethylated, 1: methylated) and the total RNA expression in tumor samples were studied. Methylation influences a change in gene expression. Samples in quantile 1 have the lowest RNA expression and samples in quantile 4 have the highest RNA expression. For each quantile and probe_ID the corresponding methylation distribution out of the methylation dataset is visualized by a boxplot.

For combining DNA methylation and RNA expression data we obtained a list of overlapping differential genes and used the Wasserstein distance metric, a way to compare the probability distributions, where one variable is derived from the other by small, non-uniform random or deterministic perturbations. We defined three metrics that combine the statistical separability and the actual separation of the two subtype distributions. These metrics were first Wasserstein distance* ks score, second Wasserstein distance* ks score, and median fold change*ks score on the intersection of the top-500 probes for RNA expression and methylation that leads to 41 genes. Second, we merged the data for RNA expression and methylation probes on the genes level and took the multiplications of the aggregated values for the three metrics; the overlap of the top-100 gave 28 gene.

6. Survival analysis

Univariate and multivariate survival analysis were performed between the expression profiles of immune modulating gene groups (high vs. low expression), patient and tumor characteristics. Patient factors associated with overall survival ($p<0.1$) were included in the multivariate analysis. Age and the TNM tumor-stage (T1, T2 or T3) reached the significance threshold ($p<0.05$) in the multivariate analysis. The hazards ratios and 95% confidence intervals were used to estimate the pretreatment gene group contribution on predicting overall survival.

References

1 Dedeurwaerder, S. et al. A comprehensive overview of Infinium HumanMethylation450 data processing. Brief Bioinform 15, 929-941, doi:bbt054 [pii]10.1093/bib/bbt054 (2014).

2 Hicks, S. C. et al. Smooth quantile normalization. Biostatistics 19, 185-198, doi:3949169 [pii]10.1093/biostatistics/kxx028 (2018).

Extended Data Table 1. Top 41 gene list for best separation of NSCLC subtypes

Chromosome	Gene	Start	Stop	Strand	Fold change
chr15	BNC1	83255903	83284716	-	15.04
chr10	CALML3	5524009	5526771	+	13.32
chr5	IRX4	1877413	1887236	-	12.64
chr18	DSC3	30990008	31042815	-	10.34
chr1	MIR205HG	209428820	209432838	+	4.79
chr3	TP63	189631416	189897279	+	3.89
chr2	DQX1	74518131	74526336	-	3.13
chr11	TRIM29	120111275	120185529	-	2.73
chr9	CEL	133061978	133087355	+	2.70
chr14	TGM1	24249114	24264432	-	2.47
chr7	SOSTDC1	16461481	16530580	-	2.42
chr3	CSTA	122325244	122341972	+	1.46
chr7	AKR1B10	134527592	134541408	+	1.37
chr17	RAPGEFL1	40177010	40195656	+	1.14
chr1	SLC16A1	112911847	112957013	-	0.98
chr18	KCTD1	26454910	26657401	-	0.97
chr8	SNAI2	48917690	48921740	-	0.89
chr1	VANGL2	160400586	160428678	+	0.84
chr14	FRMD6	51489100	51730727	+	0.82
chr6	DST	56457987	56954628	-	0.73
chrX	EFNB1	68828997	68842147	+	0.51
chr7	FSCN1	5592823	5606655	+	0.45
chr19	FXYD3	35115879	35124324	+	0.44
chr3	DLG1	197042560	197299300	-	0.38
chr16	ABCC1	15949577	16143074	+	0.37
chr12	ZNF385A	54369133	54391298	-	0.36
chr3	ACTL6A	179562880	179588408	+	0.30
chr17	JUP	41754604	41786931	-	0.20
chrX	ZDHHC9	129803288	129843909	-	-0.22
chr12	DRAM1	101877351	102012130	+	-0.28
chr12	KRT7	52232520	52252186	+	-0.43
chr21	CLIC6	34669389	34718227	+	-0.43
chr13	ATP11A	112690329	112887168	+	-0.43
chr4	HOPX	56647988	56681899	-	-0.46
chr6	SLC44A4	31863192	31879046	-	-0.56
chr1	PLEKHA6	204218851	204377665	-	-0.57
chr15	ALPK3	84816680	84873482	+	-0.61
chr4	SLC4A4	71187286	71572087	+	-0.67
chr14	NKX2-1	36516392	36521149	-	-0.68
chr14	SFTA3	36473288	36513829	-	-0.71
chr17	HNF1B	37686432	37745247	-	-0.84

Extended Data Table 2. Association of immune modulating groups with survival

			COX regression univariate			COX regression multivariate		
Covariate	**Factor**	**Comparison**	**P-value**	**HR**	**95% CI**	**P-value**	**HR**	**95% CI**
Categorical	COSTIM	High vs. low	0.822	1.022	(0.847, 1.232)	0.834	1.041	(0.714, 1.517)
Categorical	AGPRES	High vs. low	0.966	1.004	(0.833, 1.210)	0.116	0.786	(0.583, 1.061)
Categorical	COINHIB	High vs. low	0.486	1.069	(0.886, 1.289)	0.754	1.069	(0.704, 1.624)
Categorical	CYTOCHEM	High vs. low	0.955	0.995	(0.825, 1.200)	0.890	1.020	(0.776, 1.340)
Categorical	Tumor type	SCC vs. adeno	0.601	1.051	(0.872, 1.267)			
Categorical	Gender	Female vs. male	0.270	1.114	(0.919, 1.351)			
Continuous	Age (years)		0.031	1.011	(1.001, 1.022)	0.005*	1.018	(1.006, 1.032)
Categorical	Smoking	Lifelong non-smoker vs. current/ex- smoker	0.072	1.338	(0.975, 1.836)	0.099	1.374	(0.942, 2.002)
Continuous	Pack years		0.893	1.000	(1.000, 1.000)			
Continuous	Tumor stage		0.000	1.487	(1.346, 1.646)	0.253	1.172	(0.893, 1.540)
Continuous	T-stage*		0.000	1.440	(1.279, 1.622)	0.011*	1.266	(1.055, 1.532)
Continuous	N-stage		0.000	1.416	(1.256, 1.597)	0.130	1.204	(0.947, 1.532)
Continuous	M-stage		0.000	2.349	(1.535, 3.594)	0.401	1.351	(0.670, 2.723)

Pretreatment immune status adjusted for clinical prognostic factors in 1026 patient with non-small cell lung cancer is not associated with overall survival. Univariate and multivariate analysis of the association between the expression profiles of immune modulating gene groups (high vs. low expression), (patient) factors and overall survival. Factors were incorporated as categorical or continuous variables. Patient factors associated with overall survival ($p<0.1$) were included in the multivariate analysis. Age and the TNM tumor-stage (T1, T2 or T3) reached the significance threshold ($p<0.05$) in the multivariate analysis. Abbreviations: hazard ratio (HR), 95% confidence interval (95% CI), adenocarcinoma (adeno).

Extended Data Table 3. Patient characteristics

Age at tumor biopsy (years)		
Median (range)	67	(33 - 90)
Gender, M/F	614/410	
Smoking status, n (%)		
Never smoker	93	(9)
Former smoker > 15 years	219	(21)
Former smoker ≤ 15 years	421	(41)
Former smoker, unspecified duration	9	(1)
Current smoker	256	(25)
Unknown	26	(3)
Total	1024	(100)
Follow-up (of censored patients; months)		
Median (range)	23	(0 - 242)
Tumor stage, n (%)		
I	524	(51)
II	286	(28)
III	169	(17)
IV	33	(3)
Unknown	12	(1)
Total	1024	(100)
T stage, n (%)		
T1	286	(28)
T2	574	(56)
T3	118	(12)
T4	43	(4)
Tx	3	
Total	1024	(100)
N stage, n (%)		
N0	655	(64)
N1	230	(22)
N2	114	(11)
N3	7	(1)
Nx	17	(2)
Unknown	1	
Total	1024	(100)
M stage, n (%)		
M0	765	(74)
M1	32	(3)
Mx	219	(23)
Unknown	8	
Total	1024	(100)

Abbreviations: number (n), squamous cell lung cancer (SCC).

Extended Data Table 4. Immune modulating gene groups

COSTIMULATORY		COINHIBITORY		AGPRES	CYTOCHEM
Receptor	**Ligand**	**Receptor**	**Ligand**		
CD28	CD80, CD86	CD272	VTCN1	HLAA	TGFB1
CD134	OX40L	CD279	PDCD1LG1, PDCD1LG2	HLAB	TNF
CD137	4-1BBL	CD94, NKG2A	HLAE	HLAC	IL6
CD40L	CD40	CTLA4	CD80, CD86	CIITA	IL10
CD278	ICOSL	TIGIT	CD155, CD112, CD113	LMP2	IFNG
CD27	CD70	CD160	HVEM	TAP1	IDO
HVEM	LIGHT	PD1HR	PD1H	LMP7	
LIGHT	HVEM	2B4	CD48	TAPBP	
DR3	TL1A	TIM3	LGALS9, PS		
GITR	GITRL				
CD30	CD30L				
TIM1	TIM4				
SLAM	SLAM				
CD2	CD48, CD58				
CD226	CD155, CD112				

Four known clusters of genes involved in stimulating and inhibiting T lymphocyte responses, antigen presentation (AGPRES), and cyto- and chemokines (CYTOCHEM).

Extended Data Figure 1. Main canonical pathways based on DNA methylation.

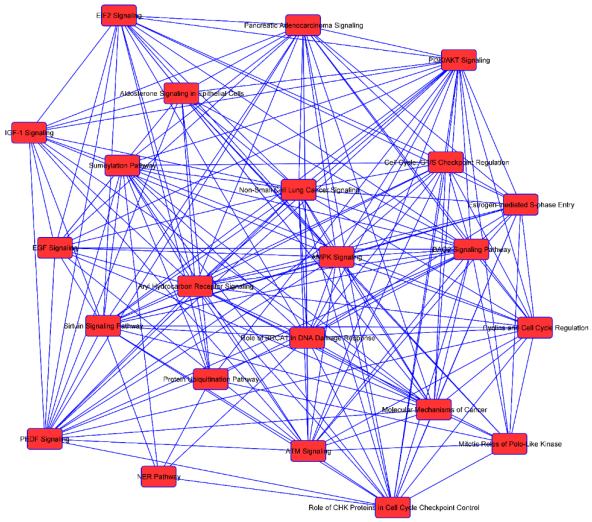

Main canonical pathways of 2,101 mapped genes with at least one probe and with ks-score ≥ 0.95 that are most distinct for NSCLC subtypes based on DNA methylation.

Extended Data Figure 2. Gene groups involved in antigen presentation and co-stimulation

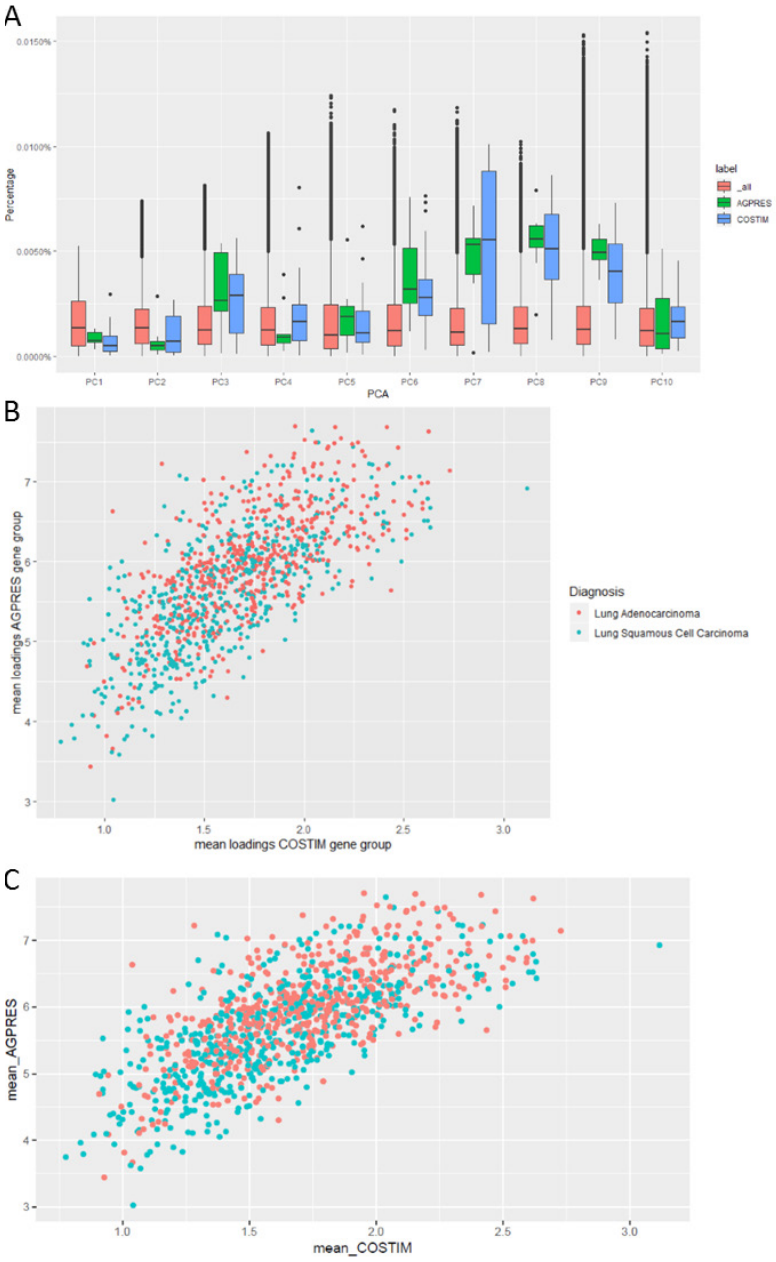

(A) Principal component analysis of gene expression can distinguish antigen presentation and costimulatory genes from other genes. (B) In both NSCLC subtypes, the higher expression of antigen presenting genes is associated with higher expression of costimulatory genes; (C) and similar in non-small cell lung cancer tissue and non-cancerous tissue.

CHAPTER 11

11

CD45RA+CCR7- CD8+ T cells lacking co-stimulatory receptors demonstrate enhanced frequency in peripheral blood of NSCLC patients responding to nivolumab

Andre Kunert*, Edwin A. Basak*, Daan P. Hurkmans, Hayri E. Balcioglu, Yarne Klaver, Mandy van Brakel, Astrid A.M. Oostvogels, Cor H.J. Lamers, Sander Bins, Stijn L.W. Koolen, Astrid A.M. van der Veldt, Stefan Sleijfer, Ron H.J. Mathijssen, Joachim G.J.V. Aerts*, Reno Debets*

*Shared first/senior authorship

Journal for ImmunoTherapy of Cancer, June 2019, 7: 149

Abstract

Introduction: Checkpoint inhibitors have become standard care of treatment for non-small cell lung cancer (NSCLC), yet only a limited fraction of patients experiences durable clinical benefit, highlighting the need for markers to stratify patient populations.

Materials and Methods: To prospectively identify patients showing response to therapy, we have stained peripheral blood samples of NSCLC patients treated with 2nd line nivolumab (n = 71), as well as healthy controls, with multiplex flow cytometry. By doing so, we enumerated 18 immune cell subsets and assessed expression for 28 T cell markers, which was followed by dimensionality reduction as well as rationale-based analyses.

Results: In patients with a partial response (PR), representing best overall response (BOR) according to RECIST v1.1, the number of CD8 T cells at baseline and during treatment is similar to those of healthy controls, but 2-fold higher than in patients with progressive and stable disease (PD and SD). CD8 T cell populations in PR patients show enhanced frequencies of T effector memory re-expressing CD45RA (TEMRA) cells, as well as T cells that express markers of terminal differentiation ($CD95^{+}$) and egression from tumor tissue ($CD69^{-}$). In PR patients, the fraction of CD8 T cells that lacks co-stimulatory receptors (CD28, ICOS, CD40L, 4-1BB, OX40) correlates significantly with the total numbers and differentiated phenotype of CD8 T cells.

Discussion: This study demonstrates that high numbers of peripheral CD8 T cells expressing differentiation markers and lacking co-stimulatory receptors at baseline are associated with response to nivolumab in NSCLC patients.

INTRODUCTION

The onset of T cell activation and differentiation, generally a consequence of the T cell receptor (TCR) recognizing its cognate antigen, is usually accompanied by up-regulated expression of co-inhibitory receptors such as programmed-death 1 (PD-1), proving a negative feedback mechanism to keep T cell activity 'in check' [1, 2]. Many types of cancer exploit this adaptive immunity and demonstrate high expression levels of co-inhibitory ligands such as PD-L1 to resist anti-tumor T cell responses. Clinical use of nivolumab, a monoclonal antibody targeting PD-1, showed promising results in metastatic melanoma [3], NSCLC [4, 5] as well as various other types of cancer [6]. Collectively, however, study results reveal that only a limited subset of patients experiences durable clinical benefit [7]. This highlights the need for markers that would identify patients prone to responding to treatment at an early time point and select these patients for extended treatment, thereby avoiding further exposure of patients with limited benefit to a potentially toxic and costly treatment.

Initial searches for predictive markers focused on the expression of PD-L1 [8, 9], but despite FDA approval for patient stratification based on PD-L1 expression in primary tumor tissue of NSCLC patients, interpretation of such immune stainings with respect to cell type and optimal cut off percentage remains challenging [10, 11]. Similarly, investigations assessing tumor mutational burden (TMB), mismatch repair deficiency (dMMR) and microsatellite instability (MSI) reveal that a high score on each of these markers correlates with enhanced responsiveness to anti-PD-1 therapy [12, 13], but on their own these markers may not be sufficiently discriminative to predict clinical response. Also, CD8 T cell density within tumor biopsies has been shown to predict anti-PD-1 response in patients diagnosed with advanced melanoma [14]. Interestingly, local CD8 T cell immunity is affected by escape mechanisms [15], and profiles based on multiple immune parameters, such as the presence of effector cells, MHC molecules, suppressor cells, as well as immune and metabolic checkpoints provide predictive value exceeding that of single markers such as PD-L1 or mutational load [16,17,18]. However, limited availability of biopsy tissue and its invasiveness, especially in case of visceral tumors, often limits in situ determination of such markers. Multi-parameter analysis of immune cell subsets in blood is an easily employable screening method anticipated to reveal surrogate markers for clinical responses. Indeed, the absolute number of lymphocytes in blood samples correlates with clinical outcome in melanoma patients treated with ipilimumab, a monoclonal antibody targeting the co-inhibitory receptor CTLA-4 [19]. And more recently, Ki67 expression in a subset of $PD^{-}1^{+}$ $CD8^{+}$ T cells has been reported as a measure of effector T cell invigoration in patients with advanced melanoma and NSCLC who were treated with antibodies targeting the PD-1/PD-L1 axis [20,21,22].

In the current study, we have enumerated 18 immune cell populations and performed both cluster and selected analyses to assess differential frequencies of multiple T cell

subsets using 28 markers of T cell activation, maturation, co-signaling and chemotaxis in NSCLC patients treated with 2nd line nivolumab in order to obtain prospective immune markers identifying those patients showing a clear response to therapy.

MATERIALS AND METHODS

Study design

The MULTOMAB study (local ethics board study number MEC16–011) was originally designed by the Laboratory of Translational Pharmacology, Dept Medical Oncology at the Erasmus MC Cancer Institute (PIs: R. Mathijssen; J. Aerts and R. Debets). Patients asked to participate in the reported analysis are suffering from NSCLC and receiving treatment in the form of nivolumab (BMS936558, Opdivo®). Written informed consent was obtained from all participants prior to inclusion into the study.

Patients and collection of specimens

Data was prospectively collected from NSCLC patients treated with 3 mg/kg of nivolumab (intravenously every 2 weeks) between May 5th 2016 and November 1st 2017, with a minimum follow-up of three months. Patient characteristics are provided in Additional file 1: Table S1. Blood was drawn at 3 time points (pre-treatment ("baseline") and prior to 2nd and 3rd administration of nivolumab (visits (V) 1 and 2). For an overview of patient treatment and sample acquisition, see Additional file 1: Figure S1. Freshly obtained, whole blood was used to enumerate immune cell populations, whereas PBMCs were isolated using ficoll gradient and stored using standard protocols and thawed at later time points to assess frequencies of T cell subsets. Healthy control samples were obtained from 15 donors that were matched with patients for age and gender-distribution (median age: 65 years (60–69); 6 female (40%) and 9 male (60%) donors) (Sanquin, Amsterdam, The Netherlands).

Assessment of tumor volume and clinical response

Baseline tumor burden was defined as the sum of the longest diameter of all target lesions. Best overall response (BOR) was assessed according to RECIST v1.1. Partial response (PR) was defined as a minimal decrease of 30% in the sum of diameters of the target lesions, taking as reference the sum of diameters at baseline, while progressive disease (PD) was defined as a minimal increase of 20% in the sum of diameters of the target lesions, taking as reference the smallest sum of diameters while on study and a minimal absolute increase of 5 mm. Stable disease (SD) was defined as insufficient change in tumor sizes to qualify for either PR or PD and if duration of SD was 90 days or more. Patients with non-measurable lesions were excluded from analysis. All three BOR response groups displayed similar medians and ranges with regard to age, sex and histology of primary lung tumor.

Flow cytometry

Whole blood was stained and after lysis of red blood cells analyzed by multi-color FCM on a BD 3-laser Celesta flow cytometer using FACSDIVA 8.x software. Absolute cell counts were determined using Flow-Count Fluorospheres (Beckman Coulter). Cryopreserved PBMC samples were thawed and stained with a master mix of antibodies. Please refer to Additional file 1: Table S2 for an overview of staining panels and utilized markers; all panels were optimized, compensated using Fluorescence minus one (FMO) controls and measurements were corrected for background fluorescence; a detailed list of antibodies is available upon request. Data were gated and analyzed using FlowJo software (Tree Star). Please refer to Additional file 1: Table S3 for an overview of our data analysis work scheme, in which dimensionality reduction analysis (tSNE, see below) preceded two-dimension (2D) analysis of selected markers. The latter analysis of large datasets was conducted using R.

T-distributed stochastic neighbor embedding (tSNE) analysis

tSNE analysis was performed using the Cytosplore software, with an interactive graphical user interface. CD8 T cell populations were extracted as individual .fcs files and imported into Cytosplore [23], where they were down-sampled to at most 1000 cells per sample, and tSNE analysis was performed on these 211,000 ± 6000 data points (cells from 71 patients, 3 time points each). Clustering was carried out with gradients of density plots, where first a threshold (sigma) of 26 was used, which provided 22 ± 8 clusters per combination of markers (see Additional file 1: Table S2, panels 2–6). This threshold was iteratively increased to a lower number of clusters in such a way that differential marker intensities were not compromised, providing a total of 12 ± 4 clusters per combination of markers. A total of 58 clusters was identified across all markers. The marker intensity profiles and contributions of individual BORs in these clusters were extracted from Cytosplore to excel sheets (Microsoft) for visualization.

Statistics

tSNE-identified clusters were tested for differential abundance among BOR groups and time points using the Student's T-test of the scipy stats package in python, while 2D analysis of selected markers was conducted using the Kruskal Wallis test. Descriptive statistics included median, standard deviation and range for continuous variables. For comparison of median differences between individual BOR groups the Mann–Whitney U test was used. For normally distributed data, significant changes of median cell numbers or frequencies within BOR groups over time were determined using two-sided, paired Student's T-test. Correlations between continuous variables were determined by Pearson's r coefficient. Differences were considered significant with a p-value below 0.05.

Data reporting

In this discovery study, experiments were not randomized and the investigators were not blinded to patient sample allocation during experiments and outcome assessment.

RESULTS

NSCLC patients with PR to nivolumab harbor normal, non-decreased numbers of CD8 T cell numbers in blood in contrast to PD and SD

Availability of freshly obtained, peripheral blood of 32 of the 71 NSCLC patients enrolled in this study allowed us to conduct enumeration of 18 major immune cell populations prior to and following nivolumab treatment (for treatment and patient details, please refer to Additional file 1: Figure S1 and Additional file 1: Table S1). Patients were assessed for their best overall response (BOR) according to RECIST v1.1 within a follow-up time of at least 90 days (except for patients experiencing progressive disease (PD) within that timeframe) and categorized into patients with partial response (PR; n = 7), stable disease (SD; n = 10) or PD (n = 15). For reference purposes, the same immune cell populations were enumerated in a control group of age and gender-matched healthy individuals (n = 15). **Figure 1** depicts the numbers of immune cells detected per µl of peripheral blood at baseline, after the 1st treatment cycle (2 weeks after baseline, visit (V)1) and 2nd treatment cycle (4 weeks after baseline, V2). Numbers remained unchanged after onset of therapy for the majority of immune cell populations, except for eosinophils, which increased in numbers, independent of BOR, and T cells, which differed significantly between PR and PD patients after onset of therapy (see below). When compared to healthy reference values at baseline (see Additional file 1: Figure S2), numbers of granulocytic and myeloid cell populations were enhanced in all BOR groups, i.e., mature neutrophils, monocytes and M-MDSCs, while numbers of lymphocytes (i.e. B and NK cells), were decreased. At baseline, SD patients displayed an enhanced number of immature neutrophils compared to PR patients, who in turn displayed significantly lowered numbers of these cells compared to healthy controls samples. On the other hand, compared to these healthy reference values, median numbers of T cells at baseline were significantly decreased only in PD and SD, but not in PR patients (see Additional file 1: Figure S2). When assessing the major T cell populations, we observed that αβ-T cells, but in particular their CD8-positive subset represented the T cell population that attributed to the difference among the BOR groups (**Fig. 2**). In example, at baseline we measured a median of 500 CD8 T cells/µl (range: 80–1450) in PR patients, while in SD and PD patients we measured 210 CD8 T cells/µl (30–900) ($p = 0.061$) and 250 CD8 T cells/µl (60–1250) ($p = 0.057$), respectively. This difference increased after onset of therapy. Namely, at time point V1 we measured a median of 560 CD8 T cells/µl (170–1900) in PR patients, while PD and SD patients showed medians of 220 CD8 T cells/µl (90–1070) ($p = 0.032$) and 230 CD8 T cells/µl (10–550) ($p = 0.01$), respectively. Neither γδ-T cells, nor

the CD4-positive αβ-T cell subset displayed significant differences between the three BOR groups.

Figure 1. Nivolumab treatment does not result in changed numbers of peripheral immune cell populations, except eosinophils and T cells

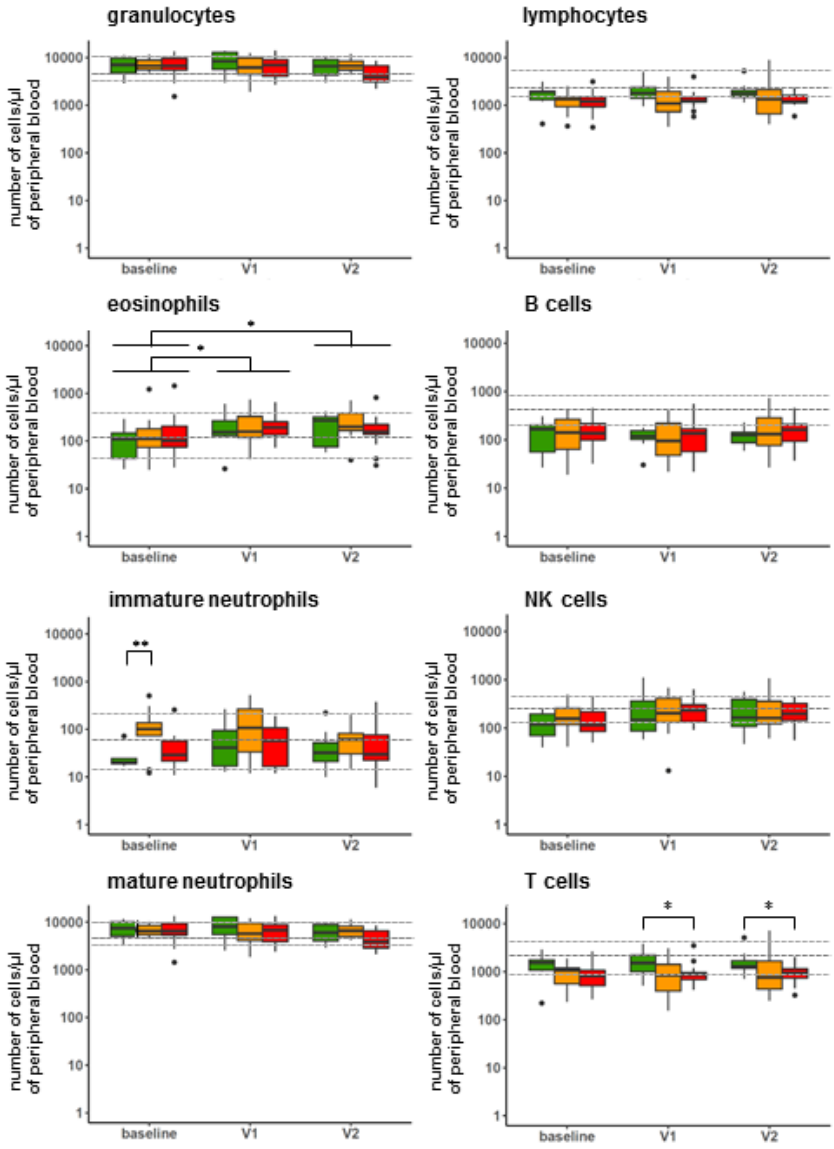

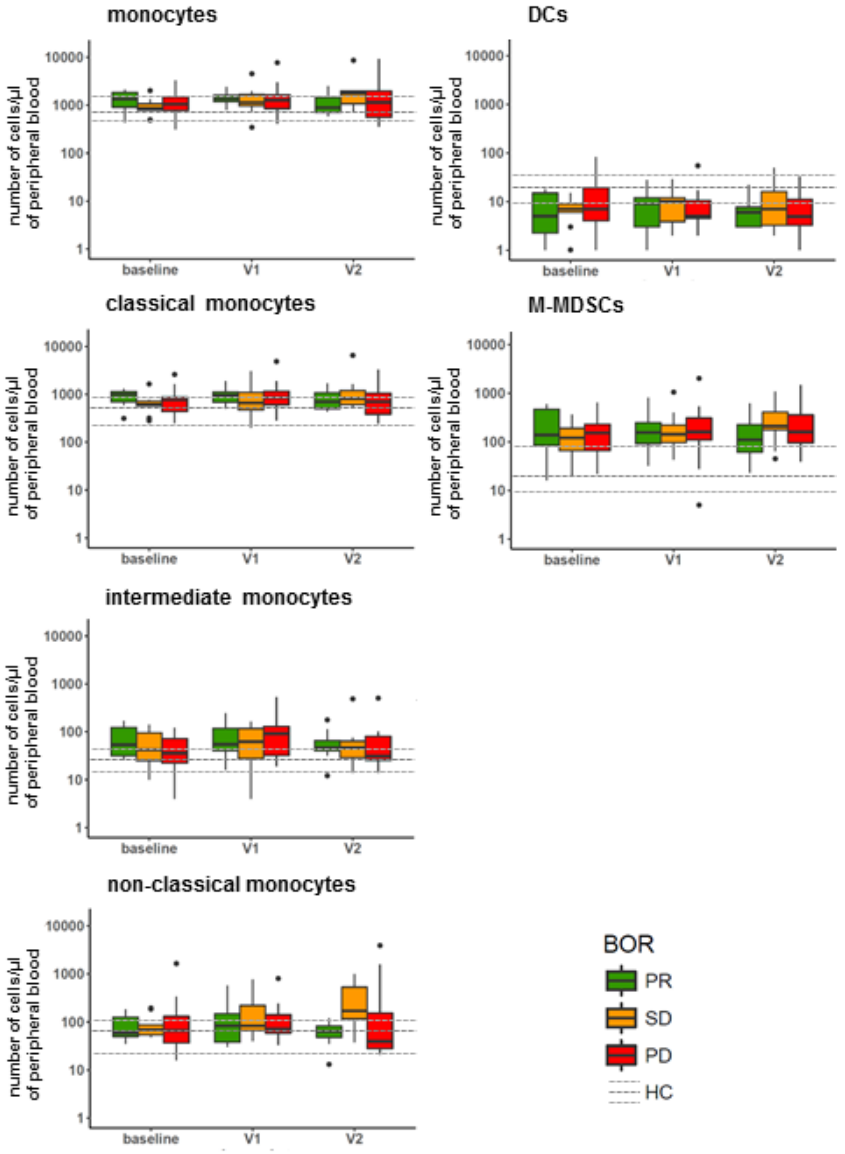

Blood samples taken from patients at baseline, V1 and V2 were stained, ery-lysed and subsequently analyzed by multi-color FCM. Immune cell populations that were enumerated and markers used are listed in Additional file 1: Table S2, panel 1. Median numbers of immune cell populations of healthy controls are indicated by a dark grey, dotted line, and upper and lower quartile ranges are indicated by light grey dotted lines. Statistically significant differences between BOR groups were determined using Mann–Whitney U test. * $p < 0.05$; ** $p < 0.01$. BOR = best overall response, PR = partial response, SD = stable disease, PD = progressive disease, HC = healthy control.

Figure 2. Patients responding to nivolumab show high numbers of CD8 T cells

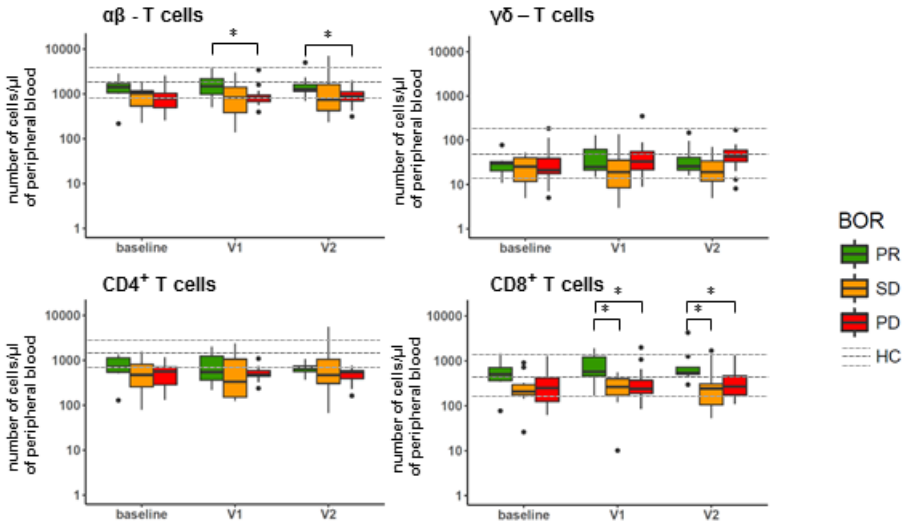

Graphs show numbers of αβ and γδ T cells in peripheral blood and the respective CD4+ and CD8+ subsets of αβ T cells. See legend to Fig. 1 for details, abbreviations and statistical testing.

PR patients show enriched frequencies of CD8 T cells with a phenotype that corresponds to enhanced T cell differentiation

As numbers of CD8 T cells differed between patients in the different BOR groups, we further investigated their particular subsets in more detail. To this end, we stained peripheral blood mononuclear cell (PBMC) samples of a total of 71 NSCLC patients (PR: n = 14; SD: n = 25; PD: n = 32) for 28 markers (Additional file 1: Tables S2 and S3), followed by dimensionality reduction as well as rationale-based analysis to identify (combinations of) markers from each of our flow cytometry panels that would reveal significant differences between BOR groups and time points within the CD8 T cell subset (identical analysis was conducted in CD4 T cells; data not shown). Starting with T cell maturation markers, and taking into account all patients and time points, density plots revealed 9 distinct clusters of which 5 were differently abundant between BOR groups and time points (Fig. 3a). In example, clusters 3 and 8 displayed higher densities in PR patients when compared to PD patients (significantly different clusters are highlighted by red lines in **Fig. 3a**; see also Additional file 1: Figure S3A). Zooming in on density plots of markers (**Fig. 3b**) and expression intensities of those markers within individual clusters (**Fig. 3c**), we observed that differences in above-mentioned clusters were mostly attributed to CD45RA, CCR7, CD95 and CD69. Instructed by these cluster analyses as well as reported combinations of T cell maturation markers, we observed that frequencies of CD8 T cells expressing single

maturation markers were not different (**Fig. 3d**, upper row), whereas frequencies of CD8 T cells expressing CD45RA and lacking CCR7 as well as those expressing CD95 and lacking CD69 were different among BOR groups (**Fig. 3d**, lower row). In fact, PR patients showed an enhanced frequency of $CD45RA^{+}CCR7-$ CD8 T cells at baseline (median: 43.1%) when compared to PD patients (29.7%). Moreover, PR but not PD patients showed a trend of increased frequency of $CD45RA^{+}CCR7^{-}$ CD8 T cells during nivolumab treatment (52 and 31% at V1 for PR and PD, respectively). Additionally, PR, SD and PD patients showed 60, 53 and 46% of $CD95^{+}CD69^{-}$ CD8 T cells at baseline, respectively (Fig. 3d; $p = 0.033$ PR v. PD). Furthermore, CD4 T cells displayed no differences between BOR groups with regard to maturation and differentiation markers (data not shown).

When assessing CD8 T cell frequencies according to markers of proliferation and regulatory T cells in an identical manner (Additional file 1: Figures S3B and S4), we identified clusters with significant, albeit low intensity differences between BOR groups. However, neither frequencies of CD8 T cells expressing individual markers nor those expressing combinations of markers, such as CD25 and FOXP3, were differently present among BOR groups. Notably, frequency of CD4 regulatory T cells showed no difference between BOR groups (data not shown). Frequencies of CD8 T cells expressing the proliferation marker Ki67 either as a single marker or in combination with PD-1 did not show significant differences between BOR groups either. It is noteworthy, however, that we did observe a significant increase in frequency of $Ki67^{+}$ CD8 T cells expressing PD-1 after onset of therapy in all BOR groups (Additional file 1: Figure S5) and that there was a positive correlation between frequency of $Ki67^{+}$ within $PD1^{+}CD8$ T cells and pre-treatment tumor volume of target lesions in NSCLC patient. This correlation, however, was not predictive of response to therapy.

Figure 3. Patients with PR show enhanced frequencies of CD8 T cells with CD45RA+ CCR7– and CD95+ CD69– phenotypes

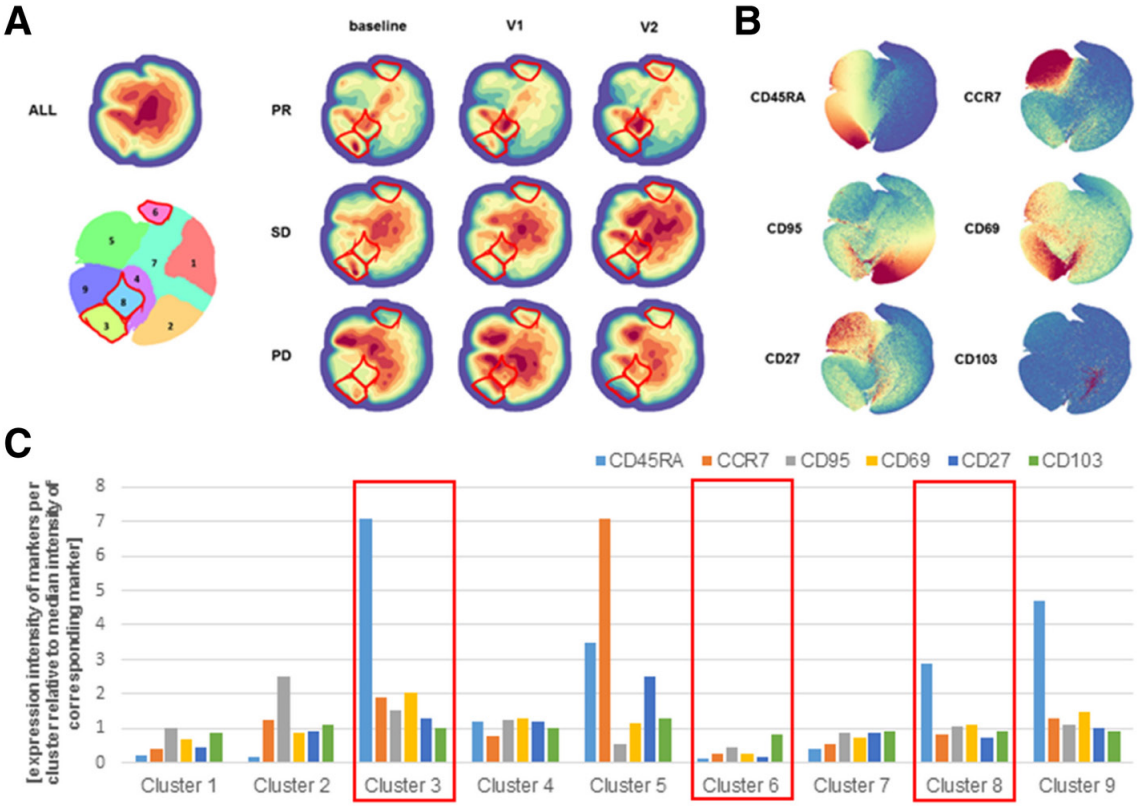

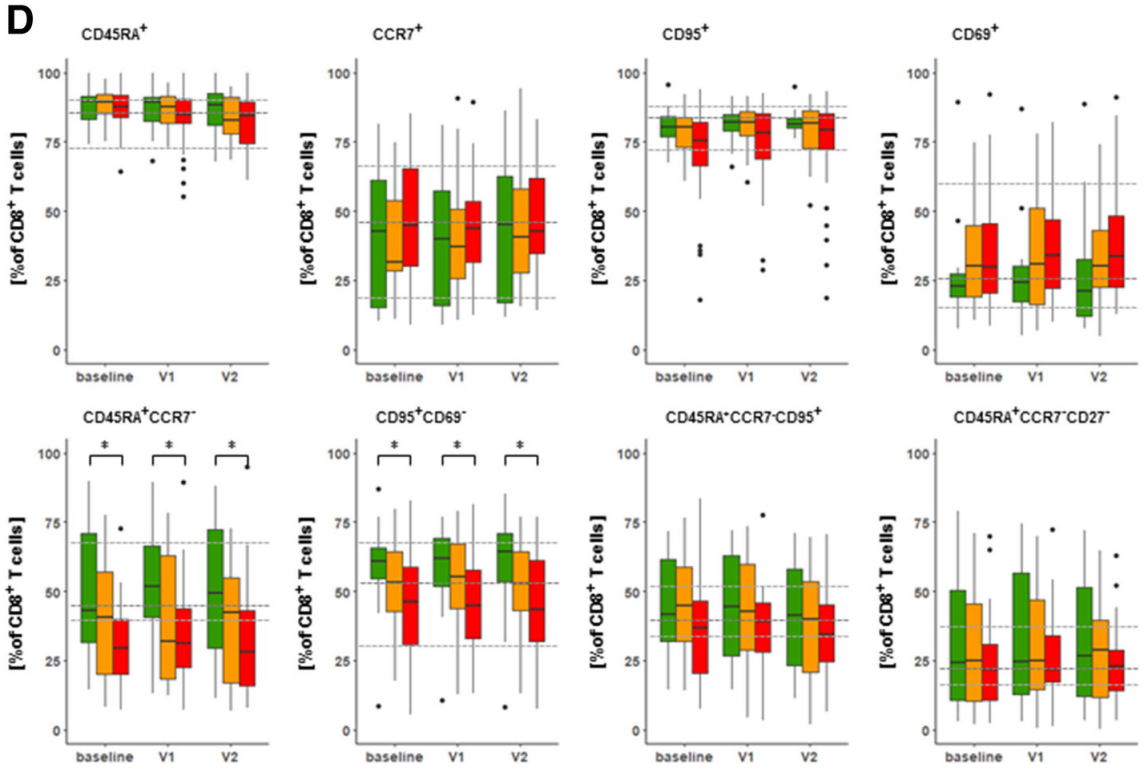

(a) Density plots of all data points (ALL: cells from 71 patients, 3 time points each) and split up according to BOR and time points. Plot with 9 clusters (lower left) is the result of gradients of density plots and iterative testing (see Materials and Methods for details). Individual clusters were assessed for significant differences between BOR groups and time points, and highlighted by red lines (see also Additional file 1: Figure S3A). (b) Density plots of individual markers and (c) expressions of markers within individual clusters according to relative intensities; clusters showing different abundance (from panel A) are highlighted by red rectangles. (d) Frequencies of CD8 T cells positive for single markers or combinations of two markers. Markers used are listed in Additional file 1: Table S2, panel 2. Statistically significant differences between BOR groups and time points were determined using Mann–Whitney U test. * $p < 0.05$.

PR patients show decreased frequencies of CD28$^+$CD40L$^+$ and CD28$^+$ICOS$^+$ CD8 T cells

When looking into expression of co-inhibitory receptors, we identified several density clusters that showed significant differences between BOR groups and time points (**Fig. 4a** and Additional file 1: Figure S3C). Differences in the majority of these clusters were attributed to CD57 and PD-1 (**Fig. 4b** and **c**). In addition to these findings, we have assessed the sum of different co-inhibitory receptors expressed by CD8 T cells (i.e., BTLA, PD-1, TIM3, LAG3), and noted that PR patients have a trend of expressing higher frequencies of CD8 T cells with 2 or more different co-inhibitory receptors when compared to PD patients at baseline (**Fig. 4d**). Instructed by these analyses, we observed that frequencies of CD8 T cells expressing a single type of co-inhibitory receptors were not different, whereas frequencies of CD8 T cells co-expressing PD-1 and TIM3 were more frequent in PR patients when compared to PD patients at baseline (**Fig. 4e**). This finding extends the observation that the frequency of highly differentiated CD8 T cells is enhanced in PR patients. Using our panel of co-stimulatory receptors, we again identified density clusters that are differentially abundant among BOR groups and time points (**Fig. 5a**, Additional file 1: Figure S3D). Interestingly, clusters that were more abundant in PR patients were marked by a decreased presence of CD28, ICOS and CD40L (clusters 3 and 8 in Fig. **5b** and **c**), whereas clusters that were more abundant in PD patients were marked by an increased presence of CD28 and CD40L (clusters 4 and 7). When assessing the sum of different receptors expressed by CD8 T cells, we noted that PR patients were marked by a higher frequency of CD8 T cells devoid of all five co-stimulatory receptors (i.e., CD28, ICOS, CD40L, 4-1BB and OX40). PR patients had lower frequencies of CD8 T cells with 2 or more different co-stimulatory receptors when compared to PD patients at baseline (**Fig. 5d**). Frequencies of CD8 T cells expressing a single type of co-stimulatory receptors, except a lower frequency of CD40L$^+$ CD8 T cells, were not different among BOR groups nor time points (**Fig. 4e**). In contrast, analysis of frequencies of CD8 T cells expressing 2 co-stimulatory receptors revealed that T cells expressing CD28 combined with another receptor, particularly CD40L or ICOS, were lowest in PR and significantly higher in PD patients (**Fig. 5e**).

Figure 4. Patients with PR display enhanced frequency of PD-1+ TIM3+ CD8 T cells at baseline

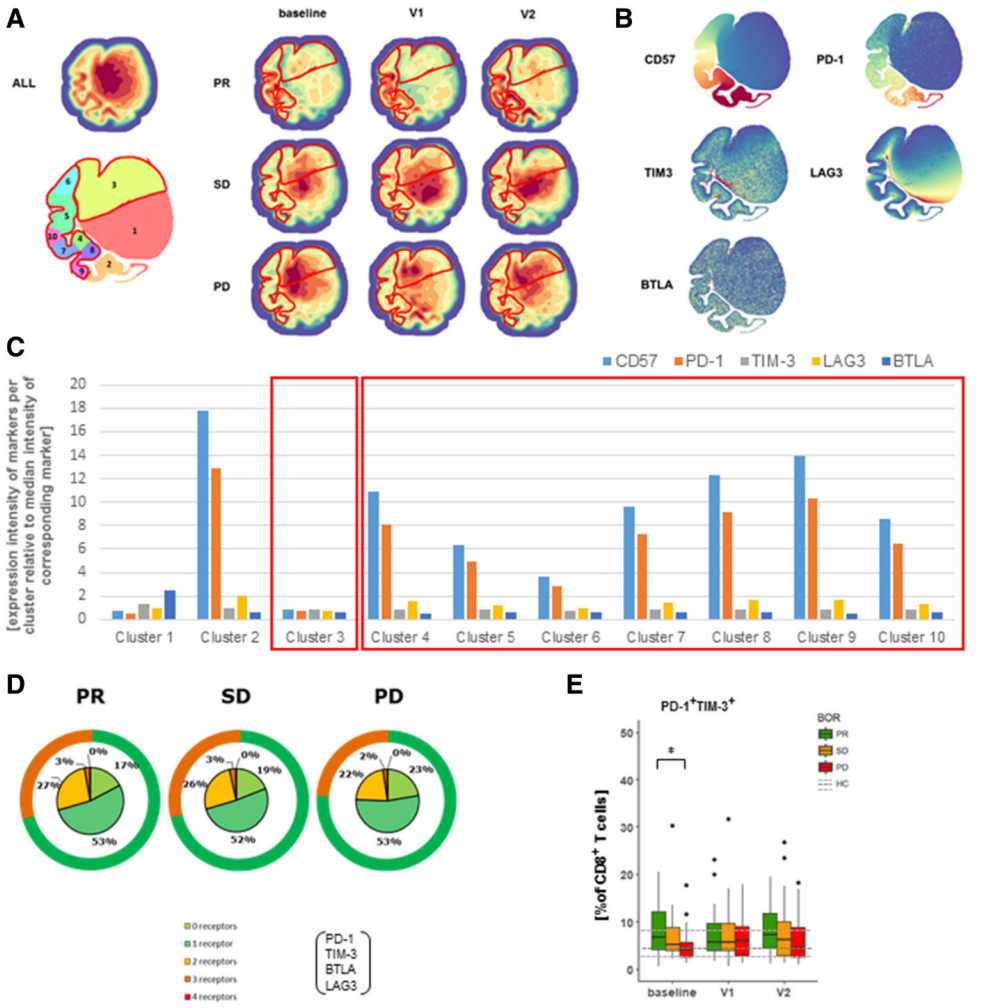

(a) Density plots of all data points (ALL: cells from 71 patients, 3 time points each) and split up according to BOR and time points. Plot with 10 clusters (lower left) is the result of gradients of density plots and iterative testing (see Materials and Methods for details). Individual clusters were assessed for significant differences between BOR groups and time points, and highlighted by red lines (see also Additional file 1: Figure S3C). (b) Density plots of individual markers and (c) expressions of markers within individual clusters according to relative intensities; clusters showing different abundance (from panel A) are highlighted by red rectangles. (d) Sum of different types of co-inhibitory receptors that are expressed by CD8 T cells (excluding CD57) at baseline. Green circles visualize fraction of CD8 T cells expressing 0 or 1 type of co-inhibitory receptors. (e) Frequencies of CD8 T cells positive for single markers or combinations of two markers showing significant differences. Markers used are listed in Additional file 1: Table S2, panel 4. Statistically significant differences between BOR groups and time points were determined using Mann–Whitney U test. * $p < 0.05$.

Figure 5. Patients with PR display reduced frequencies of CD8 T cells co-expressing CD28 and CD40L or CD28 and ICOS

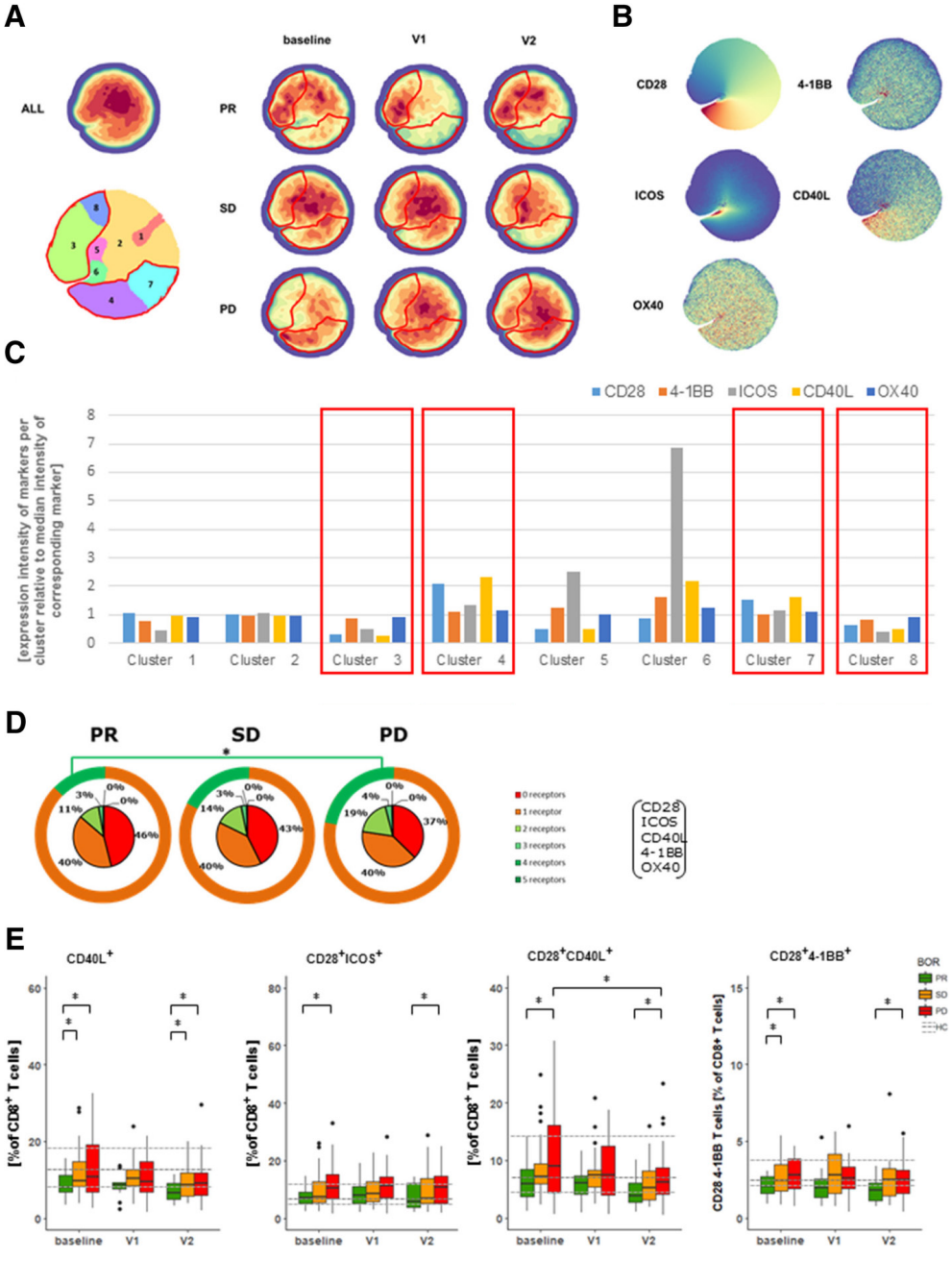

(a) Density plots of all data points (ALL: cells from 71 patients, 3 time points each) and split up according to BOR and time points. Plot with 8 clusters (lower left) is the result of gradients of

density plots and iterative testing (see Materials and Methods for details). Individual clusters were assessed for significant differences between BOR groups and time points, and highlighted by red lines (see also Additional file 1: Figure S3D). (b) Density plots of individual markers and (c) expressions of markers within individual clusters according to relative intensities; clusters showing different abundance (from panel A) are highlighted by red rectangles. (d) Sum of different types of co-stimulatory receptors that are expressed by CD8 T cells at baseline. Orange circles visualize fraction of CD8 T cells expressing 0 or 1 type of co-stimulatory receptors. (e) Frequencies of CD8 T cells positive for single markers or combinations of two markers with significant differences. Markers used are listed in Additional file 1: Table S2, panel 5. Statistically significant differences between BOR groups and time points were determined using Mann–Whitney U test. * $p < 0.05$.

Figure 6. Number of CD8 T cells in PR patients correlate with CD8 T cell maturation phenotypes

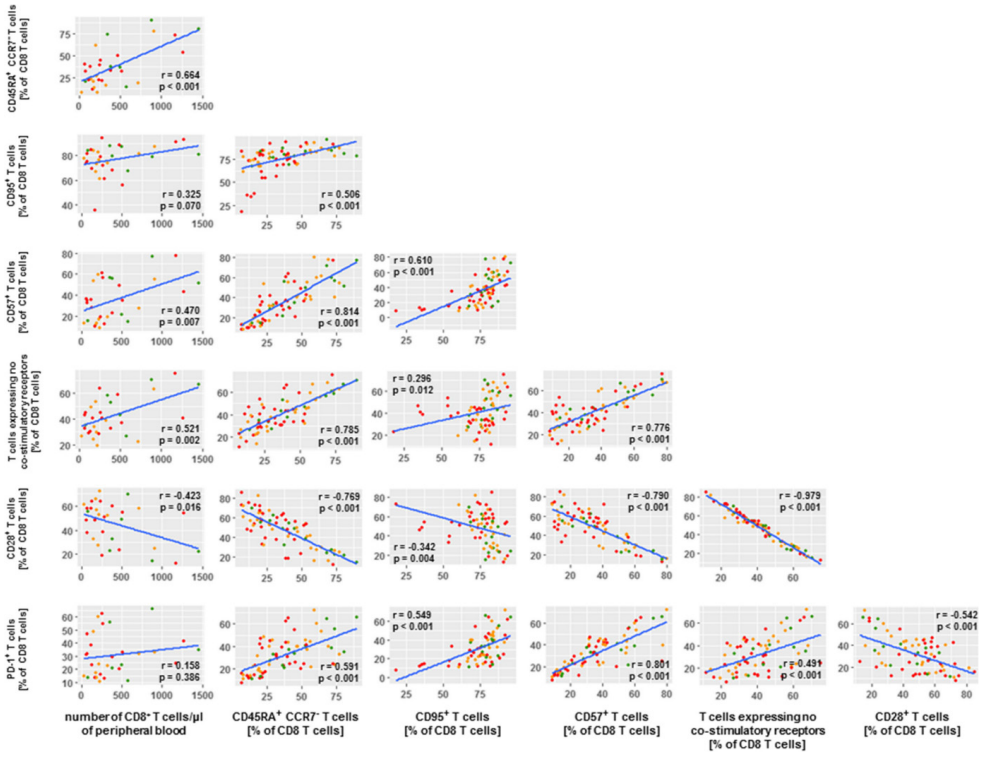

Correlation matrix depicts CD8 T cell phenotypes that were selected according to statistically significant differences between BOR groups (p values < 0.001) as well as extent of correlations with number of CD8 T cells and frequency of T cell phenotypes (r values < – 0.5 and > 0.5). Correlations were statistically assessed via Spearman's test.

In PR patients, the CD8 T cell differentiation phenotype coincides with a complete lack of co-stimulatory receptors

To study whether and how the differential numbers of CD8 T cells as well as the differential frequencies of defined CD8 T cell phenotypes among BOR groups were inter-related, we conducted extensive correlation studies with all immune markers measured in this study. **Figure 6** displays the resulting matrix of immune parameters with the highest correlations (r values < -0.5 or > 0.5 and p values < 0.001) with number of CD8 T cells and the CD8 phenotypes. Enhanced numbers of CD8 T cells in PR patients relate most clearly to frequencies of $CD45RA^{+}CCR7-$ CD8 T cells as well as CD8 T cells with no co-stimulatory receptors. In turn, frequencies of $CD45RA^{+}CCR7-$ CD8 T cells predominantly relate to frequencies of $CD95^{+}$ CD8 T cells, $CD57^{+}$ CD8 T cells, PD-1^{+} CD8 T cells and again CD8 T cells with no co-stimulatory receptors.

DISCUSSION

In this explorative study, we set out to discover potential immune markers in NSCLC patients that correspond with response to nivolumab therapy. The distribution of BOR in this prospective study of 71 patients is reflective of clinical outcome in large clinical trials with NSCLC patients [4, 5] with about 20% of treated patients showing response. Using our prospectively collected cohort of patients, we have enumerated immune cell populations and assessed clusters of T cell markers and frequencies of T cells subsets in blood samples drawn prior to and during therapy, using reference values from age- and gender-matched healthy controls.

Most studies evaluating systemic immune profiles generally rely on frozen PBMC samples, resulting in a bias towards immune cell populations that show high stability throughout the freeze/thaw procedure [24]. To address this issue, we have determined numbers of 18 different immune cell populations in freshly obtained blood. Amongst the significant differences in numbers of major immune cell populations between the three BOR groups, we detected a general increase in numbers of eosinophils during nivolumab therapy. Such an increase in peripheral eosinophils has previously been identified as a prognostic marker for survival in metastatic melanoma patients treated with various types of immune therapy [25]. However, increase in eosinophils was not associated with BOR in our NSCLC cohort as this increase occurred irrespective of BOR. At baseline, only immature neutrophils and T cells, in particularly CD8 T cells, showed differences among BOR groups. The increased number of immature neutrophils in SD patients is interpreted with caution since this finding may have been the result of exclusion of several outliers in this particular BOR group at baseline, part of our downstream analysis, which may have reduced the spread in this immune cell subset. The reduced number of CD8 T cells in SD and PD patients prior to therapy on the other hand shows a relatively low spread and is consistent over time. The

latter observation may explain the lack of responsiveness to therapy and is supported by previous findings of reduced numbers of T cells ($CD45^+CD3^+$) during immune checkpoint inhibition [19]. Besides therapy-induced changes, we also observed changed numbers of immune cell populations at baseline when compared with healthy controls. Increased numbers of mature neutrophils and monocytes correspond with an inflamed tumor microenvironment that may drive the proliferation of these cells and their detection in the periphery [26]. Also, our finding of increased numbers of M-MDSCs is in line with multiple reports, and may be of interest since these cells have been described as main suppressors of immune responses [27, 28]. The role of activated NK cells (expressing MIP-1β and CD69) in the context of anti PD-1 therapy of melanoma patients has recently been highlighted by Hodi and colleagues [29]. These authors observed increased frequencies of these cells as well as NK cells in patients showing response to therapy. Important to note that numbers of neutrophils, M-MDSCs, B or NK cells, neither by themselves nor in combination with other immune cell populations, did correlate with BOR in the present study, indicating that immune response in NSCLC patients may be mostly driven by T cells, rather than NK, B or other effector cells.

To follow-up on the different CD8 T cell numbers, we conducted a dimensionality reduction as well as 2D analyses to identify marker combinations and T cell subsets. Notably, we observed that reduced numbers of CD8 T cells in SD and PD patients were not due to changed frequencies of CD8 regulatory T cells nor a general lack of T cell proliferation (Additional file 1: Figure S4). Although the presence of CD4 Treg cells within the tumor microenvironment has been described as a potential driver of tumor immune escape (reviewed in [30]), peripheral frequencies of this subset may not be sufficiently reflective of local conditions. An increase in the frequency of $PD\text{-}1^+$ CD8 T cells and an enhanced frequency of $PD\text{-}1^+$ CD8 T cells that express Ki67 has previously been observed in NSCLC patients undergoing anti-PD-1/anti-PD-L1 therapy [20, 31]. Similar to this study, we found an increase in $PD\text{-}1^+$ CD8 T cells expressing Ki67, yet no correlation between their frequencies after onset of therapy and the clinical response according to RECIST1.1 (see Additional file 1: Figure S5). Huang and colleagues demonstrated that the ratio between $Ki67^+PD\text{-}1^+$ CD8 T cells and pre-therapy tumor burden was indicative of a clinical response of melanoma patients to pembrolizumab [21]. While we observed a similar correlation between 1D tumor measurements and frequencies of $Ki67^+PD\text{-}1^+$ CD8 T cells, albeit to a lower degree (see Additional file 1: Figure S5C), we were unable to demonstrate this ratio to be of discriminatory value among BORs in our NSCLC patient cohort. Although we cannot exclude that increased frequencies of $Ki67^+PD\text{-}1^+$CD8 T cells depend on tumor type, mutational load and/or certain patient subgroups, our findings do argue that further studies are required to better define how the Ki67 marker relates to clinical response to checkpoint inhibition. When conducting similar tSNE and 2D analysis of chemo-attractant receptors, we observed that the frequency of CD8 T cells expressing such receptors did not yield differences between BOR groups or time points (Additional file 1: Figure S6).

When looking into maturation states of T cells, we detected significantly higher frequencies of CD45RA$^+$CCR7– CD8 T cells, a phenotype often related to terminal T cell differentiation [32], in PR patients compared to PD patients at baseline and during treatment. Moreover, in PR patients we observed higher frequencies of CD95$^+$CD69– CD8 T cells. While CD95 has been recognized for FAS-mediated apoptosis, there is evidence for FAS-mediated T cell proliferation and differentiation as well [33]. High numbers of CD95$^+$ CD8$^+$ tumor infiltrating lymphocytes have previously been demonstrated to have predictive value in breast cancer patients [34] and an enhanced frequency of CD95$^+$ T cells in blood of stage IV melanoma patients has been reported to associate with clinical response upon anti-PD-1 treatment [22]. CD69 is an early activation marker that shows a rapid and transient upregulated expression upon TCR-mediated activation of CD8 T cells. Additionally, CD69 has been described as a tissue retention marker, indicating that down-regulated expression of CD69 coincides with egress of T cells into the blood flow [35]. Therefore, the observed changes, with respect to both CD45RA$^+$CCR7– and CD95$^+$CD69– CD8 T cell phenotypes, may be a consequence of local antigen encounter, T cell differentiation, and tissue egression of CD8 T cells in PR patients. Interestingly, these findings are nicely in line with recent observations by Gide and colleagues showing that differentiated effector memory T cells are more abundant in melanoma patients who respond to PD1 and CTLA-4 antibody treatment [36]. Further evidence for enhanced T cell differentiation in PR patients comes from the observation that the frequency of the mentioned phenotypes highly correlates with the frequency of CD8 T cells expressing CD57, another marker of terminal exhaustion upon antigen encounter [37]. Lastly, other CD8 T cell phenotypes that have been reported to relate to late T cell differentiation, such as lack of the co-stimulatory receptor CD28 and co-expression of PD-1 and TIM3, also show enhanced frequencies in PR patients (discussed below). Analysis of co-signaling receptors revealed that clear differences between BOR groups are particularly related to a CD8 T cell subset lacking the co-stimulatory receptors CD28, ICOS, CD40L, 4-1BB and OX40. Interestingly, PR patients show an increased frequency of CD8 T cells lacking co-stimulatory receptors, in particular CD28 and CD40L or CD28 and ICOS. Moreover, the frequency of CD28$^+$ CD8 T cells showed a high and inverse correlation with the frequency of CD8 T cells lacking co-stimulatory receptors (Fig. 6). While expression of CD28 is a pre-requisite for proper activation of T cells, the absence of this receptor has been described as part of a negative feedback loop following long-term antigen stimulation [38], and fits the above-described phenotype of antigen-exposed and differentiated CD8 T cells. Further substantiating the premise that a higher frequency of CD8 T cells in PR patients have encountered antigen, is our observation that these patients contain higher frequencies of PD-1$^+$TIM3$^+$ CD8 T cells at baseline (see **Fig. 5c**). The combination of these two receptors has been well described as a sign of activation-mediated T cell differentiation and potentially exhaustion [39,40,41]. Moreover, in patients with squamous cell carcinoma of the head and neck, recent studies showed that PD-1$^+$TIM3$^+$ CD8 T cells that lack CD28 and CD27 were able to suppress

proliferation of autologous peripheral blood T cells ex vivo [42]. Of interest, the presence of intra-tumoral PD-1$^+$ CD8 T cells expressing the transcription factor Tcf has been related to tumor control in response to immunotherapy [43, 44] and these T cells may harbor stemness and yield T cells that are more differentiated. Since PD-1 primarily intervenes with CD28 co-signaling, rather than TCR signaling itself [20, 45], we cannot exclude that the frequency of CD28$^+$ T cells that co-express Ki67 and PD-1 becomes enhanced upon treatment with checkpoint inhibitor. Along these lines, it is striking that the frequency of CD8 T cells devoid of multiple co-stimulatory receptors is highest in PR patients at baseline and throughout therapy, and correlates with the total number of CD8 T cells as well as frequencies of CD8 T cells showing a CD45RA$^+$CCR7− phenotype.

CONCLUSIONS

In conclusion, we found that NSCLC patients with a PR upon treatment with nivolumab demonstrate enhanced numbers of CD8 T cells and a phenotype corresponding with late differentiation at baseline. Collectively, our findings argue that a large fraction of CD8 T cells in PR patients has been exposed to tumor antigen and subsequently matured and egressed into the bloodstream. This enhanced CD8 T cell differentiation was accompanied by a higher frequency of PD-1 and TIM3 and a complete loss of co-stimulatory receptors. We propose that a panel comprising the markers CD45RA, CCR7, CD95, CD69, CD57, PD-1 as well as CD28, CD40L, and ICOS should be validated in larger cohorts of patients and used to develop a model aiding in the identification of NSCLC patients prone to show tumor regression upon anti-PD-1 therapy. While novel approaches are emerging that include assessment of tumor material with regard to T cell exclusion and exhaustion [18], to our knowledge this is the first description of peripheral immune markers able to identify NSCLC patients showing response to nivolumab treatment prior to onset of therapy (see Additional file 1: Figure S7 for a schematic overview of our findings).

REFERENCES

1. Keir ME, Butte MJ, Freeman GJ, Sharpe AH. PD-1 and its ligands in tolerance and immunity. Annu Rev Immunol. 2008;26:677–704.
2. Wherry EJ. T cell exhaustion. Nat Immunol. 2011;12(6):492–9.
3. Robert C, Long GV, Brady B, Dutriaux C, Maio M, Mortier L, et al. Nivolumab in previously untreated melanoma without BRAF mutation. N Engl J Med. 2015;372(4):320–30.
4. Borghaei H, Paz-Ares L, Horn L, Spigel DR, Steins M, Ready NE, et al. Nivolumab versus docetaxel in advanced nonsquamous non-small-cell lung Cancer. N Engl J Med. 2015;373(17):1627–39.
5. Brahmer J, Reckamp KL, Baas P, Crino L, Eberhardt WE, Poddubskaya E, et al. Nivolumab versus docetaxel in advanced squamous-cell non-small-cell lung Cancer. N Engl J Med. 2015;373(2):123–35.
6. Callahan MK, Postow MA, Wolchok JD. Targeting T cell co-receptors for Cancer therapy. Immunity. 2016;44(5):1069–78.
7. Topalian SL, Drake CG, Pardoll DM. Immune checkpoint blockade: a common denominator approach to cancer therapy. Cancer Cell. 2015;27(4):450–61.
8. Gettinger S, Herbst RS. B7-H1/PD-1 blockade therapy in non-small cell lung cancer: current status and future direction. Cancer J. 2014;20(4):281–9.
9. Sundar R, Cho BC, Brahmer JR, Soo RA. Nivolumab in NSCLC: latest evidence and clinical potential. Ther Adv Med Oncol. 2015;7(2):85–96.
10. Ribas A, Hu-Lieskovan S. What does PD-L1 positive or negative mean? J Exp Med. 2016;213(13):2835–40.
11. Rijnders M, van der Veldt AAM, Zuiverloon TCM, Grunberg K, Thunnissen E, de Wit R, et al. PD-L1 antibody comparison in urothelial carcinoma. Eur Urol. 2018.
12. Le DT, Uram JN, Wang H, Bartlett BR, Kemberling H, Eyring AD, et al. PD-1 blockade in tumors with mismatch-repair deficiency. N Engl J Med. 2015; 372(26):2509–20.
13. Zhu J, Armstrong AJ, Friedlander TW, Kim W, Pal SK, George DJ, et al. Biomarkers of immunotherapy in urothelial and renal cell carcinoma: PD-L1, tumor mutational burden, and beyond. J Immunother Cancer. 2018;6(1):4.
14. Tumeh PC, Harview CL, Yearley JH, Shintaku IP, Taylor EJ, Robert L, et al. PD1 blockade induces responses by inhibiting adaptive immune resistance. Nature. 2014;515(7528):568–71.
15. Debets R, Donnadieu E, Chouaib S, Coukos G. TCR-engineered T cells to treat tumors: seeing but not touching? Semin Immunol. 2016;28(1):10–21.
16. Charoentong P, Finotello F, Angelova M, Mayer C, Efremova M, Rieder D, et al. Pan-cancer Immunogenomic analyses reveal genotypeImmunophenotype relationships and predictors of response to checkpoint blockade. Cell Rep. 2017;18(1):248–62.
17. Thorsson V, Gibbs DL, Brown SD, Wolf D, Bortone DS, Ou Yang TH, et al. The immune landscape of Cancer. Immunity. 2018;48(4):812–30 e14.
18. Jiang P, Gu S, Pan D, Fu J, Sahu A, Hu X, et al. Signatures of T cell dysfunction and exclusion predict cancer immunotherapy response. Nat Med. 2018;24(10):1550–8.

19. Weide B, Martens A, Hassel JC, Berking C, Postow MA, Bisschop K, et al. Baseline biomarkers for outcome of melanoma patients treated with Pembrolizumab. Clin Cancer Res. 2016;22(22):5487–96.
20. Kamphorst AO, Pillai RN, Yang S, Nasti TH, Akondy RS, Wieland A, et al. Proliferation of PD-1+ CD8 T cells in peripheral blood after PD-1-targeted therapy in lung cancer patients. Proc Natl Acad Sci U S A. 2017;114(19):4993–8.
21. Huang AC, Postow MA, Orlowski RJ, Mick R, Bengsch B, Manne S, et al. T-cell invigoration to tumour burden ratio associated with anti-PD-1 response. Nature. 2017;545(7652):60–5.
22. Krieg C, Nowicka M, Guglietta S, Schindler S, Hartmann FJ, Weber LM, et al. High-dimensional single-cell analysis predicts response to anti-PD-1 immunotherapy. Nat Med. 2018;24(2):144–53.
23. van Unen V, Hollt T, Pezzotti N, Li N, Reinders MJT, Eisemann E, et al. Visual analysis of mass cytometry data by hierarchical stochastic neighbor embedding reveals rare cell types. Nat Commun. 2017;8(1):1740.
24. Kadic E, Moniz RJ, Huo Y, Chi A, Kariv I. Effect of cryopreservation on delineation of immune cell subpopulations in tumor specimens as determinated by multiparametric single cell mass cytometry analysis. BMC Immunol. 2017;18(1):6.
25. Moreira A, Leisgang W, Schuler G, Heinzerling L. Eosinophilic count as a biomarker for prognosis of melanoma patients and its importance in the response to immunotherapy. Immunotherapy. 2017;9(2):115–21.
26. Uribe-Querol E, Rosales C. Neutrophils in Cancer: two sides of the same coin. J Immunol Res. 2015;2015:983698.
27. Pogoda K, Pyszniak M, Rybojad P, Tabarkiewicz J. Monocytic myeloidderived suppressor cells as a potent suppressor of tumor immunity in nonsmall cell lung cancer. Oncol Lett. 2016;12(6):4785–94.
28. de Goeje PL, Bezemer K, Heuvers ME, Dingemans AC, Groen HJ, Smit EF, et al. Immunoglobulin-like transcript 3 is expressed by myeloid-derived suppressor cells and correlates with survival in patients with non-small cell lung cancer. Oncoimmunology. 2015;4(7):e1014242.
29. Subrahmanyam PB, Dong Z, Gusenleitner D, Giobbie-Hurder A, Severgnini M, Zhou J, et al. Distinct predictive biomarker candidates for response to anti-CTLA-4 and anti-PD-1 immunotherapy in melanoma patients. J Immunother Cancer. 2018;6(1):18.
30. Chaudhary B, Elkord E. Regulatory T cells in the tumor microenvironment and Cancer progression: role and therapeutic targeting. Vaccines (Basel). 2016;4(3).
31. Mazzaschi G, Facchinetti F, Missale G, Canetti D, Madeddu D, Zecca A, et al. The circulating pool of functionally competent NK and CD8+ cells predicts the outcome of anti-PD1 treatment in advanced NSCLC. Lung Cancer. 2019; 127:153–63.
32. Thome JJ, Farber DL. Emerging concepts in tissue-resident T cells: lessons from humans. Trends Immunol. 2015;36(7):428 –35.
33. Paulsen M, Janssen O. Pro- and anti-apoptotic CD95 signaling in T cells. Cell Commun Signal. 2011;9:7.
34. Blok EJ, van den Bulk J, Dekker-Ensink NG, Derr R, Kanters C, Bastiaannet E, et al. Combined evaluation of the FAS cell surface death receptor and CD8+ tumor infiltrating lymphocytes as a prognostic biomarker in breast cancer. Oncotarget. 2017;8(9):15610 –20.

35. Mackay LK, Braun A, Macleod BL, Collins N, Tebartz C, Bedoui S, et al. Cutting edge: CD69 interference with sphingosine-1-phosphate receptor function regulates peripheral T cell retention. J Immunol. 2015;194(5):2059–63.
36. Gide TN, Quek C, Menzies AM, Tasker AT, Shang P, Holst J, et al. Distinct immune cell populations define response to anti-PD-1 monotherapy and anti-PD-1/anti-CTLA-4 combined therapy. Cancer Cell. 2019;35(2):238–55 e6.
37. Verma K, Ogonek J, Varanasi PR, Luther S, Bunting I, Thomay K, et al. Human CD8+ CD57- TEMRA cells: too young to be called "old". PLoS One. 2017; 12(5):e0177405.
38. Weng NP, Akbar AN, Goronzy J. CD28(–) T cells: their role in the ageassociated decline of immune function. Trends Immunol. 2009;30(7):306–12.
39. Sakuishi K, Apetoh L, Sullivan JM, Blazar BR, Kuchroo VK, Anderson AC. Targeting Tim-3 and PD-1 pathways to reverse T cell exhaustion and restore anti-tumor immunity. J Exp Med. 2010;207(10):2187–94.
40. Severson JJ, Serracino HS, Mateescu V, Raeburn CD, McIntyre RC Jr, Sams SB, et al. PD-1+Tim-3+ CD8+ T lymphocytes display varied degrees of functional exhaustion in patients with regionally metastatic differentiated thyroid Cancer. Cancer Immunol Res. 2015;3(6):620–30.
41. Kim JE, Patel MA, Mangraviti A, Kim ES, Theodros D, Velarde E, et al. Combination therapy with anti-PD-1, anti-TIM-3, and focal radiation results in regression of murine gliomas. Clin Cancer Res. 2017;23(1):124–36.
42. Pfannenstiel LW, Diaz-Montero M, Tian YF, Scharpf J, Ko J, Gastman B. Immune-checkpoint blockade opposes CD8+ T-cell suppression in human and murine Cancer. Cancer Immunol Res. 2019.
43. Siddiqui I, Schaeuble K, Chennupati V, Fuertes Marraco SA, Calderon-Copete S, Pais Ferreira D, et al. Intratumoral Tcf1(+)PD-1(+)CD8(+) T cells with stemlike properties promote tumor control in response to vaccination and checkpoint blockade immunotherapy. Immunity. 2019;50(1):195–211 e10.
44. Kurtulus S, Madi A, Escobar G, Klapholz M, Nyman J, Christian E, et al. Checkpoint blockade immunotherapy induces dynamic changes in PD1(–)CD8(+) tumor-infiltrating T cells. Immunity. 2019;50(1):181–94 e6.
45. Hui E, Cheung J, Zhu J, Su X, Taylor MJ, Wallweber HA, et al. T cell costimulatory receptor CD28 is a primary target for PD-1-mediated inhibition. Science. 2017;355(6332):1428–33.

SUPPLEMENTARY INFORMATION

Figure S1.

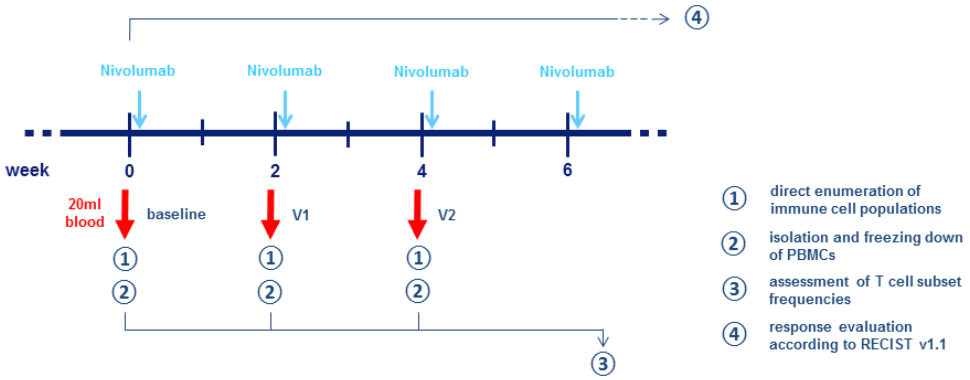

For immune monitoring, 20 ml of peripheral blood was taken at three time points: prior to therapy (baseline), prior to the second therapy cycle (V1, 2 weeks after baseline) and prior to the third therapy cycle (V2, 4 weeks after baseline). Blood was stained, ery-lysed and 18 different immune cell populations were enumerated by multiplex flow cytometry. PBMCs were isolated and cryopreserved, and stained for 28 markers (for a detailed panel overview, please refer to Table S2) followed by dimensionality reduction as well as rationale-based analyses.

Figure S2.

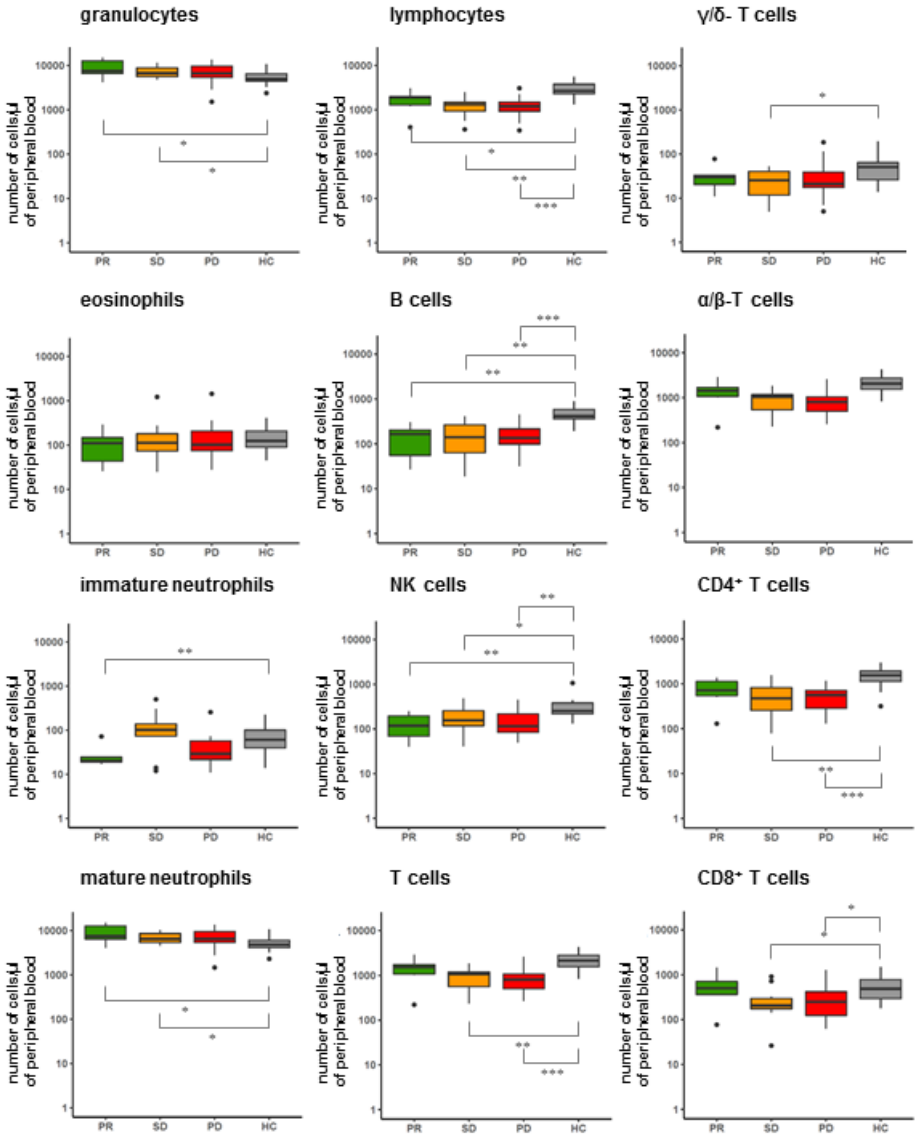
granulocytes
lymphocytes
γ/δ- T cells
eosinophils
B cells
α/β-T cells
immature neutrophils
NK cells
CD4⁺ T cells
mature neutrophils
T cells
CD8⁺ T cells
number of cells/µl of peripheral blood
PR
SD
PD
HC

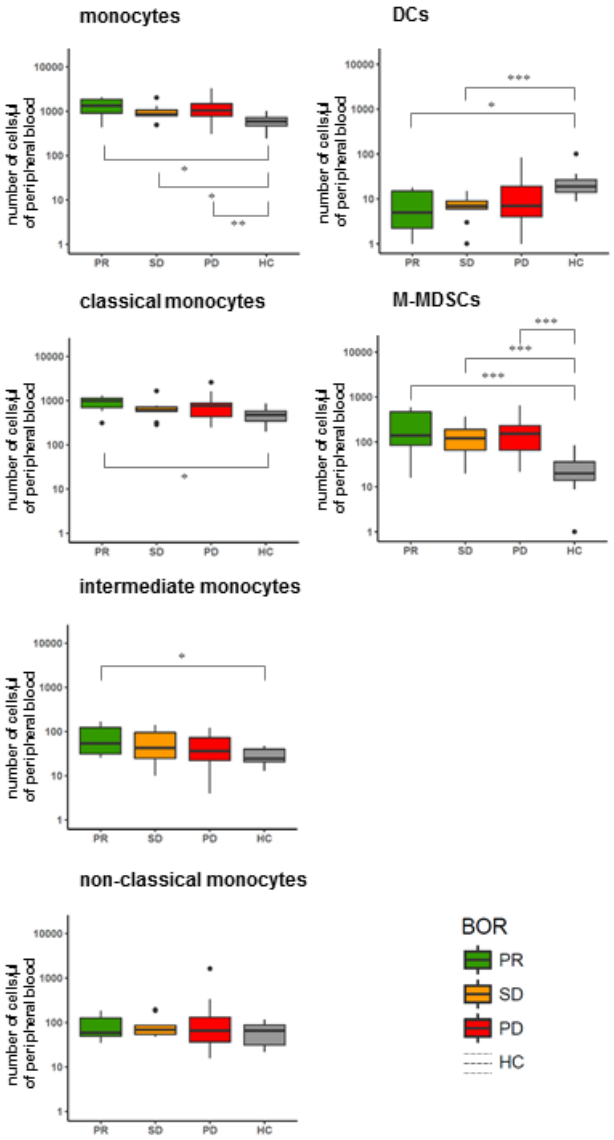

Blood samples were taken from NSCLC patients at baseline as well as from healthy controls (HC), and were stained, ery-lysed and subsequently analyzed by multi-color FCM. See legend to Figure S1 and Table S2 for details. Statistically significant differences between BOR groups and HC were determined using Mann–Whitney U test. * * $p < 0.05$, ** $p < 0.01$, *** $p < 0.005$.

Figure S3.

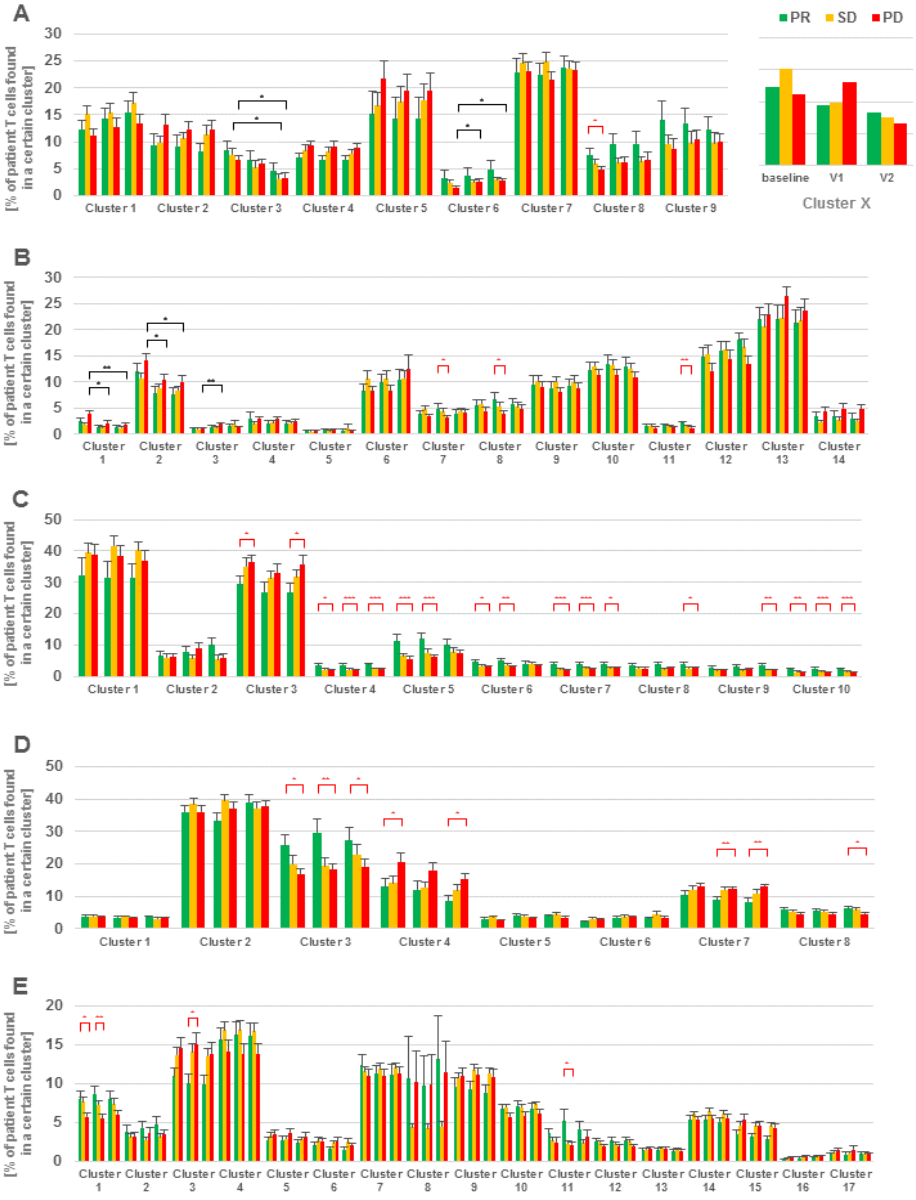

Graphs depict % of CD8 T cells (mean + SD) present in tSNE clusters according to BOR groups and time points and categorized by panels of markers (as described in Table S2), namely: (A) T cell maturation, (B) proliferation/regulatory T cell markers, (C) co-inhibitory receptors, (D) costimulatory receptors and (E) chemo-attractant receptors. See legends to Figs. 3, 4, 5, S4 and S6 for details. Red lines indicate differences between BOR groups within the same time point, black lines indicate differences within the same BOR group but between time points. Statistically significant differences were determined using Student's T test. * $p < 0.05$; ** $p < 0.01$; *** $p < 0.005$.

Figure S4.

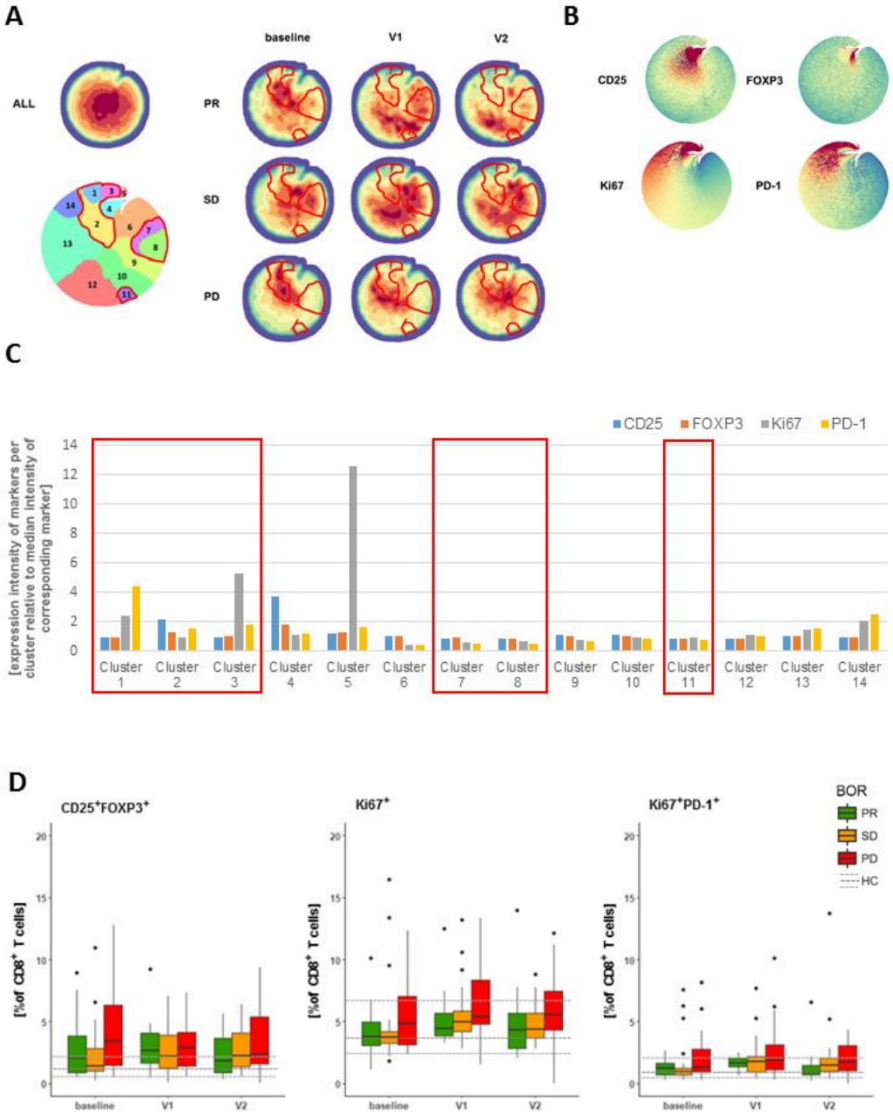

(A) Density plots of all data points (ALL: cells from 71 patients, 3 time points each) and split up according to BOR and time points. Plot with 14 clusters (lower left) is the result of gradients of density plots and iterative testing (see Materials and Methods for details). Individual clusters were assessed for significant differences between BOR groups and time points, and highlighted by red lines (see also Figure S3B). (B) Density plots of individual markers and (C) expressions of markers within individual clusters according to relative intensities; clusters showing different abundance (from panel A) are highlighted by red rectangles. (D) Frequencies of CD8 T cells positive for single markers or combinations of two markers. Markers used are listed in Table S2, panel 3. Statistically significant differences between BOR groups and time points were determined using Mann–Whitney U test. * $p < 0.05$.

Figure S5.

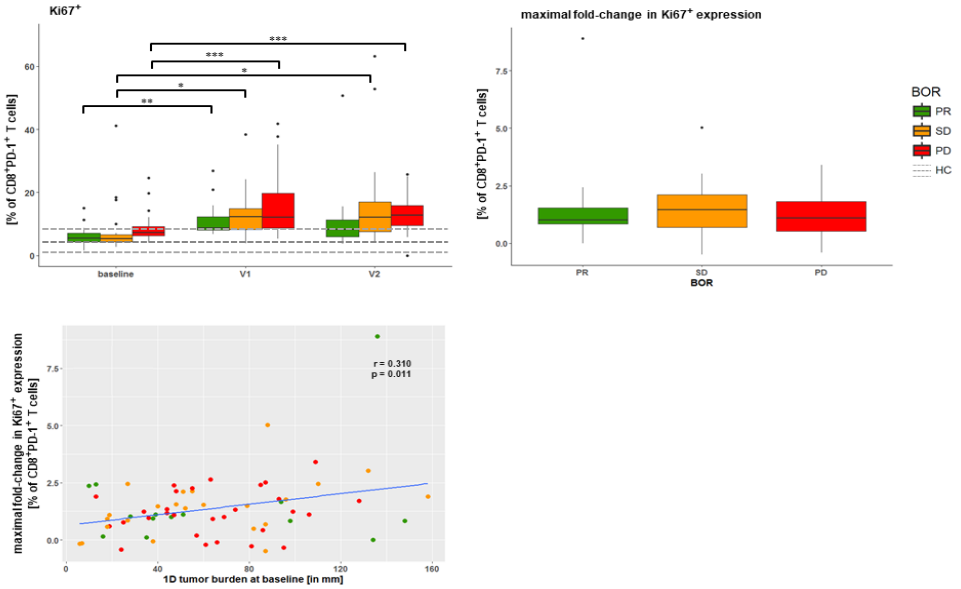

Graph in (A) shows frequency of Ki67+ cells within PD-1+CD8 T cells. Graph (B) presents the difference in frequency of Ki67+ within PD1+CD8 T cells between BOR groups. Graph in (C) depicts correlation between 1D tumor burden at baseline according to radiology (see methods for details) and maximum change in frequency of Ki67+ within PD1+CD8 T cells (delta between either V1 or V2 and baseline). Correlations were statistically assessed via Spearman's test. Statistically significant differences between BOR groups and time points were determined using Mann–Whitney U test and paired Student's T-test, respectively. * $p < 0.05$, ** $p < 0.01$, *** $p < 0.005$.

Figure S6.

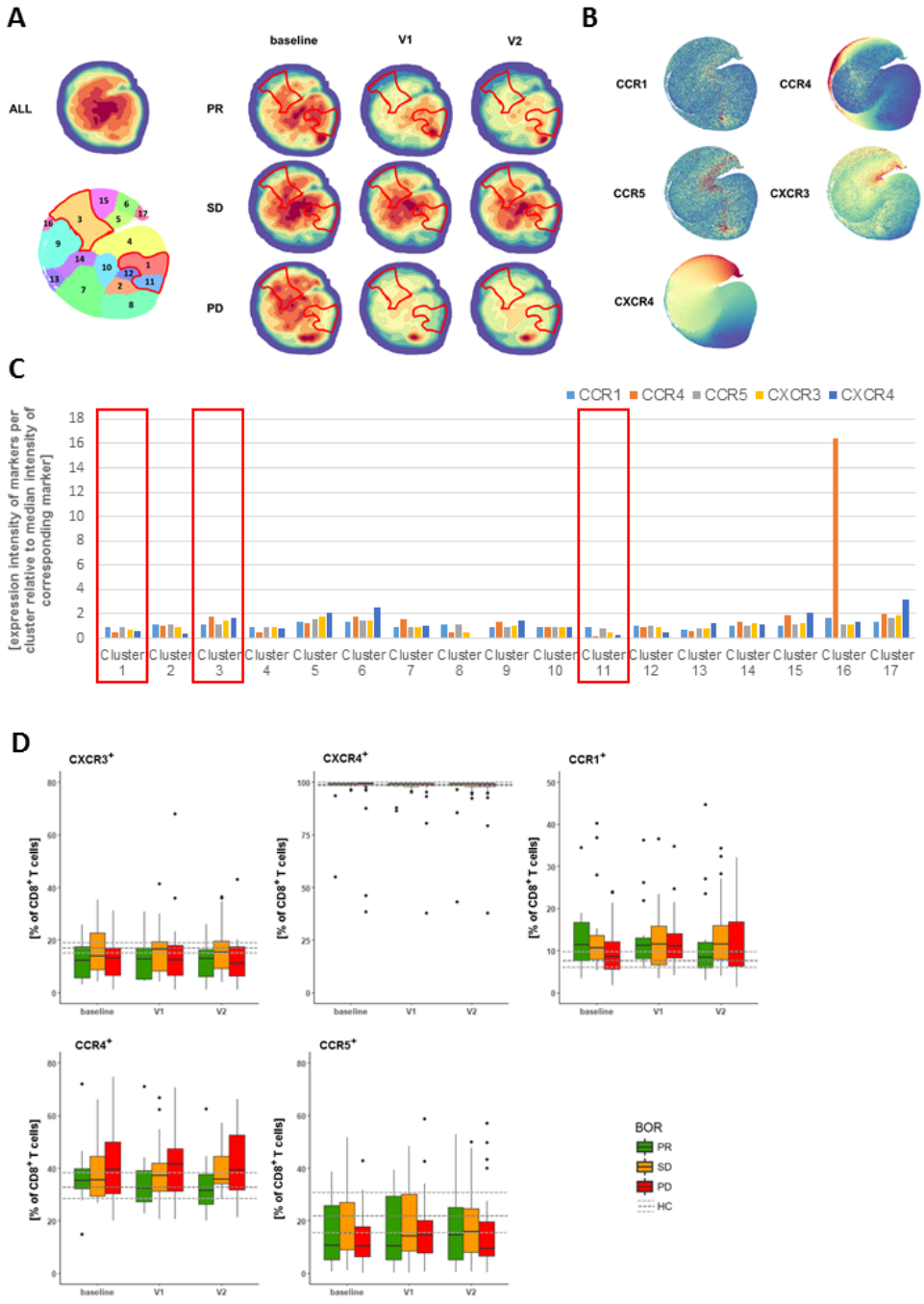
A
baseline
V1
V2
ALL
PR
SD
PD
B
CCR1
CCR4
CCR5
CXCR3
CXCR4
C
CCR1 CCR4 CCR5 CXCR3 CXCR4
[expression intensity of markers per cluster relative to median intensity of corresponding marker]
Cluster 1
Cluster 2
Cluster 3
Cluster 4
Cluster 5
Cluster 6
Cluster 7
Cluster 8
Cluster 9
Cluster 10
Cluster 11
Cluster 12
Cluster 13
Cluster 14
Cluster 15
Cluster 16
Cluster 17
D
CXCR3+
CXCR4+
CCR1+
CCR4+
CCR5+
[% of CD8+ T cells]
BOR
PR
SD
PD
HC

(A) Density plots of all data points (ALL: cells from 71 patients, 3 time points each) and split up according to BOR and time points. Plot with 17 clusters (lower left) is the result of gradients of density plots and iterative testing (see Materials and Methods for details). Individual clusters were assessed for significant differences between BOR groups and time points, and highlighted by red lines (see also Figure S3E). (B) Density plots of individual markers and (C) expressions of markers within individual clusters according to relative intensities; clusters showing different abundance (from panel A) are highlighted by red rectangles. (D) Frequencies of CD8 T cells positive for single markers or combinations of two markers. Markers used are listed in Table S2, panel 6. Statistically significant differences between BOR groups and time points were determined using Mann–Whitney U test. *$p < 0.05$.

Figure S7.

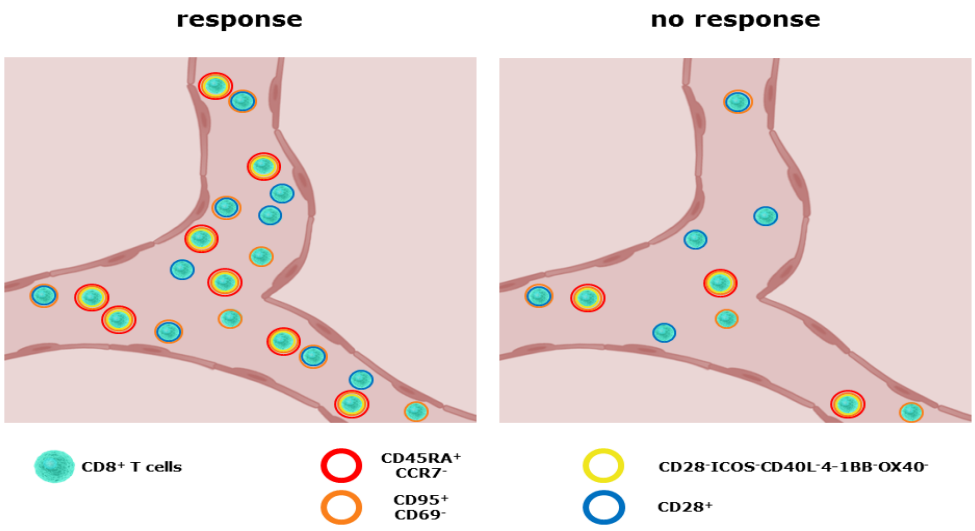

This figure depicts main findings of this study, indicating that patients responding to therapy (PR) prior to start of therapy display higher numbers of peripheral CD8 T cells, with enhanced frequencies of the phenotypes CD45RA+CCR7−, CD95+CD69− and lack of CD28, ICOS, CD40L, 4-1BB and OX40.

Supplementary Table I. Patient characteristics

Tumor type:		**NSCLC**	
Treatment[a]:		Nivolumab, Q2W, 3mg/kg	
Median age *(years, range)*		65 (35-79)	
Sex:	Female	30 (42.3%)	
	male	41 (57.7%)	
WHO performance status:	0	16 (22.5%)	
	1	37 (52.1%)	
	unknown	18 (25.4%)	
Histology of primary lung tumor:	adenocarcinoma	48 (67.6%)	
	squamous cell carcinoma	21 (29.6%)	
	great cell carcinoma	2 (2.8%)	
BOR:	progressive disease (PD)	32 (45.1%) [b]	15 (46.9%) [c]
	stable disease (SD)	25 (35.2%)	10 (31.2%)
	partial response (PR)	14 (19.7%)	7 (21.9%)
Median follow-up *(days, range)*		242 (35-544)	

[a] all patients received platinum-containing pre-treatment
[b] all patients enrolled in this study (71 in total) underwent staining for 28 T cell markers in frozen PBMC samples
[c] 32 of these 71 patients underwent enumeration of immune cell populations in fresh blood samples

Supplementary Table II. Multiplex flow cytometry panels

1[a]	markers		markers
granulocytes	$CD45^+$ SSC	**eosinophils**	$CD15^+CD16^-$
		mature neutrophils	$CD15^{high}CD16^{high}$
		immature neutrophils	$CD15^+CD16^+$
monocytes	$CD45^+$ SSC	**classical monocytes**	$CD14^+CD16^-$
		intermediate monocytes	$CD14^+CD16^+$
		non-classical monocytes	$CD14^-CD16^+$
		DCs	$CD14^-CD16^-CD11c^+$
		M-MDSCs	$CD14^+CD16^-$ $CD11b^+HLA\text{-}DR^{low}$
lymphocytes	$CD45^+$ SSC	**B cells**	$CD3^-CD19^+$
		NK cells	$CD3^-CD56^+$ $CD16^{+/-}$
		T cells	$CD3^+$
		αβ - T cells	$CD3^+TCR\alpha\beta^+CD4^+$ or $CD8^+$
		γδ - T cells	$CD3^+TCR\gamma\delta^+$

2[b]	T cell maturation markers	CCR7(CD197), CD45RA, CD95, CD69, CD27, CD103
3[b]	T cell proliferation/ regulatory T cell markers	Ki67, CD25, FOXP3, PD-1(CD279)
4[b]	T cell co-inhibitory receptors	CD57, LAG3(CD223), BTLA(CD272), PD-1(CD279), TIM3(CD366)
5[b]	T cell co-stimulatory receptors	CD28, OX40(CD134), 4-1BB(CD137), CD40L, ICOS(CD278)
6[b]	T cell chemoattractant receptors	CXCR3(CD183), CXCR4(CD184), CCR1(CD191), CCR4(CD194), CCR5(CD195)

[a] enumeration of immune cell populations in fresh blood sample
[b] assessment of T cell subset frequencies in PBMC samples

Supplementary Table III. Analysis work scheme

clinical parameters	best overall response (SD/PR/PD)[a]
time points	baseline, V1 (2 weeks after baseline), V2 (4 weeks after baseline)
change	Δbaseline-V1, Δbaseline-V2, Δmax[b]

Order of analysis				
1	**2**	**3**	**4**	**5**
immune cell populations (panel 1)	**tSNE cluster analysis**	**defined CD4/CD8 T cells subsets (panels 2, 3)**	**CD4/CD8 T cells subsets according to single and combination of markers (panels 4-6[c])**	**CD4/CD8 T cells subsets according to accumulation of markers (panels 4-6[c])**

[a] see Methods for details on response assessment
[b] defined as maximal change from baseline measurement
[c] testing of specific marker combinations was guided by significance and was only conducted when markers yielded $p<0.05$ comparing all three BOR groups (Kruskal-Wallis).

PART III

Treatment selection in melanoma, and across tumors

CHAPTER 13

13

Extracellular matrix biomarkers are correlated with clinical outcome after PD-1 blockade in metastatic melanoma patients

Daan P. Hurkmans*, Christina Jensen*, Stijn L.W. Koolen, Joachim G.J.V. Aerts, Morten Asser Karsdal, Ron H.J. Mathijssen, Nicholas Willumsen

*Shared first authorship

Journal for ImmunoTherapy of Cancer, October 2020, 8: 1193

Background: Immune checkpoint inhibitors that target the PD-1 receptor induce a response in only a subgroup of metastatic melanoma patients. Previous research suggests that TGF-β signaling and a collagen-rich peritumoral stroma (tumor fibrosis), may negatively interfere with the interaction between T cells and tumor cells and thereby contribute to resistance mechanisms by immune-exclusion, while increased tumor infiltration of M1-like macrophages enhances T cell activity. Hence, the current study aimed to assess the relationship between blood-based markers of collagen or vimentin turnover (reflecting M1 macrophage activity) and clinical outcome in metastatic melanoma patients after PD-1 inhibition.

Methods: Metastatic melanoma patients who were treated with anti-PD-1 monotherapy between May 2016 and March 2019 were included in a prospective observational study. Type III collagen formation (PRO-C3) and cross-linking (PC3X), matrix metalloprotease (MMP)-degraded type III (C3M) and IV collagen (C4M), granzyme B degraded type IV collagen (C4G), and citrullinated and MMP-degraded vimentin (VICM) were measured with immunoassays in serum before (n=107), and six weeks after the first administration of immunotherapy (n=94). Biomarker levels were associated with overall survival (OS) and progression-free survival (PFS).

Results: Multivariate Cox regression analysis identified high baseline PRO-C3 (Q4) as a predictor of worse PFS (HR=1.81, 95%CI=1.06-3.10, p=0.030) and OS (HR=2.08, 95%CI=1.06-4.09, p=0.035), after correction for lactate dehydrogenase (LDH). High PC3X also independently predicted worse PFS (HR=1.86, 95%CI= 1.09-3.18, p=0.023), whereas a high C3M/PRO-C3 ratio was associated with improved OS (HR=0.42, 95%CI=0.20-0.90, p=0.025) after correction for LDH. An increase in VICM ($p<0.0001$; in 56% of the patients) was observed after six weeks of treatment, and an increase in VICM was associated with better OS when adjusted for WHO performance status and brain metastases (HR=0.28, 95%CI=0.10-0.76, p=0.013) and LDH (HR=0.42, 95%CI=0.20-0.91, p=0.028).

Conclusions: Blood-based biomarkers reflecting excessive type III collagen turnover were associated with worse OS and PFS after PD-1 inhibition in metastatic melanoma. Moreover, an increase in VICM levels after six weeks of treatment was associated with improved OS. These findings suggest that type III collagen and vimentin turnover contribute to resistance/response mechanisms of PD-1 inhibitors and hold promise of assessing extracellular matrix- and stroma derived components to predict immunotherapy response.

Abstract

INTRODUCTION

Over the last decade, immune checkpoint inhibitors (ICIs) have improved the overall survival (OS) of patients with metastatic cancer. Monoclonal antibodies directed to the programmed cell death protein 1 (PD-1) receptor have emerged as frontline therapies for cancers such as metastatic melanoma. However, there is an unmet need for biomarkers to guide treatment decisions, as the efficacy of ICIs is highly variable across individual patients. Although the expression of its ligand programmed death-ligand 1 (PD-L1) has been positively associated with clinical outcome in metastatic melanoma, the predictive performance remains limited, which may partly be explained by tumor heterogeneity [1]. Similarly, other biomarkers, such as $CD8^+$ T cell infiltration and tumor mutational burden, individually or combined, have been considered as biomarkers [2,3]. Interestingly, recent evidence suggests that transforming growth factor beta (TGF-β), cancer associated fibroblasts (CAFs) and immune-exclusion in tumor tissue are associated with worse clinical outcome after PD-L1 or PD-1 inhibition in solid cancer [4–6]. Those immune-excluded tumors are characterized by a collagen-rich peritumoral stroma (tumor fibrosis) that blocks the interaction between $CD8^+$ T cells and tumor cells [4–6]. The main collagens of the interstitial matrix (type I and III collagen) and the basement membrane (type IV collagen) are upregulated in immune-excluded tumors that are accompanied by a peritumoral location of $CD8^+$ T cells [7]. Moreover, components of proteolytic extracellular matrix (ECM) turnover appear to affect the response mechanisms to ICIs by regulating steps in the cancer-immunity cycle [8]. Melanoma is characterized by a highly reactive and fibrotic tumor stroma [9,10]. Increased stroma activity leads to increased matrix metalloproteinase (MMP)-mediated collagen degradation resulting in the generation and release of small protein fragments into the blood circulation [11,12]. These ECM protein fragments can be used as non-invasive biomarkers measured in blood, and may be used to assess processes such as MMP-mediated collagen degradation and collagen formation and cross-linking by evaluating its blood-based signature [12]. This has been demonstrated by our previous study showing that biomarkers measuring type III collagen formation (PRO-C3) or MMP-degraded type IV collagen (C4M) are associated with worse clinical outcome after CTLA-4 ICIs in metastatic melanoma patients [13]. The two collagen derived biomarkers assess different components of the ECM in the tumor microenvironment (TME) by reflecting a dense stromal interstitial matrix and fibrotic activity (PRO-C3) and degradation of the basement membrane (C4M) [14].

The current study aimed to investigate the relationship of tissue-derived biomarkers and clinical outcome after PD-1 inhibition in patients with metastatic melanoma. Protein fragments reflecting type III collagen formation (PRO-C3) and cross-linking (PC3X), MMP-degraded type III (C3M) and IV collagen (C4M), granzyme B degraded type IV collagen (C4G), and citrullinated and MMP-degraded vimentin (VICM) were measured in serum

obtained before and six weeks after the first administration of PD-1 ICIs. Moreover, the dynamics of collagen turnover and VICM during treatment were assessed.

MATERIALS AND METHODS

Study design and data collection

Patients with metastatic melanoma who were treated with anti-PD-1 monotherapy (pembrolizumab or nivolumab) at the Erasmus MC Cancer Institute (Rotterdam, The Netherlands) were prospectively included in the MULTOMAB immune-monitoring trial (Dutch Trial Registry number NL6828) between May 2016 and March 2019. Pembrolizumab was administered as a three-weekly infusion of 2 mg/kg, and nivolumab as a two-weekly infusion of 3 mg/kg. Patients who were treated with a prior line of immunotherapy or who received combination ICI therapy were excluded. The study was approved by the independent ethics committee board (reference number: MEC 16-011; Medical Ethical Board Erasmus MC, Rotterdam, The Netherlands) and all patients provided written informed consent. Serum samples drawn at baseline and after six weeks (median: 6, IQR 6-9 weeks) of treatment and were available for the assessment of selected ECM biomarkers. All biomarker assays were performed blinded to clinical outcome and patients were assigned to a subject number. Progression-free survival (PFS) was defined as the time from the first administration of PD-1 ICI until progressive disease (PD; based on Response Evaluation Criteria in Solid Tumors version 1.1 [RECIST v1.1]) [15] or death, whichever occurred first. OS was defined as the time from the first administration of PD-1 ICI until death. After treatment initiation, radiological evaluation by computed tomography was usually performed every 3 months. For the determination of the best overall response (BOR) by RECIST v1.1, a minimum duration of 90 days for stable disease (SD) was required. Confirmation of partial response (PR) or complete response (CR) was not required.

Assessment of biomarkers of extracellular matrix turnover in serum

Levels of ECM biomarkers were assessed in duplicates in serum samples using immunoassays (Nordic Bioscience, Herlev, Denmark) as previously described [1]. In short, type III collagen formation were measured with a competitive enzyme-linked immunosorbent assay (ELISA) targeting the N-terminal pro-peptide of type III collagen (PRO-C3). Moreover, type III collagen formation and cross-linking were measured with a sandwich ELISA targeting cross-linked N-terminal pro-peptides of type III collagen. Granzyme B-mediated degradation of type IV collagen was measured with a competitive electro-chemiluminescence assay (C4G). Lastly, MMP-degraded type III collagen (C3M), MMP-degraded type IV collagen (C4M), and MMP-degraded and citrullinated vimentin (VICM) were measured with competitive ELISAs.

Statistical analysis

Firstly, patient survival (PFS and OS) was visualized by the Kaplan-Meier approach and log-rank tests were used to determine differences between the curves after stratification of patients into quartile groups based on biomarker levels. Kaplan-Meier survival curves were also used to analyze survival outcomes in patients with a low type III collagen degradation to formation (C3M/PRO-C3) ratio (<1) compared to a high C3M/PRO-C3 ratio (>1). Moreover, survival outcomes were analyzed in patients with an evident increase in biomarkers (>20%) at week 6 compared to baseline versus the rest of the patients. The association with survival (PFS and OS) was further analyzed using univariate and multivariate Cox regression analysis. Correction for potential confounding factors was performed, variables with a p-value of ≤ 0.05 were considered for multivariate analyses. Test variables (ECM biomarkers) were included as continuous variable and stratified by the 75th percentile cutoff. Secondly, to study the association of baseline ECM biomarker levels with BOR: patients with PD were compared to patients with SD/PR/CR and analyzed using the Mann-Whitney test. Lastly, the dynamics of ECM biomarkers were studied by determining the difference over time of individual ECM biomarkers, indicating an increase or decrease comparing baseline levels to levels during therapy using the Wilcoxon matched-pairs rank test. A Pearson correlation was used to examine biomarker correlations. Analyses were performed using MedCalc (v16.8.4), IBM SPSS Statistics version 24.0.0.1 (Chicago, IL) and Graphpad Prism 8.3.0 (Graphpad Software, LLC). A p-value of $p<0.05$ was considered statistically significant.

RESULTS

Serum from a total of 107 metastatic melanoma patients at baseline and paired serum from 94 patients (88% of all patients) that was obtained six weeks (median: 6, IQR 6-9 weeks) after PD-1 ICI therapy was available for analysis. The baseline patient characteristics including demographic and clinical data are shown in **Table 1**. All 107 patients were evaluable for the OS analysis, with a median OS of 36.2 months. Three patients (3%) were not evaluable for determination of BOR, i.e. because of early clinical progression, resulting in a disease control rate (the proportion of patients with a BOR of SD, PR or CR) of 63.5%. The serum levels of the six different ECM biomarkers were evaluated at baseline: PRO-C3, PC3X, C4G, C3M, C4M and VICM. The distribution of those baseline measurements is shown in **Suppl. Fig. 1**. For all six ECM biomarkers, there was a right-skewed distribution of data.

Table 1. Patient characteristics

Patient factor	N	(%)
Gender		
Male	62	(58%)
Female	45	(42%)
Primary tumor		
Melanoma		
WHO performance		
0	69	(64%)
1	30	(28%)
2	2	(2%)
Unknown	6	(6%)
Treatment regimen		
Nivolumab	62	(58%)
Pembrolizumab	45	(42%)
Prior systemic treatment lines		
0	88	(82%)
1	18	(17%)
2	1	(1%)
Brain metastases		
Present at baseline	18	(17%)
Absent at baseline	48	(45%)
No screening performed	41	(38%)
BOR		
CR	15	(14%)
PR	38	(35.5%)
SD	13	(12%)
PD	38	(35.5%)
Not evaluable	3	(3%)
Continuous variables	**Median**	**(IQR)**
Age	66	(55-73)
LDH at baseline	216	(183-306)

Abbreviations: Best overall response (BOR), complete response (CR), partial response (PD), stable disease (SD), progressive disease (PD), lactate dehydrogenase (LDH).

Baseline levels of PRO-C3 and PC3X are negatively associated with survival outcomes

Firstly, the relationship between ECM-derived biomarkers at baseline and clinical outcome after PD-1 inhibition in patients with metastatic melanoma were investigated. For PRO-C3 and PC3X, statistically significant differences among PFS curves were observed across the quartiles of biomarker levels (median PFS of PRO-C3 Q1: 28.4 months, Q2:

not reached, Q3: 12.9 months and Q4: 2.6 months, p=0.028 and median PFS of PC3X Q1: 26.9 months, Q2: 9.1 months, Q3: 23.3 months and Q4: 3.2 months, p=0.035; **Fig. 1a,b**). Similarly, the association of ECM biomarkers with OS was assessed (**Fig. 2a-f**), resulting in a corresponding trend for PRO-C3 and PC3X (median OS of PRO-C3 Q1: 42.3 months, Q2: not reached, Q3: 36.2 months and Q4: 13.9 months, p=0.056 and median OS PC3X Q1: not reached, Q2: 29.7 months, Q3: not reached and Q4: 17.0 months, p=0.064; **Fig. 2a,b**). The baseline levels of C4G, C3M, C4M or VICM were not significantly associated with PFS or OS (**Fig. 1a-f** and **Fig. 2a-f**). Of note, PRO-C3 and PC3X levels were moderately correlated with each other at baseline (Pearson r=0.60, p<0.0001), while C3M and C4M were strongly correlated at baseline (Pearson r=0.86, p<0.0001; **Suppl. Table 1)**. Interestingly, patients with a high C3M/PRO-C3 ratio (>1) at baseline had improved PFS (median PFS: 15.5 *vs.* 2.8 months, p=0.020) and OS (median OS: 42.3 *vs.* 4.6 months, p<0.001) compared to patients with a low C3M/PRO-C3 ratio (<1; **Fig. 3a,b**).

Figure 1. Association of ECM biomarkers measured at baseline and progression free survival

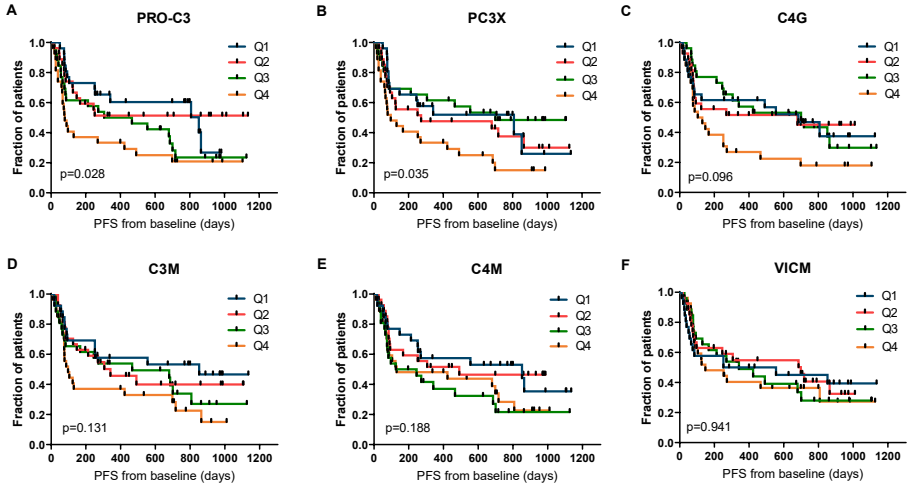

Kaplan-Meier plots demonstrating the association of ECM biomarkers with progression free survival (PFS) for metastatic melanoma patients. A) PRO-C3, B) PC3X, C) C4G, D) C3M, E) C4M and F) VICM were dichotomized into quartiles (Q4, representing the highest levels of the biomarker). P-values are based on the log-rank test.

Excessive type III collagen turnover are independent predictors of worse outcome

Univariate and multivariate Cox regression analyses were performed of all ECM biomarkers corrected for common (prognostic) baseline patient risk factors. In the

univariate analysis, PRO-C3, PC3X, C4G and C3M levels as continuous test variables were negatively correlated with PFS (**Table 2**). Additionally, the predictive value was evaluated by using the 75th percentile cut-point (Q4), based on the observation that patients with high biomarker levels (Q4) had worse survival outcomes compared to patients with low biomarker levels (Q1-3; **Fig. 1a-d** and **Fig. 2a,b**). Here, higher baseline levels of PRO-C3 (HR=1.96, 95%CI=1.17-3.30, p=0.011), PC3X (HR=2.05, 95%CI=1.23-3.43, p=0.006), C4G (HR=1.93, 95%CI=1.15-3.26, p=0.014) and C3M (HR=1.75, 95%CI=1.04-2.93, p=0.036) were significantly associated with worse PFS compared to lower levels (**Table 2**). For OS, the results were comparable for PRO-C3 and PC3X. In the univariate analysis, PRO-C3 and PC3X as continuous test variables were negatively associated with OS, while higher PRO-C3 (HR=2.41, 95%CI=1.26-4.60, p=0.008) and PC3X (HR=2.21, 95%CI=1.14-4.28, p=0.019) was associated with worse OS compared to lower levels (**Table 3**). Again, a high C3M/PRO-C3 ratio (>1) was associated with improved PFS (HR=0.51, 95%CI=0.29-0.91, p=0.023) and OS (HR=0.33, 95%CI=0.16-0.65, p=0.001) compared to a low ratio (**Table 3**). Importantly, baseline lactate dehydrogenase (LDH) had a significant impact on PFS (HR=1.00, 95%CI=1.00-1.00, p=0.014) and OS (HR= 1.00, 95%CI=1.00-1.00, p<0.0001). In the multivariate analysis, PRO-C3 and PC3X levels were both independently associated to worse PFS after correction for LDH (HR=1.81, 95%CI=1.06-3.10, p=0.030 and HR=1.86, 95%CI=1.09-3.18, p=0.023, respectively; **Table 2**), although baseline PRO-C3 and PC3X were moderately correlated with baseline LDH (p<0.0001; **Suppl. Table 1**). Importantly, PRO-C3 remained significantly associated to worse OS after adjustment for LDH (HR=2.08, 95%CI=1.06-4.09, p=0.035), with a similar trend for PC3X that did not however meet statistical significance (HR=1.78, 95%CI=0.88-3.60, p=0.106; **Table 3**). The WHO performance score of patients (HR=3.10, 95%CI=1.64-5.86, p<0.001) and the presence of cerebral metastases before start of treatment (HR=2.39, 95%CI=1.01-5.68, p=0.049) were also associated with OS in the univariate analysis, attenuating the association of all biomarkers and OS (data not shown).

In line with previous findings, a high C3M/PRO-C3 ratio had a positive relationship with OS when adjusted for LDH (HR=0.42, 95%CI=0.20-0.90, p=0.025; **Table 3**).

Baseline levels of PRO-C3 are associated with progressive disease

The relationship between baseline levels of the ECM biomarkers and the BOR was assessed. When comparing patients with PD to patients achieving disease control (BOR of SD, PR or CR), baseline PRO-C3 levels were significantly elevated in PD patients (median 10.5 ng/ml; 95%CI=8.3-12.7 *vs.* 8.8 ng/ml; 95%CI=7.6-9.9, p=0.046; **Suppl. Fig 2a**). No significant differences were observed for the remaining five biomarkers (**Suppl. Fig. 2b-f**).

Figure 2. Association of ECM biomarkers measured at baseline and overall survival

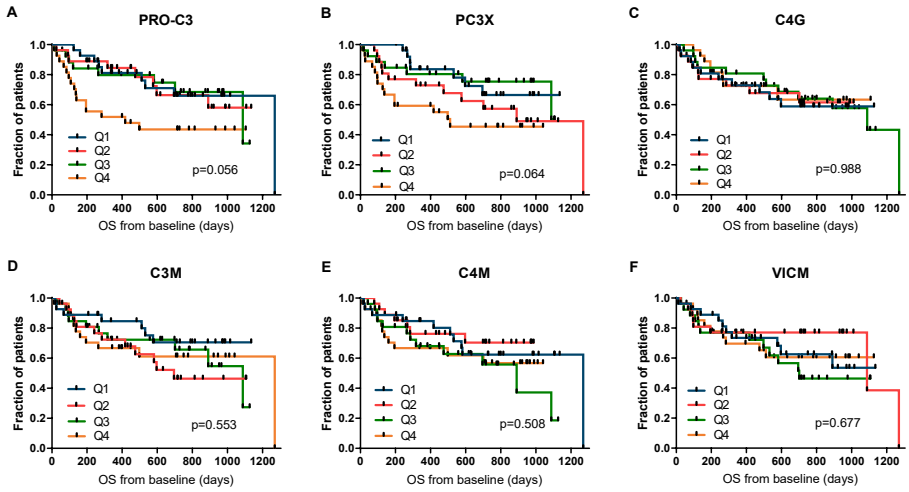

Kaplan-Meier plots demonstrating the association of ECM biomarkers with overall survival (OS) for metastatic melanoma patients. A) PRO-C3, B) PC3X, C) C4G, D) C3M, E) C4M and F) VICM were dichotomized into quartiles (Q4, representing the highest levels of the biomarker). P-values are based on the log-rank test.

An increase of VICM levels during treatment was positively associated with clinical outcome

The dynamics of collagen and VICM turnover were assessed during PD-1 inhibition by comparing the baseline biomarker levels to the levels after PD-1 ICI therapy. For PRO-C3, PC3X and VICM, an increase of serum levels was observed after six weeks of therapy compared to baseline (PRO-C3: 10.2 ng/ml; 95%CI=9.4-12.1 *vs.* 9.0 ng/ml; 95%CI=8.3-9.9; p<0.0001, PC3X: 5.7 ng/ml; 95%CI=5.2-6.3 *vs.* 4.9 ng/ml; 95%CI=4.4-5.6; p=0.003 and VICM: 21.4 ng/ml; 95%CI=17.0-25.7 *vs.* 15.0 ng/ml 95%CI=12.6-18.1; p<0.0001; **Suppl. Fig 3**). Neither C4G, C3M or C4M changed significantly after treatment. Of note, the levels of all six biomarkers were highly correlated before and after 6 weeks of treatment (**Suppl. Table 2**). Biomarker levels during therapy were associated to PFS and OS. By the Kaplan-Meier approach, moderate significant differences of PFS were observed for quartile groups of PRO-C3 (p=0.011), C4G (p=0.017) and C4M (p=0.046) levels (**Suppl. Fig. 4).** The levels of the ECM biomarkers after six weeks of treatment were not significantly associated to OS (**Suppl. Fig. 5**). Next, stratification was performed into patients who had an evident increase of the ECM biomarker during therapy (of more than 20% from baseline) and patients who did not have an evident increase (the remaining patients). Patients with an increase of VICM during therapy seemed to have, although not significant,

an improved PFS (median PFS: 28.4 *vs.* 8.4 months, HR=0.59, 95%CI=0.35-1.01, p=0.056). The OS in these patients was significantly improved (median OS: 42.3 *vs.* 36.2 months, HR=0.39, 95%CI=0.19-0.86, p=0.018). VICM remained significant after correction for WHO performance status and brain metastases (HR=0.28, 95%CI=0.10-0.76, p=0.013) and LDH (HR=0.42, 95%CI=0.20-0.91, p=0.028; **Fig. 4c,f**). No significant differences were observed for PRO-C3 or PC3X (**Fig. 4a,b,d,e**), although a trend could be observed for PRO-C3 and PC3X levels and worse PFS.

Table 2. Univariate and multivariate Cox regression analysis of the association of patient factors and ECM biomarkers with progression-free survival (PFS)

		Univariate		Multivariate	
Factor	**Test variable**	**HR (95% CI)**	**P-value**	**HR (95% CI)**	**P-value**
Gender	Male vs. Female	1.14 (0.69-1.86)	0.611		
Age	Continuous (yr)	1.00 (0.99-1.02)	0.744		
WHO	≥1 vs 0	1.60 (0.98-2.62)	0.061		
Brain metastasis	Present vs. absent	1.00 (0.52-1.94)	0.997		
LDH	Continuous (U/L)	1.00 (1.00-1.00)	0.014*		
PRO-C3	Continuous (ng/ml)	1.02 (1.00-1.04)	0.031*		
	4.0-12.5 ng/ml, Q1-Q3	1.00	-	Adjusted for LDH	
	12.6-84.7 ng/ml, Q4	1.96 (1.17-3.30)	0.011*	1.81 (1.06-3.10)	0.030*
PC3X	Continuous (ng/ml)	1.04 (1.00-1.07)	0.046*		
	1.2-7.6 ng/ml, Q1-Q3	1.00	-	Adjusted for LDH	
	7.6-30.2 ng/ml, Q4	2.05 (1.23-3.43)	0.006**	1.86 (1.09-3.18)	0.023*
C4G	Continuous (ng/ml)	1.01 (1.00-1.02)	0.019*		
	7.8-27.3 ng/ml, Q1-Q3	1.00	-	Adjusted for LDH	
	27.4-125.7 ng/ml, Q4	1.93 (1.15-3.26)	0.014*	1.91 (1.13-3.23)	0.016*
C3M	Continuous (ng/ml)	1.04 (1.00-1.09)	0.038*		
	8.2-19.5 ng/ml, Q1-Q3	1.00	-	Adjusted for LDH	
	19.6-36.0 ng/ml, Q4	1.75 (1.04-2.93)	0.036*	1.67 (0.99-2.82)	0.054
C4M	Continuous (ng/ml)	1.01 (1.00-1.03)	0.158		
VICM	Continuous (ng/ml)	1.01 (1.00-1.02)	0.121		
				Adjusted for LDH	
C3M/PRO-C3	>1 vs <1	0.51 (0.29-0.91)	0.023*	0.59 (0.32-1.11)	0.102

HR were calculated by univariate and multivariate cox regression analysis. By the multivariate analysis, the individual biomarkers were adjusted for LDH. Abbreviations: WHO performance score (WHO), lactate dehydrogenase (LDH), 95% confidence interval (95% CI), hazard ratio (HR). Significance is marked with stars.

Table 3. Univariate and multivariate Cox regression analysis of the association of patient factors and ECM biomarkers with overall survival (OS)

		Univariate		Multivariate	
Factor	**Test variable**	**HR (95% CI)**	**P-value**	**HR (95% CI)**	**P-value**
Gender	Male vs. Female	1.31 (0.68-2.51)	0.426		
Age	Continuous (yrs)	1.01 (0.99-1.03)	0.410		
WHO	≥1 vs 0	3.10 (1.64-5.86)	<0.001***		
Brain metastases	Present vs. absent	2.39 (1.01-5.68)	0.049*		
LDH	Continuous (U/L)	1.00 (1.00-1.00)	<0.0001****		
PRO-C3	Continuous (ng/ml)	1.03 (1.01-1.05)	0.004**		
	4.0-12.6 ng/ml, Q1-Q3	1.00	-	¤1.78 (0.66-4.82)	0.254
	12.7-84.7 ng/ml, Q4	2.41 (1.26-4.60)	0.008**	#2.08 (1.06-4.09)	0.035*
PC3X	Continuous (ng/ml)	1.04 (1.00-1.09)	0.045*		
	1.2-7.6 ng/ml, Q1-Q3	1.00	-	¤1.08 (0.40-2.95)	0.880
	7.6-30.2 ng/ml, Q4	2.21 (1.14-4.28)	0.019*	#1.78 (0.88-3.60)	0.106
C4G	Continuous (ng/ml)	1.00 (0.98-1.02)	0.693		
C3M	Continuous (ng/ml)	1.02 (0.96-1.08)	0.484		
C4M	Continuous (ng/ml)	1.01 (0.99-1.04)	0.237		
VICM	Continuous (ng/ml)	1.01 (0.99-1.02)	0.344		
				¤0.42 (0.15-1.19)	0.101
C3M/PRO-C3	>1 vs <1	0.33 (0.16-0.65)	0.001*	#0.42 (0.20-0.90)	0.025*

HR were calculated by univariate and multivariate cox regression analysis. By the multivariate analysis, the individual biomarkers were adjusted for LDH (indicated by #) or adjusted for WHO and brain metastases (indicated by ¤). Abbreviations: WHO performance score (WHO), lactate dehydrogenase (LDH), 95% confidence interval (95% CI), hazard ratio (HR). Significance is marked with stars.

Figure 4. Increase in VICM after anti-PD-1 treatment associates with PFS and OS

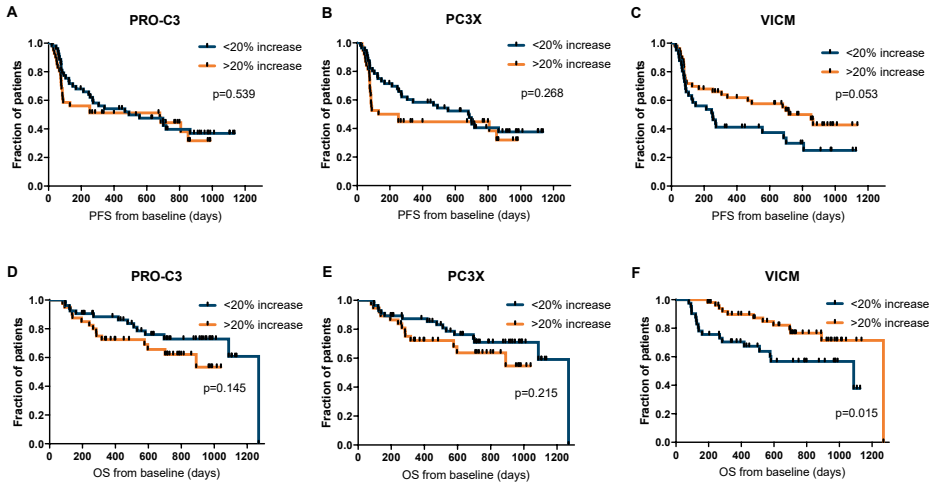

Kaplan-Meier plots demonstrating the association of change in PRO-C3 (A, D), PC3X (B, E) and VICM (C, F) with progression-free survival (PFS) and overall survival (OS) six weeks after start of anti-PD-1 ICI therapy after stratification of patients based on an increase of more than 20% from baseline versus <20% increase. P-values are based on the log-rank test.

DISCUSSION

The present study demonstrates that blood-based biomarkers of protease-generated neo-epitopes on protein fragments reflecting altered ECM turnover are associated with clinical outcome after PD-1 ICI therapy in metastatic melanoma. Baseline serum levels of ECM protein fragments PRO-C3 and PC3X, indicating a collagen-rich peritumoral stroma, were associated with resistance to PD-1 inhibition. Moreover, upregulation of VICM during therapy, reflecting M1 macrophage activity, was associated with improved survival.

Patients with higher PRO-C3 and PC3X levels had worse clinical outcome after PD-1 inhibition compared to patients with lower levels. Interestingly, as PRO-C3 and PC3X are released to the blood circulation during excessive collagen formation and cross-linking [16], the findings suggest that those markers identify tumors with an immune-excluded phenotype. Immune-exclusion is characterized by dense collagen stroma that limits the entry of tumor infiltrating lymphocytes into the TME, which is considered as an important biological mechanism of therapy resistance [4,17]. Cytotoxic T cell activity towards cancer cells in the TME is suggested to be an independent factor of the PD-L1 tumor proportion score and tumor mutation burden [2,18].

Although these protease-generated protein fragments were significantly correlated to LDH levels, we demonstrated that higher PRO-C3 independent of LDH was associated with worse PFS and OS and that higher PC3X was associated with worse PFS. LDH is known as a marker of tumor burden and a clinically significant adverse prognostic factor for metastatic melanoma, which is also confirmed in this immune-oncology setting [19]. Elevated LDH levels is integrated as a suffix to the M1 subcategories in recent TNM cancer staging protocols[20], providing additional prognostic value. Interestingly, similar observations for PRO-C3 were previously seen in metastatic melanoma patients who were treated with CTLA-4 ICI therapy [13], suggesting that the non-invasive biomarker may be considered across different ICIs.

Dense collagen stroma may also affect the diffusion and distribution of the therapeutic antibodies [21], in addition to its effect in limiting the entry of tumor infiltrating lymphocytes into the TME. Previous work by Jensen et al. demonstrated additional prognostic value of the ratio of type III collagen degradation to formation (C3M/PRO-C3) after CTLA-4 inhibition in metastatic melanoma [13]. The present findings confirm that patients with a high C3M/PRO-C3 ratio (>1) are linked to better clinical outcome after PD-1 inhibition, thereby providing additional evidence for the hypothesis that patients with relatively low net fibrosis/collagen deposition are more likely to respond to ICIs. PRO-C3 and PC3X are associated with a higher activity of CAFs. In addition to the desmoplastic, collagen rich TME related to immune-exclusion, CAFs have also shown to contribute to a diminished immune function by expressing TGF-β, PD-L1/PD-L2 and by inducing immune checkpoints on T cells [6,22–24].

We demonstrated that patients with an increase in VICM during treatment had improved clinical outcome. VICM is released from activated inflammatory M1 macrophages [25], which may be an important factor for response to ICIs compared to the immune-suppressive M2 macrophage phenotype. For example, PD-L1 inhibition was demonstrated to polarize macrophages into a more pro-inflammatory phenotype, which was associated with enhanced T cell activity [26]. In mice, PD-1 inhibition was found to increase macrophage phagocytosis, and was associated with better survival in a macrophage dependent fashion [27]. Our results support these findings and additionally suggest that blood-based VICM levels has potential value for monitoring early response to PD-1 inhibition.

Whereas higher C4M levels at baseline were previously demonstrated to be associated with worse clinical outcome after CTLA-4 inhibition in metastatic melanoma [13], we could not confirm this observation after PD-1 inhibition. C4M mirrors basement membrane remodeling, which is strongly associated with malignant progression of cancer [28]. These inconsistent results may be explained either by the difference of mechanism of action of CTLA-4 and PD-1 inhibition or by the higher efficacy of PD-1 inhibition in this immune-oncology setting [13].

Interestingly, C4G levels were previously associated with improved OS after CTLA-4 inhibition in metastatic melanoma (Jensen et al., AACR abstract 2020, in press). This C4G

biomarker measures a neo-epitope of granzyme B mediated degradation of type IV collagen that may reflect cytotoxic T-cell infiltration in the TME [29]. Nevertheless, we could not observe a relationship between C4G levels and clinical outcome after PD-1. Granzyme B is a key serine protease that is secreted by activated T and NK cells to induce apoptosis [30]. While it is suggested to contribute to response mechanisms of PD-1 inhibition in metastatic lung cancer, illustrated by an inverse relationship of both granzyme B levels as well as germline variation of *GZMB* and clinical outcome (Hurkmans JITC 2020, in press), further research is needed to elaborate on the differences between ICIs and tumor types [31].

Despite the interesting findings, this study also has some limitations. Patients were treated with two different ICIs (nivolumab or pembrolizumab) and not designed/powered to differentiate between the two. Although these are highly similar monoclonal antibodies directed to the PD-1 receptor, this may have an impact on the results. Furthermore, the sample size was too small to correct for multiple testing or for splitting the patients into a discovery and validation group. Nevertheless, in the current analysis we were able to demonstrate strong associations with survival outcomes for a selection of ECM biomarkers. Though, ECM turnover is a physiological process taking place throughout the body, the assessments of specific post-translational modifications (neo-epitopes) may reduce the systemic background of healthy turnover and instead increase the specificity of ECM turnover in the TME [12,32]. Lastly, even though our main objective was to investigate the association of markers with clinical outcome, the findings do not address the predictive performance of the biomarkers, for which prospective external validation is needed in cohorts randomized to different modalities.

CONCLUSIONS

In conclusion, we demonstrated that the ECM protein fragments PRO-C3 and PC3X in baseline serum, representing a dense collagen stroma, were associated with worse clinical outcome after PD-1 inhibition in metastatic melanoma. Moreover, increasing VICM levels early during therapy was associated with improved survival. VICM levels correspond with M1 macrophage activity by its specific release of MMP-degraded and citrullinated vimentin in the blood circulation. After validation, these biomarkers may provide a robust non-invasive tool for patient stratification and therapeutic decision-making in immuno-oncology.

REFERENCES

1 Jessurun CAC, Vos JAM, Limpens J, *et al.* Biomarkers for response of melanoma patients to immune checkpoint inhibitors: A systematic review. *Front Oncol* 2017;**7**:233. doi:10.3389/fonc.2017.00233

2 Hurkmans DP, Kuipers ME, Smit J, *et al.* Tumor mutational load, CD8+ T cells, expression of PD-L1 and HLA class I to guide immunotherapy decisions in NSCLC patients. *Cancer Immunol Immunother* 2020;**69**:771–7. doi:10.1007/s00262-020-02506-x

3 Tarhini A, Kudchadkar RR. Predictive and on-treatment monitoring biomarkers in advanced melanoma: Moving toward personalized medicine. Cancer Treat. Rev. 2018;**71**:8–18. doi:10.1016/j.ctrv.2018.09.005

4 Mariathasan S, Turley SJ, Nickles D, *et al.* TGFβ attenuates tumour response to PD-L1 blockade by contributing to exclusion of T cells. *Nature* 2018;**554**:544–8. doi:10.1038/nature25501

5 Wang L, Saci A, Szabo PM, *et al.* EMT- and stroma-related gene expression and resistance to PD-1 blockade in urothelial cancer. *Nat Commun* 2018;**9**:3503. doi:10.1038/s41467-018-05992-x

6 Chakravarthy A, Khan L, Bensler NP, *et al.* TGF-β-associated extracellular matrix genes link cancer-associated fibroblasts to immune evasion and immunotherapy failure. *Nat Commun* 2018;**9**:4692. doi:10.1038/s41467-018-06654-8

7 Okrah K, Tarighat S, Liu B, *et al.* Transcriptomic analysis of hepatocellular carcinoma reveals molecular features of disease progression and tumor immune biology. *npj Precis Oncol* 2018;**2**:25. doi:10.1038/s41698-018-0068-8

8 Mushtaq MU, Papadas A, Pagenkopf A, *et al.* Tumor matrix remodeling and novel immunotherapies: The promise of matrix-derived immune biomarkers. *J Immunother Cancer* 2018;**6**:65. doi:10.1186/s40425-018-0376-0

9 Ziani L, Safta-Saadoun T Ben, Gourbeix J, *et al.* Melanoma-associated fibroblasts decrease tumor cell susceptibility to NK cell-mediated killing through matrix-metalloproteinases secretion. *Oncotarget* 2017;**8**:19780–94. doi:10.18632/oncotarget.15540

10 Hutchenreuther J, Leask A. Why target the tumor stroma in melanoma? *J Cell Commun Signal* 2018;**12**:113–8. doi:10.1007/s12079-017-0419-1

11 Kessenbrock K, Plaks V, Werb Z. Matrix Metalloproteinases: Regulators of the Tumor Microenvironment. *Cell* 2010;**141**:52–67. doi:10.1016/j.cell.2010.03.015

12 Leeming DJ, Bay-Jensen AC, Vassiliadis E, *et al.* Post-translational modifications of the extracellular matrix are key events in cancer progression: Opportunities for biochemical marker development. *Biomarkers* 2011;**16**:193–205. doi:10.3109/1354750X.2011.557440

13 Jensen C, Madsen DH, Hansen M, *et al.* Non-invasive biomarkers derived from the extracellular matrix associate with response to immune checkpoint blockade (anti-CTLA-4) in metastatic melanoma patients. *J Immunother Cancer* 2018;**6**:152. doi:10.1186/s40425-018-0474-z

14 Willumsen N, Ali SM, Leitzel K, *et al.* Collagen fragments quantified in serum as measures of desmoplasia associate with survival outcome in patients with advanced pancreatic cancer. *Sci Rep* 2019;**9**:19761. doi:10.1038/s41598-019-56268-3

15 Eisenhauer EA, Therasse P, Bogaerts J, *et al.* New response evaluation criteria in solid tumours: Revised RECIST guideline (version 1.1). *Eur J Cancer* 2009;**45**:228–47. doi:10.1016/j.ejca.2008.10.026

16 Nielsen MJ, Nedergaard AF, Sun S, *et al.* The neo-epitope specific PRO-C3 ELISA measures true formation of type III collagen associated with liver and muscle parameters. *Am J Transl Res* 2013;**5**:303–15.

17 Chen DS, Mellman I. Elements of cancer immunity and the cancer–immune set point. *Nature* 2017;**541**:321–30. doi:10.1038/nature21349

18 Rizvi NA, Hellmann MD, Snyder A, *et al.* Mutational landscape determines sensitivity to PD-1 blockade in non. *Science (80-)* 2016;**348**:124–9.

19 Weide B, Martens A, Hassel JC, *et al.* Baseline biomarkers for outcome of melanoma patients treated with pembrolizumab. *Clin Cancer Res* 2016;**22**:5487–96. doi:10.1158/1078-0432.CCR-16-0127

20 Gershenwald JE, Scolyer RA, Hess KR, *et al.* Melanoma staging: Evidence-based changes in the American Joint Committee on Cancer eighth edition cancer staging manual. *CA Cancer J Clin* 2017;**67**:472–92. doi:10.3322/caac.21409

21 Francis DM, Thomas SN. Progress and opportunities for enhancing the delivery and efficacy of checkpoint inhibitors for cancer immunotherapy. *Adv Drug Deliv Rev* 2017;**114**:33–42. doi:10.1016/j.addr.2017.04.011

22 Ahmadzadeh M, Rosenberg SA. TGF-β1 Attenuates the Acquisition and Expression of Effector Function by Tumor Antigen-Specific Human Memory CD8 T Cells. *J Immunol* 2005;**174**:5215–23. doi:10.4049/jimmunol.174.9.5215

23 Nissen NI, Karsdal M, Willumsen N. Collagens and Cancer associated fibroblasts in the reactive stroma and its relation to Cancer biology. *J Exp Clin Cancer Res* 2019;**38**:115. doi:10.1186/s13046-019-1110-6

24 Gorchs L, Moro CF, Bankhead P, *et al.* Human pancreatic carcinoma-associated fibroblasts promote expression of co-inhibitory markers on CD4+ and CD8+ T-cells. *Front Immunol* 2019;**10**. doi:10.3389/fimmu.2019.00847

25 Mortensen JH, Guo X, De Los Reyes M, *et al.* The VICM biomarker is released from activated macrophages and inhibited by anti-GM-CSFRα-mAb treatment in rheumatoid arthritis patients. *Clin Exp Rheumatol* 2019;**37**:73–80.

26 Xiong H, Mittman S, Rodriguez R, *et al.* Anti-PD-L1 treatment results in functional remodeling of the macrophage compartment. *Cancer Res* 2019;**79**:1493–506. doi:10.1158/0008-5472.CAN-18-3208

27 Gordon SR, Maute RL, Dulken BW, *et al.* PD-1 expression by tumour-associated macrophages inhibits phagocytosis and tumour immunity. Nature. 2017;**545**:495–9. doi:10.1038/nature22396

28 Cox TR, Erler JT. Remodeling and homeostasis of the extracellular matrix: Implications for fibrotic diseases and cancer. *DMM Dis Model Mech* 2011;**4**:165–78. doi:10.1242/dmm.004077

29 Prakash MD, Munoz MA, Jain R, *et al.* Granzyme B promotes cytotoxic lymphocyte transmigration via basement membrane remodeling. *Immunity* 2014;**41**:960–72. doi:10.1016/j.immuni.2014.11.012

30 Voskoboinik I, Whisstock JC, Trapani JA. Perforin and granzymes: Function, dysfunction and human pathology. Nat. Rev. Immunol. 2015;**15**:388–400. doi:10.1038/nri3839

31 Wei SC, Levine JH, Cogdill AP, *et al.* Distinct Cellular Mechanisms Underlie Anti-CTLA-4 and Anti-PD-1 Checkpoint Blockade. *Cell* 2017;**170**:1120–33.e17. doi:10.1016/j.cell.2017.07.024

32 Karsdal MA, Henriksen K, Leeming DJ, *et al.* Novel combinations of Post-Translational Modification (PTM) neo-epitopes provide tissue-specific biochemical markers-are they the cause or the consequence of the disease? *Clin Biochem* 2010;**43**:793–804. doi:10.1016/j.clinbiochem.2010.03.015

SUPPLEMENTARY INFORMATION

Supplementary Figure 1. Histograms showing the distribution of serum levels of ECM biomarkers

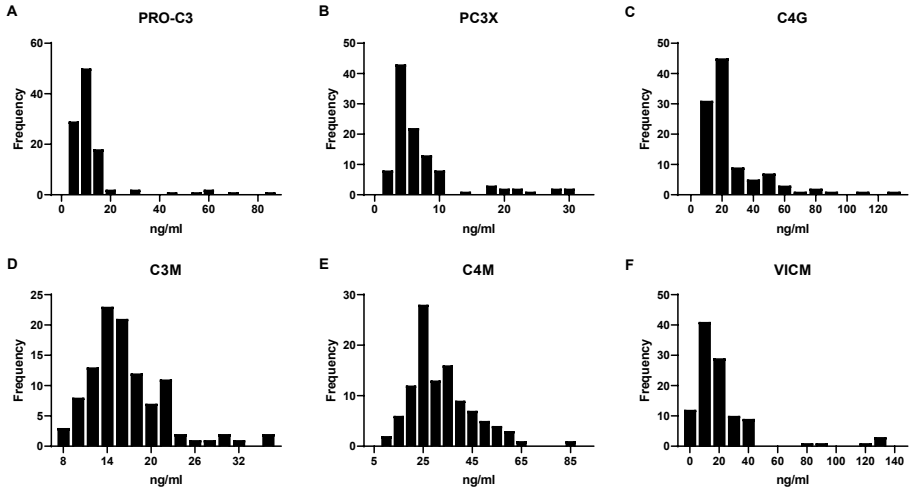

Histograms showing the distribution of serum levels of the studied ECM biomarkers at baseline A) PRO-C3, B) PC3X, C) C4G, D) C3M, E) C4M and F) VICM. The distribution of levels is generally skewed to the right.

Supplementary Figure 2. Relationship between baseline levels of the ECM biomarkers and therapy response

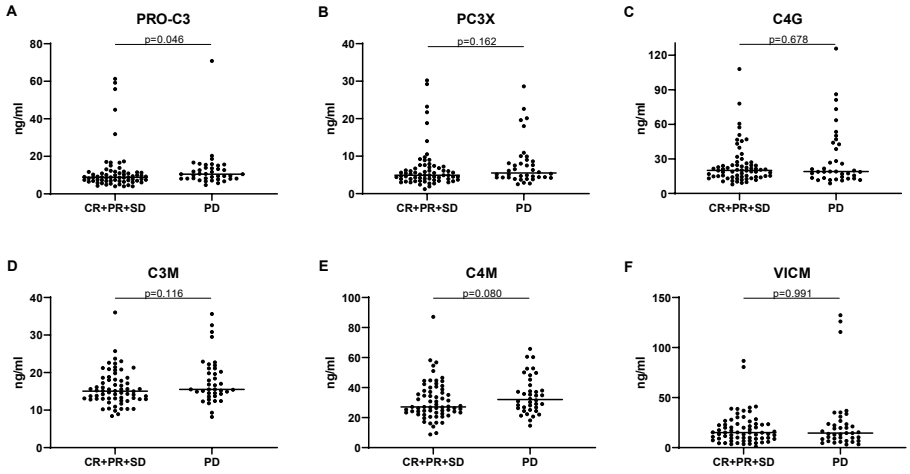

Relationship between the ECM biomarkers A) PRO-C3, B) PC3X, C) C4G, D) C3M, E) C4M and F) VICM with therapy response. Therapy response was based on RECIST v1.1. Patients with progressive disease (PD) were compared to patients with stable disease (SD), partial response (PR) or complete response (CR) with Mann-Whitney test.

Supplementary Figure 3. Relationship between ECM biomarker levels at baseline and week six

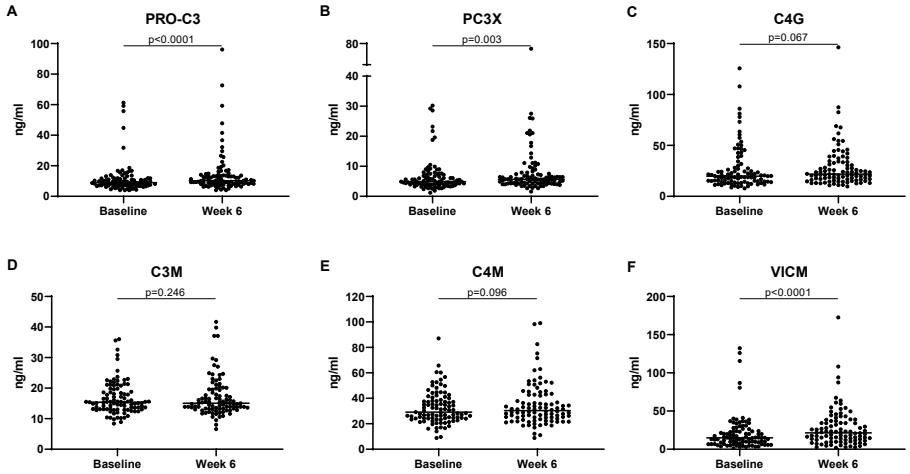

The graphs show the serum levels of ECM biomarkers at baseline and 6 weeks after start of PD-1 ICI therapy: A) PRO-C3, B) PC3X, C) C4G, D) C3M, E) C4M and F) VICM. The black lines represent the median value of patients. Serum levels were compared using Wilcoxon matched-pairs test.

Supplementary Figure 4. Association of ECM biomarkers measured at week six and progression free survival

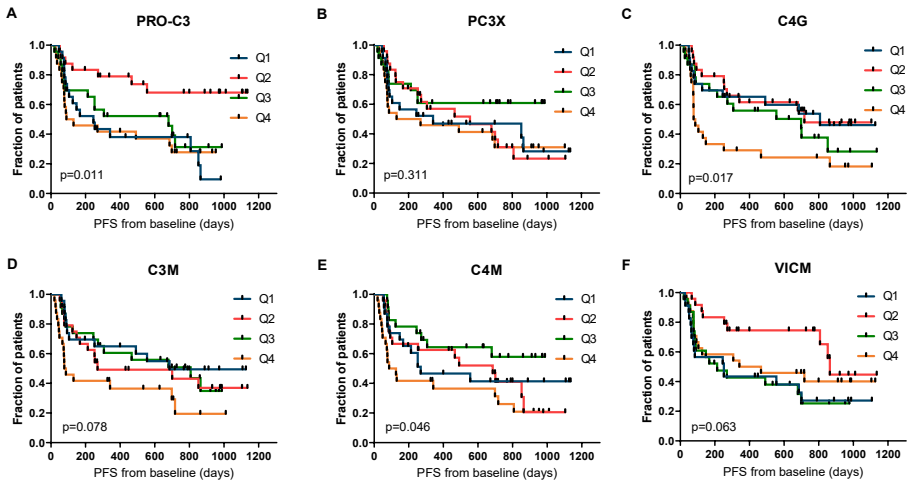

Kaplan-Meier plots demonstrating the association of ECM biomarkers with progression free survival (PFS) for metastatic melanoma patients. A) PRO-C3, B) PC3X, C) C4G, D) C3M, E) C4M and F) VICM were dichotomized into quartiles (Q4, representing the highest levels of the biomarker). P-values are based on the log-rank test.

Supplementary Figure 5. Association of ECM biomarkers measured at week six and overall survival

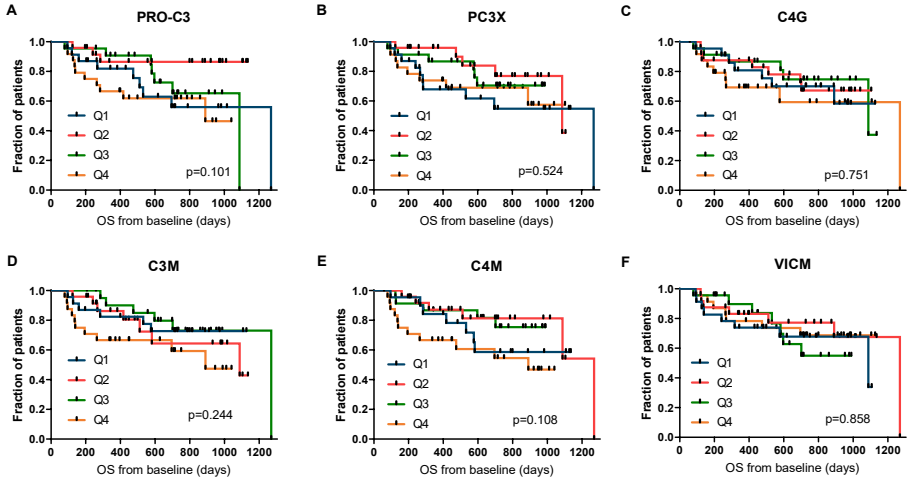

Kaplan-Meier plots demonstrating the association of ECM biomarkers with overall survival (OS) for metastatic melanoma patients. A) PRO-C3, B) PC3X, C) C4G, D) C3M, E) C4M and F) VICM were dichotomized into quartiles (Q4, representing the highest levels of the biomarker). P-values are based on the log-rank test.

Supplementary Table 1. Correlation matrix showing the association of ECM biomarkers and lactate dehydrogenase (LDH) at baseline

LDH	Pearson Correlation	-0.03						
	Sig. (2-tailed)	0.743						
	N	107						
PRO-C3	Pearson Correlation	0.03	0.56					
	Sig. (2-tailed)	0.724	<0.0001****					
	N	107	107					
PC3X	Pearson Correlation	-0.06	0.41	0.60				
	Sig. (2-tailed)	0.532	<0.0001****	<0.0001****				
	N	107	107	107				
C4G	Pearson Correlation	-0.03	-0.11	-0.07	0.04			
	Sig. (2-tailed)	0.757	0.279	0.479	0.699			
	N	106	106	106	106			
C3M	Pearson Correlation	0.05	0.06	0.11	0.27	0.22		
	Sig. (2-tailed)	0.642	0.514	0.277	0.005**	0.027*		
	N	107	107	107	107	106		
C4M	Pearson Correlation	0.11	0.18	0.11	0.28	0.06	0.86	
	Sig. (2-tailed)	0.274	0.060	0.257	0.003**	0.524	<0.0001****	
	N	107	107	107	107	106	107	
VICM	Pearson Correlation	0.03	-0.13	-0.04	0.18	0.01	0.21	0.26
	Sig. (2-tailed)	0.730	0.176	0.700	0.069	0.928	0.034*	0.006**
	N	107	107	107	107	106	107	107
		Age	**LDH**	**PRO-C3**	**PC3X**	**C4G**	**C3M**	**C4M**

Pearson correlation. Abbreviations: significance (sig.), number (N).

Supplementary Table 2. Correlation matrix showing the association of baseline and week six measurements of the ECM biomarkers

	PRO-C3	PC3X	C4G	C3M	C4M	VICM
Pearson Correlation	0.68	0.67	0.83	0.72	0.70	0.45
Sig. (2-tailed)	<0.0001****	<0.0001****	<0.0001****	<0.0001****	<0.0001****	<0.0001****
N	94	94	93	94	94	94

Pearson correlation was used. Abbreviations: Sig significance (sig.), number (N).

CHAPTER 14

14

Blood-based kinase activity profiling; a potential predictor of response to immune checkpoint inhibition in metastatic cancer

Daan P. Hurkmans*, Els M.E. Verdegaal*, Sabrina A. Hogan, Rik de Wijn, Lies Hovestad, Dianne M.A. van den Heuvel, Rob Ruijtenbeek, Marij J.P. Welters, Mandy van Brakel, Edwin A. Basak, Herbert M. Pinedo, Cor H.J. Lamers, Harmen J.G. van de Werken, John P. Groten, Reno Debets, Mitchell P. Levesque, Reinhard Dummer, Ellen Kapiteijn, Ron H.J. Mathijssen, Joachim G.J.V. Aerts*, Sjoerd H. van der Burg*

*Shared first/senior authorship

Journal for ImmunoTherapy of Cancer, December 2020, 8: 1607

Abstract

Background: Many cancer patients do not obtain clinical benefit from immune checkpoint inhibition. Checkpoint blockade targets T-cells, suggesting that tyrosine kinase activity profiling of baseline peripheral blood mononuclear cells may predict clinical outcome.

Methods: Here a total of 160 patients with advanced melanoma or non-small-cell lung cancer (NSCLC), treated with anti-CTLA-4 or anti-PD-1, were divided in 5 discovery and cross-validation cohorts. The kinase activity profile was generated by analyzing phosphorylation of PBMC lysates in a micro-array comprising of 144 peptides derived from sites that are substrates for protein tyrosine kinases. Binary grouping into patients with or without clinical benefit was based on RECISTv1.1. Predictive models were trained using partial least square discriminant analysis (PLS-DA), performance of the models was evaluated by estimating the Correct Classification Rate (CCR) using cross-validation.

Results: The kinase phosphorylation signatures segregated responders from non-responders by differences in canonical pathways associated with governing T-cell migration, infiltration and co-stimulation. PLS-DA resulted in a CCR of 100% and 93% in the anti-CTLA-4 and anti-PD1 melanoma discovery cohorts, respectively. Cross-validation cohorts to estimate the accuracy of the predictive models showed CCRs of 83% for anti-CTLA-4 and 78% or 68% for anti-PD-1 in melanoma or NSCLC, respectively.

Conclusions: Blood-based kinase activity profiling for response prediction to ICIs in melanoma and NSCLC revealed increased kinase activity in pathways associated with T cell function and lead to a classification model with a highly accurate classification rate in cross-validation groups. The predictive value of kinase activity profiling is prospectively verified in an ongoing trial.

INTRODUCTION

Tumors can evade T cell-mediated destruction via the expression of immune checkpoints, including the programmed cell death ligand-1 (PD-L1) and CD80 or CD86, that inhibit T cells that express programmed cell death 1 (PD-1) or cytotoxic T lymphocyte antigen 4 (CTLA-4), respectively. Immune checkpoint inhibitors (ICIs) against these receptors have been approved for a variety of malignancies and revolutionized their clinical management, in particular that of melanoma and non-small cell lung cancer (NSCLC)[1-4]. However, durable responses are only obtained in a minority of patients, whereas ICIs are associated with considerable side effects and costs. Therefore, robust and reliable predictive biomarkers to predict treatment response are urgently needed.

The cognate interaction between T cells and antigen presenting cells (APCs) via interaction of the T cell receptor (TCR) with antigen presented in the context of HLA, results in activation of T cells after which T cells quickly upregulate CTLA-4 and/or PD-1 as part of a negative feedback loop. As a result, T cells may display a reduced capacity to become activated, proliferate and exert specific effector functions. Currently, CTLA-4 is thought to play a major role during priming of a T cell response in the lymph node where it directly prevents co-stimulation of T cells via interaction of CD28 with its ligand CD80/86 on APCs. Moreover, CTLA-4 is constitutively expressed on regulatory T cells (Tregs), and Tregs can reduce expression of CD80/86 by trans-endocytosis thereby preventing activation of effector T cells[5]. PD-1 inhibits activation of pre-existing tumor-specific T cells during the effector phase and is thought to dampen an immune response after antigen eradication in order to prevent immune pathology. Eventually, tumor eradication by T cells relies on TCR-mediated activation and downstream co-stimulatory signaling, which is tightly regulated by different tyrosine kinase mediated signaling pathways. For instance, activation of PI3K and deactivation of PTEN results in recruitment and activation of downstream signaling molecules like AKT, enhancing T cell survival, proliferation and effector functions[6]. Under normal conditions, ligation of the inhibitory receptors CTLA-4 and PD-1 results in recruitment of SHP2 phosphatases that dampens TCR signaling as well as CD28 signaling[7-9]. As such, kinase activity may reflect anti-tumor T cell activity and consequently could act as a predictor for clinical outcome after ICI therapy. In fact, peptide micro-array technology to evaluate global kinase activities in tumor or blood has recently been applied as a biomarker strategy for response prediction to chemo- or targeted-therapy in several cancer types.[6,10-13]

Previous efforts to predict the clinical response to ICI therapy yielded various biomarkers, including tumor mutational burden (TMB) and PD-L1 expression in tumor tissue for NSCLC[14,15]. The predictive performance of these biomarkers may be sufficient in some studies[16,17], yet are complicated by both the availability of tissue and both inter- and intra-tumoral heterogeneity. Interestingly, a number of blood parameters have been associated with response to CTLA-4 and PD-1/PD-L1. For example, the total number and

composition of circulating leukocytes were associated with clinical outcome, amongst which high lymphocyte and eosinophil counts, low monocyte count and low neutrophil to lymphocyte ratio (NLR). In addition, the absence of myeloid-derived suppressor cells and presence of classical monocytes or previously activated T cells was associated with better response rates or survival after ICI.[18-28] Collectively, these studies indicate that the activation status and number of several immune cells in blood may provide minimally invasive predictive biomarkers that are suitable for routine clinical use.

Whereas commonly used methods, including transcriptomics and high-dimensional flowcytometry may reveal the outcome of certain incoming signals, they do not reveal the whole network of signal transduction pathways activated in cells, nor show at which point they are deregulated in certain patients. Protein kinases are a large family of highly influential proteins which modify the activity, affinity and location of many cellular proteins in order to regulate cellular processes, in particular signal transduction. Here, we argued that if some of the complex biological tumor-immune cell interactions determining the response to ICIs are also reflected in the plethora of immune cells in the blood, then kinase activity profiling of peripheral blood mononuclear cells (PBMCs) may be able to capture this. Therefore, we have explored the predictive performance of kinase activity profiling in PBMCs from advanced melanoma and NSCLC patients treated with anti-PD-1 or anti-CTLA-4 monotherapy.

MATERIALS AND METHODS

Patient population and study workflow

Patients with irresectable stage III/IV advanced melanoma or stage IV NSCLC were included if they had received intravenous monotherapy with either ipilimumab (anti-CTLA4; 3 mg/kg every 3 weeks for 4 courses), nivolumab (anti-PD-1; 3 mg/kg every 2 weeks until a maximum of 2 years) or pembrolizumab (anti-PD1; 2 mg/kg every 3 weeks until a maximum of 2 years) as standard of care at the Erasmus University Medical Center (Rotterdam, The Netherlands), Leiden University Medical Center (Leiden, The Netherlands) or University Hospital Zürich (Zürich, Switzerland), all being referral hospitals. Patients who received ICI combination therapy or who were treated with a prior line of any form of immunotherapy were excluded, pretreatment of corticosteroids was not considered. The study was approved by the independent ethics committee board (reference numbers: MEC 16-011, P11-016, and MEC 14-0425, respectively) and in accordance with the revised WMA Declaration of Helsinki on human rights. Following written informed consent of the patients, blood samples were collected before the first administration of ICIs and after the last administration of any previous treatment if applicable .

Data collection

Binary grouping was performed according to patients with (responders) or without (non-responders) clinical benefit based on response evaluation criteria in solid tumors (RECIST) version 1.1. For determination of best overall response (BOR), confirmation of a complete or partial response (CR/PR) was not required, but a minimum duration of 90 days was required for stable disease (SD). Patients with a CR, PR or SD as BOR were considered to have obtained clinical benefit after ICIs and were defined as responders. Patients with progressive disease (PD) were defined as non-responders. Additionally, binary grouping was performed according to progression-free survival (PFS), measured from start of treatment to death or the first evaluation time point that PD is detected; the two groups included late (> 140 days) or no progression (responders) versus patients with early progression within 140 days (non-responders). Clinical parameters and chemistry or blood parameters were evaluated at baseline and included age, gender, WHO performance score, pathological tumor type, presence of brain metastases and serum lactate dehydrogenase (LDH) levels.

Preparation of PBMC lysate

Venous blood of patients was collected at baseline using either sodium-heparin or EDTA as anticoagulant, and isolation of PBMCs was done within 4 hours or within 24 hours depending on the local study protocol (**Suppl. Table 1**). PBMC were isolated by density gradient centrifugation and cryopreserved until further use. Erythrocyte lysis was only performed in the Mel-CTLA4-B cohort if PBMC still contained considerable erythrocyte contamination after isolation. Importantly, kinase activity was affected by erythrocyte lysis during PBMC isolation (**Suppl. Fig. 1a**). Moreover, overall reduced kinase activity was observed in PBMCs that were isolated after 24 hour from blood collected in EDTA anticoagulated tubes (**Suppl. Fig. 1b**).

Cryopreserved cells were thawed, washed with phosphate buffered saline, and lysed using ice-cold M-PER lysis buffer (Mammalian Protein Extraction Reagent, Thermo Fisher Scientific, MA, USA) containing 1:100 Protease Inhibitor Cocktail (Thermo Fisher Scientific). Cell lysate was obtained by centrifugation at 14.000 × g for 10 min at 4°C. After centrifugation the supernatant was snap-frozen in aliquots and stored at -80°C. The protein concentration was determined using the Bradford Assay (Thermo Fisher Scientific) with bovine serum albumin (BSA) as the standard.

Kinase activity profiling

PBMC kinomic activity was measured using protein tyrosine kinase (PTK) PamChip-96 microarrays (catalog # 86311, PamGene International BV, 's-Hertogenbosch, The Netherlands) using standard manufacturer protocol. In short, the microarrays were blocked with 2% BSA (Calbiochem # 126609) to prevent non-specific binding. After blocking the arrays were washed three times with 1x PK buffer (50 mM Tris-HCl pH 7.5,

10 mM $MgCl_2$, 0.01% Brij35, 2 mM DTT). For kinomic profiling 2 µg PBMC lysate protein was used in 40 µl PTK assay buffer (1x PK buffer, 10mM DTT, 400 µM ATP, 1x PTK additive (PamGene International BV), 1:400 Halt Phosphatase Inhibitors (Thermo Fisher Scientific, MA, USA), 0.01% BSA (Calbiochem), and fluorescein isothiocyanate (FITC)-labeled antiphosphotyrosine antibody (PamGene). During incubation the reaction mixture was pumped up and down through the porous membrane for 60 cycles at 2 cycles/min. Incubation and read-out of the microarrays was performed with 96 arrays in parallel on a PamStation-96. Typically, 3-4 technical replicates of each sample were measured in the same run. Time courses of peptide phosphorylation were followed by recording fluorescent images which were quantified by automated image analysis in Bionavigator 6.3.67 (PamGene). Analysis of signals was performed after local background subtraction in Bionavigator 6.3.67 interfaced to the open source statistical program R 3.3.1 (R-project, www.rproject.org).

Analysis was specifically performed per cohort and comprised a quality check, removal of outlier replicates, data transformation and averaging of the kinase signal replicates. To check data quality, the first step was exclusion of a low portion of arrays that showed clear visual defects (e.g. broken membrane, large stains) or technical replicates clearly deviating from the other replicates of the same samples. In the second step, data is log-transformed (CTLA-4 cohorts: Mel-CTLA4-A, Mel-CTLA4-B) or normalized using the VSN method (PD-1 cohorts: Mel-PD1-A, Mel-PD1-B, NSCLC-PD1). Prior to log-transformation, a small fraction of negative values in the (background corrected) signals was handled by setting all signals <1 or equal to 1. Signal-positive spots were required to show a positive trend in the recorded phosphorylation time course. Peptides for which such a trend could not be detected in > 75% of the samples were excluded from further analysis. Effectively, 88-113 peptides were included for further analysis. Technical replicates of each patient sample were averaged resulting in a single kinase activity profile per included patient for subsequent analysis.

Principal Component Analysis (PCA) was performed on the transformed and filtered data and PCA scores were used to identify systematic variation, e.g. as a result of different sub-cohorts and/or the use of different PamStation-96 microarray plates. Systematic variation was handled by applying ComBat[29] batch correction, and outlier patient samples were removed. For the small Mel-CTLA4-A cohort no such correction was necessary. For the Mel-CTLA4-B cohort a batch effect was observed and corrected for the batches in which samples were lysed together. A small number (ranging from 1 to 8) of outlier samples according to PCA scores or heat map visualizations of the transformed profiles were removed. In most cases these were samples showing low overall kinase activity. Other reasons for removing measured patient samples from the analysis was unavailability of clinical data or if, after reevaluation, patients were observed not to fulfill the selection criteria.

Statistical analysis and bioinformatics

Kinase activity profiles were correlated to the clinical response to ICIs. Univariate (per peptide) analysis was performed using a two-sided two sample t-test with binary grouping as a covariate (responders versus non-responders). Peptides with $p < 0.05$ were regarded as significant, in addition, the proportion of false discoveries in a set of significant peptides was estimated using the False Discovery Rate (FDR) method of Benjamini & Hochberg. Classification analysis was performed using Partial Least Squares Discriminant Analysis (PLS-DA) with patients divided in binary groups as previously described[13]. In short, a classification model is trained using all tested peptides, i.e., without prior peptide selection based on responder and non-responder differences. The resulting model is a set of coefficients (one for each peptide + an offset) that can be applied to new observations to obtain a score that predicts classification in either groups. For each cohort, the Correct Classification Rate (CCR) was estimated using cross validation. Approximately 90% binomial confidence intervals (CI_{90}) for the CCR estimates were obtained using the exact method (note that a CI_{90} implies with 95% confidence that the CCR is higher than the lower limit). Prediction of kinases responsible for the changes in peptide phosphorylation in the kinomic profiles were obtained using the Upstream Kinase Analysis tool in Bionavigator 6.3.67 (PamGene). Results were visualized by annotation to a kinase phylogenetic tree using the web-based Coral tool (http://phanstiel-lab.med.unc.edu)[30]. Additionally, Ingenuity Pathway Analysis (Qiagen, Hilden, Germany) was used to perform gene set enrichment analyses utilizing the delta and unadjusted p-value of each peptide (two-sided two sample t-tests). Pathway activation or inhibition were predicted by the z-score statistic, and further explored by the MAP tool (Qiagen, Hilden, Germany). Full access of the datasets generated during the current study is provided in the supplementary materials (**Suppl. Tables 2-6**).

RESULTS

A total of 174 advanced cancer patients were enrolled and 160 patients were evaluable for analysis (**Fig. 1**) because in 14 cases (8%) the patient samples had to be removed as they did not comply with the quality check (**Suppl. Fig. 2**). The study protocols between the centers were different with regard to the PBMC isolation protocol and the anti-coagulant used for blood collection. As a consequence, the different patient cohorts were not pooled for analysis, resulting in five distinct cohorts (**Fig. 1**), and protocol differences could be assessed for their effect on kinase activities. The baseline patient characteristics are provided in **Table 1**. Patient cohort *Mel-CTLA4-A* was used as a discovery cohort for anti-CTLA-4 and consists of 10 melanoma patients selected based on an equal distribution of responders and non-responders. All responders in this cohort had SD >90 days, thus precluding selection bias based on exceptionally good and worse responders, only.

The patients had a baseline blood LDH level that was not above 2x the upper limit of normal (ULN, i.e. < 250 U/ml) to avoid bias towards a known independent prognostic factor. The 29 patients in cohort *Mel-PD1-A* functioned as discovery cohort for anti-PD-1 and had an almost equal distribution of responders (n=14) and non-responders (n=15). The mean baseline blood LDH level was not elevated above 2x ULN in the *Mel-PD1-A* discovery cohort, although some individual patients did have an elevated LDH above this threshold. The patients in the three other cohorts were used for cross-validation to assess the performance of response prediction by kinase activity profiling. Because of the lower response rate, patients in the *MEL-CTL-B* cohort were selected on equal distribution of responsers and non-responders, but again not based on patients with an exceptionally good or bad response. Patients in the other cohorts were not selected, apart from the exclusion criteria that they should not have received prior immunotherapy or combination checkpoint blockade. The mean baseline blood LDH level was higher and the range of values of individual patients larger in the cross-validation cohorts when compared to the discovery cohorts (**Table 1**).

Kinase activity profiles in PBMC of patients responding to checkpoint blockade

The correlation of kinase activity profiles with treatment response is visualized for the discovery cohort *Mel-CTLA4-A* using a heat map (**Fig. 2a**). A profound difference in kinase activity was observed between the responder and non-responders. Generally, the phosphorylation signal of peptides was higher in responders compared to non-responders. For 83% of the target peptides, a significantly higher signal was found in responders compared to non-responders (two-sided two sample t-test, p-value < 0.05; FDR < 5%). This overall increase in kinase activity was confirmed in the cross-validation cohort *Mel-CTLA4-B* (**Fig. 2b**), although less pronounced since only 23% of the target peptides displayed a significantly higher signal in responders compared to non-responders (two-sided two sample t-test, p-value < 0.05, FDR = 18%). In addition, the relative increase in signal was higher in the *Mel-CTLA4-A* cohort (median Log2 Fold Change= 0.84; SD = 0.15; ~ 80% increase) compared to the *Mel-CTLA4-B* cohort (median Log2 Fold Change = 0.40; SD = 0.17; ~ 30% increase). This increase in signal appears to reflect systemic, non-specific signaling in the responders compared to the non-responders.

Figure 1. Schematic overview of the study.

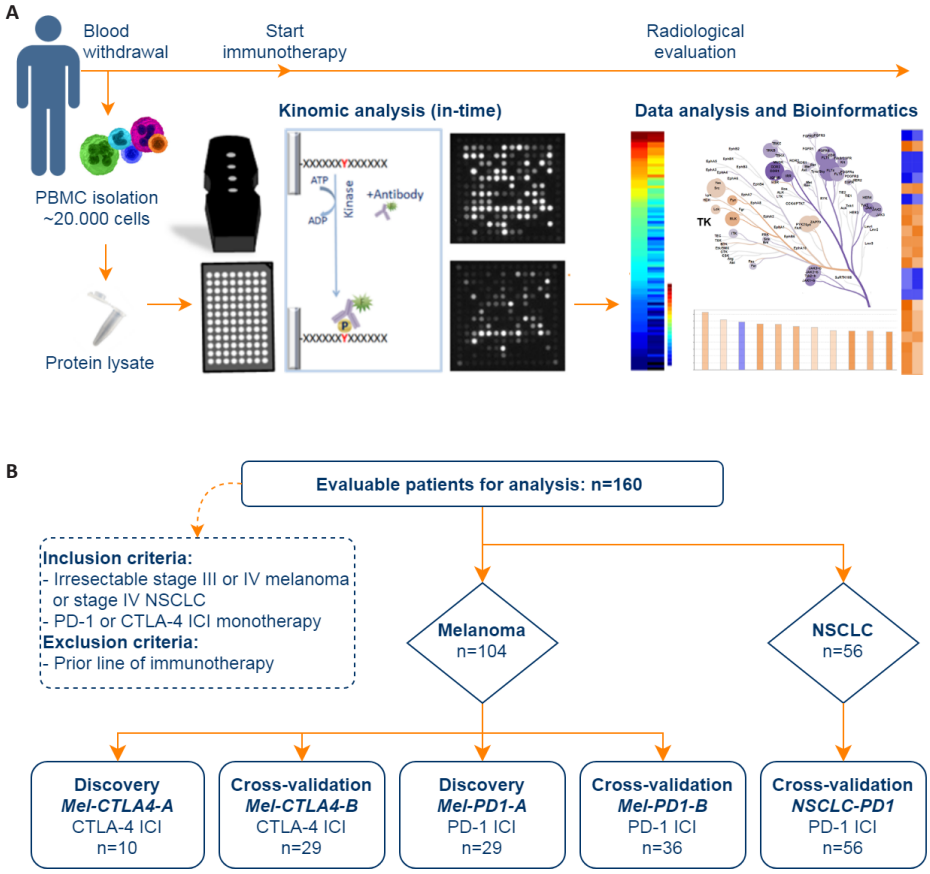

A) Work flow showing that kinase activity was measured in baseline PBMC samples using a peptide microarray system consisting of identical arrays, each containing 144 unique protein tyrosine kinase phosphorylation sites. PBMC samples were isolated from blood collected before onset of immune checkpoint inhibitor therapy. The kinase activity profile is analyzed using BioNavigator (PamGene), Coral tool (Courtesy Cell Signaling Technologies) to annotate kinases onto a phylogenetic tree and Ingenuity Pathway Analysis software (Qiagen) to perform gene set enrichment analyses. B) Flow chart of the patient selection process.

Table 1. Baseline patient characteristics

	Mel-CTLA4-A	Mel-CTLA4-B	Mel-PD1-A	Mel-PD1-B	NSCLC-PD1
Total, n	10	29	29	36	56
Age, median (range)	59.3 (26-79)	58.3(35-86)	64.0 (39-84)	61.6 (31-83)	63.1 (35-81)
Gender, n					
Male	4	13	16	21	36
Female	6	16	13	15	20
Primary tumor, n					
Melanoma	10	29	29	36	0
NSCLC	0	0	0	0	56
Adenocarcinoma	0	0	0	0	37
SCC	0	0	0	0	17
Large cell carcinoma	0	0	0	0	2
Treatment regimen, n					
Anti-PD1	0	0	29	36	56
Nivolumab	0	0	1	14	50
Pembrolizumab	0	0	28	22	6
Anti-CTLA4					
Ipilimumab	10	29	0	0	0
Prior therapy lines, n (%)					
0	4 (40%)	-	20 (69%)	30 (83%)	1 (2%)
1	4 (40%)	-	9 (31%)	6 (17%)	46 (82%)
2	2 (20%)	-	0 (0%)	0 (0%)	7 (12%)
>2	0 (0%)	-	0 (0%)	0 (0%)	2 (4%)
Prior immunotherapy, n					
No	10	29	29	36	56
Yes	0	0	0	0	0
Cerebral metastasis, n (%)					
No	6 (60%)	-	17 (59%)	15 (42%)	0 (0%)
Yes	2 (20%)	-	11 (38%)	2 (5%)	0 (0%)
Unknown	2 (20%)	-	1 (3%)	19 (53%)	56 (100%)
LDH (U/L), median (range)	207 (168-247)	369 (283-881)	229 (124-359)	315 (128-1523)	269 (133-860)

All patients received immune checkpoint inhibitor monotherapy and did not receive any prior line of immunotherapy. Abbreviations: lactate dehydrogenase (LDH), squamous cell carcinoma (SCC).

Figure 2. Baseline kinase activity profiles and response classification of patients treated with CTLA-4 blockade

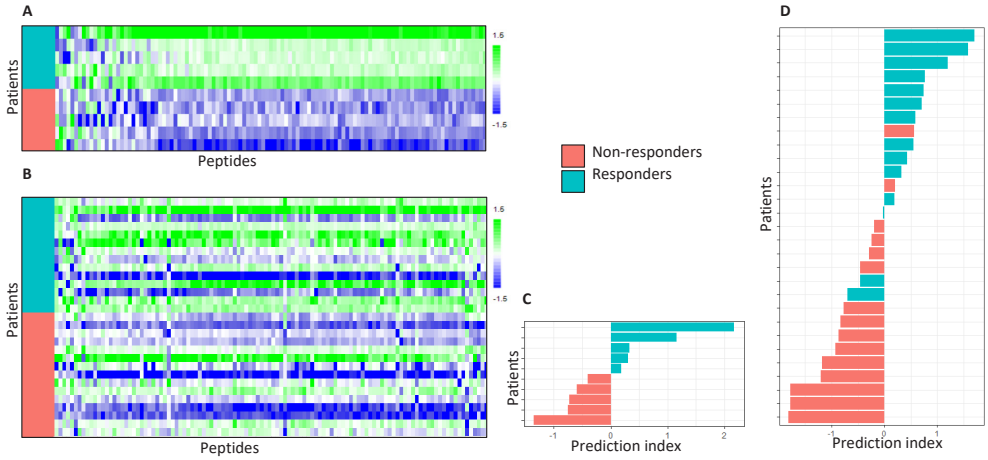

Heat maps showing kinase activity of separate cohorts of melanoma patients who were treated with CTLA-4 ICIs: A) discovery cohort Mel-CTLA4-A and B) cross-validation cohort Mel-CTLA4-B. Binary grouping of patients that either benefited or not from treatment (responders and non-responders, respectively)are shown . The columns represent patients sorted from left to right according to treatment response; the rows represent peptides sorted according to Pearsons correlation coefficient with treatment response, such that the peptides with a relatively higher phosphorylation signal in the non-responders are shown at the top of the map and the peptides with a relatively high signal in the responders are shown at the bottom of the map. The values are scaled per row to zero mean and unit variance. Furthermore, classification analyses of these cohorts are shown: C) discovery cohort Mel-CTLA4-A and D) cross-validation cohort Mel-CTLA4-B. The bar graphs show for each patient the prediction index obtained by cross validation of a PLS-DA model (see methods section). If the prediction index > 0 the patient is predicted to be a responder. The color of the bars indicates the actual clinical response class.

Discovery cohort *Mel-PD1-A* included melanoma patients who were treated with anti-PD-1. The profound higher kinase activities as observed in the responders in the two anti-CTLA-4 cohorts was not observed in the three anti-PD-1 cohorts. Therefore, the data was normalized for overall kinase activity using the VSN method. As a consequence, the data reflects differences in the ratio between peptides on the array rather than the overall differences. Responder patients showed a different kinase activity profile when compared to non-responders (**Fig. 3a).** For 17% of the peptides in cohort *Mel-PD1-A*, a significant different signal was found in responders compared to non-responders (two-sided two sample t-test, $p < 0.05$; FDR = 29%). These differentially phosphorylated peptides represented both higher and lower signals in responders compared to non-responders. Likewise, differential peptide phosphorylation was observed in the cross-validation

cohorts *Mel-PD1-B* and *NSCLC-PD1* (**Fig. 3b-c)**. In *Mel-PD1-B,* 16 peptides (18%) displayed significantly differential signals for response (two-sided two sample t-test, $p < 0.05$, FDR = 25%) whereas *NSCLC-PD1,* 18 peptides (19%) were significantly differently phosphorylated in responders compared to non-responders (two-sided two sample t-test, $p < 0.05$, FDR = 24%). The specific differences in kinase activities differentiating responders and non-responders varied between cohorts.

A high percentage of patients is correctly classified for response by their kinase activity profile

To investigate the potential use of kinase activity profiling as a biomarker for response to ICI therapy, classification analysis was performed using the binary grouping of responders and non-responders. Because of the kinase profile variation between the CTLA-4 and PD-1 ICIs cohorts, a separate PLS-DA classification model was trained for each cohort and predictive scores for each patient were obtained using cross-validation. This resulted in a correct classification rate (CCR) of 100% (90%CI 74-100%) in the discovery cohort *Mel-CTLA4-A* and 83% (64-93%) in cross-validation cohort *Mel-CTLA4-B* (**Fig. 2c,d**). The CCR was 93% (80-99%) in the discovery cohort *Mel-PD1-A,* 78% (63-88%) in cross-validation cohort *Mel-PD1-B*, and 68% (56-78%) in the second cross-validation cohort *NSCLC-PD1* (**Fig. 3d-f**).

Upstream kinase and canonical pathway analysis identify kinases associated with T cell function

Bioinformatics was applied to interrogate the biological processes underlying response or resistance to ICIs. Here, we have zoomed in on the anti-PD-1 cohorts as the overall increase of kinase activity in anti-CTLA-4 responders hampered proper identification of relevant and recognized peptide targets. Identified kinases were annotated to a phylogenetic tree for protein tyrosine kinases (**Fig. 4**). In the discovery cohort *Mel-PD1-A*, predictions revealed that the VEGF family kinases and FES/FER have relatively higher activity in responders compared to non-responders. Similarly, but less pronounced, the activity of TYRO-3, AXL and MER kinases of the TAM-family and the TRK-family were positively correlated with response in this cohort. In the cross-validation cohort *Mel-PD1-B*, however, the activity of several kinases, including the SRC family kinases, were negatively correlated with response. Interestingly, the above observations were corroborated in the second cross-validation cohort *NSCLC-PD1*, where VEGF kinases were found to have higher activity and the SRC family kinases to have lower kinase activity in responders compared to non-responders. Canonical pathway analysis using *Mel-PD1-A* and *NSCLC-PD1* cohorts revealed the importance of peptide targets involved in immune cell migration/leukocyte extravasation and co-stimulation of T helper cells. Finally, increased kinase activity in the STAT3-, ERBB-, VEGF- and EGF-signaling pathways were found to be related to response to anti-PD-1, whereas the PTEN activation was associated with resistance to anti-PD-1 (**Fig. 5** and **Suppl. Fig. 3**).

Figure 3. Baseline kinase activity profiles and response classification of patients treated with PD-1 blockade

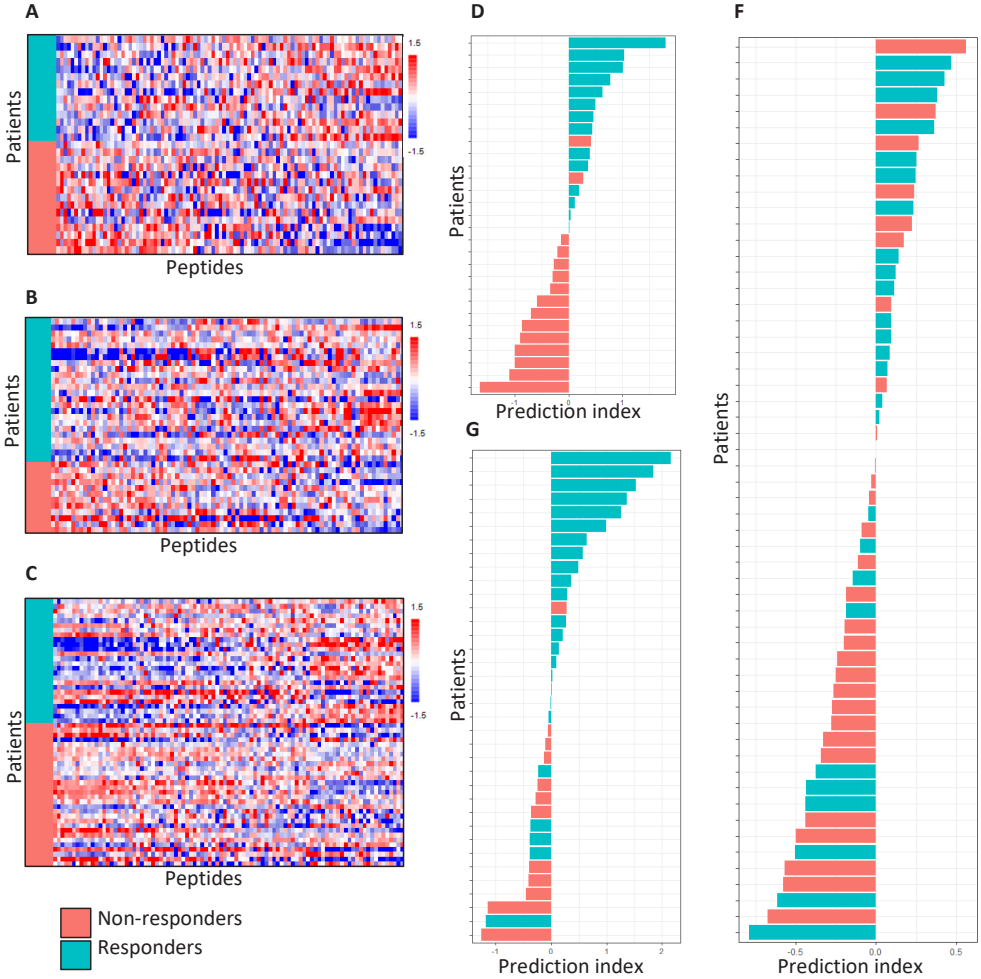

Heat maps showing the kinase activity of separate cohorts of melanoma patients who were treated with PD-1 ICIs: A) disovery cohort Mel-PD1-A, B) cross-validation cohort Mel-PD1-B and C) second cross-validation cohort NSCLC-PD1. See legend to Figure 2 for details. Furthermore, the classification analysis of these cohorts are shown: D) discovery cohort Mel-PD1-A, E) cross-validation cohort Mel-PD1-B and F) second cross-validation cohort NSCLC-PD1. Again, see legend to Figure 2 for details.

Figure 4. Identification of involved kinase families by phylogenetic tree analysis

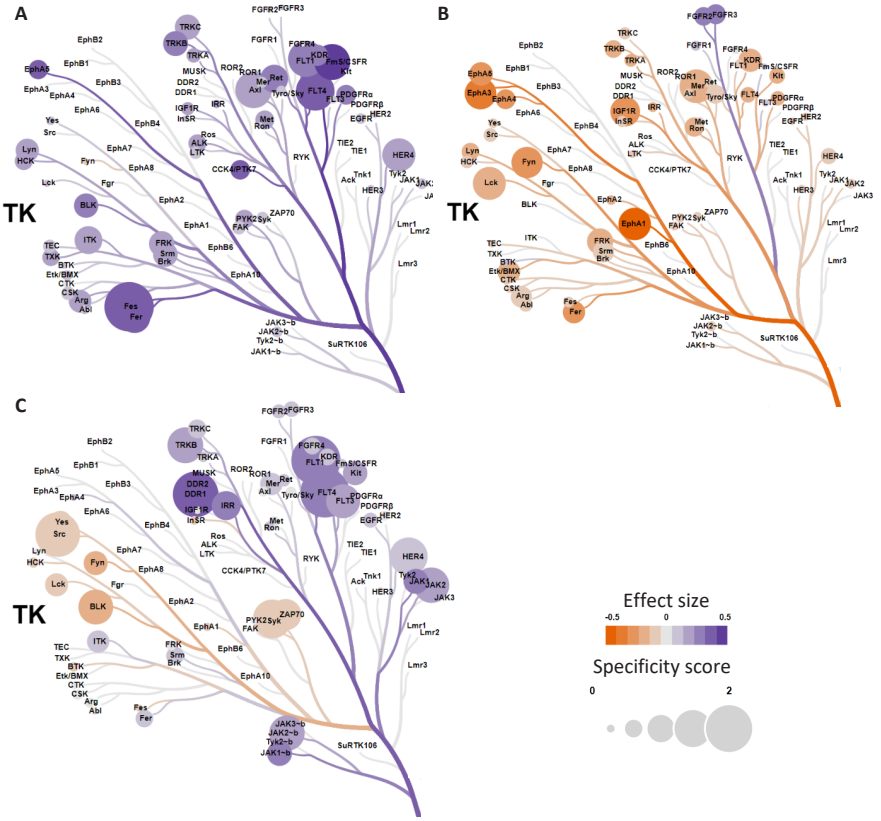

Kinase activities that were measured for the anti-PD1 treated cohorts, Mel-PD1-A (A), Mel-PD1-B (B), and NSCLC-PD1 (C) were exposed to the Coral tool to annotate kinases onto a phylogenetic tree (Courtesy Cell Signaling Technologies Inc.). The coloring indicates the effect size (purple: increased phosphorylation; and orange: decreased phosphorylation in responders compared to non-responders), and the size of the circle indicates the specificity score of the corresponding kinase (a higher score indicates a higher likelihood to contribute to the observed phosphorylation changes).

Figure 5. Differential kinase activity involves canonical pathways associated with T cell function analysis

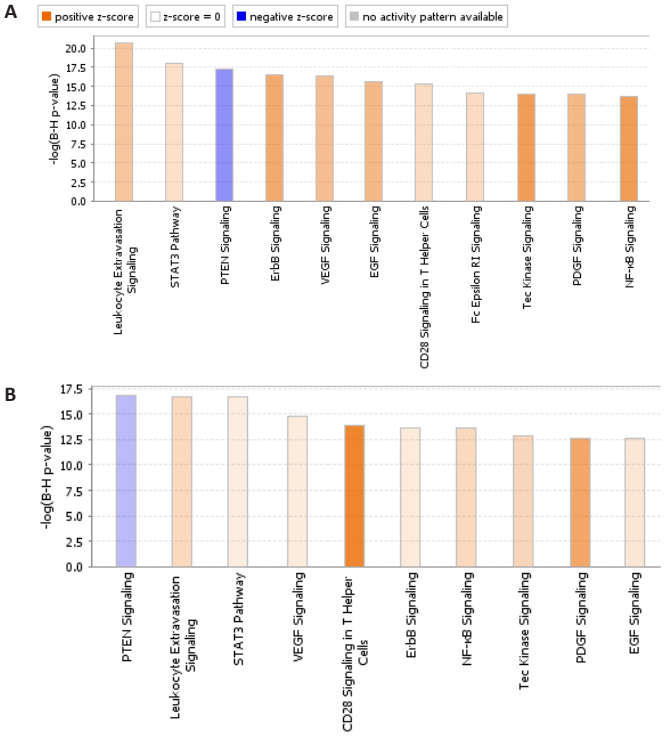

Top canonical pathways according to kinase activities are schematically shown for cohort A) Mel-PD1-A and B) NSCLC-PD1. Orange (positive z-score) indicates a predicted upregulation of the pathway in patients who benefit from treatment (responders), blue (negative z-score) indicates a predicted downregulation of the pathway in responders. Gray represents canonical pathways without a predicted activity pattern. The significance value indicates the probability that involved kinases are associated with the canonical pathway by random chance alone, cutoff was set at a B-H p-value >12. Ranking was based on the trend and z-score.

DISCUSSION

In this study we have investigated whether the clinical response to ICIs is reflected by the kinase activity profile in PBMC. We observed differential kinase activity profiles between patients with and without clinical benefit, which were subsequently used to develop a predictive model with a high correct classification rate (68 to 100%) in metastatic cancer patients who were treated with ICI monotherapy.

The predictive power of kinase activity profiling positively compares to currently recognized biomarkers for response to ICIs. For instance, PD-L1 expression in the tumor has a sensitivity and specificity ranging from 58 to 85% and 49 to 60%, respectively, depending on the tumor type, applied cutoff or type of anti-PD-1 antibody[31]. A similar predictive performance has been reported for TMB[32]. The kinase activity profile, reported here, demonstrated a lower predictive performance for response to PD-1 inhibitors in NSCLC compared to melanoma. Potentially this is due to prior systemic treatments since nearly all (98%) NSCLC but not (28%) melanoma patients included in this study were pretreated, this may have impacted the outcomes of the kinase profiles.

Responsiveness to CTLA-4 ICIs in melanoma was associated with higher overall kinase activity at baseline in responders when compared to non-responders, suggesting a generally more active immune system in responder patients. Indeed, higher pre-existing T cell activity has been associated with a better response to CTLA-4 blockade in mouse models[33,34]. In line with reports on circulating immune-suppressive cells in metastasized patients[35], our findings may implicate that immune suppression is less pronounced in responder patients.

The melanoma or NSCLC patients showing a clinical response to PD-1 blockade displayed a more restricted kinase profile. Upstream and canonical pathway analysis of differentially activated peptide targets extend earlier reports on the mechanism of action of PD-1 ICIs. First, high activity of TAM-family kinases, such as TYRO-3, AXL and MERTK, in responders fits findings by others that MERTK becomes activated in $CD4^+$ and $CD8^+$ T cells downstream of TCR signaling[36]. Secondly, identification of pathways, such as extravasation and CD28 costimulation, extends outcomes of studies demonstrating the key importance of T cell recruitment and T cell co-stimulation in anti-PD-1 responses[7,37,38]. Thirdly, higher activity in the VEGF pathway in responding patients with melanoma and NSCLC was in line with the finding that VEGF-A enhances the expression of PD-1 by cytotoxic lymphocytes in the tumor microenvironment in a mouse model[30]. Also, in cancer patients, VEGF is implicated to (in)directly enhance PD-1 expression by intra-tumoral T cells, which may be reflected by higher PD-1 expression on circulating $CD4^+$ cells and its association with better clinical outcome after ICI in melanoma[20]. Finally, we also observed lower activity of the PTEN pathway in responding patients with melanoma or NSCLC. This may seem counterintuitive as loss of PTEN in tumor cells was associated to anti-PD-1 therapy resistance[39,40]. However, in T cells PTEN functions as a negative regulator of TCR-signaling. In the absence of PTEN, TCR-mediated activation of T cells is strongly enhanced and thresholds for T cell activation become less dependent on CD28-costimulation[41]. Taken together, the above four lines of evidence argue that kinase acivities and pathways that are differentially present in melanoma and NSCLC patients who respond to anti-PD1 reflect the presence of circulating tumor-specific T cells[38].

Recently, the serine threonine kinase (STK) activity profiles in PBMCs from a small group of 28 metastatic NSCLC patients treated with nivolumab as well as healthy individuals were

reported[10]. Baseline activity of the CAMK-family and AGC-family was higher in the group of patients with relatively lower survival after PD-1 blockade when compared to patients with longer survival or healthy individuals. The authors suggested that this probably reflects multiple lines of prior systemic treatment (including tyrosine kinase inhibitors [14%] or bevacizumab [39%]). We did not observe differences in these kinase families because we determined the PTK instead of STK activity profiles in PBMC lysates.

Our study has some limitations. Although cross-validation led to correct classification rates that varied from 68% to 100% in separate patient cohorts, the underlying kinase activity profiles were not fully consistent. This may be due to differences in the study populations. For instance, the baseline serum LDH levels showed a greater heterogeneity between patients of cohort *Mel-PD1-B* (median LDH 315 U/L; range 128-1523) when compared to cohort *Mel-PD1-A* (median 229 U/L; range 124-359). Serum LDH is considered a clinically significant prognostic factor for metastatic melanoma[26] and is incorporated in the M1 subcategory of current TNM cancer staging protocols[42]. More importantly, differences in the kinase activity profiles may also be affected by the fact that for this exploratory study we did not apply standardized protocols for PBMC isolation across the patient cohorts, neither was pretreatment of patients with corticosteroids or systemic treatment other than immunotherapy taken into account. We did notice that the overall kinase activity was affected by erythrocyte lysis during PBMC isolation and by the timespan between PBMC isolation and blood collection when EDTA was used as an anticoagulant. Indeed, EDTA by capturing Ca^{2+} may negatively influence PTK activity[43]. Moreover, considering the relatively large number of kinase spots that were determined in modest patient cohorts, prospective validation with sufficient power is needed before it may be clinically applicable for treatment selection. Finally, the kinase activities point at major involvement of T cell pathways governing migration, tissue infiltration and co-stimulation. In this study, we used PBMC lysates for kinase activity profiling of individual patients, yet, kinase activity profiling of specific immune subsets may further improve the response prediction and provide more detailed insights in the biological mechanisms of response and resistance to ICIs.

In conclusion, we have demonstrated the potential of kinase activity profiling of PBMCs for response prediction after ICI in separate cross-validation patient cohorts. In a first attempt to address the remaining challenges, the standardization of PBMC isolation protocols and the interrogation of kinase activity in subsets of immune cells has been incorporated in a currently ongoing prospective study to validate the predictive value of kinase activity profiles in PBMCs for ICI response.

REFERENCES

1. Borghaei H, Paz-Ares L, Horn L, et al. Nivolumab versus Docetaxel in Advanced Nonsquamous Non-Small-Cell Lung Cancer. *N Engl J Med.* 2015;373(17):1627-1639.
2. Brahmer J, Reckamp KL, Baas P, et al. Nivolumab versus Docetaxel in Advanced Squamous-Cell Non-Small-Cell Lung Cancer. *N Engl J Med.* 2015;373(2):123-135.
3. Larkin J, Chiarion-Sileni V, Gonzalez R, et al. Combined Nivolumab and Ipilimumab or Monotherapy in Untreated Melanoma. *N Engl J Med.* 2015;373(1):23-34.
4. Robert C, Long GV, Brady B, et al. Nivolumab in previously untreated melanoma without BRAF mutation. *N Engl J Med.* 2015;372(4):320-330.
5. Qureshi OS, Zheng Y, Nakamura K, et al. Trans-endocytosis of CD80 and CD86: a molecular basis for the cell-extrinsic function of CTLA-4. *Science.* 2011;332(6029):600-603.
6. Ree AH, Flatmark K, Saelen MG, et al. Tumor phosphatidylinositol 3-kinase signaling in therapy resistance and metastatic dissemination of rectal cancer: opportunities for signaling-adapted therapies. *Crit Rev Oncol Hematol.* 2015;95(1):114-124.
7. Hui E, Cheung J, Zhu J, et al. T cell costimulatory receptor CD28 is a primary target for PD-1-mediated inhibition. *Science.* 2017;355(6332):1428-1433.
8. Kamphorst AO, Pillai RN, Yang S, et al. Proliferation of PD-1+ CD8 T cells in peripheral blood after PD-1-targeted therapy in lung cancer patients. *Proc Natl Acad Sci U S A.* 2017;114(19):4993-4998.
9. Nirschl CJ, Drake CG. Molecular pathways: coexpression of immune checkpoint molecules: signaling pathways and implications for cancer immunotherapy. *Clin Cancer Res.* 2013;19(18):4917-4924.
10. Noe G, Bellesoeur A, Golmard L, et al. Differential Kinase Activation in Peripheral Blood Mononuclear Cells from Non-Small-Cell Lung Cancer Patients Treated with Nivolumab. *Cancers (Basel).* 2019;11(6).
11. Tahiri A, Røe K, Ree AH, et al. Differential inhibition of ex-vivo tumor kinase activity by vemurafenib in BRAF(V600E) and BRAF wild-type metastatic malignant melanoma. *PLoS One.* 2013;8(8):e72692.
12. Folkvord S, Flatmark K, Dueland S, et al. Prediction of response to preoperative chemoradiotherapy in rectal cancer by multiplex kinase activity profiling. *Int J Radiat Oncol Biol Phys.* 2010;78(2):555-562.
13. Arni S, Le THN, de Wijn R, et al. Ex vivo multiplex profiling of protein tyrosine kinase activities in early stages of human lung adenocarcinoma. *Oncotarget.* 2017;8(40):68599-68613.
14. Hellmann MD, Ciuleanu TE, Pluzanski A, et al. Nivolumab plus Ipilimumab in Lung Cancer with a High Tumor Mutational Burden. *N Engl J Med.* 2018;378(22):2093-2104.
15. Topalian SL, Taube JM, Anders RA, Pardoll DM. Mechanism-driven biomarkers to guide immune checkpoint blockade in cancer therapy. *Nat Rev Cancer.* 2016;16(5):275-287.
16. Bodor JN, Boumber Y, Borghaei H. Biomarkers for immune checkpoint inhibition in non-small cell lung cancer (NSCLC). *Cancer.* 2020;126(2):260-270.
17. Hurkmans DP, Kuipers ME, Smit J, et al. Tumor mutational load, CD8(+) T cells, expression of PD-L1 and HLA class I to guide immunotherapy decisions in NSCLC patients. *Cancer Immunol Immunother.* 2020.

18. Martens A, Wistuba-Hamprecht K, Geukes Foppen M, et al. Baseline Peripheral Blood Biomarkers Associated with Clinical Outcome of Advanced Melanoma Patients Treated with Ipilimumab. *Clin Cancer Res.* 2016;22(12):2908-2918.
19. Wistuba-Hamprecht K, Martens A, Heubach F, et al. Peripheral CD8 effector-memory type 1 T-cells correlate with outcome in ipilimumab-treated stage IV melanoma patients. *Eur J Cancer.* 2017;73:61-70.
20. Jacquelot N, Roberti MP, Enot DP, et al. Predictors of responses to immune checkpoint blockade in advanced melanoma. *Nat Commun.* 2017;8(1):592.
21. Buder-Bakhaya K, Hassel JC. Biomarkers for Clinical Benefit of Immune Checkpoint Inhibitor Treatment-A Review From the Melanoma Perspective and Beyond. *Front Immunol.* 2018;9:1474.
22. Voong KR, Feliciano J, Becker D, Levy B. Beyond PD-L1 testing-emerging biomarkers for immunotherapy in non-small cell lung cancer. *Ann Transl Med.* 2017;5(18):376.
23. Ferrucci PF, Ascierto PA, Pigozzo J, et al. Baseline neutrophils and derived neutrophil-to-lymphocyte ratio: prognostic relevance in metastatic melanoma patients receiving ipilimumab. *Ann Oncol.* 2016;27(4):732-738.
24. Bagley SJ, Kothari S, Aggarwal C, et al. Pretreatment neutrophil-to-lymphocyte ratio as a marker of outcomes in nivolumab-treated patients with advanced non-small-cell lung cancer. *Lung Cancer.* 2017;106:1-7.
25. Jiang T, Qiao M, Zhao C, et al. Pretreatment neutrophil-to-lymphocyte ratio is associated with outcome of advanced-stage cancer patients treated with immunotherapy: a meta-analysis. *Cancer Immunol Immunother.* 2018;67(5):713-727.
26. Weide B, Martens A, Hassel JC, et al. Baseline Biomarkers for Outcome of Melanoma Patients Treated with Pembrolizumab. *Clin Cancer Res.* 2016;22(22):5487-5496.
27. Krieg C, Nowicka M, Guglietta S, et al. High-dimensional single-cell analysis predicts response to anti-PD-1 immunotherapy. *Nat Med.* 2018;24(2):144-153.
28. Kunert A, Basak EA, Hurkmans DP, et al. CD45RA(+)CCR7(-) CD8 T cells lacking co-stimulatory receptors demonstrate enhanced frequency in peripheral blood of NSCLC patients responding to nivolumab. *J Immunother Cancer.* 2019;7(1):149.
29. Fujimoto D, Sato Y, Uehara K, et al. Predictive Performance of Four Programmed Cell Death Ligand 1 Assay Systems on Nivolumab Response in Previously Treated Patients with Non-Small Cell Lung Cancer. *J Thorac Oncol.* 2018;13(3):377-386.
30. Metz KS, Deoudes EM, Berginski ME, et al. Coral: Clear and Customizable Visualization of Human Kinome Data. *Cell Syst.* 2018;7(3):347-350 e341.
31. Diggs LP, Hsueh EC. Utility of PD-L1 immunohistochemistry assays for predicting PD-1/PD-L1 inhibitor response. *Biomark Res.* 2017;5:12.
32. Rizvi NA, Hellmann MD, Snyder A, et al. Cancer immunology. Mutational landscape determines sensitivity to PD-1 blockade in non-small cell lung cancer. *Science.* 2015;348(6230):124-128.
33. Yamazaki T, Pitt JM, Vetizou M, et al. The oncolytic peptide LTX-315 overcomes resistance of cancers to immunotherapy with CTLA4 checkpoint blockade. *Cell Death Differ.* 2016;23(6):1004-1015.

34. Hannani D, Vetizou M, Enot D, et al. Anticancer immunotherapy by CTLA-4 blockade: obligatory contribution of IL-2 receptors and negative prognostic impact of soluble CD25. *Cell Res.* 2015;25(2):208-224.
35. Xia A, Zhang Y, Xu J, Yin T, Lu XJ. T Cell Dysfunction in Cancer Immunity and Immunotherapy. *Front Immunol.* 2019;10:1719.
36. Peeters MJW, Dulkeviciute D, Draghi A, et al. MERTK Acts as a Costimulatory Receptor on Human CD8(+) T Cells. *Cancer Immunol Res.* 2019;7(9):1472-1484.
37. Herbst RS, Soria JC, Kowanetz M, et al. Predictive correlates of response to the anti-PD-L1 antibody MPDL3280A in cancer patients. *Nature.* 2014;515(7528):563-567.
38. Tumeh PC, Harview CL, Yearley JH, et al. PD-1 blockade induces responses by inhibiting adaptive immune resistance. *Nature.* 2014;515(7528):568-571.
39. George S, Miao D, Demetri GD, et al. Loss of PTEN Is Associated with Resistance to Anti-PD-1 Checkpoint Blockade Therapy in Metastatic Uterine Leiomyosarcoma. *Immunity.* 2017;46(2):197-204.
40. Peng W, Chen JQ, Liu C, et al. Loss of PTEN Promotes Resistance to T Cell-Mediated Immunotherapy. *Cancer Discov.* 2016;6(2):202-216.
41. Buckler JL, Walsh PT, Porrett PM, Choi Y, Turka LA. Cutting edge: T cell requirement for CD28 costimulation is due to negative regulation of TCR signals by PTEN. *J Immunol.* 2006;177(7):4262-4266.
42. Gershenwald JE, Scolyer RA, Hess KR, et al. Melanoma staging: Evidence-based changes in the American Joint Committee on Cancer eighth edition cancer staging manual. *CA Cancer J Clin.* 2017;67(6):472-492.
43. Luconi M, Krausz C, Forti G, Baldi E. Extracellular calcium negatively modulates tyrosine phosphorylation and tyrosine kinase activity during capacitation of human spermatozoa. *Biol Reprod.* 1996;55(1):207-216.

SUPPLEMENTARY INFORMATION

Supplementary Figure 1. Effect of anticoagulant for blood collection on PTK activity

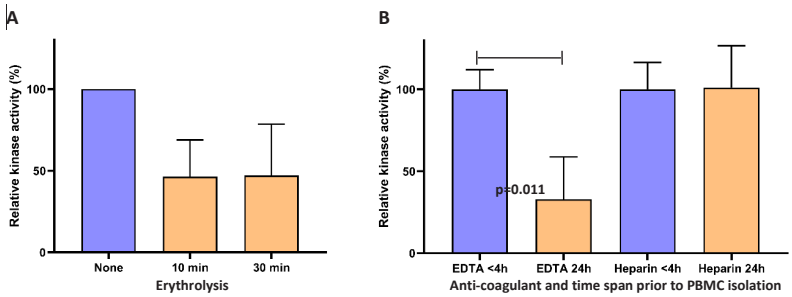

Erythrocyte lysis, anti-coagulant and time prior to PBMC isolation affect overall kinase activity. The overall kinase activity is depicted as relative kinase activity (%) compared to controls which were set at 100 % (blue bars). A) The kinase activity was determined after erythrocyte lysis for 10 or 30 minutes during PBMC processing and is compared to PBMC prepared without erythrocyte lysis (none, blue bars). B) Blood of healthy donors (n=4) was collected in EDTA or sodium heparin collection tubes and PBMCs were isolated either within 4 or 24h following collection of blood, depicted in blue and orange bars, respectively. Paired t-tests were used to compare different experimental conditions; error bars indicate the SD. Abbreviations: ethylenediaminetetraacetic acid collection tube (EDTA), sodium heparin collection tube (heparin).

Supplementary Figure 2. Detailed flow chart

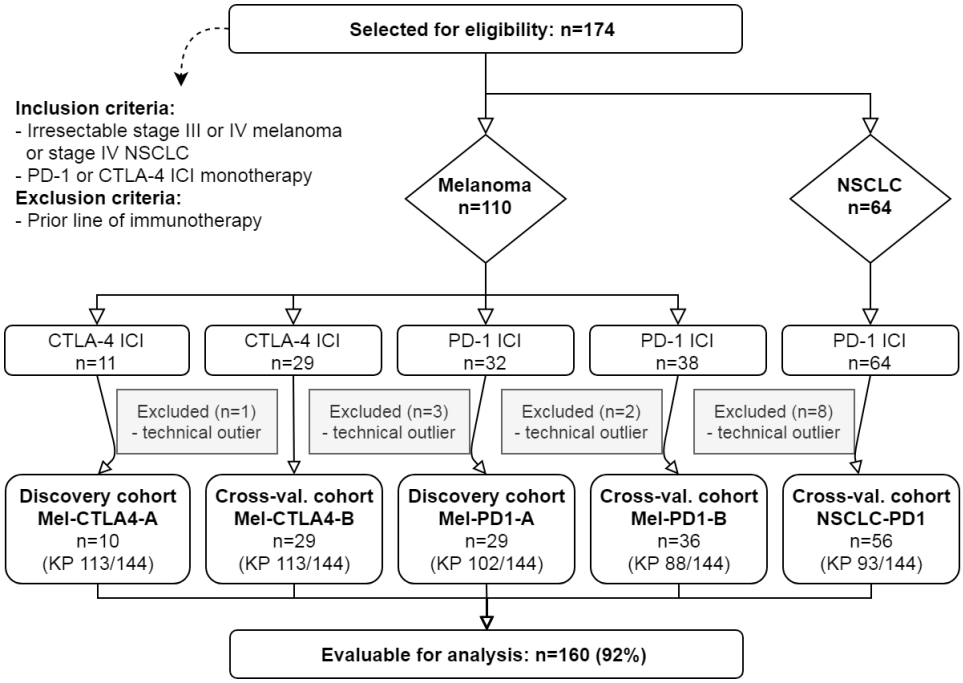

The extended flow chart of the patient selection process is shown. 174 patients were assessed for eligibility, and 14 technical outliers were removed (8%). As described in the supplementary text, signal-positive spots required a positive trend in the recorded phosphorylation time course. Peptides for which such a trend could not be detected in > 75% of the samples were removed, which yielded 88-113 peptides (depending on cohort) for further analysis. Abbreviations: kinase profile (KP), cross-validation (cross-val.).

Supplementary Figure 3. Comparison analysis of two anti-PD-1 cohorts

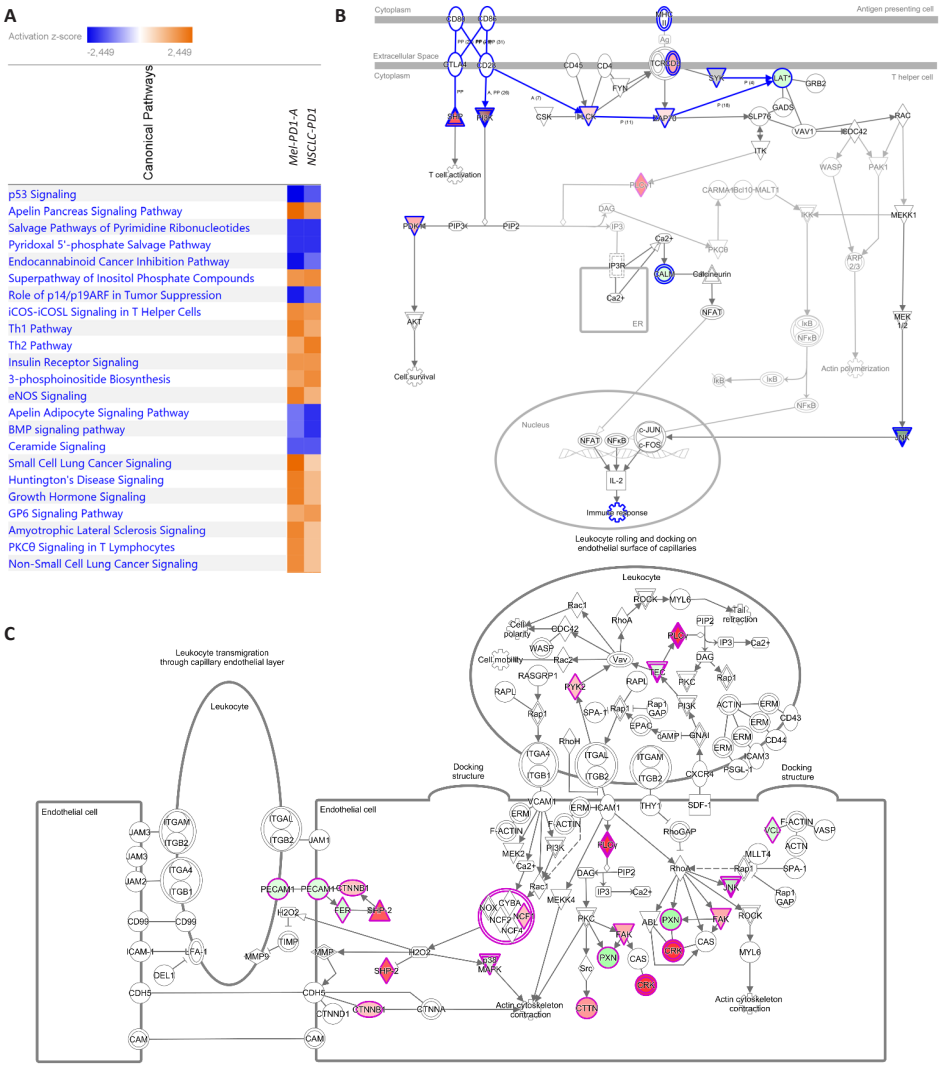

A) Comparison analysis of cohort Mel-PD1-A and NSCLC-PD1. Orange (positive z-score) indicates a predicted upregulation of the pathway in responders, blue (negative z-score) indicates a predicted downregulation of the pathway in responders. Gray represents canonical pathways without an expected activity pattern. B) CD28 signaling in Th cells as well as C) immune cell extravasation have predicted upregulated activity in responders.

Supplementary Table 1. Site-specific study protocols

Cohort	ICI	Study site	Anticoagulant	PBMC isolation within	Erythrolysis
Mel-CTLA4-A	CTLA-4	Center A	Na-Hep	4 h	no
Mel-CTLA4-B	CTLA-4	Center B	EDTA	24 h	yes
Mel-PD1-A	PD-1	Center A	Na-Hep	4 h	no
Mel-PD1-B	PD-1	Center C	EDTA	24 h	no
NSCLC-PD1	PD-1	Center C	EDTA	24 h	no

Five patient cohorts were evaluated in this study. The cohorts are based on the malignancy (melanoma or NSCLC patients), the type of ICI therapy administered and the center were the samples were collected. Patient number per cohort and anticoagulant used for blood collection are listed. An erythrocyte lysis step was performed during PBMC isolation for cohort Mel-CTLA4-B. Abbreviations: ethylenediaminetetraacetic acid collection tube (EDTA), sodium heparin (Na-Hep).

Supplementary Tables 2-6. Datasets generated by kinase activity profiling

Included as separate online .txt files (http://jitc.biomedcentral.com)

CHAPTER 15

15

Overt thyroid dysfunction and anti-thyroid antibodies predict response to anti-PD-1 immunotherapy in cancer patients

Edwin A. Basak*, Jan W.M. van der Meer*, Daan P. Hurkmans, Marco W.J. Schreurs, Esther Oomen - de Hoop, Astrid A.M. van der Veldt, Sander Bins, Arjen Joosse, Stijn L.W. Koolen, Reno Debets, Robin P. Peeters, Joachim G.J.V. Aerts, Ron H.J. Mathijssen, Marco Medici

*Shared first authorship

Thyroid, July 2020, 30: page 966-973

Abstract

Introduction: Thyroid dysfunction is among the most common adverse effects during anti-PD-1 immunotherapy, and alongside correlations with elevated anti-thyroid antibodies (ATAb), studies have found correlations with survival. However, the exact relations remain to be clarified. We therefore aimed to clarify the relationship between thyroid dysfunction, ATAbs and survival in anti-PD-1 treated cancer patients.

Materials and Methods: We included 168 patients with non-small-cell lung carcinoma, renal cell carcinoma, and metastatic melanoma treated with nivolumab or pembrolizumab. TSH and free T4 (FT4) levels were measured before each anti-PD-1 infusion. ATAb levels (anti-thyroid peroxidase (TPO) and anti-thyroglobulin (Tg)) were measured at baseline and after 2 months of treatment. Although the vast majority of patients had detectable levels of ATABs, only few patients had positive ATAbs when using conventional cut-offs. To study the consequences of detectable ATABs, the cut-off levels were *a priori* set at the median concentrations at baseline in the study population. Tumor progression was classified according to RECIST v1.1.

Results: Patients who acquired overt thyroid dysfunction during treatment had significantly higher overall survival (OS) (HR=0.18 [95%CI: 0.04-0.76]; p=0.020) and progression free survival (PFS) (HR=0.39 [0.15-0.998]; p=0.050) than patients without thyroid dysfunction with one-year OS rates of 94% *vs* 59% and one-year PFS rates of 64% *vs* 34%. During treatment, patients with ATAb levels above the median had a higher OS (HR=0.39 [0.21-0.72]; p=0.003) and PFS (HR=0.52 [0.33-0.81]; p=0.004) than patients with ATAb levels below the median, with one-year OS rates of 83% *vs* 49% and PFS rates of 54% *vs* 20%, respectively. When analyzing ATAb levels over time, patients with a persistent ATAb level above the median had a higher OS (HR=0.41 [0.19-0.89], p=0.025) and PFS (HR=0.54 [0.31-0.95], p=0.032) compared to patients with a persistent ATAb level below the median. Patients whose ATAb levels increased above the median during treatment had an improved OS (HR=0.27 [0.06-1.22], p=0.088) and PFS (HR=0.24 [0.07-0.77], p=0.017) compared to patients whose ATAb levels decreased below the median.

Discussion: Acquired overt thyroid toxicity and above median ATAb levels during anti-PD-1 treatment are associated with improved PFS and OS. Additionally, our results suggest that ATAb levels at baseline are of clinical relevance for PFS and OS.

INTRODUCTION

Immunotherapies against immune checkpoints that inhibit T cell activation (cytotoxic T lymphocyte antigen 4 (CTLA-4) and programmed cell death 1 (PD-1)) are rapidly emerging treatments in oncology. While these treatments have impressively improved survival for various metastatic malignancies, they are associated with many immune related adverse events (1-3). Thyroid toxicity is among the most common (5-15%) immune related adverse events during anti-PD-1 immunotherapy.[1-3] In most cases, it presents itself as a transient thyrotoxicosis followed by hypothyroidism, thereby resembling the course of a classical thyroiditis, but its exact cause remains unclear.[4,5] Previous studies have suggested that thyroid toxicity during anti-PD-1 treatment may be associated with improved overall survival (OS), but these studies were limited by small sample sizes, included only patients with non-small-cell lung carcinoma (NSCLC), and showed inconsistent effects on progression-free survival (PFS).[6,7] While thyroid autoimmunity, the presence of anti-thyroid antibodies (ATAbs), prior to immunotherapy has been related to the development of thyroid toxicity during immunotherapy,[8,9] the ATAb status at baseline showed no relation with improved survival.[10] We therefore hypothesized that the occurrence of thyroid toxicity during anti-PD-1 treatment and thyroid antibody status may predict treatment outcomes in anti-PD-1 treated patients. This hypothesis was investigated in patients with various cancer types in a large prospective cohort study.

MATERIALS AND METHODS

A total of 168 patients with metastatic melanoma, NSCLC, and renal cell carcinoma (RCC) who started anti-PD-1 treatment, nivolumab (every 2 weeks) or pembrolizumab (every 3 weeks), between April 2016 and July 2017 at the Erasmus Medical Center (Rotterdam, the Netherlands) were eligible for the MULTOMAB-trial[11-13] (Dutch Trial Registry #NL6828). The goal of the MULTOMAB-trial was to set up a biobank of prospectively collected blood samples for pharmacokinetic analyses of monoclonal antibodies and immunophenotyping. All adult patients beginning anti-PD-1 treatment were eligible for the MULTOMAB-trial, in which we serially collected serum samples and isolated peripheral blood mononuclear cells. Therapy was terminated in case of complete response, disease progression, severe side effects, or patients' wish. The study was approved by the local ethics board committee.

OS was defined as the period between the start of therapy until death, while PFS was calculated until tumor progression, based on standard Response Evaluation Criteria In Solid Tumors (RECIST) v1.1, or death. Patients who were lost to follow-up were censored. Serum was collected prior to each drug administration (every 2 or 3 weeks) in order to determine TSH and free T4 (FT4) levels. Serum TSH and FT4 levels were measured via

immunoassays on Siemens Immulite 2000XPi (reference range: 0.4-4.3 mU/L) and Ortho Vitros ECiQ (reference range: 11-25 pmol/L), respectively. Thyroid toxicity was scored as 'subclinical' when TSH levels were increased (subclinical hypothyroidism) or decreased (subclinical hyperthyroidism) and FT4 levels were normal. Thyroid toxicity was scored as 'overt' when TSH levels were increased and FT4 levels decreased (overt hypothyroidism), or *vice versa* (overt hyperthyroidism). Patients who acquired overt thyroid toxicity after they had acquired subclinical thyroid toxicity were scored as 'overt'. Patients were monitored for thyroid toxicity until tumor progression. This was done because this research investigates possible prospective markers for which events occurring after tumor progression are not of any predictive value. Patients with abnormal TSH levels or receiving thyroid medication within 3 months before the start of immunotherapy were categorized as having a pre-existing thyroid disorder.

Antibodies directed against thyroid peroxidase (anti-TPO) and thyroglobulin (anti-Tg) were measured on a Phadia 250 at baseline and 2 months after start of treatment, or the last available sample in case of death. The lower limit of quantification (LLoQ) for anti-TPO was 33 IU/mL and for anti-Tg it was 244 IU/mL, as reported by the supplier. The lower limit of detection (LLoD) for both values was 1 IU/mL. The vast majority of patients had detectable levels of ATAbs, only 7 patients at baseline and 14 patients during follow-up had positive antibodies when using conventional cut-offs for anti-TPO and anti-Tg positivity as provided by the assay manufacturers (60 and 280 IU/mL, respectively). To avoid underpowered analyses and to study the consequences of detectable ATAbs- as a reflection of an auto-immune reaction, the cut-off levels were *a priori* set at the median concentrations at baseline in the study population (anti-TPO: 3.05 IU/mL, anti-Tg: 22.35 IU/mL). Patients with any antibody level above these cut-offs were categorized as patients with 'above median' ATAb levels and patients with anti-TPO and anti-Tg levels below these cut-offs were categorized as patients with 'below median' ATAb levels.

Categorical variables were tested using X^2 tests (or Fisher's exact test when X^2 test assumptions were not valid). Age distribution between groups was analyzed using one-way ANOVA. To study relationships between thyroid toxicity and PFS or OS, Cox regression analysis was used where thyroid toxicity was added to the model as a time-dependent covariate. This method takes into account the fact that thyroid toxicity emerges during the follow-up period and can only emerge when the patient survives long enough to develop the toxicity. Hence, false positive results due to immortal time bias are prevented. Conventional Cox regression was used for relationships between ATAb status and PFS or OS. Patients using glucocorticoids were excluded in sensitivity analyses, as these could both interfere with thyroid toxicity and ATAb.

All analyses were corrected for cancer type, as it was a confounder in the relationship between thyroid toxicity and survival. A p-value <0.05 was considered statistically significant and STATA (v15.1 StataCorp. College Station, TX) was used for all statistical analyses.

RESULTS

Baseline characteristics of all patients (n=168) are shown in **Table 1**. The median follow-up time of patients still alive was 14.9 (IQR:9.2-18.4) months. During the study period, 34 patients (20%) developed subclinical thyroid dysfunction and 20 patients (12%) developed overt thyroid dysfunction. Twenty-seven patients (16%) had pre-existing thyroid dysfunction, consisting of 9 cases with hyperthyroidism and 18 cases with hypothyroidism. Twenty-two of those patients only had subclinical thyroid disease. Eighty patients (48%) developed no thyroid dysfunction during the study period. For 7 patients (4%) it was impossible to determine thyroid dysfunction due to missing TSH values. Median time to development of all types of thyroid dysfunction was 2.8 (IQR: 1.3-4.2) months, whereas for overt thyroid dysfunction it was 2.1 (IQR: 1.2-3.7) months. There were no differences in age, sex, cancer type, and drug administered between patients who developed thyroid dysfunction and those who did not (**Table 2**). Patients with above median ATAb levels at baseline (p=0.374) or acquired above median ATAb levels during therapy (p=0.349) did not have a different risk of acquired thyroid toxicity than patients with below median baseline ATAb levels.

Table 1. Baseline characteristics of study cohort

	Patients (n=168)
Sex (number (%))	
Male	103 (61%)
Female	65 (39%)
Age at start of treatment (years)	
Median (IQR)	65 (58-70)
Cancer type (number (%))	
Non-small-cell lung carcinoma	93 (55%)
Melanoma	63 (38%)
Renal cell carcinoma	12 (7%)
Drug treatment (number (%))	
Nivolumab	118 (70%)
Pembrolizumab	50 (30%)
Follow-up time (months)[a]	
Median (IQR)	14.9 (9.2-18.4)

[a]Follow-up time for patients who were alive at end of study

Table 2. Patient characteristics by thyroid toxicity groups

					P-value
Thyroid toxicity group	None (n=80; 48%)	Acquired subclinical (n=34; 20%)	Acquired overt (n=20; 12%)	Pre-existing (n=27; 16%)	
Sex (number (%))					0.17
Male	53 (67%)	23 (63%)	11 (53%)	12 (46%)	
Female	27 (33%)	11 (37%)	9 (47%)	15 (54%)	
Age at start of treatment(years)					0.18
Mean (IQR)	64.5 (58-71)	64 (56-70)	67.5 (60-72.25)	69 (62.5-73.5)	
Cancer type (number (%))					0.08
Non-small-cell lung carcinoma	40 (53%)	23 (67%)	11 (53%)	14 (50%)	
Melanoma	37 (43%)	6 (19%)	8 (41%)	10 (38%)	
Renal cell carcinoma	3 (4%)	5 (15%)	1 (6%)	4 (12%)	
Drug (number (%))					0.53
Nivolumab	53 (68%)	26 (74%)	13 (65%)	21 (77%)	
Pembrolizumab	27 (32%)	8 (26%)	7 (35%)	6 (23%)	
One-year survival rate (%)					
Overall survival	64%	54%	94%	68%	
Progression free survival[a]	33%	34%	64%	45%	

[a] PFS could not be calculated for 3 patients

Patients who acquired overt thyroid dysfunction had longer OS (HR=0.18 [CI-95%: 0.04-0.76], p=0.020) as well as PFS (HR=0.39 [0.15-0.998], p=0.050) than patients without thyroid dysfunction. No difference was found in OS (HR=1.54 [0.79-2.98], p=0.201) and PFS HR=0.99 [0.52-1.91], p=0.998) in patients with subclinical thyroid dysfunction or with pre-existing thyroid dysfunction (OS: HR=0.92 [0.44-1.90], p=0.816; PFS: HR=0.71 [0.40-1.26], p=0.243) when compared to patients without thyroid dysfunction (**Figure 1**). These effects remained significant after excluding patients using glucocorticoids for PFS (p=0.020). For OS, a trend to significance was observed (p=0.078).

Median time to the measurement of ATAbs during treatment was 2.1 (IQR:2.0-2.3) months. ATAb level distributions are described in **Supplementary Table 1**. Age and sex were divided proportionally over the ATAb status groups, in contrast to cancer type and drugs administered (**Table 3**). Within this cohort, patients with NSCLC and RCC were predominantly treated with nivolumab, while patients with metastatic melanoma were predominantly treated with pembrolizumab. Patients with ATAb levels above the median did not differ in OS (HR=0.97 [0.55-1.72], p=0.930) and PFS (HR=0.99 [0.64-1.54], p=0.981) when compared to patients with ATAb levels below the median (**Figure 2**). However, during treatment, patients with ATAb levels above the median had improved OS (HR=0.39

[0.21-0.72], p=0.003) and PFS (HR=0.52 [0.33-0.81], p=0.004) when compared to patients with ATAb levels below the median with one-year survival rates of 83% vs 49% for OS and 54% vs 20% for PFS, respectively. These effects remained significant after excluding patients treated with glucocorticoids for OS (p=0.010) and PFS (p=0.010).

Furthermore, we analyzed the changes of ATAbs over time (**Figure 3**). In 84% of patients, the ATAb status did not change from baseline until the end of treatment. We found that the 70 patients (48%) with a persistent ATAb level above the median, had a significantly improved OS (HR=0.41 [0.19-0.89], p=0.025) and PFS (HR=0.54 [0.31-0.95], p=0.032) compared to the 53 patients (36%) with a persistent ATAb level below the median. The 15 patients (10%) whose ATAb levels increased above the median during treatment had an improved OS (HR=0.27 [0.06-1.22], p=0.088) and PFS (HR=0.24 [0.07-0.77], p=0.017) compared to the 9 patients (6%) whose ATAb levels decreased below the median (**Figure 3**).

Finally, **Supplementary Figure 1** provides the thyroid toxicity courses in patients experiencing thyroid toxicity. This swimmers plot shows a variety of patterns. In many cases a hyperthyroid phase was followed by a hypothyroid phase which is classical for a thyroiditis, while only rarely a hypothyroid phase was followed by a hyperthyroid phase.

Figure 1. Thyroid toxicity and survival

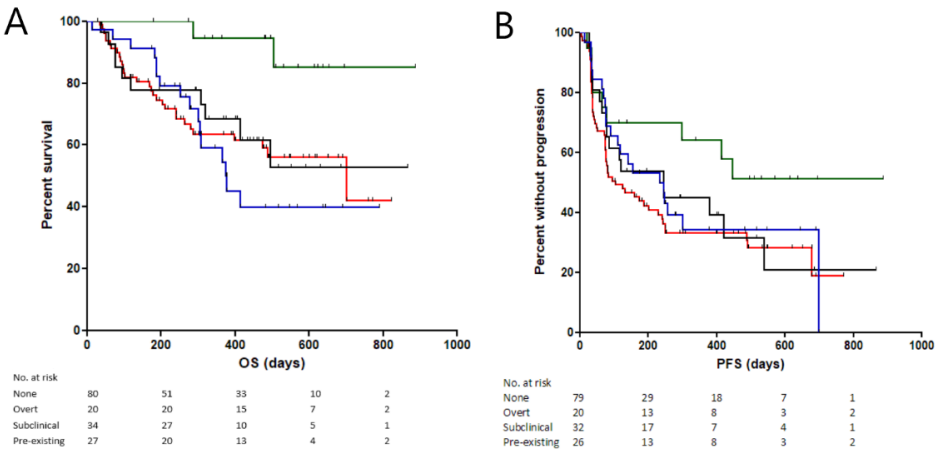

Kaplan-Meier curves of patients with acquired overt thyroid toxicity (in green), acquired subclinical thyroid toxicity (in blue), pre-existing thyroid dysfunction (in black), or without thyroid dysfunction (in red). a) OS and b) PFS. OS: Overt vs without: HR=0.18 (CI-95%: 0.04-0.76), p=0.020; Subclinical vs without: HR=1.54 (0.79-2.98), p=0.201; Pre-existing vs without: HR=0.92 (0.44-1.90), p=0.816. PFS: Overt vs without: HR=0.39 (0.15-0.998), p=0.050; Subclinical vs without: HR=0.99 (0.52-1.91), p=0.998; Pre-existing vs without: HR=0.71 (0.40-1.26), p=0.243

Table 3. Patient characteristics by anti-thyroid antibody status groups

	Antibodies at Baseline (n=156)		**P-value**	**Antibodies during Treatment (n=158)**		**P-value**
	Below median (n=69; 44%)	Above median (n=87; 56%)		Below median (n=65; 41%)	Above median (n=93; 59%)	
Sex (number (%))			0.24			0.30
Male	46 (67%)	50 (57%)		43 (66%)	54 (58%)	
Female	23 (33%)	37 (43%)		22 (34%)	39 (42%)	
Age (years)			0.34			0.14
Median (IQR)	64 (57-69.5)	65 (59-72)		64 (56.5-68)	67 (58.5-72)	
Cancer type (number (%))			<0.001			<0.001
NSCLC	54 (78%)	34 (39%)		51 (78%)	35 (38%)	
Melanoma	11 (16%)	46 (53%)		10 (15%)	50 (54%)	
Renal cell carcinoma	4 (6%)	7 (8%)		4 (6%)	8 (9%)	
Drug (number (%))			<0.001			<0.001
Nivolumab	63 (91%)	47 (54%)		60 (92%)	53 (57%)	
Pembrolizumab	6 (9%)	40 (46%)		5 (8%)	40 (43%)	

Figure 2. Anti-thyroid antibodies and survival

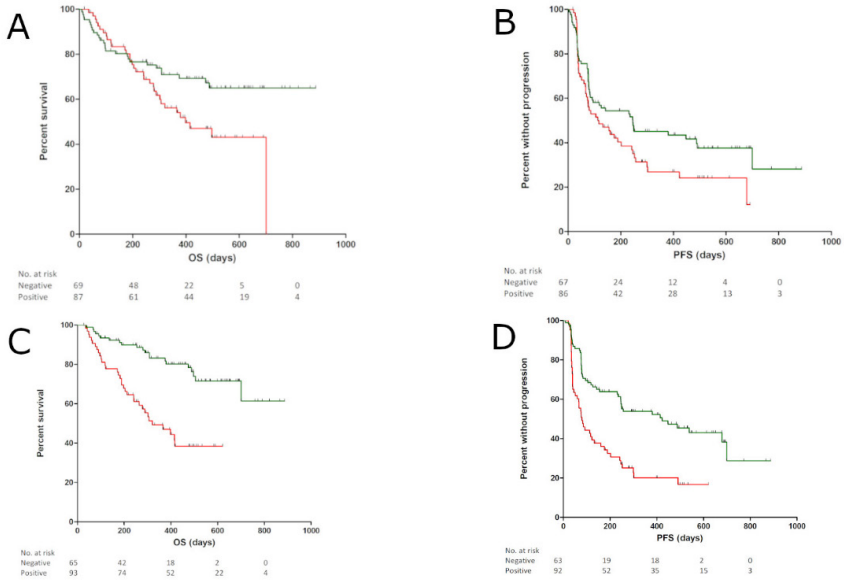

Kaplan-Meier curves of patients with anti-thyroid antibodies above median (in green) or below median (in red). a) OS for antibody status at baseline (HR=0.97 (0.55-1.72), p=0.930), b) PFS for antibody status at baseline (HR=0.99 (0.64-1.54), p=0.981), c) OS for antibody status during treatment (HR=0.39 (0.21-0.72), p=0.003), and d) PFS for antibody status during treatment (HR=0.52 (0.33-0.81), p=0.004).

Figure 3. Changes in anti-thyroid antibody status and survival

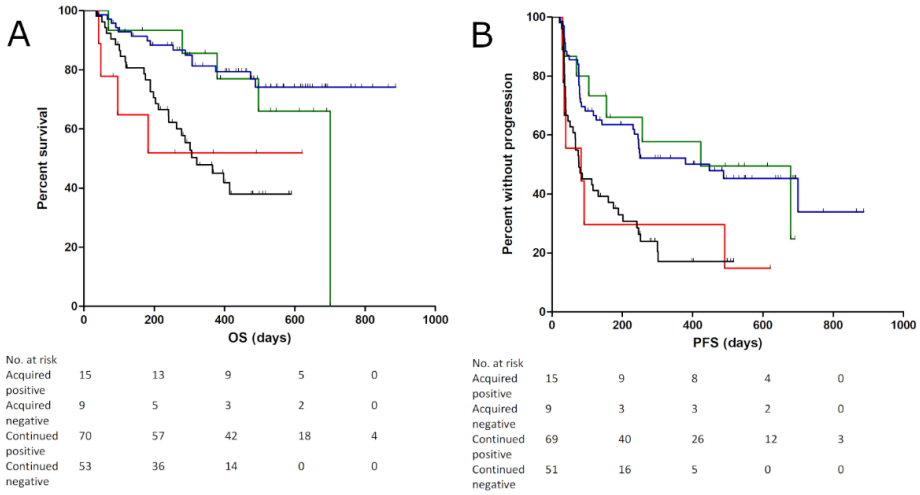

Kaplan-Meier curves of patients with acquired anti-thyroid antibodies above median (in green), acquired anti-thyroid antibodies below median (in red), continued anti-thyroid antibodies above median (in blue), or continued anti-thyroid antibodies below median (in black). a) OS and b) PFS. OS: Acquired above median vs acquired below median: HR=0.27 (0.06-1.22), p=0.088; Persistentabove median vs persistentbelow median: HR=0.41 (0.19-0.89), p=0.025. PFS: Acquired above median vs acquired below median: HR=0.24 (0.07-0.77), p=0.017; Persistent above median vs Persistentbelow median: HR=0.54 (0.31-0.95), p=0.032

DISCUSSION

Anti-PD-1 treated patients with metastatic melanoma, NSCLC, and RCC and acquired overt thyroid toxicity and/or higher ATAb levels during treatment have clinically relevant prolonged OS and PFS compared to patients without thyroid toxicity and/or low ATAbs. We hypothesize that these patients represent a group with a higher susceptibility to autoimmunity, which in turn could be beneficial in the anti-cancer treatment via autoimmune dependent pathways, leading to longer survival. This is supported by various studies in recent years showing that the occurrence of immune related adverse events in anti-PD-1 treated patients is associated with improved response and survival.[14-25] However, most of these studies were limited by their retrospective study design and/or small sample size, while in the current large prospective study we observed effect sizes for thyroid toxicity on OS which are much stronger compared to published associations with other immune related adverse events.[14-25]

Our finding that ATAb status at baseline is not correlated with OS or PFS is in line with the results of Toi *et al*.[10] However, we found that a very large portion of patients did not change in ATAb status from baseline until end of treatment and significantly improved OS and PFS were observed for patients with persistent ATAb levels above the median when compared to patients with persistent ATAb levels below the median. Finally, patients whose ATAb levels rose above the median during treatment had significantly improved survival compared to patients whose ATAb levels decreased below the median, leading to the observed difference in survival between patients with ATAb levels above and below the median during treatment. These results suggests that a predisposition for higher susceptibility to autoimmunity could already exist at baseline, but may be influenced during --and possibly by-- the treatment, which is a new finding.

An important finding in our study is that only a few patients had positive ATAbs when using conventional cut-off thresholds. As these thresholds are specifically used for diagnosing Hashimoto's thyroiditis, rather than detecting autoimmunity, the cut-off levels in our study were *a priori* set at the median concentrations at baseline in the study population. The fact that these lower cut-off thresholds can serve as a strong predictive marker suggest that more subtle increases in ATAb levels are involved and relevant in this setting when compared to diagnosing Hashimoto's hypothyroidism.

Alternative models are available to describe response in patients treated with immunotherapy, like iRECIST (immune related response criteria). However, we used RECIST v1.1 since this is currently still standard in the oncology field for patients treated with immunotherapy.[26,27] The scoring of thyroid toxicity in our study was purely based on the interpretation of serum TSH and FT4 levels to determine the presence of subclinical or overt thyroid dysfunction. This is because the decision to treat thyroid toxicity in practice is predominantly guided by this endocrine classification and therefore has clinical relevance. This in contrast to Common Terminology Criteria for Adverse Events (CTCAE), a common method used within oncology, which describes the severity of organ toxicity for patients receiving cancer therapy, with a score ranging from 0 (no adverse event) up to 5 (death).

Another important advantage of the current analysis is that we adjusted our results for time dependent effects, while others did not, thereby preventing misinterpretation of the effects of thyroid toxicity on survival. It may be possible that patients with a longer follow-up time are more likely to develop thyroid toxicity. However, median duration to overt thyroid toxicity was 2.1 months, whereas the median follow-up time in our study was 14.9 months, well exceeding the median duration to thyroid toxicity.

The number of patients with pre-existing thyroid dysfunction in our cohort was high (16%), which is likely explained by our definition of thyroid dysfunction. Out of 27 patients with pre-existing thyroid disease, 22 patients were classified as having subclinical thyroid dysfunction, which we classified as such when having one aberrant TSH value prior start with immunotherapy. We intentionally used these very strict criteria to define pre-existing

thyroid disease to avoid including any patient with pre-existing mild thyroid dysfunction which could interfere with our study aim .

The presence of non-thyroidal illness (NTI) may complicate the interpretation of thyroid function tests in severely ill patients. NTI is more common among intensive care patients, but none of our patients were hospitalized in the intensive care unit. Moreover, the most important associations in our cohort were found in patients with overt thyroid toxicity, the biochemical fingerprint of which does not resemble NTI, and was also supported by the observed thyroid toxicity courses (**Supplementary Figure 1**). Therefore, it is unlikely that the potential presence of NTI among study participants substantially influenced the study results. When evaluating the course of thyroid dysfunction over time, a variety of patterns was observed, an important part of which resembled a thyroiditis. The fact that a hypothyroid phase was not always preceded by a hyperthyroid phase might be due to the fact that the hyperthyroid phase was short and occurred between the time of thyroid function testing.

Despite correlations between ATAb status and and thyroid toxicity and OS, no associations were found between ATAb status and thyroid toxicity in our cohort. This could be explained by the fact that the number of patients with thyroid toxicity in the separate ATAb status groups were low. Therefore, further studies should investigate this relationship in larger groups of patients.

In conclusion, this study shows that acquired overt thyroid toxicity and higher ATAbs during treatment are strong predictive markers for response to anti-PD-1 treatment in three cancer types studied. If validated in an independent study, these parameters may serve as novel predictive markers.

REFERENCES

1. Champiat S, Lambotte O, Barreau E, et al. Management of immune checkpoint blockade dysimmune toxicities: a collaborative position paper. *Ann Oncol.* 2016;27(4):559-574.
2. Michot JM, Bigenwald C, Champiat S, et al. Immune-related adverse events with immune checkpoint blockade: a comprehensive review. *Eur J Cancer.* 2016;54:139-148.
3. Cukier P, Santini FC, Scaranti M, Hoff AO. Endocrine side effects of cancer immunotherapy. *Endocr Relat Cancer.* 2017;24(12):T331-T347.
4. Chalan P, Di Dalmazi G, Pani F, De Remigis A, Corsello A, Caturegli P. Thyroid dysfunctions secondary to cancer immunotherapy. *J Endocrinol Invest.* 2018;41(6):625-638.
5. Byun DJ, Wolchok JD, Rosenberg LM, Girotra M. Cancer immunotherapy - immune checkpoint blockade and associated endocrinopathies. *Nat Rev Endocrinol.* 2017;13(4):195-207.
6. Osorio JC, Ni A, Chaft JE, et al. Antibody-mediated thyroid dysfunction during T-cell checkpoint blockade in patients with non-small-cell lung cancer. *Ann Oncol.* 2017;28(3):583-589.
7. Kim HI, Kim M, Lee SH, et al. Development of thyroid dysfunction is associated with clinical response to PD-1 blockade treatment in patients with advanced non-small cell lung cancer. *Oncoimmunology.* 2017;7(1):e1375642.
8. Kobayashi T, Iwama S, Yasuda Y, et al. Patients With Antithyroid Antibodies Are Prone To Develop Destructive Thyroiditis by Nivolumab: A Prospective Study. *J Endocr Soc.* 2018;2(3):241-251.
9. Kimbara S, Fujiwara Y, Iwama S, et al. Association of antithyroglobulin antibodies with the development of thyroid dysfunction induced by nivolumab. *Cancer Sci.* 2018;109(11):3583-3590.
10. Toi Y, Sugawara S, Sugisaka J, et al. Profiling Preexisting Antibodies in Patients Treated With Anti-PD-1 Therapy for Advanced Non-Small Cell Lung Cancer. *JAMA Oncol.* 2019;5(3):376-383.
11. Basak EA, Koolen SLW, Hurkmans DP, et al. Correlation between nivolumab exposure and treatment outcomes in non-small-cell lung cancer. *Eur J Cancer.* 2019;109:12-20.
12. Kunert A, Basak EA, Hurkmans DP, et al. CD45RA(+)CCR7(-) CD8 T cells lacking co-stimulatory receptors demonstrate enhanced frequency in peripheral blood of NSCLC patients responding to nivolumab. *J Immunother Cancer.* 2019;7(1):149.
13. Hurkmans DP, Basak EA, van Dijk T, et al. A prospective cohort study on the pharmacokinetics of nivolumab in metastatic non-small cell lung cancer, melanoma, and renal cell cancer patients. *J Immunother Cancer.* 2019;7(1):192.
14. Indini A, Di Guardo L, Cimminiello C, et al. Immune-related adverse events correlate with improved survival in patients undergoing anti-PD1 immunotherapy for metastatic melanoma. *J Cancer Res Clin Oncol.* 2019;145(2):511-521.
15. Chan L, Hwang SJE, Kyaw M, et al. The oncological survival and prognosis of individuals receiving PD-1 inhibitor with and without immunologic cutaneous adverse events. *J Am Acad Dermatol.* 2019.
16. Verzoni E, Carteni G, Cortesi E, et al. Real-world efficacy and safety of nivolumab in previously-treated metastatic renal cell carcinoma, and association between immune-related adverse events and survival: the Italian expanded access program. *J Immunother Cancer.* 2019;7(1):99.

17. Cortellini A, Chiari R, Ricciuti B, et al. Correlations Between the Immune-related Adverse Events Spectrum and Efficacy of Anti-PD1 Immunotherapy in NSCLC Patients. *Clin Lung Cancer.* 2019;20(4):237-247 e231.
18. Lei M, Michael A, Patel S, Wang D. Evaluation of the impact of thyroiditis development in patients receiving immunotherapy with programmed cell death-1 inhibitors. *J Oncol Pharm Pract.* 2019;25(6):1402-1411.
19. Ricciuti B, Genova C, De Giglio A, et al. Impact of immune-related adverse events on survival in patients with advanced non-small cell lung cancer treated with nivolumab: long-term outcomes from a multi-institutional analysis. *J Cancer Res Clin Oncol.* 2019;145(2):479-485.
20. Shafqat H, Gourdin T, Sion A. Immune-related adverse events are linked with improved progression-free survival in patients receiving anti-PD-1/PD-L1 therapy. *Semin Oncol.* 2018;45(3):156-163.
21. Owen DH, Wei L, Bertino EM, et al. Incidence, Risk Factors, and Effect on Survival of Immune-related Adverse Events in Patients With Non-Small-cell Lung Cancer. *Clin Lung Cancer.* 2018;19(6):e893-e900.
22. Sato K, Akamatsu H, Murakami E, et al. Correlation between immune-related adverse events and efficacy in non-small cell lung cancer treated with nivolumab. *Lung Cancer.* 2018;115:71-74.
23. Judd J, Zibelman M, Handorf E, et al. Immune-Related Adverse Events as a Biomarker in Non-Melanoma Patients Treated with Programmed Cell Death 1 Inhibitors. *Oncologist.* 2017;22(10):1232-1237.
24. Teraoka S, Fujimoto D, Morimoto T, et al. Early Immune-Related Adverse Events and Association with Outcome in Advanced Non-Small Cell Lung Cancer Patients Treated with Nivolumab: A Prospective Cohort Study. *J Thorac Oncol.* 2017;12(12):1798-1805.
25. Toi Y, Sugawara S. Survivorship Bias in Analyses of Immune Checkpoint Inhibitor Trials-In Reply. *JAMA Oncol.* 2019.
26. Kim HK, Heo MH, Lee HS, et al. Comparison of RECIST to immune-related response criteria in patients with non-small cell lung cancer treated with immune-checkpoint inhibitors. *Cancer Chemother Pharmacol.* 2017;80(3):591-598.
27. Hodi FS, Hwu WJ, Kefford R, et al. Evaluation of Immune-Related Response Criteria and RECIST v1.1 in Patients With Advanced Melanoma Treated With Pembrolizumab. *J Clin Oncol.* 2016;34(13):1510-1517.

SUPPLEMENTARY INFORMATION

Supplementary Figure 1.

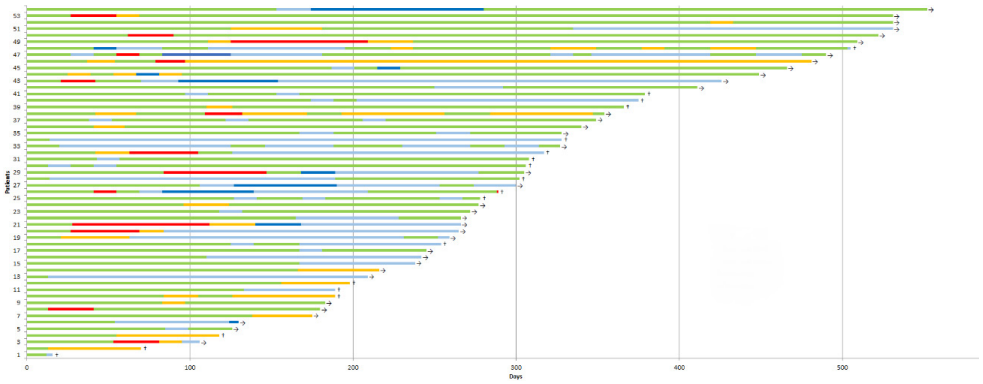

Thyroid toxicity patterns in patients with acquired thyroid toxicity (euthyroidism in green; subclinical hypothyroidism in light blue; subclinical hyperthyroidism in yellow; overt hypothyroidism in dark blue; overt hyperthyroidism in red). →: Patient did not die nor was lost to follow-up. †: Patient died or was lost to follow-up.

Supplementary Table 1. Distribution of anti-TPO and anti-Tg levels

	Baseline (n=156)		**Follow-up (n=158)**	
	Anti-TPO (IU/ml)	Anti-Tg (IU/ml)	Anti-TPO (IU/ml)	Anti-Tg (IU/ml)
Median (IQR)	3.1 (0-7.9)	22.4 (0-46.5)	3.4 (0-8.3)	23.1 (0-49.5)
Range (min-max)	0-2,011.2	0-931.3	0-2341.1	0-16,332.7

CHAPTER 16

16

Donor-derived cell-free DNA detects kidney transplant rejection during nivolumab treatment

Daan P. Hurkmans*, Jeroen G.H.P. Verhoeven*, Kitty de Leur, Karin Boer, Arjen Joosse, Carla C. Baan, Jan H. von der Thüsen, Ron H.N. Van Schaik, Ron H.J. Mathijssen, Astrid A.M. Van der Veldt*, Dennis A. Hesselink*

*Shared first/senior authorship

Journal for ImmunoTherapy of Cancer, July 2019, 7: 182

Abstract

Background: In solid organ transplant (SOT) recipients, transplant rejection during immune checkpoint inhibitor (ICI) treatment for cancer is a clinical problem. Donor-derived cell-free DNA (dd-cfDNA) can be detected in blood and is a sensitive biomarker for diagnosis of acute rejection in SOT recipients. To our best knowledge, this is the first case report of a kidney transplant recipient with advanced cancer treated with ICI who was monitored with dd-cfDNA.

Case presentation: A 72-year old female with a long-standing renal transplant was diagnosed with advanced melanoma in 2018 and was treated with the anti-PD1 antibody nivolumab. Within 12 days after the first administration of nivolumab, dd-cfDNA ratio increased to 23%, suggesting allograft rejection. Her kidney transplant function deteriorated and acute rejection was confirmed by renal transplant biopsy. As the rejection could not be controlled despite immunosuppressive treatment, a transplant nephrectomy was necessary and haemodialysis was started. Immunological analysis of the renal explant showed infiltration of alloreactive, nivolumab-saturated, PD1+ cytotoxic T cells. After transplant nephrectomy, she experienced nivolumab-related toxicity and rapid disease progression.

Conclusion: Clinicians prescribing ICIs should be aware that SOT recipients are at risk of transplant rejection as a result of T cell activation. Dd-cfDNA is a sensitive biomarker and should be further studied for early detection of transplant rejection. Immunological analysis of the kidney explant showed marked graft infiltration with alloreactive PD-1^{+} cytotoxic T cells that were saturated with nivolumab,

INTRODUCTION

Immune checkpoint inhibitors (ICIs) have significantly improved the overall survival of patients with advanced malignancies, including advanced stage melanoma [1]. The monoclonal antibody nivolumab blocks the inhibitory immune checkpoint receptor programmed death-1 (PD-1), thereby promoting the anti-tumor immune response [2]. This is particularly hazardous for solid organ transplant (SOT) recipients who may develop acute rejection as a result of enhanced T cell activation [3]. As SOT recipients have an increased risk to develop ICI-responsive malignancies, including melanoma and cutaneous squamous cell carcinoma [4,5], ICI-induced SOT rejection is a clinical problem. For adequate patient counselling and early intervention during ICI treatment, biomarkers for early detection of acute rejection are needed. However, conventional biomarkers to monitor SOT integrity have a low sensitivity and specificity [6].

Donor-derived cell-free DNA (dd-cfDNA) can be detected in blood and urine of SOT recipients and has been shown to be a potentially useful biomarker for the early diagnosis of acute rejection of kidney transplants [7]. In kidney transplant recipients, dd-cfDNA levels of <1% of total cfDNA appear to reflect the absence of active rejection whereas levels >1% seem to indicate active rejection [7]. However, many questions regarding the clinical utility of dd-cfDNA monitoring following SOT remain and this is not standard practice (reviewed in Verhoeven et al.). Here, a kidney transplant recipient is described who experienced severe acute allograft rejection during ICI therapy for metastatic melanoma. In the current analysis, dd-cfDNA was evaluated as a potential sensitive biomarker for detection of transplant rejection in a cancer patient treated with ICIs. Second, to understand the pathophysiology of this ICI-induced rejection, graft-infiltrating leucocytes were isolated and characterized.

MATERIALS AND METHODS

Genotyping, isolation and measurement of dd-cfDNA

Peripheral blood mononuclear cells of the recipient and spleen cells of the donor were used for automated purification of DNA (Maxwell, Promega, Leiden, the Netherlands). Donor and recipient were genotyped and discriminated by using a panel of 10 preselected different single-nucleotide polymorphisms (SNP). Blood samples for dd-cfDNA were collected in CellSave BCT tubes (Menarini, San Diego, CA). Blood collection tubes were stored at 4°C within 3 hours after collection, and within 2 days post draw, plasma was separated by centrifugation at 1,600 × *g* for 20 minutes and stored at -80°C. Post thaw, plasma was centrifuged for a second time at 16,000 × *g* for 10 minutes and cfDNA was extracted immediately using the Circulating Nucleic Acid kit (Qiagen, Venlo, The Netherlands)). For the droplet digital PCR (ddPCR), droplets were manually generated

with the QX200 Droplet Generator (Bio-Rad, Lunteren, The Netherlands). The samples were run on a the T100™ Thermal Cycler (Biorad, Lunteren, The Netherlands). Dd-cfDNA was quantified based on differences in SNPs between donor and recipient (3 different SNPs that were able to distinguish between ddcfDNA and cfDNA) using the QX200™ Droplet Reader (Biorad, Lunteren, The Netherlands). Analysis was performed with QuantaSoft Analysis Pro (Bio-Rad, Lunteren, The Netherlands).

Immunohistochemical stainings

Four µm sections of Formalin-Fixed Paraffin-Embedded (FFPE) tissue were mounted serially on adhesive glass slides and deparaffinized. Antigen retrieval was performed by CC1 antigen retrieval solution (ref. 950-124, Ventana Medical Systems, Inc., Oro Valley, Arizona). Specimens were incubated with the primary antibody. The following antibodies were used; CD3 (ref. 790-4341, Ventana Medical Systems, Inc., Oro Valley, Arizona), CD4 (ref. 790-4423, Ventana Medical Systems, Inc., Oro Valley, Arizona), CD8 (ref. 790-4460, Ventana Medical Systems), CD20 (790-2531 Ventana Medical Systems), Granzyme B (262R-18, Cell Marque Corporation, Rocklin, California), Ki-67 (ref. 790-4286 Ventana Medical Systems) and PD-1 (ref. 760-4895, Cell Marque). Detection was performed with OptiView DAB (ref. 760-700, Ventana Medical Systems, Inc.) or UltraView-DAB (ref. 760-500, Ventana Medical Systems, Inc) and amplification was done with the Amplification Kit (ref: 760-080 or OptiView Amplification Kit ref: 760-099, Ventana Medical Systems, Inc.). Next, the specimens were counterstained with haematoxylin II (ref: 790-2208, Ventana Medical Systems, Inc.) and cover-slipped in order to keep the specimens pressed flat. Each slide contained a positive control. All stainings were performed on the VENTANA BenchMark ULTRA (Ventana Medical Systems, Inc.).

Flow cytometric phenotyping of graft infiltrating lymphocytes (GILs)

GILs were stained with the following monoclonal antibodies (MoAb) in order to determine their phenotype: CD3, CD4, CD8, and PD-1. In order to measure the capacity of the cells to produce pro-inflammatory cytokines, the GILs were stimulated for 4 hours with 0.5 µg/mL phorbol myristate acetate (PMA) and 10 µg/mL ionomycin (Sigma-Aldrich, St. Louis, MO) at 37°C. Intracellular accumulation of cytokines was enhanced by the addition of monensin and brefeldin A. The reaction was stopped by the addition of ethylene-diamine-tetra-acetic acid. Subsequently, cells were stained with CD3 brilliant violet 510 (BV510; Biolegend, San Diego, CA), CD4 brilliant violet 421 (BV421; Biolegend), CD8 phycoerythrin-cyanine7 (Pe-Cy7; BD), PD-1 allophycocyanin-Cy7 (APC-Cy7; Biolegend), and the viability marker 7-aminoactinomycin (7-AAD; Biolegend). After surface staining, the cells were immediately fixed with FACS lysing solution (BD) and permeabilized with PERM II (BD). Intracellular staining was performed with the following MoAb: TNFα PE (Biolegend), IFNγ fluorescein isothiocyanate (FITC; BD) and IL-2 APC (BD). Samples were measured on the FACSCanto II (BD).

In order to determine free binding places of nivolumab (Bristol-Myers Squibb, New York, NY), was labelled with the SiteClick™ R-PE Antibody Labeling Kit (ThermoFisher, Waltham, MA). The GILs from the patient and the control patient were not stimulated. Cells were phenotyped with the following monoclonal antibodies: CD3 brilliant violet 510 (Biolegend), CD4 brilliant violet 421 (Biolegend), CD8 phycoerythrin-cyanine7 (BD), Nivolumab-PE, and the viability marker 7-aminoactinomycin (Biolegend). After surface staining, the cells were measured on the FACSCanto II (BD). Analysis was performed with Kaluza 1.5a software (Beckman Coulter, Brea, CA).

CASE PRESENTATION

In 2018, a 72-year-old female with a long-standing renal transplant was diagnosed with metastatic BRAF-wildtype melanoma, five years after a cutaneous melanoma (Breslow thickness 0.8 mm) had been radically excised. She presented with a solitary large left axillary metastasis of 6 cm which encased the axillary artery and the plexus brachialis, resulting in edema and paralysis of her left arm. The patient had received a deceased donor kidney transplant in 2013 due to end-stage renal disease caused by hypertensive nephropathy and a unilateral nephrectomy because of renal cell carcinoma (T2N0M0) in 2006. Apart from the development of post-transplantation diabetes mellitus, the clinical course after her transplantation had been uneventful. At the time of melanoma diagnosis, she had a stable renal function with limited proteinuria (urinary protein to creatinine ratio of 33 g/mol) and a serum creatinine concentration of 150 umol/L, corresponding to an eGFR of 30 mL/min per 1.73 m^2 (CKD-EPI formula) [8].

The large left axillary mass was considered unresectable. After radiotherapy combined with hyperthermia, she had progressive disease with pulmonary and distant lymph node metastases. She was carefully counselled about ICI-associated side effects, specifically about the possibility of renal allograft rejection. Progressive axillary metastasis with severe vascular and neurologic complications led to the shared decision to start first-line nivolumab (3 mg/kg Q2W). The immunosuppressive regimen consisting of tacrolimus (1.5 mg q.d.) and mycophenolate mofetil (500 mg b.i.d.) was switched to prednisolone (20 mg q.d.) and nivolumab was administered one week thereafter.

Twelve days after first nivolumab administration, the patient presented with nausea, vomiting, loose stools and abdominal pain located at the site of her transplant. Laboratory investigation demonstrated severe renal insufficiency with a serum creatinine of 549 umol/L. A kidney transplant biopsy was performed and demonstrated extensive acute ischemic changes with capillary endothelial necrosis, tubular epithelial degeneration, edema and haemorrhage, consistent with infarction (**Figure 3A)**. These findings were interpreted as acute kidney transplant rejection and methylprednisolone pulse therapy (1000 mg intravenously for 3 consecutive days) and haemodialysis were initiated.

Because of ongoing rejection despite methylprednisolone treatment, prednisolone was discontinued and transplant nephrectomy was performed. Because of advanced malignancy, T lymphocyte-depleting antibodies were not administered.

After transplant nephrectomy, nivolumab was continued for a period of 8 weeks. As she experienced immune-related adverse events, including pneumonitis grade 2 and colonoscopy-conformed colitis grade 2 (common terminology criteria for adverse events version 4.03), nivolumab was discontinued and prednisolone was initiated. Three months after the start of nivolumab, ^{18}F-FDG PET-CT revealed progressive disease with new lung and lymph node metastases (**Figure 1**). The patient decided to stop haemodialysis and died five months after the start of nivolumab.

Figure 1.

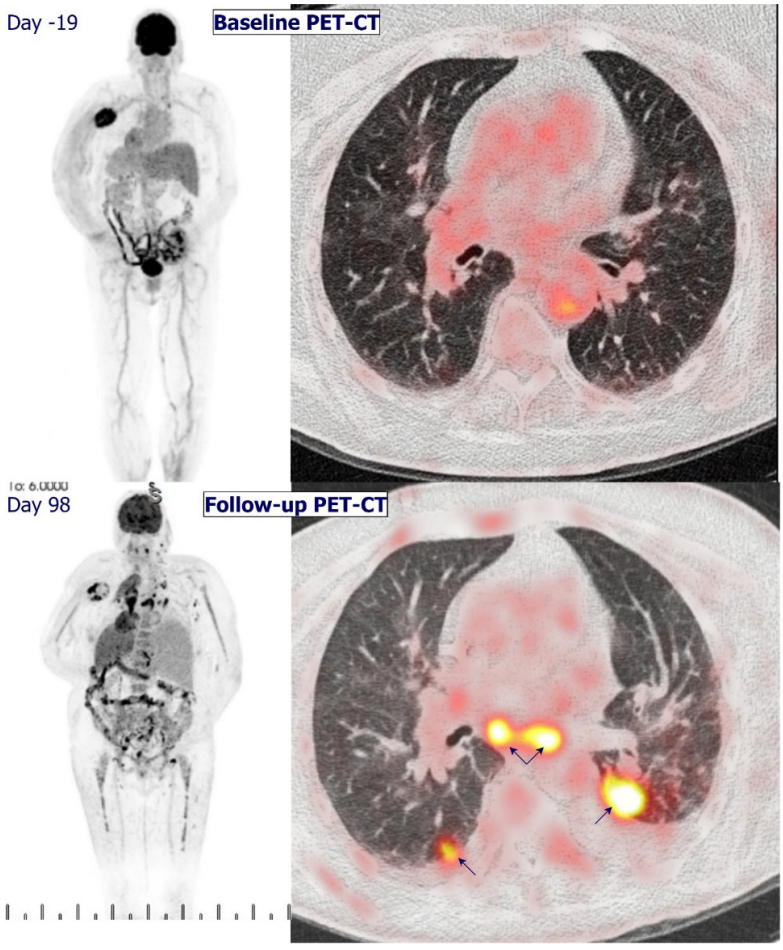

Three months after the start of nivolumab, ^{18}F-FDG PET-CT revealed progressive disease with new lung and lymph node metastases. Pleural effusion was present.

Dd-cfDNA reveals acute allograft rejection

The patient participated in the MULTOMAB clinical trial, (see Dutch Trial Register number NTR7015), in which blood is collected prospectively for translational purposes. After kidney transplant rejection, previously obtained blood samples were analyzed for dd-cfDNA. Dd-cfDNA was expressed as a percentage of total cfDNA (see methods section below). Prior to administration of nivolumab, dd-cfDNA was low (0.9%; **Figure 2**). One week after administration of nivolumab, dd-cfDNA increased to 2.9%, indicating active rejection of the allograft. At the time of rejection, 12 days after first administration of nivolumab, dd-cfDNA increased to a maximum of 23.1%. Dd-cfDNA levels declined to 8.8%, 0.1% and 0.0% at 3-5 hours, 22 days and 77 days after transplant explantation, respectively, corresponding with the half-life of dd-cfDNA [9].

Figure 2.

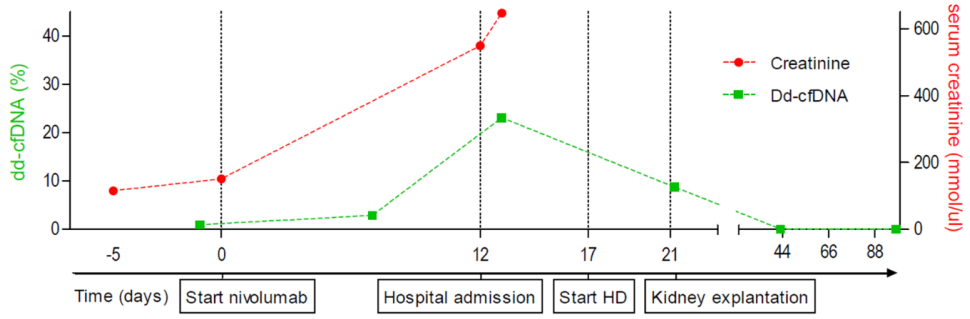

Time course of the percentage plasma dd-cfDNA (green) and serum creatinine concentration (red), in relation to important clinical events. During the hospital admission, hemodialysis (HD; day 17) was initiated. Dd-cfDNA levels declined from 23% to 8.8% 3-5 hours after kidney explantation. Dotted lines are added to connect separate measurements of creatinine and dd-cfDNA. Of note, no comparative serum creatinine measurement was performed at 7 days after the first administration of nivolumab.

Acute vascular rejection with viable graft infiltrating lymphocytes

Histopathological examination of the explanted kidney allograft demonstrated severe vascular, acute T-cell mediated rejection with an almost entirely necrotic kidney parenchyma with hemorrhage and moderate endothelialitis with focal fibrin deposition (**Figure 3B**). $CD3^+$ T lymphocytes were found subendothelially (**Figure 3C**) and included both $CD4^+$ (**Figure 3D**) and $CD8^+$ T cells (**Figure 3E**). No $CD20^+$ B lymphocytes were identified (**Figure 3F**). The cytotoxic $CD8^+$ T cells were active and viable, as evidenced by the presence of intracellular granzyme B (**Figure 3G**) and Ki-67 (**Figure 3H**), reflecting their cytotoxic potential and proliferation, respectively. $PD\text{-}1^+$ staining was also seen in the vessel wall (**Figure 3I**).

Despite the necrotic status of the renal explant, viable lymphocytes were revealed, which mainly consisted of $CD3^+$ T cells (59%). Within the total $CD3^+$ T cell population, the $CD4^+$:$CD8^+$ ratio was approximately 1:3 (22% $CD4^+$ and 73% $CD8^+$, **Figure 4A**). Cytokines, such as IFN-γ, TNF and IL-2, play an important role in the immune response that mediate allograft rejection. The amount of these pro-inflammatory cytokines, produced by T-cells, indicates whether these cells are activated. After polyclonal stimulation, the capacity of the T cells to produce IFN-γ, TNFα and IL-2 was measured [10]. $CD8^+$ T cells had a higher capacity than $CD4^+$ T cells to produce IFN-γ (91% *vs.* 37%; **Figure 4B**) and TNFα (66% *vs.* 34%), whereas $CD4^+$ T cells showed a higher capacity for IL-2 production (5% *vs.* 17%).

Nivolumab PD-1 occupancy on graft infiltrating lymphocytes

Further immunological analysis was performed to examine whether nivolumab was successfully bound to the graft infiltrating lymphocytes (GILs), which were considered to have caused rejection. Among the GILs, PD-1 was expressed on both the $CD4^+$ and $CD8^+$ T cells (31% and 34%, respectively; **Figure 4C**), indicating that the receptor for nivolumab was present on the surface of these cells. To determine the amount of free PD-1 binding places on the GILs in the explant, conjugated nivolumab was added to the explant of both the current and a control patient, who experienced an acute rejection without ICI. In the renal explant of the control patient, nivolumab binding capacity was 49% of $CD4^+$ and 37% $CD8^+$ T-cells (**Figure 4D**), whereas conjugated nivolumab was not able to bind $CD4^+$ and $CD8^+$ T-cells (0% and 0%, respectively) in the nivolumab-treated patient.

Figure 3.

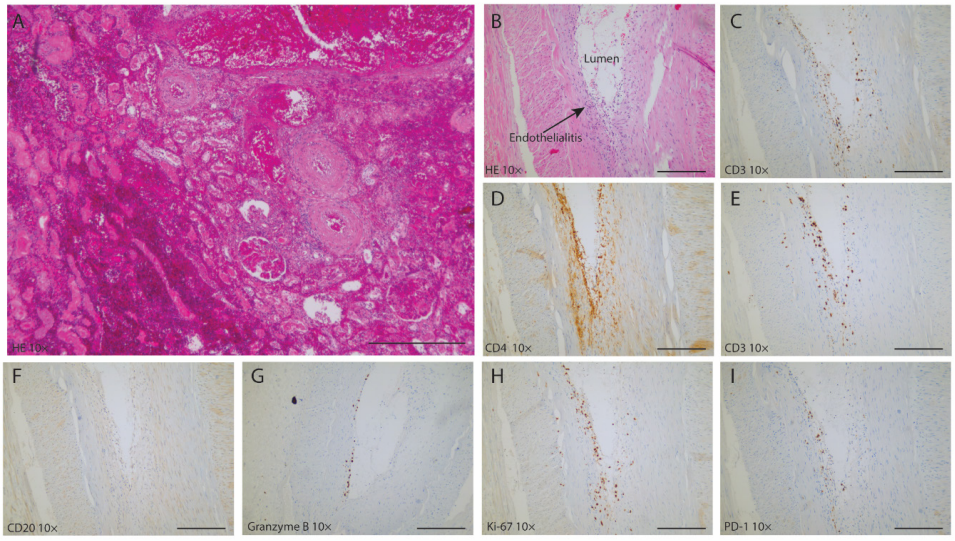

Histology of the renal graft at the time of the kidney transplant biopsy and the explantation under nivolumab treatment (250 µm scale bar). Immunohistochemistry of the explanted kidney. A: HE staining of the kidney biopsy shows diffuse cortical necrosis, hemorrhage and glomerular congestion. B: HE staining of the renal explant shows moderate endothelialitis with focal fibrin deposition. C-I: immunohistochemistry of the explanted kidney. C-E: $CD3^+$, $CD4^+$ and $CD8^+$ T-cells are present. F: no $CD20^+$ B-cells are present. G and H: indicates the presence granzyme producing cells and proliferating cells (Ki-67) cells. Overall, there is influx of PD-1^+ granzyme B-producing $CD8^+$ T-cells in the vascular wall with endothelialitis. Magnification: 10x.

Figure 4.

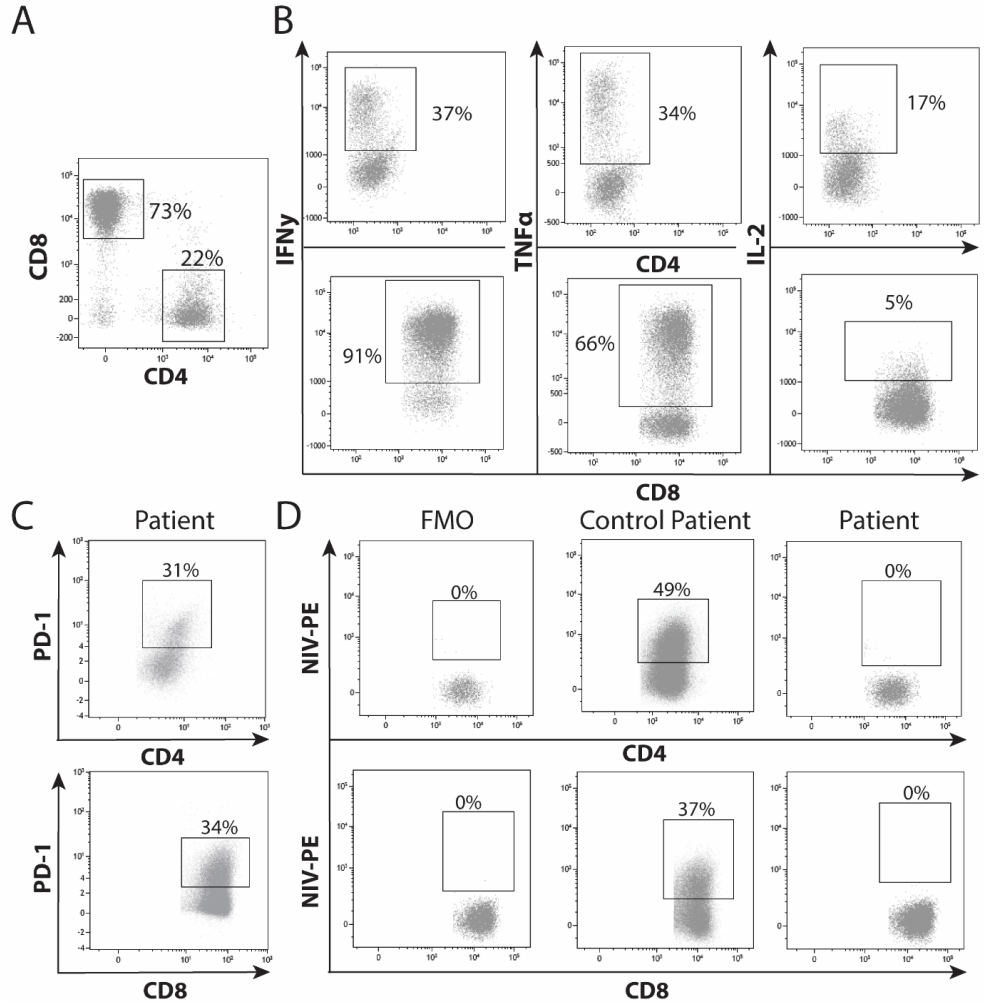

Phenotyping of the graft infiltrating lymphocytes isolated from the explanted kidney during nivolumab treatment. A: Unstimulated graft infiltrating-lymphocytes were gated by size and granularity in the forward and side scatter. $CD4^+$ and $CD8^+$ T cells were gated within total $CD3^+$ cells. B: Intracellular IFN-γ, TNFα and IL-2 was determined in $CD3^+CD8^-$ (representing the $CD4^+$ population) and $CD8^+$ T cells at 3 hours of stimulation with PMA/ionomycin. C: Presence of the presence of PD-1 in $CD4^+$ and $CD8^+$ T-cells was also determined. D: Blockade of the PD-1 receptor by nivolumab was demonstrated by adding conjugated nivolumab to these cells and was compared with graft infiltrating lymphocytes of a rejected kidney from a patient who was not treated with nivolumab.

DISCUSSION

Here a melanoma patient with a kidney transplant is reported who developed a fulminant acute kidney allograft rejection two weeks after the start of nivolumab treatment. Dd-cfDNA was measured in this cancer patient to monitor allograft integrity and detect potential allograft rejection at an early stage during treatment with an ICI. Previously, it has been reported that quantification of so called dd-cfDNA can be useful to detect allograft rejection. Cell-free DNA is degraded into non-encapsulated DNA and released after cell death, or by active secretion of cells. During SOT rejection, the cells of donor origin are damaged and their content is released into the bloodstream. [7] Detection of dd-cfDNA is based on chimerism: donor cells are genetically distinct from that of the transplant recipient [6].

Immunological analysis of the kidney explant showed marked graft infiltration with alloreactive PD-1^{+} cytotoxic T cells that were saturated with nivolumab, demonstrating nivolumab-mediated inhibition of PD-1. This indicated that nivolumab was bound to the T cells which likely caused allograft rejection. The graft infiltrating T cell population had the capacity to mount an effector response.

As indications of ICIs are expected to expand and SOT recipients have an increased risk to develop malignancies, e.g. advanced hepatocellular carcinoma in liver transplant patients, the use of ICIs in SOT recipients is a clinical problem, the magnitude of which is likely to increase in the near future [11]. However, clinical trials of ICIs excluded SOT patients. Apart from case reports and case series [12-16], the efficacy and toxicity of ICI in transplanted patients with malignancies have not been studied extensively but do indicate the high risk of allograft rejection. Serum creatinine, which estimates the glomerular filtration rate, is not specific nor sensitive for kidney transplant rejection [17].

The findings of the present case study suggest that dd-cfDNA may be a valuable biomarker for early detection of ICI-induced transplant rejection. It remains unclear at this stage if this novel biomarker outperforms conventional biomarkers such as serum creatinine. The first serum creatinine measurement in this case was only performed 12 days after the first administration of nivolumab and not at the same time of the dd-cfDNA measurement.

In conclusion, physicians prescribing ICIs should be aware of the increased risk of allograft rejection as a result of T cell activation. We believe that a combined measurement of dd-cfDNA and conventional biomarkers may assist physicians to diagnose transplant rejection in this particular setting at an early stage but this should be studied prospectively. The transplant rejection was caused by alloreactive cytotoxic T cells that were positive for PD-1 and were saturated with nivolumab, which is in line with the anti-tumor effect of this drug.

REFERENCES

1. Robert C, Long GV, Brady B, et al. Nivolumab in previously untreated melanoma without BRAF mutation. *N Engl J Med.* 2015;372(4):320-330.
2. Callahan MK, Postow MA, Wolchok JD. Targeting T Cell Co-receptors for Cancer Therapy. *Immunity.* 2016;44(5):1069-1078.
3. Aguirre LE, Guzman ME, Lopes G, Hurley J. Immune Checkpoint Inhibitors and the Risk of Allograft Rejection: A Comprehensive Analysis on an Emerging Issue. *Oncologist.* 2018.
4. Ramsay HM, Fryer AA, Hawley CM, Smith AG, Harden PN. Non-melanoma skin cancer risk in the Queensland renal transplant population. *Br J Dermatol.* 2002;147(5):950-956.
5. Vajdic CM, McDonald SP, McCredie MR, et al. Cancer incidence before and after kidney transplantation. *JAMA.* 2006;296(23):2823-2831.
6. Verhoeven J, Boer K, Van Schaik RHN, et al. Liquid Biopsies to Monitor Solid Organ Transplant Function: A Review of New Biomarkers. *Ther Drug Monit.* 2018;40(5):515-525.
7. Bloom RD, Bromberg JS, Poggio ED, et al. Cell-Free DNA and Active Rejection in Kidney Allografts. *J Am Soc Nephrol.* 2017;28(7):2221-2232.
8. Levey AS, Stevens LA, Schmid CH, et al. A new equation to estimate glomerular filtration rate. *Ann Intern Med.* 2009;150(9):604-612.
9. Yao W, Mei C, Nan X, Hui L. Evaluation and comparison of in vitro degradation kinetics of DNA in serum, urine and saliva: A qualitative study. *Gene.* 2016;590(1):142-148.
10. Walsh PT, Strom TB, Turka LA. Routes to transplant tolerance versus rejection; the role of cytokines. *Immunity.* 2004;20(2):121-131.
11. Xu F, Jin T, Zhu Y, Dai C. Immune checkpoint therapy in liver cancer. *J Exp Clin Cancer Res.* 2018;37(1):110.
12. Barnett R, Barta VS, Jhaveri KD. Preserved Renal-Allograft Function and the PD-1 Pathway Inhibitor Nivolumab. *N Engl J Med.* 2017;376(2):191-192.
13. Kittai AS, Oldham H, Cetnar J, Taylor M. Immune Checkpoint Inhibitors in Organ Transplant Patients. *J Immunother.* 2017;40(7):277-281.
14. Kwatra V, Karanth NV, Priyadarshana K, Charakidis M. Pembrolizumab for metastatic melanoma in a renal allograft recipient with subsequent graft rejection and treatment response failure: a case report. *J Med Case Rep.* 2017;11(1):73.
15. Ong M, Ibrahim AM, Bourassa-Blanchette S, Canil C, Fairhead T, Knoll G. Antitumor activity of nivolumab on hemodialysis after renal allograft rejection. *J Immunother Cancer.* 2016;4:64.
16. Spain L, Higgins R, Gopalakrishnan K, Turajlic S, Gore M, Larkin J. Acute renal allograft rejection after immune checkpoint inhibitor therapy for metastatic melanoma. *Ann Oncol.* 2016;27(6):1135-1137.
17. Josephson MA. Monitoring and managing graft health in the kidney transplant recipient. *Clin J Am Soc Nephrol.* 2011;6(7):1774-1780.

PART IV

Summary and General discussion

CHAPTER 17

17

Summary and Future Perspectives

PHARMACOLOGY OF IMMUNE CHECKPOINT INHIBITORS

The pharmacokinetics (PK) of immune checkpoint inhibitors (ICIs) were studied in **Part I** of this thesis. In the studies described in this thesis, an association was found between drug exposure and PD-1 ICI response for non-small-cell lung cancer (NSCLC; **Chapter 2**), while earlier phase I studies established that a relationship was lacking between drug dose and therapy response[1]. This was an unexpected finding as drug dosing is usually positively correlated with drug exposure, and has been the motif for subsequent PK studies.

Cancer cachexia pathways may lead to higher drug clearance

We presume that the association between drug exposure and therapy response might be the result of inter-patient variability of drug clearance. This hypothesis was confirmed by Turner *et al*. for a PD-1 ICI (pembrolizumab) in solid tumors[2]. Here, drug clearance was negatively correlated with drug exposure and this correlation was equivalent across different dose levels.[2] Hence, patients with rapid disease progression or unfavorable prognostic characteristics were found to have a higher elimination rate of the drug and consequently have worse survival outcome regardless of the dose they received.

For clarification, **Table 1** shows the paradoxical association between exposure and response in two hypothetical patients with variation in dosing and drug clearance. Higher drug clearance of patient B (0.45 L/day) results in lower exposure (156 *vs.* 467 mg/L*day for a 70 mg dose; 1560 *vs.* 4670 mg/L*day for a 700 mg dose) and represents a patient with a more advanced disease status or reflects disease progression during immunotherapy. Even though the absolute drug exposure of patient B for the 700 mg dose is higher than patient A's systemic exposure for the 70 mg dose, patient B does not benefit of treatment. This is irrespective of the dosage (70 or 700 mg). For that reason, an exposure-response relationship may be observed within dose levels.

Table 1. Hypothetical patients with distinct levels of drug clearance

	CL (L/day)	Dose (mg)	AUC (mg/L*day)	BOR	Dose (mg)	AUC (mg/L*day)	BOR
Patient A	0.15	70	467	PR	700	4670	PR
Patient B	0.45	70	156	PD	700	1560	PD

Table 1. Two hypothetical patients (patient A and B) with respectively lower and higher drug clearance, who were treated with low or high dose immune checkpoint inhibitors. Patient B had impaired response irrespective of exposure. Table adapted from Badawi et al.3 Abbreviations: drug clearance (CL), area under the curve (AUC), best overall response (BOR), partial response (PR), progressive disease (PD).

Next, we explored patient characteristics that predominantly impact the rate of drug clearance. In **Chapter 3** and **4**, we described the first real-world population PK model

for nivolumab and pembrolizumab. Here, we found that the relationship between drug clearance and therapy response was most profound in stage IV NSCLC treated with nivolumab, which could be confirmed for pembrolizumab. Furthermore, baseline albumin levels were negatively associated with drug clearance, suggesting a key role of cancer cachexia in the PK of ICIs. Elimination of ICIs primarily occurs through metabolic breakdown into amino acids[4], while the extended half-life time is the result of recycling mechanisms, similar to endogenous immunoglobulins. Potentially, higher drug clearance may represent a more advanced disease status, which may result in cancer cachexia and induces catabolism of immunoglobulins. Hence, we propose that cachexia pathways as a result of cancer progression may lead to higher target elimination of ICIs. Based on these findings, we postulate that the observed association between drug exposure or clearance with therapy response is a reflection of the patients' metabolism (**Figure 1;** upper part of the figure).

TREATMENT SELECTION OF NSCLC

A serum profile involved in the acute phase response may reflect cancer cachexia and is associated with resistance to ICIs

In the second part of the thesis (Part II), we focused on treatment selection of ICIs in NSCLC. The role of cancer cachexia in NSCLC was also underlined by studying the serum proteome (Chapter 5). Enrichment analysis of the serum proteome, consisting of more than one thousand different proteins, identified IL-6 as a key upstream regulator of therapy resistance. Higher IL-6 was associated with worse clinical outcome, which was known to be strongly correlated as an acute phase protein to cancer cachexia. Interestingly, further evidence that emphasizes the role of the general metabolism was provided by a serum protein signature by mass spectrometry that stratified outcomes in patients with advanced NSCLC with second-line PD-1 ICIs (Chapter 6). A potential biological mechanism supporting the test was determined using protein set enrichment analyses methods. Consistently, patients were primarily stratified based on proteins involved in the acute phase response, acute inflammatory response, wound healing and complement activation, which was upregulated in patients with a worse clinical outcome after PD-1 inhibition. No significant association with progression-free survival (PFS) or overall survival (OS) was observed in a comparable cohort of advanced NSCLC patients treated with docetaxel. This demonstrates a predictive value of this specific serum protein signature, while previous research that showed the involvement of these mechanisms of resistance refrained from demonstrating predictive value[5,6]. Hence, although cancer cachexia is considered a prognostic factor, cancer cachexia related pathways have also been suggested to be specific for immunotherapeutic response.

Figure 1. Pharmacokinetics and the tumor-immune interaction impacts tumor response after ICIs

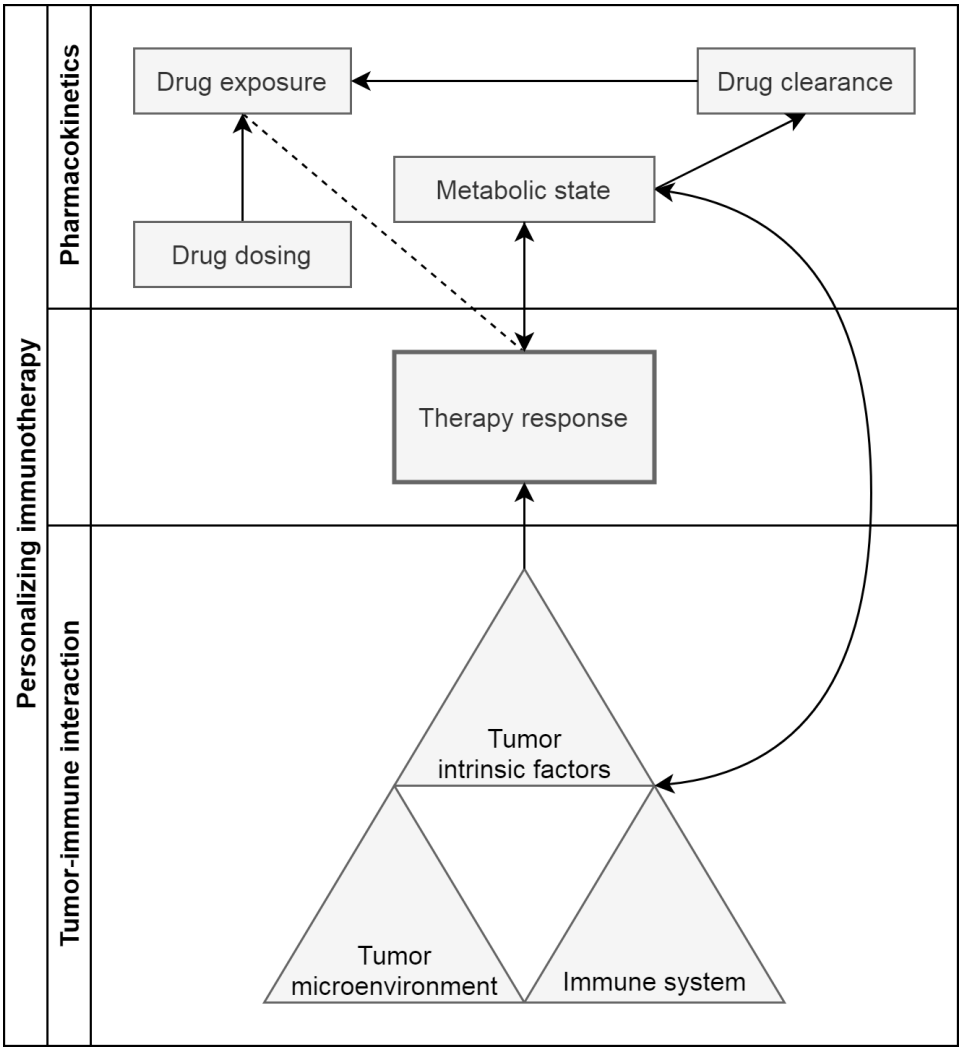

The following model was proposed in this thesis, in which the therapy response to immune checkpoint inhibitors or tumor-immune factors direct the metabolic state of patients (progressive disease or malignant grade are associated with catabolism). Cancer cachexia is suggested to lead to higher drug clearance and lower drug exposure, which may also be a result of lower dosing. The association between drug exposure or drug clearance is the result of differences in the metabolic state of patients. As a consequence, we propose that there is no causal relationship between drug exposure or drug clearance and therapy response, despite our findings that indicate an exposure-response relationship at the start of this thesis. Moreover, there is no true dose-response relationship in patients that are treated with ICIs as standard of care (either fixed or weight based dosing strategies). Of note, other factors rather than the tumor-immune interaction may also contribute to patients' general metabolism, such as intrinsic, genetic or physiologic features.

Tumor growth rate as tool for better evaluation of tumor response after ICIs

The clinical outcome after ICIs is generally based on the patient's survival or radiological evaluation of tumor lesions over time. Radiological evaluation allows classification into patients who have progressive disease, stable disease or partial/complete response. Classically, this is done according to the Response Evaluation Criteria in Solid Tumors (RECIST v1.1)[7]. However, new methods of radiological evaluation have been studied, as cancer patients that are treated with immunotherapy sometimes show initial tumor growth with subsequent tumor shrinkage, defined as pseudo-progression. Treatment past progression is needed to recognize these tumor growth dynamics. Therefore, tools such as immune-related RECIST have been proposed by Nishino *et al.*[8] to evaluate patients in this immune-oncology setting, but also experimental biomarkers might contribute to identify pseudo-progression during treatment. Circulating tumor DNA (ctDNA) is proposed to be a useful biomarker for this purpose: melanoma patients with pseudo-progression have demonstrated to have a profound decrease of ctDNA, which was not observed in patients with true progression[9].

In addition, considerable tumor growth acceleration may occur, that could be characterized as hyper-progressive disease (HPD; **Figure 2**)[10]. The growth patterns are very specific for immunotherapy, in contrast to other regimens such as chemotherapy or targeted therapies, and can only be determined by assessment of the tumor growth rate before in relation to after start of ICIs. We determined the volumetric growth rate before and after start of treatment in NSCLC patients (**Chapter 7**) to study the significance of these growth patterns after ICI treatment. Here, a significant relationship between tumor growth rate and OS could be determined, and a minority of patients (7%) had HPD. HPD was correlated with worse OS of only 2 months, which was in line with the observations by Champiat *et al.*[11]

Different strategies for response evaluation have thus been considered, as RECIST v1.1. does not adequately reflect response to ICIs. Tumor growth dynamics seem to provide additional information, particularly to distinguish patients with the poorest prognosis, compared to alternatively used evaluation methods.

Figure 2. Hyper-progressive disease

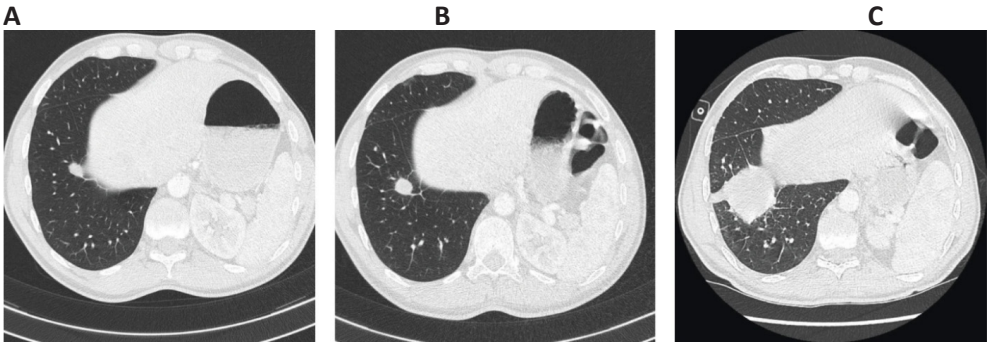

Patient with stage IV NSCLC showing hyper-progressive disease. CT scans were performed A) 10 weeks before start, B) at baseline and C) at first disease evaluation 3 weeks after start of PD-1 ICIs. The blue arrow indicates the prominent tumor lesion. Figure adapted from Champiat et al.[10].

A combination of tumor-immune markers improves prediction

The importance of the tumor-immune interaction in patient stratification was determined in **Chapter 8**, where we combined several factors that were considered to have predictive value. This combination involved tumor intrinsic factors (tumor mutation burden [TMB], PD-L1 expression, expression of classical HLA) and information about the tumor microenvironment (TME; cytotoxic tumor infiltrating lymphocytes [TILs]). Strikingly, cluster analysis based on all markers revealed one cluster pattern that almost exclusively identified patients that did not benefit from ICIs. Here, patients with lower rates of cytotoxic TILs had worse OS than patients with higher rates, which was only in patients with either higher TMB, higher PD-L1 expression or strong classical HLA expression. Hence, a rational combination of markers improved response prediction.

Distorted function of cytotoxic TIL is associated with resistance to ICIs

Distorted effector function of cytotoxic TILs lead to reduced tumor cell death after ICIs, even when these cells are activated. Cytotoxic TILs are generally known to represent $CD8^+$ T cells that have been primed by antigen presenting cells to recognize tumor antigens and to subsequently induce apoptosis of tumor cells. Because granzyme B is a key serine protease secreted by cytotoxic TILs, we hypothesized that a common germline variant of the *GZMB* gene (occurring in approximately one third of the European population) could lead to ICI resistance resulting from an incapability of TILs to induce tumor lysis[12]. Here, we showed that both germline variation of the *GZMB* gene and lower serum levels of granzyme B are associated with therapy resistance in NSCLC (**Chapter 9**). Moreover, *GZMB* variation was associated with serum levels: patients with the heterozygous or homozygous variant of *GZMB* had lower serum levels than patients with the wild type. Notably, we determined

that germline variation of *GZMB* was also significantly associated with impaired PFS and OS in metastatic melanoma (**Chapter 12**), which will be further discussed in the third part of the summary: *Treatment selection of melanoma, and across other tumor types*. Taken together, we demonstrated that germline genetics may significantly impact immune response mechanisms after ICIs in NSCLC and melanoma. The work indicates that the host genetics may significantly impact immune responses after ICIs.

Molecular characterization of NSCLC phenotypes demonstrates different mechanisms of immune evasion

The complexity of the tumor-immune interaction was further underlined in **Chapter 10**. We performed a genome-wide molecular characterization of lung adenocarcinoma and squamous cell carcinoma based on DNA methylation and RNA expression. While differences could be determined in the modulation and expression of key immune modulating genes, the differences were mainly regulated by a group of genes that were not involved in immune modulation. Decreased expression of genes involved in antigen presentation were observed to be the main immune related defect[13].

Characterization of pre-treatment peripheral immune cells in relation to tumor response after ICIs

The association of the peripheral immune status with therapy response was studied in **Chapter 11**. A large fraction of cytotoxic T cells of patients who benefit from treatment were found to be exposed to tumor antigen and matured and egressed in the bloodstream. NSCLC patients with higher numbers of T cells expressing differentiation markers and lacking co-stimulatory receptors were associated with therapy response. Moreover, the intracellular kinase activity profile of peripheral immune cells was determined in stage IV NSCLC and metastatic melanoma (**Chapter 14**). Interestingly, reduced activity in the phosphatase and tensin homolog (PTEN) pathway in peripheral immune cells before start of treatment was associated with therapy response. Loss of PTEN in cancer was found to be associated with therapy resistance of ICIs[14,15]. However, an inverse effect may be achieved when PTEN is downregulated in immune cells by becoming less dependent on activating co-stimulatory receptors for the recognition and elimination of tumor cells[16]. Reduced phosphorylation in the PTEN pathway may decrease the activation threshold and increase the clonal expansion of $CD8^+$ T cells after presentation of tumor-antigens by antigen-presenting cells, facilitating apoptosis of tumor cells. The findings demonstrate the potential of studying immune cell subsets in blood prior to onset of ICIs, which may provide a broader view of the host immune system and local tumor-immune interactions.

TREATMENT SELECTION OF MELANOMA, AND ACROSS TUMORS

We assume that the model for therapy response after ICIs (**Figure 1**) is applicable across tumors. Nevertheless, the factors that determine tumor-immune interactions may vary between tumors, primarily because of differences of intrinsic tumor characteristics and its preferred niche. Therefore, we have also studied the pharmacokinetics of PD-1 ICIs in metastatic melanoma, renal cell carcinoma, urothelial cell carcinoma and mesothelioma (**Chapter 3 and 4**), as well as treatment selection of PD-1 ICIs in metastatic melanoma.

Distorted function or exclusion of cytotoxic TIL associates to ICI resistance

We determined that germline variation of *GZMB* was associated with impaired clinical outcome in both NSCLC (**Chapter 9**) and metastatic melanoma (**Chapter 12**), although the association of *GZMB* variation in metastatic melanoma was much weaker than in NSCLC. The associations in metastatic melanoma did not retain significance after correction for baseline patient characteristics. On the other hand, a common germline variant in *PDCD1*, the gene encoding for PD-1, was strongly associated with impaired OS. Reduced fractions of peripheral PD-1^{+} CD4^{+} T cells were observed in patients with this specific germline variant in *PDCD1*, suggesting that it may affect ICI response by decreasing transcriptional initiation and PD-1 expression. Once more, the findings indicate that host genetics may impact immune responses after ICIs, but also indicate differences between NSCLC and melanoma.

Importantly, distorted function of effector T cells may not only result from an incapability of TILs to induce tumor lysis, for instance as a consequence of germline variation of *GZMB*, but is also heavily affected by the architecture of the TME[11]. Tumors that are excluded of cytotoxic TILs are characterized by collagen-rich stroma that blocks the tumor-immune interaction. An immune-excluded phenotype has been associated with therapy resistance[11], and specific pro-peptides of type III collagen are suggested to reflect the immune-excluded tumor type. In metastatic melanoma patients, we demonstrated that two main components of desmoplasia (pro-C3 and PC3X; pro-peptides of type III collagen) measured in blood were associated with resistance of ICIs (**Chapter 13**). The findings display the possibility to predict response after ICIs by assessment of stroma derived components in blood.

Immune-related toxicity and solid organ transplant rejection after ICI therapy

After initiation of ICI therapy, also self-tolerant immune cells may become activated that may result in immune-related toxicity or adverse effects. In fact, the occurrence of immune-related toxicity has been suggested to be related to tumor response after ICI. The relationship between ICI response and the occurrence of immune-related toxicity, thyroid autoimmune phenomena, was studied in patients with various solid tumors

(**Chapter 15**). Here, we could observe that acquired thyroid toxicity during treatment were associated with therapy response. Interestingly, elevated thyroid specific antibodies prior to initiation of ICIs were correlated with response. The findings suggest additional value for treatment selection or early screening in these patients for on-treatment autoimmune thyroid toxicity, and suggests the importance of the host immune system on response mechanisms after ICIs.

Likewise, in solid organ transplant recipients, transplant rejection may be triggered during ICI therapy. A patient example of a kidney recipient with metastatic melanoma who was treated with immunotherapy was described in **Chapter 16**. Given that donor cells are genetically distinct from that of the transplant recipient, this patient was closely monitored by determining the levels of donor-derived cell-free DNA. Although it remains unclear whether this cell-free DNA outperforms conventional markers (e.g. serum creatinine) in this setting, the findings suggest that it has potential for early detection of transplant rejection induced by ICIs.

PERSPECTIVES ON THE PHARMACOKINETICS

To date, fixed and less frequent dosing of ICIs have been established for the treatment of stage IV NSCLC, among other tumor types. These new dosing strategies have been conducted *in silico* through the use of population PK modeling and simulation[17,18], which results in overall similar drug exposure. Fixed dosing is usually preferred compared to weight-based dosing since it would reduce costs associated with drug preparation and administration. Also, less frequent dosing means that patients may reduce their visits to daycare units in medical centers. With this intention, new dosing strategies should be investigated.

Improving dosing strategies by dose de-escalation, dose personalization or applying a loading dose

Lower dosage of ICIs leads to cost savings by decreasing the demand of resources. Different strategies may be implemented for this purpose. Generally, dose de-escalation can be conducted by lowering the dose of each drug administration, less frequent dosing while establishing the dose of each drug administration, or a combination of these options. A shorter duration of therapy, especially when its early therapeutic effect has been shown, might also be considered for certain tumor types. Currently, the minimum effective concentration is unknown, so we need prospective data to validate such strategies.

Personalized dosing may be considered given the large inter-patient variability of ICIs. We provided understanding in the patient factors that are responsible for the interpatient variability (**Chapters 3** and **4**). For nivolumab, men had a 20% higher drug clearance than women and important variables that explain variability included body surface area

(BSA) and serum albumin. A possible methodology would be to calculate an optimal dose and interval for each individual based on gender, BSA and blood chemistry (e.g. serum albumin). Personalized dosing would be challenging as disease dynamics may influence the patients' metabolism in such way that patients with progressive disease had significantly higher drug clearance.

Moreover, a loading dose may be applied to further optimize the dosing scheme, as the drug is generally well-tolerated[19]. We have presented in **Chapter 3** that biological half-life time of nivolumab is approximately 25 days, which results in an estimated time to reach steady state of 12 weeks (a rule of thumb is that 87.5% of the steady state concentration will be achieved after five half-lives). This has already been applied for other therapeutic monoclonal antibodies (such as cetuximab or trastuzumab[20,21]), and would reduce the time before the rate of drug input is equal to the rate of drug clearance.

Figure 3. Body distribution of PD-1 ICIs

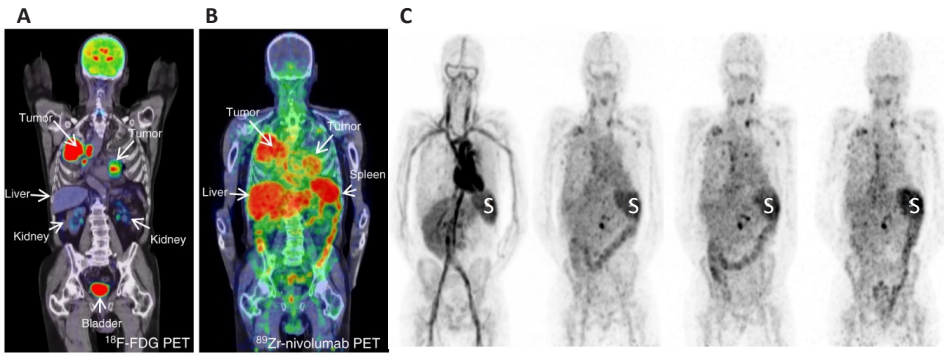

A) ^{18}F-FDG PET demonstrated high glucose metabolism of tumors in both lungs and mediastinal lymph nodes. B) ^{89}Zr-labeled nivolumab PET demonstrate heterogeneous tracer uptake within and between tumors 7 days after infusion of radio-labeled nivolumab. High accumulation can be observed in the liver, spleen and gastrointestinal tract. C) the kinetics of ^{89}Zr-labeled nivolumab on day 0, 3, 5 and 7, showing increasing tissue accumulation and decreasing concentration in the blood circulation over time. Figure adapted from Niemeijer et al.[23]. Abbreviations: spleen (S).

Importance of further understanding the pharmacology of ICIs

Unfortunately, biological understanding of the relationship between PK and the immune-modulating activity in the tumor and TME remains incomplete. Current evidence from studies suggests that peripheral pharmacodynamics markers such as PD-1 receptor occupancy was not associated with therapy response. A saturation of the PD-1 receptor (>80%) was reached at very low exposures of ICIs (corresponding to an approximate nivolumab dose of 0.3 mg/kg Q2W)[22]. However, the receptor occupancy in blood may

not represent its activity in the TME, as it may not necessarily mean that the drug would reach the tumor. Recently, understanding of the distribution was expanded by positron emission tomography (PET) studies with radio-labeled nivolumab[23]. Nivolumab seemed gradually cleared from the circulation by the liver, spleen and gastro-intestinal tract and specifically accumulate at the target site (**Figure 3**). Non-invasive, whole body visualization may contribute to our understanding of the pharmacokinetics of ICIs.

In conclusion, we presume that future research should prospectively study the efficacy of dose de-escalation strategies of ICIs, because costs continue to be a problem for both patients and society. Importantly, profound differences between tumor types are expected, illustrated by a strong inverse drug clearance-OS relationship for patients with advanced-stage NSCLC, which was not apparent for metastatic melanoma (**Chapter 3** and **4**). The underlying biological mechanism is not yet understood. We propose that surrogate markers for faster catabolism of (endogenous) immunoglobulins and relevant patient factors might be convenient for selecting patients for dose de-escalation. Ideally, this may be accompanied by PK monitoring to determine the minimal effective drug concentration. Further insights in context of the exact distribution of ICIs through the body and its immune-modulating activity in the TME is warranted, because it is unlikely that the pharmacologic response solely depends on drug binding to its target. As the relationships connecting drug elimination and cancer cachexia may be the key to our understanding of the ICI pharmacokinetics, it would be interesting to relate PK to cancer cachexia pathways.

PERSPECTIVES ON TREATMENT SELECTION

In addition to PD-L1 expression in tumor tissue, many predictive biomarkers have been considered in clinical trials for ICIs. PD-L1 expression in tumor tissue was shown to have a sensitivity and specificity ranging from 58–85% and 49–60%, respectively, depending on the tumor type or ICI[24]. In the *Introduction,* an overview was provided of the research that has been done up to the start of this thesis. In the following, we provide an updated literature overview (summarized in **Table 2**), and discuss future perspectives of treatment selection.

Potential for the early on-treatment assessment of the immunological response after ICIs

To date, ICIs directed towards the PD-1 receptor or its ligand PD-L1 are now standard of care for many types of cancer, whether or not combined with chemotherapy or CTLA-4 inhibitors. In murine melanoma cell line and models, checkpoint blockade targets only specific subsets of TIL populations, with major differences between PD-1 and CTLA-4 ICIs. Here, anti-PD-1 predominantly induces the proliferation of exhausted-like $CD8^+$

T cells, while anti-CTL-4 also induces the expansion of $CD4^+$ T cells.[25] In patients with advanced NSCLC, Kamphorst *et al.* focused on the peripheral immunological response after PD-1 ICIs. Here, an increase of peripheral $PD1^+$ $CD8^+$ T cells early on-treatment was observed in patients with a radiological response. These peripheral cells had an effector-like phenotype, expressed costimulatory molecules and CTLA-4.[26] The findings were confirmed by the same group and specific peripheral $CD8^+$ T cell clones were found to be activated in patients with melanoma[27]. Although differentiated $CD8^+$ T cells (**Chapter 11**) and the absolute numbers or ratios of a wide variety of immune subsets have been suggested to be predictive for response[28-35], of which most findings were confirmed in independent patient cohorts, the predictive performance remains limited. Attempts to increase the predictive value of blood biomarkers with the combination of apparent prognostic markers, such as the ratio between T cell reinvigoration with tumor load reported by Huang *et al.*[36], should not be considered for future treatment selection. Such combination biomarkers with information on the likely course of disease (irrespective of treatment type) should be avoided because this dilutes the predictive value.

Although patterns of the peripheral immunological response after treatment start in patients are generally specific for reactive tumors - with differences across ICIs but similarities across tumor types (NSCLC or melanoma) – previous reports about pre-treatment patterns in peripheral blood are less consistent. Early on-treatment assessment of the immunological response have been shown to be more predictive.

Response to ICIs relies on tumor-immune interactions

The number of TILs, their spatial distribution and the state of effector T cells are found to be essential for an adequate immunological response after PD-1 inhibition[65,71]. A general increase in TILs could be determined with identified transcriptome signatures related to IFN-γ[72,73], but this was determined by investigation of mixed immune and tumor cells together, which complicates correct interpretation. Therefore, single-cell techniques have been developed to further differentiate immune subsets with tumor or stroma tissue. Actually, tumor reactivity after PD-1 ICIs seems to be restricted to TIL subsets with high expression levels of PD-1 in NSCLC. These TIL subsets are highly distinctive based on its transcriptional signature, with the capacity of tumor recognition.[64] In metastatic melanoma, two major phenotypes of CD8+ T cells were identified by single-cell transcriptomic analysis, of which the ratio of memory-like and exhausted $CD8^+$ T cells was suggested to be related with response after PD-1 ICIs[65]. Nevertheless, it was incompletely understood whether the T cell response to ICIs relies on pre-existing TILs, or on recruitment of TILs. And so, longitudinal single-cell transcriptome analysis of tumor samples were performed. In patients with advanced skin basal and squamous cell carcinoma, it was demonstrated that response to PD-1 inhibition depends on recruitment of novel T cell populations.[74]

Table 2. Literature overview (updated) of proposed biomarkers for immune checkpoint inhibitors

Agent	Tumor	Marker	Association	Reference
Peripheral blood cells				
PD-1 inhibitors	NSCLC	CD8+ T cells[a]	Positive	Kamphorst et al., Proc Nal Acad Sci USA 2017[26]
PD-1 inhibitors	MM	T_{ex}/TB[b]	Positive	Huang et al., Nature 2017[36]
PD-1 inhibitors	NSCLC	ALC, AEC ANC	Positive Negative	Tanizaki et al., J Thorac Oncol 2018[28]
PD-1	MM	$CD8^+$ T cells[c]	Positive	Wieland et al., Cancer Immunol Immunother 2018[27]
PD-1	MM	Classical monocytes	Positive	Krieg et al., Nat Med 2018[37]
Blood-based molecules				
PD-1 or CTLA-4 inhibitors	MM	sPD-1/sPD-L1	Negative	Zhou et al., Cancer Immunol Res 2017[38]
PD-1 inhibitors	NSCLC	sPD-L1	Negative	Costantini et al., Oncoimmunology 2018[39]
PD-1 inhibitors	MM	IFN-γ, IL-6, IL-10	Positive	Yamazaki et al., Cancer Sci 2017[6]
PD-(L)1 inhibitors	NSCLC	dNLR/LDH[d]	Negative*	Mezquita et al., JAMA Oncol. 2018[29]
PD-1 inhibitors	MM	Exosomal PD-L1	Negative	Chen et al., Nature 2018[40]
PD-1 inhibitors	NSCLC	Exosomal PD-1 mRNA	Positive	Del Re et al., Br J Cancer 2018[41]
ICIs (meta analysis)	NSCLC	LDH	Negative*	Zhang et al., Cancer Med 2019[42]
Chemo, ICIs	NSCLC	dNLR/LDH	Negative*	Kazandjian et al., JAMA Oncol 2019[43]
Tumor genome				
PD-(L)1 inhibitors	NSCLC	*EGFR* or *ALK* mutation	Negative	Lee et al., J Thor Oncol 2017[44]
PD-1 inhibitors	MM and NSCLC	*B2M* mutation	Negative	Gettinger et al., Cancer Discov 2017[45]
PD-1 inhibitors	MM and NSCLC	*B2M* mutation	Negative	Sade-Feldman et al., Nat Commun 2017[46]
PD-1 inhibitors	Solid tumors	MMR deficiency	Positive	Le et al., Science 2017[47]
PD-1 and in combination with CTLA-4 inhibitors	NSCLC	TMB	Positive	Hellman et al., N Engl J Med 2018[48]
PD-1 and CTLA-4 inhibitors	NSCLC	TMB	Positive	Hellmann et al., Cancer Cell 2018[49]
PD-(L)1 inhibitors	NSCLC	TMB	Positive	Rizvi et al., J Clin Oncol 2018[50]
PD-L1 inhibitors	NSCLC	bTMB	Positive	Gandara et al., Nat Med 2018[51]
PD-L1 inhibitors	NSCLC	bTMB	Positive	Rizvi et al., Ann Oncol 2018[52]
PD-1 and CTLA-4 inhibitors	NSCLC	*STK11* mutation *PTEN/KEAP1* mutation	Negative Negative	Hellmann et al., Cancer Cell 2018[53]
PD-(L)1 inhibitors	NSCLC	*EGFR* or *ALK* mutation	Negative	Rizvi et al., J Clin Oncol 2018[50]
PD-(L)1 and/or CTLA-4 inhibitors	NSCLC	*MET* mutation	Negative	Sabari et al., Ann Oncol 2018[54]
PD-1 inhibitors	NSCLC	*STK11* mutation	Negative	Skoulidis et al., Cancer Discov 2018[55]
PD-(L)1 inhibitors	NSCLC	bTMB	Positive	Wang et al., JAMA Oncol 2019[56]
PD-(L)1 inhibitors	NSCLC	bTMB	Positive	Wang et al., J Thorac Oncol 2020[57]
PD-(L)1 and/or CTLA-4 inhibitors	NSCLC	*NOTCH* mutation	Positive	Zhang et al., Clin Cancer Res 2020[58]

Tumor microenvironment				
PD-L1 inhibitors	NSCLC	PD-L1	Positive	Rittmeyer et al., Lancet 2017[59]
CTLA-4 inhibitors	MM	PD-L1 on T cells	Positive	Jacquelot et al., Nat Commun 2017[60]
PD-1 or CTLA-4 inhibitors	MM	$CD8^+$ TIL	Positive	Tietze et al. Eur J Cancer 2017[61]
CTLA-4 inhibitors	MM	$FOXP3^+$ and $CD8^+$ Tcells in lymph nodes	Positive	Balatoni et al., Cancer Immunol Immunother 2018[62]
PD-1 inhibitors	NSCLC	EPIMMUNE profile[e] Unmethyl. FOXP1	Positive Positive	Duruisseaux et al. Lancet Respir Med 2018[63]
PD-1 inhibitors	NSCLC	$PD\text{-}1^{high}$ TIL	Positive	Thommen et al., Nat Med 2018[64]
PD-1 inhibitors	MM	$TCF7^+/TCF7^-$ $CD8^+$ TIL[f]	Positive	Sade-Feldman et al., Cell 2018[65]
PD-1 and in combination with CTLA-4 inhibitors	MM	$EOMES^+CD69^+CD45RO^+$ TIL[g]	Positive	Gide et al., Cancer Cell 2019[66]
CTLA-4 inhibitors	MM and RCC	$CD20^+$ TIL[h]	Positive	Helmink et al., Nature 2020[67]
Commensal microbiotica				
PD-1 inhibitors	MM	*B longum, C aerofaciens, E faecium*	Positive	Matson et al., Science 2018[68]
CTLA-4 inhibitors	MM	*Faecalibacterium* family	Positive	Chaput et al., Ann Oncol 2019[69]
PD-1 inhibitors	MM	*Ruminococcaceae* family	Positive	Gopalakrishnan et al., Science 2018[70]

Updated overview from March 2017 of biomarkers with probable predictive value after immune checkpoint inhibitors for metastatic melanoma (MM) or non-small cell lung cancer (NSCLC). Abbreviations: absolute lymphocyte count (ALC), absolute neutrophil count (ANC), absolute eosinophil count (AEC), tumor infiltrating lymphocyte (TIL), soluble PD-1 or PD-L1 (sPD-1 or sPD-L1), interferon-γ (IFN-γ), mismatch repair (MMR), tumor mutation burden (TMB), blood TMB (bTMB). *Likely prognostic biomarkers. [a]Proliferating $CD8^+$ T cells early on-treatment, [b]the ratio between peripheral exhausted-phenotype $CD8^+$ T cells (T_{ex}) and pretreatment tumor burden (TB) defined by the sum of diameters according to RECIST v1.1, [c]proliferating $CD8^+$ T cells with an effector-like-phenotype and co-stimulation CD28/CD27 was required for ICI response, [d]the ratio between derived neutrophils/leukocytes minus neutrophils (dNLR) to lactate dehydrogenase (LDH), [e]EPIMMUNE DNA methylation profile of tumor tissue, [f]the ratio between memory-like and exhausted $CD8^+$ T cells based on TCF7 marker, [g]effector memory-phenotype T cells and activated T cell signatures (interferon-related genes) and [h]tumor infiltrating B cells, presence of tertiary lymphoid structures and related exosomes.

While the role of T cell invigoration is well-studied and fairly established, other immune cell populations may also contribute to mechanisms of response or resistance of ICIs. Recently, higher expression of B cell markers have been determined in patients with melanoma or RCC who benefit from CTLA-4 ICIs. Histological examination demonstrated the localization of B cells within organized lymphoid aggregates.[67] Interestingly, T cells with high expression levels of PD-1, reported to be essential for immunological response after PD-1 ICIs, are found to be in close proximity with B cell infiltrates and primarily produce CXCL13[64]. CXCL13 is a cytokine that mediates the formation of organized lymphoid aggregates in tumor[75]. These lines of evidence suggest that specific tumor-

associated T cells initiate the formation of organized lymphoid aggregates in patients with immunological response after ICIs. However, its precise role remains to be elucidated.

Need for prospective evidence and further biological understanding of blood-based molecules such as exosomes

Serum LDH was suggested to be a negative predictive biomarker for survival after ICIs in NSCLC[42]. However, this relationship has also been determined for chemotherapy, and is likely prognostic[35,76-78], as discussed for melanoma in the *Introduction* of this thesis. Accumulating evidence taking LDH and the neutrophil-to-lymphocyte ratio (NLR) into account demonstrate only prognostic value. Here, a pre-treatment index of NLR and LDH was significantly associated with better survival in patients with NSCLC who were treated with ICIs, irrespective of treatment type[28,43,79-81]. On the other hand, blood-based molecules in the PD-1 pathway have also been related to ICI efficacy. Patients with higher levels of serum soluble PD-L1 are associated with poorer response to PD-1 and CTLA-4 ICIs[38,39], which was preliminarily suggested to be derived from alternate splicing activities and tumor cell death. Moreover, a subtype of extracellular vesicles, known as exosomes, are suggested to play a role in intercellular communication[82]. Higher protein levels of PD-L1 in exosomes are proposed to be associated with response to PD-1 ICIs in metastatic melanoma[40], while a decrease of exosomal PD-1 mRNA was demonstrated to be associated to therapy response in NSCLC. Although these markers are closely linked to known immunotherapy pathways, the source and role in cancer of soluble/exosomal PD-L1 are largely unknown.

The prospect of the tumor (epi)genetics to predict response after ICIs

Advances have been made in further understanding the role of tumor genetics in response and resistance mechanisms of ICIs. After March 2017, TMB has been of interest in particular. TMB was reported to have a similar test performance as PD-L1[83] and may independently predict response to ICIs, which has the potential to combine with other biomarkers improve prediction (**Chapter 7**). Although the application of TMB as predictive biomarker is debated because of some negative prospective trials, most clinical studies demonstrate that tumor or blood-based TMB are positively associated with better clinical outcome after PD-(L)1 ICIs in NSCLC and melanoma[48-52,56,57,84], which may be explained by its association with tumor immunogenicity.

Retrospective work has shown that *TP53/KRAS* co-mutation is related with better clinical outcome after ICIs[85,86]. *KRAS*-mutated NSCLC is generally smoking-related, effects DNA damage repair (DDR) mechanisms and correlate with higher TMB[87], and may explain the positive relationship of KRAS mutations with ICI response. On the contrary, mutations related to reduced antigen presentation were consistently related to ICI resistance[45,46]. The effect of specific genetic alterations in *EGFR* or *ALK* have been related to worse clinical outcome after ICIs in NSCLC[44,50], particularly when compared with alternative treatment

options such as tyrosine kinase inhibitors with superior survival outcomes. Data about other targetable mutations is insufficiently available but suggests that these patients are generally less likely to respond to ICIs. For example, patients with *MET* exon 14 mutated NSCLC express PD-L1 but have significant lower TMB compared to unselected patients[54]. Tumors with *EGFR, ALK* or *MET* oncogenic drivers are generally associated with younger age of cancer onset and with never-smoking[88]. Hence, these tumors have co-occurrence of lower TMB and are probably related to lower number of tumor antigens that can be recognized by cytotoxic T cells, which are considered as less immunogenic tumors.

Recently, *STK11* or *KEAP1* mutated NSCLC was associated with worse clinical outcome after PD-1[55] or PD-1/CTLA-4 ICIs[53], which was initially suggested to reflect ICI resistance mechanisms. However, a significant proportion of NSCLC patients with *STK11* or *KEAP1* mutations do benefit from PD-1 inhibition (AACR Annual Meeting 2020)[89] and those genetic alterations have been proposed to be prognostic, not predictive, in advanced NSCLC[90].

NOTCH mutations were reported as a robust predictive biomarker of ICIs in NSCLC. Here, deleterious *NOTCH* mutations were related with better clinical outcome after ICIs in four independent NSCLC cohorts (*EGFR/ALK* wild types), compared to non-deleterious mutations or wild type, which could not be determined after chemotherapy[58]. Although TMB was higher in both non- and deleterious *NOTCH* mutations, the predictive value seems to rely on higher transcription of genes related to DDR, suggesting more mutagenesis in tumors with deleterious *NOTCH* mutations.

Interestingly, genome-wide epigenetic profiling can be used for the development of predictive biomarkers of complex traits, such as smoking behaviour[91]. Here, a DNA methylation signature has been developed and validated to predict survival after PD-1 ICIs in NSCLC, which could not be determined in patients who did not receive immunotherapy[63].

Taken together, determination of the TMB, as well as specific genetic defects, hold great promise for prediction of response after ICIs. While *STK11* or *KEAP1* mutations may only have prognostic value, the exact mechanism need to clarified of other mutations that have predictive value. A crucial role is speculated for DDR pathway, but it is unknown whether the reported relationship of genetic alterations in *KRAS*, *EGFR, ALK* or *MET* are linked to distinct mechanisms of ICI response or can just be explained by their link with TMB. Importantly, novel insights in tumor epigenetics do not only demonstrate the feasibility of a DNA methylation signature as a predictive biomarker, but also provides insight in the epigenetic landscape which may serve as a target for novel therapies.

Commensal gut microbiome relate to response after ICIs

The potential of fecal microbial transplantation to affect the antitumor effects of ICIs has determined in mice models[92], however, former research in human has only determined associations between variable commensal microbiome and clinical outcome of ICIs[68-70].

Even more, a retrospective analysis of two randomized trials demonstrates reduced OS of ICIs when antibiotics are used at time of initiation in advanced NSCLC, which was less pronounced in the docetaxel group[93]. As antibiotic use is known to impact distinct gut bacteria, the findings suggest a causal relationship, but remain to be clarified in future studies.

Towards robust treatment selection

For robust treatment selection, we believe that several key factors, affecting the immune response after ICIs, should be combined in a prediction model. Such a predictive model would outperform individual biomarkers (e.g. PD-L1 expression in tumor tissue or TMB) and add to current prognostic tools (e.g. TNM cancer staging[94]). Importantly, the integration of blood-based biomarkers, patient characteristics and imaging, being minimal-invasive, has advantages over tissue-based biomarkers. However, considerable hurdles must be overcome for implementation of rapid guidance for physicians in clinical decision making. Firstly, a predictive model requires a continuous process of model update and re-evaluating as knowledge increases, and would have profound implications in the clinics. Although randomized controlled trials with sufficient power would still be needed to endorse the efficacy of novel (combination) treatments, the continuous evaluation and updating of a prediction model would be performed in the real-world setting, requiring larger trials with appropriate size, ideally being cluster-randomized studies known as impact studies[95]. Academic and peripheral medical centers should collaborate closely to collect and share patient data to re-evaluate the prediction model in the immunotherapy setting, particularly because the field is rapidly moving with the registration of novel (combination) treatments or treatment sequences. Secondly, particularly in real-world clinical setting, patients are more likely to lack one or more markers. Therefore, solutions to handle with missing data should be implicated. Thirdly, while prediction models may be useful to aid in the treatment decisions, we should prevent that treatment algorithms emerge that define subgroup indications for very similar monoclonal antibodies. This has previously led to less rational treatment algorithms for the second line ICI treatment of patients with advanced NSCLC, with different subgroup indications for monoclonal antibodies directed to the same immune checkpoint (e.g. pembrolizumab or nivolumab as second line treatment for advanced-stage IV NSCLC in palliative setting). Instead, it should assist the physician to select the right (combination) treatment or treatment sequence for the right patient. Lastly, as examined by Kappen *et al*.[95], it is essential that physicians are informed about the underlying assumptions of the model. In this immune-oncology setting, questions should be addressed, such as what parameters are included in the model and the underlying rationale. In that way, physicians prescribing ICIs would understand better how it may affect their patients.

Hence, a future predictive model for ICI response may meet the requirements as described above. Importantly, the development of a predictive model should rely on OS or robust

response evaluation, which can be supported by dynamic early on-treatment biomarkers or tumor growth dynamics. The inclusion of parameters that reflect the likely course of disease should be avoided, as it dilutes the predictive value. Based on our own findings and previous research, it should include information about tumor intrinsic factors, the TME and the host immunity apart from the PK of ICIs. Although several knowledge gaps are still present, precise and accurate treatment selection for ICIs is within reach for the clinic.

References

1. Topalian SL, Sznol M, McDermott DF, et al. Survival, durable tumor remission, and long-term safety in patients with advanced melanoma receiving nivolumab. *J Clin Oncol.* 2014;32(10):1020-1030.
2. Turner DC, Kondic AG, Anderson KM, et al. Pembrolizumab Exposure-Response Assessments Challenged by Association of Cancer Cachexia and Catabolic Clearance. *Clin Cancer Res.* 2018;24(23):5841-5849.
3. Badawi M, Coss CC, Phelps MA. Letter to the Editor: Exposure-response or clearance-response relationship in immune checkpoint therapy?-A comment on 'correlation between nivolumab exposure and treatment outcomes in non-small-cell lung cancer' by Basak et al. *Eur J Cancer.* 2019;114:25-26.
4. Centanni M, Moes D, Troconiz IF, Ciccolini J, van Hasselt JGC. Clinical Pharmacokinetics and Pharmacodynamics of Immune Checkpoint Inhibitors. *Clin Pharmacokinet.* 2019;58(7):835-857.
5. Weber JS, Sznol M, Sullivan RJ, et al. A Serum Protein Signature Associated with Outcome after Anti-PD-1 Therapy in Metastatic Melanoma. *Cancer Immunol Res.* 2018;6(1):79-86.
6. Yamazaki N, Kiyohara Y, Uhara H, et al. Cytokine biomarkers to predict antitumor responses to nivolumab suggested in a phase 2 study for advanced melanoma. *Cancer Sci.* 2017;108(5):1022-1031.
7. Eisenhauer EA, Therasse P, Bogaerts J, et al. New response evaluation criteria in solid tumours: revised RECIST guideline (version 1.1). *Eur J Cancer.* 2009;45(2):228-247.
8. Nishino M, Giobbie-Hurder A, Gargano M, Suda M, Ramaiya NH, Hodi FS. Developing a common language for tumor response to immunotherapy: immune-related response criteria using unidimensional measurements. *Clin Cancer Res.* 2013;19(14):3936-3943.
9. Lee JH, Long GV, Menzies AM, et al. Association Between Circulating Tumor DNA and Pseudoprogression in Patients With Metastatic Melanoma Treated With Anti-Programmed Cell Death 1 Antibodies. *JAMA Oncol.* 2018;4(5):717-721.
10. Champiat S, Ferrara R, Massard C, et al. Hyperprogressive disease: recognizing a novel pattern to improve patient management. *Nature Reviews Clinical Oncology.* 2018;15(12):748-762.
11. Chen DS, Mellman I. Elements of cancer immunity and the cancer-immune set point. *Nature.* 2017;541(7637):321-330.
12. McIlroy D, Cartron PF, Tuffery P, et al. A triple-mutated allele of granzyme B incapable of inducing apoptosis. *Proc Natl Acad Sci U S A.* 2003;100(5):2562-2567.
13. Horn L, Spigel DR, Vokes EE, et al. Nivolumab Versus Docetaxel in Previously Treated Patients With Advanced Non-Small-Cell Lung Cancer: Two-Year Outcomes From Two Randomized, Open-Label, Phase III Trials (CheckMate 017 and CheckMate 057). *J Clin Oncol.* 2017;35(35):3924-3933.
14. George S, Miao D, Demetri GD, et al. Loss of PTEN Is Associated with Resistance to Anti-PD-1 Checkpoint Blockade Therapy in Metastatic Uterine Leiomyosarcoma. *Immunity.* 2017;46(2):197-204.
15. Peng W, Chen JQ, Liu C, et al. Loss of PTEN Promotes Resistance to T Cell-Mediated Immunotherapy. *Cancer Discov.* 2016;6(2):202-216.

16. Locke FL, Zha YY, Zheng Y, Driessens G, Gajewski TF. Conditional deletion of PTEN in peripheral T cells augments TCR-mediated activation but does not abrogate CD28 dependency or prevent anergy induction. *J Immunol.* 2013;191(4):1677-1685.
17. Zhao X IV, Gopalakrishnan M, Shen J, Feng Y, Statkevich P. A model-based exposure–response (ER) assessment of a nivolumab 4-weekly (Q4W) dosing schedule across multiple tumor types. 2017;Proceedings of the AACR Annual Meeting. Apr 1–5.
18. Zhao X, Suryawanshi S, Hruska M, et al. Assessment of nivolumab benefit-risk profile of a 240-mg flat dose relative to a 3-mg/kg dosing regimen in patients with advanced tumors. *Ann Oncol.* 2017;28(8):2002-2008.
19. Postel-Vinay S, Aspeslagh S, Lanoy E, Robert C, Soria JC, Marabelle A. Challenges of phase 1 clinical trials evaluating immune checkpoint-targeted antibodies. *Ann Oncol.* 2016;27(2):214-224.
20. Yakes FM, Chinratanalab W, Ritter CA, King W, Seelig S, Arteaga CL. Herceptin-induced inhibition of phosphatidylinositol-3 kinase and Akt Is required for antibody-mediated effects on p27, cyclin D1, and antitumor action. *Cancer Res.* 2002;62(14):4132-4141.
21. Azzopardi N, Lecomte T, Ternant D, et al. Cetuximab pharmacokinetics influences progression-free survival of metastatic colorectal cancer patients. *Clin Cancer Res.* 2011;17(19):6329-6337.
22. Topalian SL, Hodi FS, Brahmer JR, et al. Safety, activity, and immune correlates of anti-PD-1 antibody in cancer. *N Engl J Med.* 2012;366(26):2443-2454.
23. Niemeijer AN, Leung D, Huisman MC, et al. Whole body PD-1 and PD-L1 positron emission tomography in patients with non-small-cell lung cancer. *Nat Commun.* 2018;9(1):4664.
24. Diggs LP, Hsueh EC. Utility of PD-L1 immunohistochemistry assays for predicting PD-1/PD-L1 inhibitor response. *Biomark Res.* 2017;5:12.
25. Wei SC, Levine JH, Cogdill AP, et al. Distinct Cellular Mechanisms Underlie Anti-CTLA-4 and Anti-PD-1 Checkpoint Blockade. *Cell.* 2017;170(6):1120-1133 e1117.
26. Kamphorst AO, Pillai RN, Yang S, et al. Proliferation of PD-1+ CD8 T cells in peripheral blood after PD-1-targeted therapy in lung cancer patients. *Proc Natl Acad Sci U S A.* 2017;114(19):4993-4998.
27. Wieland A, Kamphorst AO, Adsay NV, et al. T cell receptor sequencing of activated CD8 T cells in the blood identifies tumor-infiltrating clones that expand after PD-1 therapy and radiation in a melanoma patient. *Cancer Immunol Immunother.* 2018;67(11):1767-1776.
28. Tanizaki J, Haratani K, Hayashi H, et al. Peripheral Blood Biomarkers Associated with Clinical Outcome in Non-Small Cell Lung Cancer Patients Treated with Nivolumab. *J Thorac Oncol.* 2018;13(1):97-105.
29. Mezquita L, Auclin E, Ferrara R, et al. Association of the Lung Immune Prognostic Index With Immune Checkpoint Inhibitor Outcomes in Patients With Advanced Non-Small Cell Lung Cancer. *JAMA Oncol.* 2018;4(3):351-357.
30. Gebhardt C, Sevko A, Jiang H, et al. Myeloid Cells and Related Chronic Inflammatory Factors as Novel Predictive Markers in Melanoma Treatment with Ipilimumab. *Clin Cancer Res.* 2015;21(24):5453-5459.

31. Kitano S, Postow MA, Ziegler CG, et al. Computational algorithm-driven evaluation of monocytic myeloid-derived suppressor cell frequency for prediction of clinical outcomes. *Cancer Immunol Res.* 2014;2(8):812-821.
32. Martens A, Wistuba-Hamprecht K, Geukes Foppen M, et al. Baseline Peripheral Blood Biomarkers Associated with Clinical Outcome of Advanced Melanoma Patients Treated with Ipilimumab. *Clin Cancer Res.* 2016;22(12):2908-2918.
33. Meyer C, Cagnon L, Costa-Nunes CM, et al. Frequencies of circulating MDSC correlate with clinical outcome of melanoma patients treated with ipilimumab. *Cancer Immunol Immunother.* 2014;63(3):247-257.
34. Nonomura Y, Otsuka A, Nakashima C, et al. Peripheral blood Th9 cells are a possible pharmacodynamic biomarker of nivolumab treatment efficacy in metastatic melanoma patients. *Oncoimmunology.* 2016;5(12):e1248327.
35. Weide B, Martens A, Hassel JC, et al. Baseline Biomarkers for Outcome of Melanoma Patients Treated with Pembrolizumab. *Clin Cancer Res.* 2016;22(22):5487-5496.
36. Huang AC, Postow MA, Orlowski RJ, et al. T-cell invigoration to tumour burden ratio associated with anti-PD-1 response. *Nature.* 2017;545(7652):60-65.
37. Krieg C, Nowicka M, Guglietta S, et al. High-dimensional single-cell analysis predicts response to anti-PD-1 immunotherapy. *Nat Med.* 2018;24(2):144-153.
38. Zhou J, Mahoney KM, Giobbie-Hurder A, et al. Soluble PD-L1 as a Biomarker in Malignant Melanoma Treated with Checkpoint Blockade. *Cancer Immunol Res.* 2017;5(6):480-492.
39. Costantini A, Julie C, Dumenil C, et al. Predictive role of plasmatic biomarkers in advanced non-small cell lung cancer treated by nivolumab. *Oncoimmunology.* 2018;7(8):e1452581.
40. Chen G, Huang AC, Zhang W, et al. Exosomal PD-L1 contributes to immunosuppression and is associated with anti-PD-1 response. *Nature.* 2018;560(7718):382-386.
41. Del Re M, Marconcini R, Pasquini G, et al. PD-L1 mRNA expression in plasma-derived exosomes is associated with response to anti-PD-1 antibodies in melanoma and NSCLC. *Br J Cancer.* 2018;118(6):820-824.
42. Zhang Z, Li Y, Yan X, et al. Pretreatment lactate dehydrogenase may predict outcome of advanced non small-cell lung cancer patients treated with immune checkpoint inhibitors: A meta-analysis. *Cancer Med.* 2019;8(4):1467-1473.
43. Kazandjian D, Gong Y, Keegan P, Pazdur R, Blumenthal GM. Prognostic Value of the Lung Immune Prognostic Index for Patients Treated for Metastatic Non-Small Cell Lung Cancer. *JAMA Oncol.* 2019;5(10):1481-1485.
44. Lee CK, Man J, Lord S, et al. Checkpoint Inhibitors in Metastatic EGFR-Mutated Non-Small Cell Lung Cancer-A Meta-Analysis. *J Thorac Oncol.* 2017;12(2):403-407.
45. Gettinger S, Choi J, Hastings K, et al. Impaired HLA Class I Antigen Processing and Presentation as a Mechanism of Acquired Resistance to Immune Checkpoint Inhibitors in Lung Cancer. *Cancer Discov.* 2017;7(12):1420-1435.
46. Sade-Feldman M, Jiao YJ, Chen JH, et al. Resistance to checkpoint blockade therapy through inactivation of antigen presentation. *Nat Commun.* 2017;8(1):1136.

47. Le DT, Durham JN, Smith KN, et al. Mismatch repair deficiency predicts response of solid tumors to PD-1 blockade. *Science.* 2017;357(6349):409-413.
48. Hellmann MD, Ciuleanu TE, Pluzanski A, et al. Nivolumab plus Ipilimumab in Lung Cancer with a High Tumor Mutational Burden. *N Engl J Med.* 2018;378(22):2093-2104.
49. Hellmann MD, Callahan MK, Awad MM, et al. Tumor Mutational Burden and Efficacy of Nivolumab Monotherapy and in Combination with Ipilimumab in Small-Cell Lung Cancer. *Cancer Cell.* 2018;33(5):853-861 e854.
50. Rizvi H, Sanchez-Vega F, La K, et al. Molecular Determinants of Response to Anti-Programmed Cell Death (PD)-1 and Anti-Programmed Death-Ligand 1 (PD-L1) Blockade in Patients With Non-Small-Cell Lung Cancer Profiled With Targeted Next-Generation Sequencing. *J Clin Oncol.* 2018;36(7):633-641.
51. Gandara DR, Paul SM, Kowanetz M, et al. Blood-based tumor mutational burden as a predictor of clinical benefit in non-small-cell lung cancer patients treated with atezolizumab. *Nat Med.* 2018;24(9):1441-1448.
52. Rizvi NA, Cho BC, Reinmuth N, et al. Durvalumab With or Without Tremelimumab vs Standard Chemotherapy in First-line Treatment of Metastatic Non-Small Cell Lung Cancer: The MYSTIC Phase 3 Randomized Clinical Trial. *JAMA Oncol.* 2020;6(5):661-674.
53. Hellmann MD, Nathanson T, Rizvi H, et al. Genomic Features of Response to Combination Immunotherapy in Patients with Advanced Non-Small-Cell Lung Cancer. *Cancer Cell.* 2018;33(5):843-852 e844.
54. Sabari JK, Leonardi GC, Shu CA, et al. PD-L1 expression, tumor mutational burden, and response to immunotherapy in patients with MET exon 14 altered lung cancers. *Ann Oncol.* 2018;29(10):2085-2091.
55. Skoulidis F, Goldberg ME, Greenawalt DM, et al. STK11/LKB1 Mutations and PD-1 Inhibitor Resistance in KRAS-Mutant Lung Adenocarcinoma. *Cancer Discov.* 2018;8(7):822-835.
56. Wang Z, Duan J, Cai S, et al. Assessment of Blood Tumor Mutational Burden as a Potential Biomarker for Immunotherapy in Patients With Non-Small Cell Lung Cancer With Use of a Next-Generation Sequencing Cancer Gene Panel. *JAMA Oncol.* 2019;5(5):696-702.
57. Wang Z, Duan J, Wang G, et al. Allele Frequency-Adjusted Blood-Based Tumor Mutational Burden as a Predictor of Overall Survival for Patients With NSCLC Treated With PD-(L)1 Inhibitors. *J Thorac Oncol.* 2020;15(4):556-567.
58. Zhang K, Hong X, Song Z, et al. Identification of Deleterious NOTCH Mutation as Novel Predictor to Efficacious Immunotherapy in NSCLC. *Clin Cancer Res.* 2020;26(14):3649-3661.
59. Rittmeyer A, Barlesi F, Waterkamp D, et al. Atezolizumab versus docetaxel in patients with previously treated non-small-cell lung cancer (OAK): a phase 3, open-label, multicentre randomised controlled trial. *Lancet.* 2017;389(10066):255-265.
60. Jacquelot N, Roberti MP, Enot DP, et al. Predictors of responses to immune checkpoint blockade in advanced melanoma. *Nat Commun.* 2017;8(1):592.

61. Tietze JK, Angelova D, Heppt MV, et al. The proportion of circulating CD45RO(+)CD8(+) memory T cells is correlated with clinical response in melanoma patients treated with ipilimumab. *Eur J Cancer.* 2017;75:268-279.
62. Balatoni T, Mohos A, Papp E, et al. Tumor-infiltrating immune cells as potential biomarkers predicting response to treatment and survival in patients with metastatic melanoma receiving ipilimumab therapy. *Cancer Immunol Immunother.* 2018;67(1):141-151.
63. Duruisseaux M, Martínez-Cardús A, Calleja-Cervantes ME, et al. Epigenetic prediction of response to anti-PD-1 treatment in non-small-cell lung cancer: a multicentre, retrospective analysis. *Lancet Respir Med.* 2018;6(10):771-781.
64. Thommen DS, Koelzer VH, Herzig P, et al. A transcriptionally and functionally distinct PD-1(+) CD8(+) T cell pool with predictive potential in non-small-cell lung cancer treated with PD-1 blockade. *Nat Med.* 2018;24(7):994-1004.
65. Sade-Feldman M, Yizhak K, Bjorgaard SL, et al. Defining T Cell States Associated with Response to Checkpoint Immunotherapy in Melanoma. *Cell.* 2018;175(4):998-1013 e1020.
66. Gide TN, Quek C, Menzies AM, et al. Distinct Immune Cell Populations Define Response to Anti-PD-1 Monotherapy and Anti-PD-1/Anti-CTLA-4 Combined Therapy. *Cancer Cell.* 2019;35(2):238-255 e236.
67. Helmink BA, Reddy SM, Gao J, et al. B cells and tertiary lymphoid structures promote immunotherapy response. *Nature.* 2020;577(7791):549-555.
68. Matson V, Fessler J, Bao R, et al. The commensal microbiome is associated with anti-PD-1 efficacy in metastatic melanoma patients. *Science.* 2018;359(6371):104-108.
69. Chaput N, Lepage P, Coutzac C, et al. Baseline gut microbiota predicts clinical response and colitis in metastatic melanoma patients treated with ipilimumab. *Ann Oncol.* 2019;30(12):2012.
70. Gopalakrishnan V, Spencer CN, Nezi L, et al. Gut microbiome modulates response to anti-PD-1 immunotherapy in melanoma patients. *Science.* 2018;359(6371):97-103.
71. Jerby-Arnon L, Shah P, Cuoco MS, et al. A Cancer Cell Program Promotes T Cell Exclusion and Resistance to Checkpoint Blockade. *Cell.* 2018;175(4):984-997 e924.
72. Kowanetz M, Zou W, Gettinger SN, et al. Differential regulation of PD-L1 expression by immune and tumor cells in NSCLC and the response to treatment with atezolizumab (anti-PD-L1). *Proc Natl Acad Sci U S A.* 2018;115(43):E10119-E10126.
73. Fehrenbacher L, Spira A, Ballinger M, et al. Atezolizumab versus docetaxel for patients with previously treated non-small-cell lung cancer (POPLAR): a multicentre, open-label, phase 2 randomised controlled trial. *Lancet.* 2016;387(10030):1837-1846.
74. Yost KE, Satpathy AT, Wells DK, et al. Clonal replacement of tumor-specific T cells following PD-1 blockade. *Nat Med.* 2019;25(8):1251-1259.
75. Ansel KM, Ngo VN, Hyman PL, et al. A chemokine-driven positive feedback loop organizes lymphoid follicles. *Nature.* 2000;406(6793):309-314.
76. Ribas A, Hamid O, Daud A, et al. Association of Pembrolizumab With Tumor Response and Survival Among Patients With Advanced Melanoma. *Jama.* 2016;315(15):1600-1609.
77. Diem S, Kasenda B, Spain L, et al. Serum lactate dehydrogenase as an early marker for outcome in patients treated with anti-PD-1 therapy in metastatic melanoma. *Br J Cancer.* 2016;114(3):256-261.

78. Kelderman S, Heemskerk B, van Tinteren H, et al. Lactate dehydrogenase as a selection criterion for ipilimumab treatment in metastatic melanoma. *Cancer Immunol Immunother.* 2014;63(5):449-458.
79. Bagley SJ, Kothari S, Aggarwal C, et al. Pretreatment neutrophil-to-lymphocyte ratio as a marker of outcomes in nivolumab-treated patients with advanced non-small-cell lung cancer. *Lung Cancer.* 2017;106:1-7.
80. Diem S, Schmid S, Krapf M, et al. Neutrophil-to-Lymphocyte ratio (NLR) and Platelet-to-Lymphocyte ratio (PLR) as prognostic markers in patients with non-small cell lung cancer (NSCLC) treated with nivolumab. *Lung Cancer.* 2017;111:176-181.
81. Kiriu T, Yamamoto M, Nagano T, et al. The time-series behavior of neutrophil-to-lymphocyte ratio is useful as a predictive marker in non-small cell lung cancer. *PLoS One.* 2018;13(2):e0193018.
82. Yáñez-Mó M, Siljander PR, Andreu Z, et al. Biological properties of extracellular vesicles and their physiological functions. *J Extracell Vesicles.* 2015;4:27066.
83. Rizvi NA, Hellmann MD, Snyder A, et al. Cancer immunology. Mutational landscape determines sensitivity to PD-1 blockade in non-small cell lung cancer. *Science.* 2015;348(6230):124-128.
84. Krieger T, Pearson I, Bell J, Doherty J, Robbins P. Targeted literature review on use of tumor mutational burden status and programmed cell death ligand 1 expression to predict outcomes of checkpoint inhibitor treatment. *Diagn Pathol.* 2020;15(1):6.
85. Dong ZY, Zhong WZ, Zhang XC, et al. Potential Predictive Value of TP53 and KRAS Mutation Status for Response to PD-1 Blockade Immunotherapy in Lung Adenocarcinoma. *Clin Cancer Res.* 2017;23(12):3012-3024.
86. Wang Z, Zhao J, Wang G, et al. Comutations in DNA Damage Response Pathways Serve as Potential Biomarkers for Immune Checkpoint Blockade. *Cancer Res.* 2018;78(22):6486-6496.
87. Govindan R, Ding L, Griffith M, et al. Genomic landscape of non-small cell lung cancer in smokers and never-smokers. *Cell.* 2012;150(6):1121-1134.
88. Rudin CM, Avila-Tang E, Harris CC, et al. Lung cancer in never smokers: molecular profiles and therapeutic implications. *Clin Cancer Res.* 2009;15(18):5646-5661.
89. Cho BC. Abstract CT084: Relationship between STK11 and KEAP1 mutational status and efficacy in KEYNOTE-042: pembrolizumab monotherapy versus platinum-based chemotherapy as first-line therapy for PD-L1-positive advanced NSCLC. *Proceedings: AACR Annual Meeting 2020; April 27-28, 2020 and June 22-24, 2020; Philadelphia, PA.* 2020.
90. Papillon-Cavanagh S, Doshi P, Dobrin R, Szustakowski J, Walsh AM. STK11 and KEAP1 mutations as prognostic biomarkers in an observational real-world lung adenocarcinoma cohort. *ESMO Open.* 2020;5(2).
91. Bojesen SE, Timpson N, Relton C, Davey Smith G, Nordestgaard BG. AHRR (cg05575921) hypomethylation marks smoking behaviour, morbidity and mortality. *Thorax.* 2017;72(7):646-653.
92. Vétizou M, Pitt JM, Daillère R, et al. Anticancer immunotherapy by CTLA-4 blockade relies on the gut microbiota. *Science.* 2015;350(6264):1079-1084.

93. Chalabi M, Cardona A, Nagarkar DR, et al. Efficacy of chemotherapy and atezolizumab in patients with non-small-cell lung cancer receiving antibiotics and proton pump inhibitors: pooled post hoc analyses of the OAK and POPLAR trials. *Ann Oncol*. 2020;31(4):525-531.
94. Detterbeck FC, Boffa DJ, Kim AW, Tanoue LT. The Eighth Edition Lung Cancer Stage Classification. *Chest*. 2017;151(1):193-203.
95. Kappen TH, van Klei WA, van Wolfswinkel L, Kalkman CJ, Vergouwe Y, Moons KGM. Evaluating the impact of prediction models: lessons learned, challenges, and recommendations. *Diagn Progn Res*. 2018;2:11.

PART V

V

Appendix

NEDERLANDSE SAMENVATTING

Immunotherapie is een nieuwe methode van anti-kanker behandeling en neemt de laatste jaren een steeds belangrijkere plek in bij de behandeling van verschillende soorten tumoren. Immuun checkpoint remmers zijn een vorm van immunotherapie en hebben als doel om de tolerantie van het immuunsysteem (afweersysteem) naar tumorcellen te doorbreken. Hierdoor worden tumorcellen weer herkend en opgeruimd door het eigen lichaam. Hoewel de geregistreerde immuun checkpoint remmers een overlevingsvoordeel oplevert vergeleken met alternatieve therapie zoals chemotherapie, reageert maar een deel van de patiënten goed op deze vorm van therapie. Daarnaast heeft helaas een deel van de patiënten bijwerkingen, welke het resultaat zijn van een overactief en ontremd immuunsysteem. De centrale vraagstelling in dit proefschrift is om de anti-kanker behandeling met immuun checkpoint remmers te personaliseren. Oftewel, om de juiste patiënt op de juiste manier te behandelen. Hierbij is er ten eerste gekeken naar de farmacokinetiek van patiënten met gemetastaseerde (uitgezaaide) kanker. De farmacokinetiek omschrijft hoe een geneesmiddel zich in patiënten gedraagt en hoe het verschil tussen patiënten kan worden verklaard. Daarnaast beschrijft dit proefschrift verschillende onderzoeken naar de gerichte behandeling bij patiënten met gemetastaseerde longkanker en melanoom, dus hoe de juiste patiënt geselecteerd kan worden voor de juiste behandeling. Hierbij wordt ook een literatuuroverzicht gegeven over de belangrijkste ontwikkelingen (**Hoofdstuk 1** en **17**).

Immuun checkpoint remmers worden gegeven via een intraveneus infuus, waarna het middel in de bloedcirculatie terecht komt en langzaam de bloedspiegel in de tijd zal dalen tot een opvolgende gift. Aanvankelijk werd dit gedoseerd op basis van gewicht van de patiënt, en tegenwoordig wordt ook een vaste dosering gegeven. Bij de eerste registratiestudies werd gezien dat het geneesmiddel al bij een lage dosering in staat is om effectief te zijn, en dat het niet uitmaakt of een hogere dosis wordt gegeven. Ook blijken bijwerkingen niet vaker op te treden bij een hoge dosering dan bij een lagere dosering. Omdat de kosten van dit geneesmiddel niet gering zijn, zijn er bij een groot aantal patiënten die regulier worden behandeld opeenvolgende spiegelbepalingen gedaan om de farmacokinetiek te onderzoeken. In een eerste onderzoek werd er een relatie gevonden tussen de blootstelling (hoogte van de bloedspiegel) en de effectiviteit van immuun checkpoint remmers (**Hoofdstuk 2**), hoewel in registratiestudies nooit een dosis-respons relatie werd beschreven. We stellen dat dit mogelijk het gevolg is van veranderde afbraak van het geneesmiddel, waarvoor overtuigende bewijslast kwam bij patiënten die behandeld waren met verschillende doseringen. Om beter te snappen waar de verschillen tussen patiënten kunnen worden verklaard, hebben we een farmacokinetiek model ontwikkeld op basis van opeenvolgende spiegelbepalingen in honderden patiënten. De afbraak van het geneesmiddel bleek afhankelijk te zijn van specifieke patiëntkarakteristieken, mogelijk verwant aan kanker cachexie – een metabole

staat van afbraak door gevorderde ziekte (**Hoofdstuk 3** en **4**). Deze kennis kan worden gebruikt voor het optimaliseren van huidige dosis strategieën.

Hoewel de invloed en oorzaak van kanker cachexie vooral gerelateerd zal zijn aan het natuurlijk beloop van de ziekte, zijn de vereiste onderdelen voor effectiviteit van immunotherapie waarschijnlijk 1) de eigenschappen van de tumorcellen, 2) zijn interactie met de omgeving en 3) de staat van het immuunsysteem van de patiënt. In dit proefschrift dragen we bij aan de groeiende kennis over de verschillende mechanismen die een rol spelen bij het wel of niet reageren op immunotherapie. Specifieke eiwitprofielen kunnen worden herkend in bloed van patiënten met gemetastaseerd longkanker die niet reageren op immunotherapie, welke gerelateerd lijken te zijn aan kanker cachexie (**Hoofdstuk 5**) en acute ontsteking (**Hoofdstuk 6**). Daarnaast leidt het combineren van verschillende eigenschappen van tumorcellen en zijn interactie met de omgeving, tot een betere voorspelling van de effectiviteit bij patiënten met longkanker (**Hoofdstuk 8**). Wij combineerden hier een in de kliniek gebruikte voorspeller van effectiviteit na immunotherapie. Deze voorspeller combineert het percentage tumorcellen die positief zijn voor het eiwit (PD-L1) dat bindt aan de immuun checkpoint (PD-1) met de hoeveelheid mutaties van de tumorcellen, het vermogen om tumoreiwitten te presenteren (klassiek HLA) en de aanwezigheid van immuuncellen ($CD8^+$ T cellen). In een bijkomende moleculaire analyse wordt het belang van verminderde werkzaamheid of afwezigheid van presentatie van eiwitten aan immuun cellen onderstreept, wat essentieel lijkt te zijn voor beide subtypes van longkanker (**Hoofdstuk 10**). Belangrijk hierbij is dat de interactie tussen tumorcellen en immuun cellen fysiek moet kunnen plaatsvinden. Deze interactie zou kunnen worden belemmerd door bindweefselvorming in de tumor, ook wel immuun-exclusie genoemd. We zien dat dit proces gerelateerd is aan verminderde werkzaamheid van immunotherapie bij patiënten met gemetastaseerd melanoom, waarbij componenten hiervan in het bloed eenvoudig te meten zijn (**Hoofdstuk 13**). Bijdragend is ook de staat van het immuunsysteem in bloed (**Hoofdstuk 11** en **14**), en ook erfelijke eigenschappen van de patiënt (**Hoofdstuk 9** en **12**). Deze erfelijke eigenschappen lijken voor een groot deel overlappend te zijn voor de immuunrespons van verschillende tumortypes zoals longkanker of melanoom, maar er zijn ook zeker verschillen in de factoren die bepalend zijn voor het wel of niet reageren van immunotherapie. Wij zagen dat variaties in het DNA van patiënten in een gen, welke codeert voor een eiwit dat wordt uitgescheiden door immuun cellen om tumorcellen te doden (granzyme B), bepalend is voor de immuun respons bij zowel longkanker als melanoom na immunotherapie. Echter, de variatie in het DNA binnen een gen die codeert voor de immuun checkpoint PD-1 lijkt vooral een rol te spelen bij melanoom.

Aanvullend vonden wij dat radiologische evaluatie van tumoren wordt bemoeilijkt door verschillende groei patronen welke kenmerkend zijn voor immunotherapie, vergeleken met alternatieve therapieën. Bij patiënten met gemetastaseerd longkanker is de ruimtelijke groei van tumoren voorafgaand en na start van de behandeling met immuun

checkpoint remmers bepaald (**Hoofdstuk 7**). Groeipatronen van tumoren rond de start blijken sterk gerelateerd aan overleving van patiënten na immunotherapie, met name bij de patiënten met sterk versnelde tumorgroei (hyperprogressie), en dragen bij aan de huidige methoden van responsevaluatie. Daarnaast constateerden wij dat het optreden van bijwerkingen van de schildklier na immunotherapie geassocieerd is met de vorming van antistoffen en de effectiviteit (**Hoofdstuk 15**). Het gevaar van een overactief en ontremd immuunsysteem na starten van immunotherapie is daarnaast vooral ook een bedreiging bij patiënten met een orgaantransplantatie. In een casus bespreking van een patiënt na niertransplantatie met gemetastaseerd melanoom beschreven we dit fenomeen en het meten van DNA van de donor in bloed leek hierbij geschikt voor vroege detectie van afstoting van de niertransplantatie (**Hoofdstuk 16**).

LIST OF PUBLICATIONS

D.P. Hurkmans, E.M.E. Verdegaal , S.A. Hogan , R. de Wijn, L. Hovestad, D.M.A. van den Heuvel, R. Ruijtenbeek, M.J.P. Welters, M. van Brakel, E.A. Basak, H.M. Pinedo , C.H.J. Lamers, H.J.G. van de Werken, J.P. Groten, R. Debets , M.P. Levesque , R. Dummer, E. Kapiteijn, R.H.J. Mathijssen, J.G.J.V. Aerts, S.H. van der Burg.
Blood-based kinase activity profiling: a potential predictor of response to immune checkpoint inhibition in metastatic cancer.
J Immunother Cancer (Dec 2020).

L. Cantini, F. Pecci, D.P. Hurkmans, R.A. Belderbos, A. Lanese, C. Copparoni, S. Aerts, R. Cornelissen, D.W. Dumoulin, I. Fiordoliva, S. Rinaldi, J.G.J.V. Aerts, R. Berardi.
High-intensity statins are associated with improved clinical activity of PD-1 inhibitors in malignant pleural mesothelioma and advanced non-small cell lung cancer patients.
Eur J Cancer (Dec 2020).

D.P. Hurkmans, C. Jensen, S.L.W. Koolen, J. Aerts, M.A. Karsdal, R.H.J. Mathijssen, N. Willumsen.
Blood-based extracellular matrix biomarkers are correlated with clinical outcome after PD-1 inhibition in patients with metastatic melanoma.
J Immunother Cancer (Oct 2020).

E.M.W. van de Garde, L.R. van Bedaf, D.P. Hurkmans, M.M. van den Heuvel.
Antibiotic use and reduced effectiveness of second-line immunotherapy for lung cancer: all the time or just at the start of treatment?
Ann Oncol (Sep 2020).

D.P. Hurkmans, M. Tamminga, B. van Es, T. Peters T, W. Karman W, R.T.A. van Wijck, P.J. van der Spek, T. Tauber, M. Los, A. van Schetsen, T. Vu, T.J.N. Hiltermann, E. Schuuring, J.G.J.V. Aerts, S. Chen, H.J.M. Groen.
Molecular data show conserved DNA locations distinguishing lung cancer subtypes and **regulation of immune genes.**
Lung Cancer (Aug 2020).

M. Muller, K. Hummelink, D.P. Hurkmans, A.N. Niemeijer, K. Monkhorst, J. Roder, C. Oliveira, H. Roder, J.G. Aerts, E.F. Smit.
A Serum Protein Classifier Identifying Patients with Advanced Non-Small Cell Lung Cancer Who Derive Clinical Benefit from Treatment with Immune Checkpoint Inhibitors.
Clin Cancer Res (Oct 2020).

D.P. Hurkmans, E.A. Basak, N. Schepers, E. Oomen-De Hoop, C.H. van der Leest, S. el Bouazzaoui, S. Bins, S.L.W. Koolen, S. Sleijfer, A.A.M. van der Veldt, R. Debets, R.H.N. van Schaik, J.G.J.V. Aerts, R.H.J. Mathijssen.
Granzyme B is correlated with clinical outcome after PD-1 blockade in patients with stage IV non-small-cell lung cancer.
J Immunother Cancer (May 2020).

E.A. Basak, J.W.M. van der Meer, D.P. Hurkmans, M.W.J. Schreurs, E. Oomen-de Hoop, A.A.M. van der Veldt, S. Bins, A. Joosse, S.L.W. Koolen, R. Debets, R.P. Peeters, J.G.J.V. Aerts, R.H.J. Mathijssen, M. Medici.
Overt Thyroid Dysfunction and Anti-Thyroid Antibodies Predict Response to Anti-PD-1 Immunotherapy in Cancer Patients.
Thyroid (Jul 2020).

D.P. Hurkmans, M.E. Kuipers, J. Smit, R. van Marion, R.H.J. Mathijssen, P.E. Postmus, P.S. Hiemstra, J.G.J.V. Aerts, J.H. von der Thüsen, S.H. van der Burg.
Tumor Mutational Load, CD8+ T Cells, Expression of PD-L1 and HLA Class I to Guide Immunotherapy Decisions in NSCLC Patients.
Cancer Immunol Immunother (May 2020).

D.M.H.J. ten Berge, D.P. Hurkmans, I. den Besten, J.S. Kloover, R.H.J. Mathijssen, R.J.E.M.A. Debets, E.F. Smit, J.G.J.V. Aerts.
Tumour Growth Rate as a Tool for Response Evaluation During Pd-1 Treatment for Non-Small Cell Lung Cancer: A Retrospective Analysis.
ERJ Open Res (Oct 2019).

D.P. Hurkmans, E.A. Basak, T. van Dijk, D. Mercieca, M.W.J. Schreurs, A.J.M. Wijkhuijs, S. Bins, E. Oomen-de Hoop, R. Debets, M. Joerger, A. Odink, A.A.M. van der Veldt, C.H. van der Leest, J.G.J.V. Aerts, R.H.J. Mathijssen, S.L.W. Koolen.
A Prospective Cohort Study on the Pharmacokinetics of Nivolumab in Metastatic Non-Small **Cell Lung Cancer, Melanoma, and Renal Cell Cancer Patients**.
J Immunother Cancer (Jul 2019).

D.P. Hurkmans, J.G.H.P. Verhoeven, K. de Leur, K. Boer, A. Joosse, C.C. Baan, J.H. von der Thüsen, R.H.N. van Schaik, R.H.J. Mathijssen, A.A.M. van der Veldt, D.A. Hesselink.
Donor-Derived Cell-Free DNA Detects Kidney Transplant Rejection During Nivolumab Treatment.
J Immunother Cancer (Jul 2019).

A. Kunert, E.A. Basak, D.P. Hurkmans, H.E. Balcioglu, Y. Klaver, M. van Brakel, A.A.M. Oostvogels, C.H.J. Lamers, S. Bins, S.L.W. Koolen, A.A.M. van der Veldt, S. Sleijfer, R.H.J. Mathijssen, J.G.J.V. Aerts, R. Debets.
CD45RA+ CCR7- CD8+ **T Cells Lacking Co-Stimulatory Receptors Demonstrate Enhanced Frequency in Peripheral Blood of NSCLC Patients Responding to Nivolumab**.
J Immunother Cancer (Jun 2019).

K.G.A.M. Hussaarts, D.P. Hurkmans, E. Oomen-de Hoop, L.J. van Harten, S. Berghuis, R.J. van Alphen, L.E.A. Spierings, Q.C. van Rossum-Schornagel, M.B. Vastbinder, R.H.N. van Schaik, T. van Gelder, A. Jager, R.W.F. van Leeuwen, R.H.J. Mathijssen.
Impact of Curcumin (with or without Piperine) on the Pharmacokinetics of Tamoxifen.
Cancers (Mar 2019).

E.A. Basak, S.L.W. Koolen, D.P. Hurkmans, M.W.J. Schreurs, S. Bins, E. Oomen-de Hoop, A.J.M. Wijkhuijs, I.D. Besten, S. Sleijfer, R. Debets, A.A.M. van der Veldt, J.G.J.V. Aerts, R.H.J. Mathijssen.
Correlation between nivolumab exposure and treatment outcomes in non-small-cell lung cancer.
Eur J Cancer (Mar 2019).

AUTHOR AFFILIATIONS

Joachim G.J.V. Aerts	Department of Pulmonary Medicine, Erasmus University Medical Center, Rotterdam, The Netherlands
Carla C. Baan	Department of Internal Medicine, Erasmus University Medical Center, Rotterdam, The Netherlands
Hayri E. Balcioglu	Department of Medical Oncology, Erasmus University Medical Center, Rotterdam, The Netherlands
Edwin A. Basak	Department of Medical Oncology, Erasmus University Medical Center, Rotterdam, The Netherlands
Deirdre M.H.J. ten Berge	Department of Radiology, Elisabeth-TweeSteden Hospital, Tilburg, The Netherlands
Ilse den Besten	Department of Pulmonary Medicine, Erasmus University Medical Center, Rotterdam, The Netherlands
Jean-Noël Billaud	Department of Digital Insights, QIAGEN, Redwood City, California
Sander Bins	Department of Medical Oncology, Erasmus University Medical Center, Rotterdam, The Netherlands
Karin Boer	Department of Internal Medicine, Erasmus University Medical Center, Rotterdam, The Netherlands
Thierry P.P. van den Bosch	Department of Pathology, Erasmus University Medical Center, Rotterdam, The Netherlands
Samira El Bouazzaoui	Department of Clinical Chemistry, Erasmus University Medical Center, Rotterdam, The Netherlands
Mandy van Brakel	Department of Medical Oncology, Erasmus University Medical Center, Rotterdam, The Netherlands
Sjoerd H. van der Burg	Department of Medical Oncology, Leiden University Medical Center, Leiden, The Netherlands
Sissy Chen	PricewaterhouseCoopers Advisory NV, Amsterdam, The Netherlands
Reno E.M.A. Debets	Department of Medical Oncology, Erasmus University Medical Center, Rotterdam, The Netherlands

Tanja van Dijk	Department of Medical Oncology, Erasmus University Medical Center, Rotterdam, The Netherlands
Willem A. Dik	Department of Immunology, Erasmus University Medical Center, Rotterdam, The Netherlands
Reinhard Dummer	Department of Dermatology, University Hospital Zurich, University of Zurich, Zurich, Switzerland
Bram van Es	Department of Clinical Chemistry and Haematology, University Medical Center Utrecht, Utrecht, The Netherlands
Harry J.M. Groen	Department of Pulmonary Diseases, University Medical Center Groningen, Groningen, The Netherlands
John P. Groten	PamGene International B.V., 's-Hertogenbosch, The Netherlands
Dennis A. Hesselink	Department of Internal Medicine, Erasmus University Medical Center, Rotterdam, The Netherlands
Dianne M.A. van den Heuvel	PamGene International B.V., 's-Hertogenbosch, The Netherlands
Sabrina A. Hogan	Department of Dermatology, University Hospital Zurich, University of Zurich, Zurich, Switzerland
Lies Hovestad	PamGene International B.V., 's-Hertogenbosch, The Netherlands
Pieter S. Hiemstra	Department of Pulmonology, Leiden University Medical Center, Leiden, The Netherlands
Jeroen N. Hiltermann	Department of Pulmonary Diseases, University Medical Center Groningen, Groningen, The Netherlands
Karlijn Hummerlink	Department of Pathology, Netherlands Cancer Institute, Amsterdam, the Netherlands
Christina Jensen	Nordic Bioscience, Herlev, Denmark
Markus Joerger	Department of Medical Oncology and Hematology, Cantonal Hospital, St. Gallen, Switzerland
Karlijn de Joode	Department of Medical Oncology, Erasmus University Medical Center, Rotterdam, The Netherlands
Arjen Joosse	Department of Medical Oncology, Erasmus University Medical Center, Rotterdam, The Netherlands
Ellen Kapiteijn	Department of Medical Oncology, Leiden University Medical Center, Leiden, The Netherlands

Wouter Karman	PricewaterhouseCoopers Advisory NV, Amsterdam, The Netherlands
Morten Asser Karsdal	Nordic Bioscience, Herlev, Denmark
Peter D. Katsikis	Department of Immunology, Erasmus University Medical Center, Rotterdam, The Netherlands
Yarne Klaver	Department of Medical Oncology, Erasmus University Medical Center, Rotterdam, The Netherlands
Jeroen S. Kloover	Department of Pulmonary Diseases, Elisabeth-TweeSteden Hospital, Tilburg, The Netherlands
Birgit C.P. Koch	Department of Hospital Pharmacy, Erasmus University Medical Center, Rotterdam, The Netherlands
Stijn L.W. Koolen	Departments of Medical Oncology and Hospital Pharmacy, Erasmus University Medical Center, Rotterdam, The Netherlands
Merian E. Kuipers	Department of Pulmonology, Leiden University Medical Center, Leiden, The Netherlands
Andre Kunert	Department of Medical Oncology, Erasmus University Medical Center, Rotterdam, The Netherlands
Ayoub Lalouti	Department of Medical Oncology, Erasmus University Medical Center, Rotterdam, The Netherlands
Cor H.J. Lamers	Department of Medical Oncology, Erasmus University Medical Center, Rotterdam, The Netherlands
Cor H. van der Leest	Department of Pulmonology, Amphia Hospital, Breda, The Netherlands
Kitty de Leur	Department of Internal Medicine, Erasmus University Medical Center, Rotterdam, The Netherlands
Mitchell P. Levesque	Department of Dermatology, University Hospital Zurich, University of Zurich, Zurich, Switzerland
Maureen Los	PricewaterhouseCoopers Advisory NV, Amsterdam, The Netherlands
Ronald van Marion	Department of Pathology, Erasmus University Medical Center, Rotterdam, The Netherlands
Ron H.J. Mathijssen	Department of Medical Oncology, Erasmus University Medical Center, Rotterdam, The Netherlands

Marco Medici	Department of Internal Medicine, Erasmus University Medical Center, Rotterdam, The Netherlands
Jan W.M. van der Meer	Department of Medical Oncology, Erasmus University Medical Center, Rotterdam, The Netherlands
Darlene Mercieca	Department of Pulmonary Medicine, Erasmus University Medical Center, Rotterdam, The Netherlands
Kim Monkhorst	Department of Pathology, Netherlands Cancer Institute, Amsterdam, the Netherlands
Mirte Muller	Department of Thoracic Oncology, Netherlands Cancer Institute, Amsterdam, the Netherlands
Anna-Larissa Niemeijer	Department of Pulmonary Diseases, VU Medical Center, Amsterdam, the Netherlands
Arlette Odink	Department of Radiology & Nuclear Medicine, Erasmus University Medical Center, Rotterdam, The Netherlands
Carlos Oliviera	Biodesix, Boulder, Colorado
Esther Oomen-de Hoop	Department of Medical Oncology, Erasmus University Medical Center, Rotterdam, The Netherlands
Astrid A.M. Oostvogels	Department of Medical Oncology, Erasmus University Medical Center, Rotterdam, The Netherlands
Robin P. Peeters	Department of Internal Medicine, Erasmus University Medical Center, Rotterdam, The Netherlands
Tom Peters	PricewaterhouseCoopers Advisory NV, Amsterdam, The Netherlands
Herbert M. Pinedo	PamGene International B.V., 's-Hertogenbosch, The Netherlands
Piet E. Postmus	Department of Pulmonology, Leiden University Medical Center, Leiden, The Netherlands
Lisanne Putter	Department of Medical Oncology, Erasmus University Medical Center, Rotterdam, The Netherlands
Heinrich Roder	Biodesix, Boulder, Colorado
Joanna Roder	Biodesix, Boulder, Colorado
Rob Ruijtenbeek	GenMab B.V., Utrecht, The Netherlands

Sebastiaan D.T. Sassen	Department of Hospital Pharmacy, Erasmus University Medical Center, Rotterdam, The Netherlands
Ron H.N. van Schaik	Department of Clinical Chemistry, Erasmus University Medical Center, Rotterdam, The Netherlands
Nina Schepers	Department of Medical Oncology, Erasmus University Medical Center, Rotterdam, The Netherlands
Anouk van Schetsen	PricewaterhouseCoopers Advisory NV, Amsterdam, The Netherlands
Marco W.J. Schreurs	Department of Immunology, Erasmus University Medical Center, Rotterdam, The Netherlands
Ed Schuuring	Department of Pathology and Medical Biology, University Medical Center Groningen, Groningen, The Netherlands
Stefan Sleijfer	Department of Medical Oncology, Erasmus University Medical Center, Rotterdam, The Netherlands
Egbert F. Smit	Department of Thoracic Oncology, Netherlands Cancer Institute, Amsterdam, The Netherlands
Jasper Smit	Department of Pulmonology, Leiden University Medical Center, Leiden, The Netherlands
Peter J. van der Spek	Department of Pathology, Erasmus University Medical Center, Rotterdam, The Netherlands
Menno Tamminga	Department of Pulmonary Diseases, University Medical Center Groningen, Groningen, The Netherlands
Jan H. von der Thüsen	Department of Pathology, Erasmus University Medical Center, Rotterdam, The Netherlands
Tjebbe Tauber	ABN-Amro, Amsterdam, The Netherlands
Astrid A.M. van der Veldt	Department of Medical Oncology, Erasmus University Medical Center, Rotterdam, The Netherlands
Els M.E. Verdegaal	Department of Medical Oncology, Leiden University Medical Center, Leiden, The Netherlands
Jeroen G.H.P. Verhoeven	Department of Internal Medicine, Erasmus University Medical Center, Rotterdam, The Netherlands

Thu Vu	PricewaterhouseCoopers Advisory NV, Amsterdam, The Netherlands
Marij J.P. Welters	Department of Medical Oncology, Leiden University Medical Center, Leiden, The Netherlands
Harmen J.G. van de Werken	Department of Urology, Erasmus University Medical Center, Rotterdam, The Netherlands
Rogier T.A. van Wijck	Department of Pathology, Erasmus University Medical Center, Rotterdam, The Netherlands
Annemarie J.M. Wijkhuijs	Department of Clinical Chemistry, Erasmus University Medical Center, Rotterdam, The Netherlands
Rik de Wijn	PamGene International B.V., 's-Hertogenbosch, The Netherlands
Nicholas Willumsen	Nordic Bioscience, Herlev, Denmark
Mirjam de With	Department of Medical Oncology, Erasmus University Medical Center, Rotterdam, The Netherlands

DANKWOORD

Onderzoek doe je nooit alleen, vandaar dat ik veel mensen wil bedanken voor hun hulp en aanmoediging. In het bijzonder geldt dit natuurlijk voor alle patiënten die hebben deelgenomen aan de studie. Ik besef terdege hoe moedig het is om in deze fase van je leven mee te werken aan iets waar je zelf niet direct de vruchten van plukt. De impact van de ziekte is mij eens te meer duidelijk geworden; in mijn persoonlijke leven denk ik aan Peter Limmen (†2019), die in deze periode is overleden ten gevolge van kanker.

Vervolgens wil ik mijn promotoren bedanken. Prof.dr. Mathijssen en prof.dr. Aerts, jullie hebben mij wegwijs gemaakt in de wetenschappelijke wereld en de uitdagingen die hierbij horen. De afgelopen vier jaar heb ik van jullie ontzettend veel geleerd. Kenmerkend voor jullie beiden is de enorme daadkracht. □ Ron, jouw toewijding in het begeleiden van de onderzoeksgroep translationele farmacologie kent geen grenzen en is productief. Personalized medicine is je levenswerk, en ik ben er trots op dat we dit hebben voortgezet in een ook voor jou relatief nieuw veld. Het was ten slotte fantastisch om te zien hoe snel je mijn manuscripten van opmerkingen kon voorzien. Altijd binnen een dag. □ Joachim, je stond echt aan de basis van de snelle veranderingen in de behandelmogelijkheden voor patiënten met longkanker. Je wordt sterk gedreven door wetenschappelijke nieuwsgierigheid, weet degenen met wie je werkt – zo ook mij – te inspireren, en brengt hierdoor de longoncologie op een hoger plan.

Verder wil ik graag de volgende mensen bedanken. □ Dr. Koolen, beste Stijn, dank voor de prettige begeleiding en het speelse gemak waarmee je mij snel op weg hebt kunnen helpen met PK modeling. □ Prof.dr. Debets, dr. Kunert en dr. Lamers, beste Reno, Andre en Cor, dank voor de wetenschappelijke discussies en jullie zorgvuldige inbreng. Prachtig om te zien hoe jullie voorwerk ontzettend relevant is en resulteert in meerdere klinische trials. □ Dr. Van der Veldt, beste Astrid, je begeleiding was voor mij van onschatbare waarde. Dank ook voor alle uren die we samen hebben doorgebracht met het beoordelen van de radiologie. □ Femke, Florence, Bodine, Mirjam, Louwrens, Edwin, Nikki, Koen, Ruben, Marijn, Wesley, Karlijn, Leni, Stefan, Bram en Sanne; zonder jullie zouden de afgelopen jaren lang niet zo gezellig zijn geweest. Bedankt voor de fijne sfeer. Jullie zijn de beste sparringpartners die ik me kan wensen. □ Roelof, dank voor je begeleiding bij de interactiestudie, die helaas buiten dit proefschrift valt. Top dat we al zo veel weekendjes in Limburg in de blubber hebben rondgereden! □ Janneke, Els, Ria en Ingrid, bedankt voor jullie improvisatiekracht om tot een goedlopende logistiek van de Multomab studie te komen in Rotterdam en Breda. □ Dr. Van der Leest, beste Cor, dank voor je aanstekelijke enthousiasme, ideeën en steun van de studie vanuit het Amphia ziekenhuis. □ Beste Kersten, Ayoub, Stan, Nina, Lisanne, Darlene, Wim en Tanja, ik wil jullie bedanken voor de enthousiasme voor verschillende onderdelen van het onderzoek, al dan niet in het kader van een masterscriptie, en al het werk dat jullie mij uit handen konden nemen. Ik heb veel vertrouwen in jullie volgende stappen! □ Inge, Mei, Peter, Bimla, Robert, Carla, Astrid

en Mandy dank voor jullie gezelligheid. Jullie zijn de basis van een goed functionerende onderzoeksgroep en ik heb oneindig veel waardering voor de precisie en betrouwbaarheid van de werkzaamheden. □ Joanne en Bob, ondanks de regen was het super om samen met jullie op congres te gaan in Barcelona.
De leden van de leescommissie wil ik bedanken voor het lezen van het manuscript.
Ik kijk terug op veel bijzondere samenwerkingsverbanden, zowel binnen als buiten het Erasmus MC. Alle betrokken oncologen, longartsen, arts-assistenten, verpleegkundigen van de oncologie en longgeneeskunde, medewerkers van het secretariaat; dank voor jullie hulp! □ Prof.dr. Van der Spek, beste Peter, mede dankzij jou was de hackathon, die je samen met Tjebbe van ABN-Amro organiseerde, een spektakel. Dank ook voor het teamwerk met Menno en Harry van het UMCG, Rogier, Bram, Sissy, Suzanne, Wouter, Tom, Anouk van PwC, en alle andere betrokkenen. □ Prof.dr. Katsikis, Dr. Schreurs, dr. Dik, beste Peter, Marco en Wim van de afdeling Immunologie, bedankt voor het gedeelde enthousiasme voor de kanker immunologie en het schakelen bij nieuwe ideeën. Annemarie, je zorgvuldigheid was hierbij van onmisbare waarde. □ Prof.dr. Van der Burg, dr. Verdegaal en dr. Kapiteijn, beste Sjoerd, Els en Ellen, ik wil jullie bedanken voor onze samenwerking, het voelde goed om zo af en toe weer in het LUMC te zijn waar ik als student heel wat tijd heb doorgebracht. Natuurlijk is er meer in het leven dan alleen werk. Voor alle gezelligheid, wielertochten, mountainbikeroutes, surfsessies, spelmarathons, bieravonden, koffieochtenden, tenniswedstrijdjes etc. wil ik mijn vrienden bedanken. Door al deze oplaadmomenten was ik weer uitgerust en kon ik met nieuwe energie aan de werkweek beginnen. Of ik jullie nu al ken van de middelbare, uit Castricum, mijn studietijd in Leiden, als huisgenoot, uit het buitenland of na mijn studie en of ik je wekelijks of wat minder vaak zie; ik ben stuk voor stuk blij dat je er bent en kijk uit naar alle mooie momenten die nog gaan komen. □ Lieve schoonfamilie, fijn dat we altijd bij elkaar terecht kunnen in een goede sfeer en elkaar in Faucon, Utrecht, Den Haag of Enschede kunnen treffen voor een lange wandeling met de honden, een goed gesprek of beeldhouwsessie in de zomer. Ik waardeer de onuitputtelijke spelletjesenergie van de hele familie en ook het feit dat 'de koude kant' niet verplicht hoeft deel te nemen aan de Beau en Lilly-appgroep (voor extra hondencontent). □ Lieve familie, bedankt voor de fijne basis die we met elkaar hebben en de gedeelde geschiedenis. Ook voor de gezellige momenten die zijn geweest en nog gaan komen in Castricum, Bakkum, vissend aan de pier in Wijk aan Zee of met z'n allen in een huisje in Drenthe zoals afgelopen najaar. Laten we dit soort gezelligheid er met elkaar inhouden. Lieve pap en mam, bedankt voor jullie vertrouwen in mij en aanmoedigingen en jullie interesse in wat ik doe. De basis die jullie mij gegeven hebben helpt mij dagelijks. □ Liefste Linde, ik heb dit boek aan je opgedragen omdat je mijn steun en toeverlaat bent. Ik kijk uit naar alles wat wij nog samen gaan beleven!

PORTFOLIO

Summary of PhD training and teaching		
Name PhD student: Daan Hurkmans		
Erasmus University MC: Dept. of Internal Oncology and Dept. of Pulmonology		
PhD period: 2017-2020		
Promotors: prof. dr. A.H.J. Mathijssen; prof. dr. J.G.J.V. Aerts		
General courses	**Year**	**Workload**
BROK course participation	2018	1.2 ECTS
BROK course self-study assessment	2017	0.3 ECTS
Biostatistical Methods NIHES[1]	2019	2.0 ECTS
Research Integrity	2020	0.3 ECTS
Specific courses		
Workshop on Microsoft Excel 2010: Basic	2017	0.3 ECTS
Workshop on Microsoft Excel 2010: Advanced	2017	0.4 ECTS
Research management for PhD-students & Post docs	2018	1.0 ECTS
Introduction in Graphpad Prism Version 7	2017	0.3 ECTS
Clinical development (Futurelab, Leiden University)	2017	1.0 ECTS
Seminars and workshops		
Training Open Clinica	2018	2.0 ECTS
Department of Pulmonary Medicine Symposia (refereeravonden)	2019-2020	0.4 ECTS
Department of Oncology Symposia (Jonge Oncologen avonden)	2017-2019	0.4 ECTS
Presentations		
Medical oncology research meetings, Erasmus MC	2018+2019	2.0 ECTS
Translational pharmacology meetings, Erasmus MC	2017-2020	2.0 ECTS
Scientific meeting (wetenschapsmiddag), Erasmus MC	2018+2019	0.4 ECTS
ASCO poster presentation, Chicago[2]	2018	0.2 ECTS
ESMO poster presentations, Barcelona[3]	2019	0.4 ECTS
WCLC poster presentations, Barcelona[4]	2019	0.6 ECTS
NVALT oral presentation, Breda[5]	2018	0.2 ECTS
National conferences		
NVKFB conference, Nijmegen[6]	2017	1.0 ECTS
International conferences		
ASCO conference, Chicago	2018	2.0 ECTS
ESMO conference, Barcelona	2019	2.0 ECTS
WCLC, Barcelona	2019	2.0 ECTS
Other		
ERS seminar and chair session, ICM, Paris[7]	2019	0.2 ECTS
Hackathon Lung Challenge, Amsterdam	2019	2.0 ECTS
Peer reviewing (for JCO, Clinical Proteomics, International immunopharmacology, Immunotherapy)	2018-2020	0.8 ECTS
Teaching - Master thesis		
Kersten Landa	2017	1.0 ECTS
Stan Berghuis	2018	1.0 ECTS
Nina Schepers	2018	1.0 ECTS
Ayoub Lalouti	2019	1.0 ECTS
Lisanne Putter	2020	1.0 ECTS

1 Netherlands Institute for Health Sciences
2 American Society of Clinical Oncology
3 European Society of Medical Oncology
4 World Conference on Lung Cancer
5 Nederlandse Vereniging van Artsen voor Longziekten en Tuberculose
6 Nederlandse Vereniging voor Klinische Farmacologie en Biofarmacie
7 Institut du Cerveau et de La Moelle Épinière

CURRICULUM VITAE

Daniël (Daan) Petrus Hurkmans werd geboren op 1 mei 1988 in Castricum, Nederland. In 2006 voltooide hij de middelbare school, richting natuur en gezondheid, natuur en techniek, gymnasium met Latijn als klassieke taal aan het Bonhoeffer college te Castricum. In 2015 behaalde Daan de master Geneeskunde en Biomedische Wetenschappen (Cum Laude) aan Universiteit Leiden te Leiden, waarvan hij een jaar van zijn Biomedische Wetenschappen heeft volbracht aan het Karolinska Instituut en het Centrum voor Moleculaire Geneeskunde te Stockholm, Zweden. Aansluitend werkte hij als arts niet in opleiding tot specialist (ANIOS) aan het Alrijne Leiderdorp, afdeling Interne Geneeskunde, waarbij hij tevens werkzaam was voor de afdelingen Longgeneeskunde en Cardiologie. Er werd in 2017 gestart met het huidige promotieonderzoek aan de afdeling Interne Oncologie en de afdeling Longgeneeskunde en in het Erasmus Universitair MC, onder supervisie van prof. dr. A.H.J. Mathijssen en prof. dr. J.G.J.V. Aerts. Zijn onderzoek heeft zich gefocust op de farmacologie en personalisatie van immuun checkpoint remmers bij uitgezaaide vormen van kanker (m.n. melanoom, niet-kleincellig longkanker en niercelkanker). In 2019 ontving Daan een Merit Award van de European Society for Medical Oncology (ESMO) tijdens de jaarlijkse ESMO meeting in Barcelona, voor een studie binnen zijn proefschrift.